

Romanian Journal of MINERALOGY

continuation of

DĂRI DE SEAMĂ ALE ȘEDINTELOR INSTITUTULUI DE GEOLOGIE ȘI GEOFIZICĂ
COMPTES RENDUS DES SÉANCES DE L'INSTITUT DE GÉOLOGIE ET GÉOPHYSIQUE
(1. Mineralogie-Petrologie)

Founded 1906 by the Geological Institute of Romania

ISSN 1220-5621

Vol. 78

CONTENTS

Mössbauer investigation of two pumpellyites from Romania. Ș. CONSTANTINESCU, G. UDUBAȘA, S. CALOGERO.....	3
Sulphur isotope characteristics of polymetallic sulphide ores at Baia Borșa, Maramureș, Romania. N.J. COOK.....	11
Geothermobarometry of metapelitic rocks from the western part of the Preluca crystalline complex, Maramureș. D.M. RADU, A. MAIS, N.J. COOK.....	21
Geochemical studies of Gold-Silver-Tellurium mineralization in the vicinity of Săcărâmb, southern Apuseni Mts, Romania: Some preliminary results. D.H.M. ALDEIRON, G. SIMON, M. IOAN, I. PANAZAN, E. ORLANDEA, I. CSIBI.....	31
Mineralogie des topazes du Hoggar Central. Y. CHALAL, M. KESRAOUI.....	39
On the presence of garnet-spessartine-calderite in the Delinești Mn-Fe deposit. P. HÂRTOPANU, I. VANGHELIE, G. STELEA, E. CĂLINESCU.....	45
Minor elements in quartz: hydrothermal vs metamorphic. G. UDUBAȘA, P. HÂRTOPANU, Ș. ANASTASE, A. ȘERBĂNESCU.....	53
Étude géochimique sur les muscovites des pegmatites des Crișeni-Muntele Rece (Monts Apuseni). D. STUMBEA.....	61

(Contents continued on outside back cover)



Institutul Geologic al României
București - 1997



Institutul Geologic al României

GEOLOGICAL INSTITUTE OF ROMANIA

Director General **Dr. G. Udubaşa** Member of the Romanian Academy

The **Geological Institute of Romania** is now publishing the following periodicals:

Romanian Journal of Mineralogy	Romanian Journal of Tectonics and Regional Geology
Romanian Journal of Petrology	Romanian Journal of Geophysics
Romanian Journal of Mineral Deposits	Anuarul Institutului Geologic al României
Romanian Journal of Paleontology	Memoriile Institutului Geologic al României
Romanian Journal of Stratigraphy	

Romanian Journal of ... supersedes "Dări de Seamă ale Ședințelor" and "Studii Tehnice și Economice", whose apparition goes back to 1910. Beside regular volumes, each series may occasionally contain Supplements (for abstracts and excursion guides to congresses and symposia held in Romania) and Special Issues (for larger papers of special interest). "Anuarul Institutului Geologic al României" (year first issued 1908) appears also in a new form, containing both the annual activity report and review papers.

Editorial Board: Gheorghe Udubaşa (chairman), Tudor Berza, Marcel Mărunțiu, Grigore Pop, Gheorghe Popescu, Vlad Roșca, Anatol Rusu, Mircea Săndulescu

Managing Editor: Anca Andăr

Executive Secretary: Georgeta Borlea

Editorial Office:
Geological Institute of Romania
Str. Caransebeș Nr. 1
RO - 79 678 București - 32
Tel. (+40) 1 665 66 25, 665 75 30
Fax (+40) 1 312 84 44
e-mail UDUBASA@IGR.RO

The editor has changed the name as follows: Institutul Geologic al României (1910–1952), Comitetul Geologic (1953–1966), Comitetul de Stat al Geologiei (1967–1969), Institutul Geologic (1970–1974), Institutul de Geologie și Geofizică (1975–1993), Institutul Geologic al României (since 1994).

ROMANIAN JOURNAL OF MINERALOGY supersedes "Dări de Seamă ale Ședințelor", Series 1/**Mineralogie** - Petrologie - the last volume with this title being No. 74.

Scientific Editor: Gheorghe Udubaşa

Advisory Board: Gheorghe Udubaşa, Ion Hârtopanu.

Rom. J. Mineralogy is also the Bulletin of the Mineralogical Society of Romania, a member the EMU and IMA. Thus, this journal follows the rules of the Commission on New Minerals and Mineral Names of the IMA in all the matters concerning mineral names and nomenclature.

The manuscripts should be sent to the scientific editor and/or executive secretary. Correspondence concerning advertisements, announcements and subscriptions should be sent to the Managing Editor.

©GIR 1997

ISSN 1220-5621

Classification index for libraries 55(058)

Printed by the Geological Institute of Romania
Bucharest



Institutul Geologic al României



CONTENTS

Mössbauer investigation of two pumpellyites from Romania. Ș. CONSTANTINESCU, G. UDUBAȘA, S. CALOGERO.....	3
Sulphur isotope characteristics of polymetallic sulphide ores at Baia Borșa, Maramureș, Romania. N.J. COOK.....	11
Geothermobarometry of metapelitic rocks from the western part of the Preluca crystalline complex, Maramureș. D.M. RADU, A. MAIS, N.J. COOK.....	21
Geochemical studies of Gold-Silver-Tellurium mineralization in the vicinity of Săcărâmb, southern Apuseni Mts, Romania: Some preliminary results. D.H.M. ALDERTON, G. SIMON, M. IOAN, I. PANAZAN, E. ORLANDEA, I. CSIBL.....	31
Mineralogie de topazes du Hoggar Central. Y. CHALAL, M. KESRAOUI.....	39
On the presence of garnet-spessartine-calderite in the Delinești Mn-Fe deposit. P. HÂRTOPANU, I. VANGHELIE, G. STELEA, E. CĂLINESCU.....	45
Minor elements in quartz: hydrothermal vs metamorphic. G. UDUBAȘA, P. HÂRTOPANU, Ș. ANASTAS, A. ȘERBĂNESCU.....	53
Étude géochimique sur les muscovites des pegmatites des Crișeni-Muntele Rece (Monts Apuseni) D. STUMBEA.....	61
Glauconitic minerals from the Transylvanian Basin. New mineralogical data. D. POP, I. BEDELEAN.....	71
Palygorskite in magnesian skarns from Băița Bihor (Rézbanya): A second romanian occurrence and a review. ȘT. MARINCEA, M. CIULAVU, I. VANGHELIE.....	87
Sepiolite from Dealul Măgurenilor-Preluca Veche, Maramureș District, Romania. I. KALMÁR, P. KOVÁCS-PALFFY, M. FÖLDVARI.....	97
Mineral composition and bloating effect of clayshale from Mezica Pb-Zn ore deposit (Slovenia). P. TOMŠE, B. MITRIČ.....	107
Once again on the joseite-A from the skarns deposits from Băița Bihor mine (Apuseni Mts, Romania). G. CIOFLICA, M. LUPULESCU.....	113
Recent discovery of tellurides in the Vezhnali ore deposit, Lesser Caucasus. S.F. VELIZADE, A.B. SHIRALIYEV, E.N. EFENDIYEVA, N.F. NAGIYEV, T.G. MUSTAFAYEV.....	117
Paragenetic mineral associations of sulphides ores, southern slope of the Great Caucasus. S.F. VELIZADE, A.B. SHIRALIYEV, E.N. EFENDIYEVA.....	121
Plant remnants replaced by copper minerals, Rongjing copper deposit, Sichuan, China. Z.M. CAO, X.Q. HU, D.Q. SHUAL.....	125
The possibilities of geological correlation on the basis of extraterrestrial spherules occurring in Hungary. Cs. H. DETRE, Gy. DON, L. DOSZTÁLY, E. RÁLISCH-FELGENHAUER, A. SIEGL-FARKAS.....	129
On the morphological distinction between spherules of extraterrestrial, terrestrial and industrial origin by means of SEM and EDAX examination of samples taken from the placers of Crișu Negru, Romania. O. KÁKAY-SZABÓ, Á. HADNAGY.....	133
The structure of synthetic Zippeite. R. VOCHTEN, L. VAN HAVERBEKE, K. VAN SPRINGEL, N. BLATON, O.M. PEETERS.....	139
Standardisation of polytype suffixes. E.H. NICKEL.....	141
Mineral names applied to synthetic substances. E.H. NICKEL.....	143
New minerals recently approved by the Commission on New Minerals and Mineral Names International Mineralogical Association.....	145





SOCIETATEA ACADEMICĂ DIN ROMÂNIA

SOCIETATEA ACADEMICĂ DIN ROMÂNIA alcătuiește o bază de date în vederea editării, până la sfârșitul acestui an, a unui **CATALOG AL EXPERTILOR** din România.

În acest catalog vor figura profesioniști din toate domeniile care:

- * *publică în străinătate*
- * *participă la congrese, seminarii, dezbateri internaționale*
- * *au făcut sau fac parte din echipe de cercetare internaționale*
- * *sunt membri ai unor organizații profesionale internaționale*
- * *au experiența predării în instituții de învățământ superior din Occident*
- * *au beneficiat de studii, burse sau orice altă formă de specializare într-o țară occidentală*

Instituțiile și specialiștii interesați sunt invitați să ne contacteze la tel./ fax (01) 210 75 69, sau la sediul Societății Academice din România, București, Intrarea Grigore Alexandrescu nr. 3.

***NU ratați șansa de a fi prezenți în
circuitul internațional al specialiștilor***



Institutul Geologic al României

MÖSSBAUER INVESTIGATION OF TWO PUMPELLYITES FROM ROMANIA

Șerban CONSTANTINESCU

Institute of Physics and Technology of Materials, P.O. Box Mg-07, Bucharest, Romania

Gheorghe UDUBAȘA

Geological Institute of Romania, 78344, Bucharest, Romania

Sandro CALOGERO

Universita degli Studi di Venezia, Dipt. Chim.-Fisica, 30123 Venezia, Italy

Key words: Pumpellyite. Mössbauer. Maramureș. Parâng Mts.

Abstract: The authors carried out the Fe^{57} Mössbauer spectra of two pumpellyite samples from two different mineral occurrences of the Romanian Carpathians. Using a specialised computing program of the quadrupole splinting spectral parameter, **QSCOMP17**, the observed quadrupole doublets were attributed to the ferric and ferrous ions in cation octahedral sites. The refined analysis of spectral parameters permitted the authors to characterize both the oxidation state, the electronic configuration and the coordination symmetry with the distortions and occupancies of pumpellyite constituting iron ions. The spectral parameter differences observed at the two studied samples, the iron abundance, the deformation and occupancies of iron octahedra are discussed and correlated with the different pressure and temperature conditions of two pumpellyite-bearing occurrences.

Introduction

The silicate minerals of the pumpellyite group are characteristic of low grade metamorphic rocks. The crystal structure of pumpellyite was determined in earlier refined studies (Gatorade, 1965; Galli; Alberti, 1969; Allmann, Donnay, 1971; Baur, 1971). The chemical formula of this mineral can be written $\text{W}_8\text{X}_4\text{Y}_8\text{Si}_{12}\text{O}_{56-n}(\text{OH})_n$, where $\text{W}=\text{Ca}^{2+}, \text{K}^{1+}, \text{Na}^{1+}$; $\text{X}=\text{Mn}^{2+,3+}, \text{Fe}^{2+}, \text{Al}^{3+}$; $\text{Y}=\text{Fe}^{3+}, \text{Al}^{3+}, \text{Ti}^{3+,4+}$. Small quantities of Mn and Fe ions can appear in W-sites and if it is necessary Al in Si sites. The pumpellyite crystallizes in the monoclinic system, space group A2/m , with the cell parameters $a=8.83 \text{ \AA}$, $b=5.90 \text{ \AA}$, $c=19.17 \text{ \AA}$, $\beta=97^\circ 7'$ and $Z=1$. The crystal structure of this mineral is characterized by two types of independent octahedral chains, X and Y. The X octahedra are a little bigger ($r_{\text{X-O}}=1.99 \text{ \AA}$) than the Y one ($r_{\text{Y-O}}=1.92 \text{ \AA}$). The two kinds of octahedra



are shown in Figure 1. Both chains are joined by the isolated SiO_4 tetrahedra and double Si_2O_7 tetrahedra.

The samples obtained from different occurrences, the Maramureş Mts, 15c, and the Parâng Mts, 2L, have been investigated by

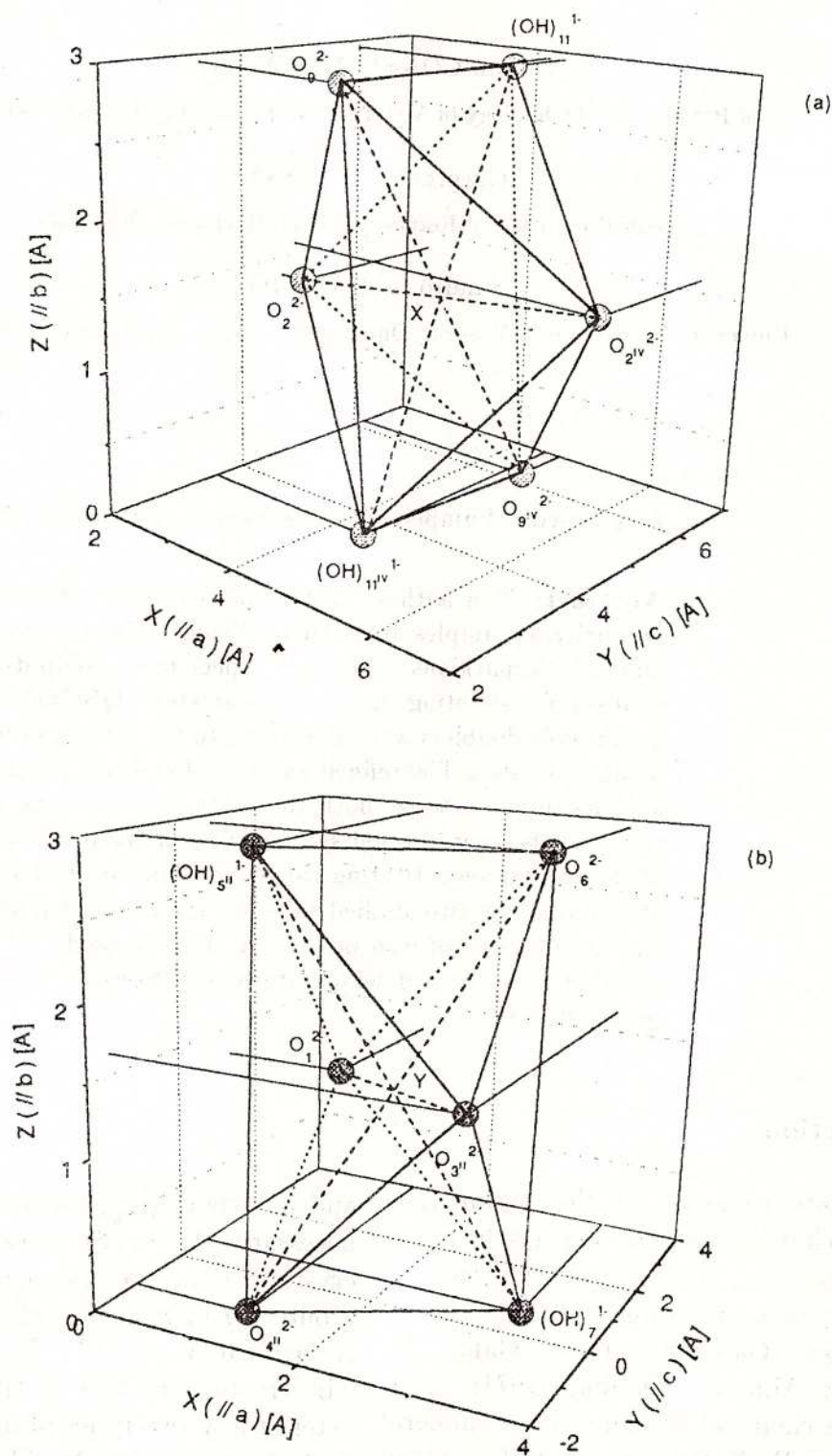


Fig. 1 – X, (a) and Y, (b) octahedra in pumpellyite crystal

Mössbauer spectroscopy technique using ^{57}Fe as Mössbauer isotope. The Mössbauer spectroscopy on ^{57}Fe isotope is a very sensitive spectroscopy for the characterization of the iron oxidation state (e.g. Fe^{2+} or Fe^{3+}), electronic configuration (e.g. high or low spin), coordination symmetry of iron atom (e.g. tetrahedral or octahedral), its distortion and the occupancies of the iron sites. The authors comparatively analyse the spectra carried out on the two samples and discuss the spectral parameters correlated with the genesis aspects of mineral occurrences.

Conditions

A $^{57}\text{Co}:\text{Rh}$ source of nominal strength (intensity) of 25mCi having a line width $\Gamma_S=0.097\text{mm/s}$ and a recoilless fraction (Mössbauer factor) $f_s=0.73$ was used. The absorbers obtained from the two above mentioned occurrences were prepared as powder-samples. Their uniform thickness has been of about $5\text{--}10\text{mgFe}/\text{cm}^2$, so they could be considered as thin samples. The spectra were carried out in the velocity range of about $\pm 4.7\text{mm/s}$, at room temperature, using a standard Mössbauer spectrometer in transmission geometry with a constant acceleration in saw tooth and in sinusoidal mode, coupled by a γ -line Na:Tl crystal detector and a multichannel-analyser.

In order to obtain the correspondence channel-energy (in velocity units) the etalon sample $\alpha\text{Fe}_2\text{O}_3+\text{Na}_2[\text{Fe}(\text{CH})_5\text{NO}]\cdot 2\text{H}_2\text{O}$ was used. A special least-squares computing program fitted the carried out etalon and experimental spectra of the investigated samples by a sum of quadrupole doublets with Lorentzian peak-shapes.

The experimental spectra have been plotted in Figure 2a,b and the Mössbauer spectral parameters, σ_{Rh} (the central shift), Δ_Q (the quadrupole splitting), $\Gamma \geq \Gamma_S + \Gamma_A$ (the line width) and the area of every quadrupole dou-

blet are given Table 1.

Discussions

The quadrupole doublet spectra of the investigated samples are corresponding to three different vicinities. The values of δ_{A-Rh} and Δ_Q of the quadrupole doublets III, II and I, in both spectra, are showing the presence of the ferric and ferrous ions respectively in the six-fold sites. The charge balance, the ionic radius and the dimension of X octahedra impose to assign the quadrupole doublet with the greater $\delta_{A-Rh}(\text{I})$ and $\Delta_Q(\text{I})$ to the Fe^{2+} in X-site.

In order to attribute the other spectral doublets (II, III) to Fe^{3+} in the X and Y sites the authors performed a numerical calculation of the lattice contribution to the electric field gradient, EFG^{latt} . The results of this calculation have been obtained in the approximation of the point charge model using the QSCOMP17 program, (Constantinescu, Tarina, 1995; 1996) with the starting fractional atomic coordinates given in (Galli, Alberti, 1969) and the net electronic charges of oxygen and hydroxyl ions extracted from (Allmann, Donnay, 1971). Moreover, supposing that iron atomic orbital of $3d^6$ electronic configuration corresponding to the ionic state ^5D and the crystal field splitting parameters, Δ_i , as given in Figure 3, the authors calculated the total quadrupole splitting parameter for Fe^{2+} in X site. The numerical calculations are given for the first surrounding anions shell. Table 2 shows the calculated values of both Δ_Q^{tot} and η^{tot} (asymmetry) parameters with the Sternheimer and antishielding factors γ_∞ , R, the nuclear quadrupole moment Q, and the ionicity factor α as given in the table and the geometrical distortions, Δ , δ^2 , given by the expressions:

$$\Delta = \frac{1}{6} \sum_{i=1}^6 \left(\frac{r_i - r}{r} \right)^2 \cdot 10^4; \quad \sigma^2 = \frac{1}{14} \sum_{k=1}^{15} \left(\frac{\Theta_k - \Theta_m}{\Theta_m} \right)^2 \quad (1)$$



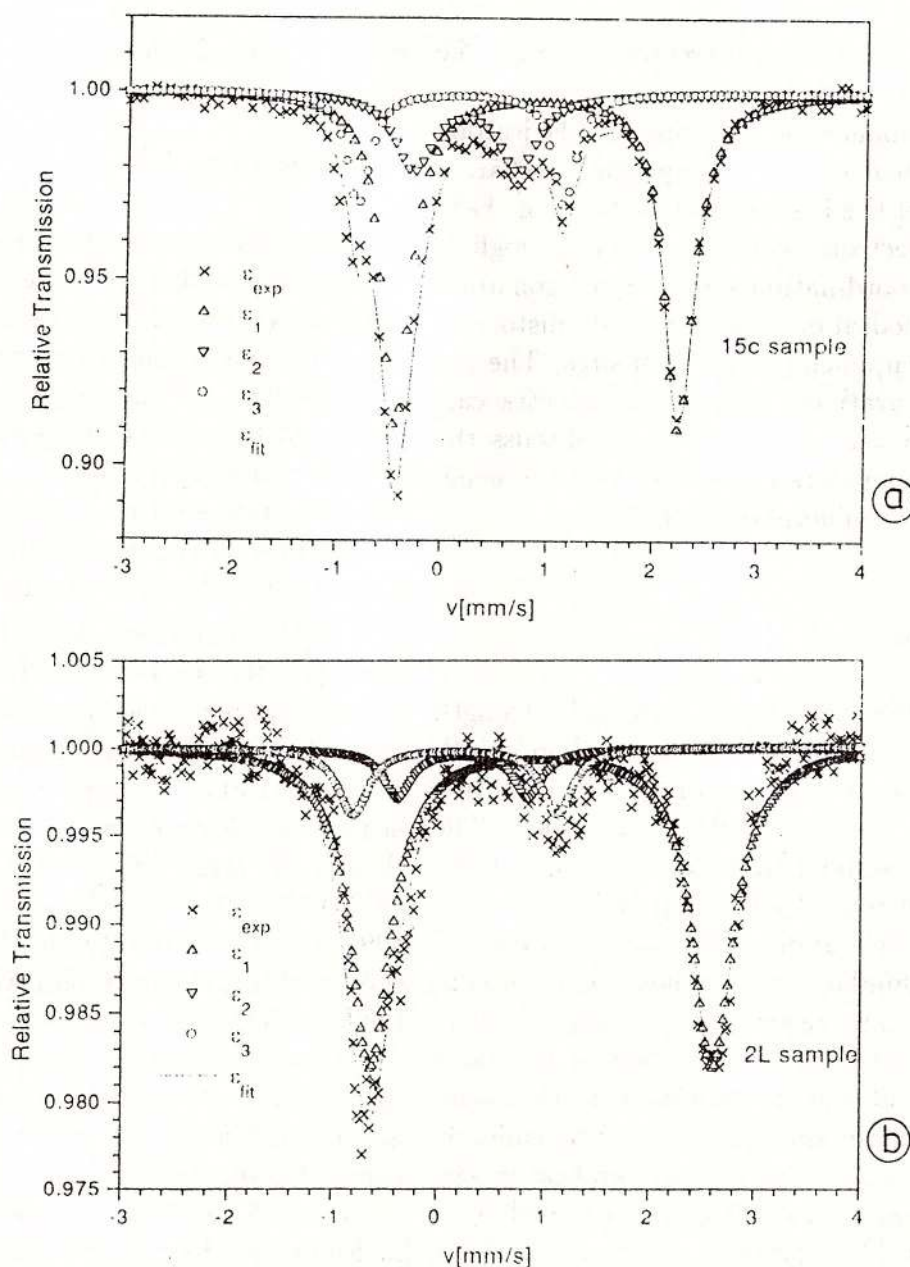


Fig. 2 – Mössbauer spectra of the sample 15c, (a) and 2L, (b)

Tab. 1

The Mössbauer spectral parameters and their errors

Sample	Quadrupole doublet	δ_{Rh}^A [mm/s]	Δ_Q [mm/s]	Γ [mm/s]	$A(i)/A_{exp}$ [%]
2L (Parâng Mts)	I	0.99(2)	3.24(4)	0.48(3)	80(3)
	II	0.35(4)	1.23(8)	0.35(9)	7(5)
	III	0.26(2)	1.93(4)	0.36(5)	13(4)
15c (Maramureş Mts)	I	0.90(2)	2.68(4)	0.34(3)	66(3)
	II	0.20(3)	0.98(6)	0.45(5)	18(4)
	III	0.16(3)	1.95(6)	0.27(4)	16(4)

$$\delta_{Rh}^A = \delta_{Fe}^A - 0.114 \text{ mm/s}$$



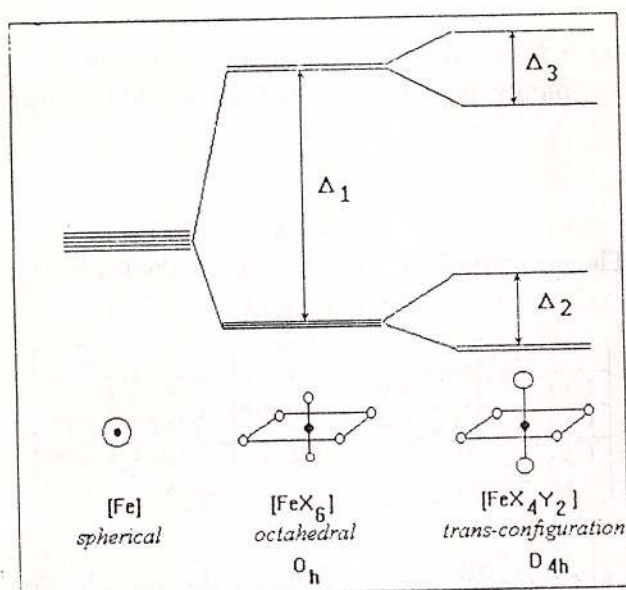


Fig. 3 - The 3d⁶ iron atomic orbital splitting in trans-configuration D_{4h} symmetry with the considered crystal field parameters

the experimental and calculated quadrupole splitting values of 15c suggested us a similar structure to pure pumpellyite one; moreover, this remarkable agreement imposes to consider the ferric ion in the high spin electronic configuration with no relevant electrons valence contribution to quadrupole splitting. The agreement between the value of the first experimental quadrupole doublet of the 15c sample and the calculated one for Fe²⁺ is suggesting us a good supposing of the electron distribution on the atomic orbital. The agreement between the octahedral distortions, Δ_x , Δ_y and the experimental Δ_Q (I), Δ_Q (II) and calculated Δ^{tot} values proved the important role of distance distortions in pumpellyite structure.

The difference between the calculated and experimental quadrupole splitting values,

Table 2

The calculated and corresponding errors value of quadrupole splitting and asymmetry parameters in the pumpellyite lattice

Site	Δ_Q^{latt} [mm/s]	η^{latt}	Δ_Q^{el} [mm/s]	η^{el}	Δ_Q^{tot} [mm/s]	η^{tot}	Geometrical distortions Δ ; δ^2
*Fe ²⁺ :X	0.86(8)	0.60	3.20(4)	0.00	2.68(8)	0.10	9.764; 0.032
Fe ³⁺ :X	0.86(8)	0.60	—	—	0.86(8)	0.60	9.764; 0.032
Fe ³⁺ :Y	1.91(10)	0.47	—	—	1.91(10)	0.47	11.12; 0.022

$$\gamma_\infty = -10; R = 0.32; Q(^{57}\text{Fe}) = 0.20 [10^{-28}\text{m}^2]; \alpha = 0.9;$$

$$\Delta_1 = 30 \text{ cm}^{-1}; \Delta_2 = 2\Delta_3 = 3 \text{ cm}^{-1}.$$

where r_i and r are the distances between the iron and octahedral anions and the average value, Θ_k ($k=i,j$) and Θ_m are the angles between the \vec{r}_i and \vec{r}_j vectors and the ideal angle on the X and Y sites in the pumpellyite mineral. Within the limits of the point charge model, of the nearest ionic neighbours, the calculated values Δ^{lat} for ⁵⁷Fe probe in X and Y sites are very close to the experimental values of the Mössbauer quadrupole doublets, Δ_Q (II) and Δ_Q (III) in 15c sample, so the authors attributed the quadrupole doublet II and III of Mössbauer spectra to Fe³⁺ in X and in Y site respectively. The concordance between

observed at the second doublet of the 2L sample, could be explained by the errors due to the low relative intensity of the quadrupole doublet, by a strong deformation of the X octahedra in this sample as the known one in the pumpellyite crystal structure, (Galli, Alberti, 1969; Allmann, Donnay, 1971) and/or by the different electrons valence contributions. On the other hand the differences of the quadrupole splittings at Fe²⁺ in X octahedra of the two samples could be explained by the last two suppositions. Supposing approximately the same contributions of the valence electrons to Δ_Q (I), the authors consider



that the deformation of X octahedra is the major cause of the observed differences in the quadrupole splittings for the two samples.

The different grade of the X octahedra deformation is partly due to the different temperature and pressure genesis conditions of the two mineral occurrences. Due to $r_{X-O} > r_{Y-O}$ a high genesis pressure of the 2L mineral occurrence will induce a greater deformation of the X octahedra and as a consequence a higher sensitivity of the Mössbauer parameters as of Y once. In addition, sample 2L represents an iron-poor pumpellyite variety or even a separate mineral species early described as lotrite. Some supplementary data on the chemical peculiarities of the "lotrite" were already emphasized (Udubaşa et al.). On the other hand taking into account other considerations the authors are supposing a lower pressure genesis condition for 2L sample occurrence as for 15c one and in consequence a higher abundance of the nonconstituting ions in the pumpellyite crystal structure.

Taking into account that our samples are thin absorbers and supposing the same recoilless factor f , the relative occupancies of the iron ions are given by the ratio of the quadrupole doublet area and the total experimental one, $a(i)/a_{exp}$. In Table 3 the occupancies C_i calculated by the expression:

$$\frac{a(i)}{a_{exp}} = \frac{C_i}{\sum_{j=1}^{nr.subr} C_j \frac{f_j \Gamma_j G_j(C_j, f_j, \delta_o)}{f_i \Gamma_i G_i(C_i, f_i, \delta_o)}} \cong \quad (2)$$

$$\frac{C_i}{\sum_{j=1}^{nr.subr} C_j}$$

where f_j, Γ_j, σ_o and G_j are the Mössbauer factor, line width, cross section factor and saturation correction of the j quadrupole doublet are shown for X and Y octahedra of the two samples.

The data presented in Table 3 point out the major differences between the Fe^{2+} and Fe^{3+} ionic occupancies of the two samples in

the octahedra, so in the sample 2L, the Fe^{3+} occupancy is smaller in both octahedra and

Table 3
The occupancies C of X and Y octahedra in the two samples

Ratio	2L	15c
$C_X(Fe^{3+})/C_X(Fe^{2+})$	7/80	18/66
$C_X(Fe^{3+})/C_Y(Fe^{3+})$	7/13	18/16
$C_X(Fe^{2+} + Fe^{3+})/C_Y(Fe^{3+})$	87/13	84/16
$C(Fe^{3+})/C(Fe^{2+})$	20/80	34/66

higher for Fe^{2+} in X one as in the sample 15c. Moreover, taking into account the thick correction, the Mössbauer spectra of 15c and 2L sample are evidencing a large difference between the effect spectral parameter $\varepsilon(v)$, corresponding to a large difference between the iron abundance.

The lines of the quadrupole doublets for 2L sample are sensitively broader as the 15c sample. That means different crystallization conditions of the samples.

The differences evidenced by the spectral parameters in the iron abundance, the deformations and occupancies of the iron octahedra, the crystallization and the iron oxidation state of 15c and 2L samples could be explained by different conditions of two pumpellyite-bearing occurrences.

In addition, sample 2L represents an iron-poor pumpellyite variety or even a separate mineral species early described as "lotrite". Some supplementary data on chemical peculiarities of the "lotrite" were already emphasized (Udubaşa et al., 1994).

A very careful analysis of the spectral parameters for the studied absorbers and correlation with the genesis data of the above mentioned geological deposit are in progress.

Acknowledgements

One of the authors, Ş. Constantinescu, thanks the University of Venice for supporting



a scientific stay in Dipartimento di Chimica-Fisica. Financial support from the Committee of CNR(Roma) and the Progetto Sistema Lagunaro Veneziano is gratefully acknowledged. Doina Russo-Săndulescu kindly put at our disposal the pumpellyite sample from Maramureş.

References

- Gatorade, G. (1965)** Die Kristallstruktur von Pumpellyit, *Tschermaks. Min. Petr. Mitt.* 3, 10, p. 115
- Galli, E., Alberti, A. (1969)** On the crystal structure of pumpellyite. *Acta Cryst.*, B25, p. 2276.
- Allmann, R., Donnay, G. (1971)** Structural relations between pumpellyite and ardenite. *Acta Cryst.*, B27, p. 1871.
- Baur, W.H. (1971)** The prediction of bond length variations in silicon-oxygen bonds. *Amer. Mineral.*, 56, p. 1573
- Constantinescu, S., Tarina, D. (1995)** Crystal field disorder in trigonal Ba, Sr and Ca germanates. *J. Roum. Phys.*, 40, p. 8.
- , **Tarina, D. (1996)** Electric field gradient at ^{57}Fe probe in metal-ligand coordination polyhedra. Report A20.1, IFA-IFTM, Bucharest.
- Shanon, R.D., Prewitt, C.T. (1969)** Effective ionic radii in oxides and fluorides. *Acta Cryst.*, B25, p. 925.
- Udubaşa, G., Mărunţiu, M., Lupulescu, M., Udubaşa S.S. (1994)** Lotrite revisited. *An. Univ. Bucureşti*, XLIII (Supl.), p. 35.





International Mineralogical Association

IMA '98 TORONTO, CANADA

IMA'98: The 17th General Meeting of the International Mineralogical Association, IMA'98, will be held from 9–15 August 1998 at the University of Toronto, Toronto, Canada. The meeting will be preceded and succeeded by field trips across Canada, including important mineral locations, ore deposits, sites of impact craters, and classic petrologic localities. For more information please contact Professor A.J. Naldrett, Department of Geology, University of Toronto, Canada M5S 3B1. Tel. [416] 978 3030, FAX [416] 978 3938. e-mail address: ima98@quartz.geology.utoronto.ca



Institutul Geologic al României

SULPHUR ISOTOPE CHARACTERISTICS OF POLYMETALLIC SULPHIDE ORES AT BAIJA BORŞA, MARAMUREŞ, ROMANIA

Nigel J. COOK

Mineralogisches Institut der Universität Würzburg. Am Hubland, 97074 Würzburg, Germany

Key words: Massive sulphide deposits. S-isotopes. Pyrite, Baia Borşa. Maramureş Mountains. East Carpathians.

Abstract: Sulphur isotope distributions have been determined in pyrite and other sulphides from the metamorphosed stratabound massive sulphide deposits at Baia Borşa, in the East Carpathians. A narrow range of $\delta^{34}\text{S}$ contents in pyrite is noted, from +7.9 to +13.6 ‰. Such values do not contradict a genetic model for the deposits involving volcanogenic deposition of the sulphides during the Cambrian. The ^{34}S -rich pyrite of the stratabound deposits is in sharp contrast to $\delta^{34}\text{S}$ contents from the superimposed hydrothermal vein-type mineralisation of the Toroiağa complex which cluster around zero ‰.

Each of the stratabound massive lenses investigated in the present study shows an extremely limited range of $\delta^{34}\text{S}$, which differs from deposit to deposit. These mild differences are interpreted to reflect fractionation brought about by slight variations in physico-chemical conditions of formation. It is considered unlikely, based on the cumulated evidence from other geographical areas, that the low-grade regional metamorphic episodes have led to large-scale homogenisation of S-isotope ratios.

Sulphide ores from Baia Borşa which, based on structural and other criteria, have been described as syn-metamorphic (?) mobilisations of syngenetic ores, have isotopic compositions largely similar to those of unmobilised ores. The $\delta^{34}\text{S}$ values of these ores allow them to be distinguished from mineralisation originating in the Neogene overprint. The two types can commonly appear in similar settings.

Introduction

The study of S-isotope signatures in pyrite and other sulphide minerals from metamorphosed massive sulphide ores can deliver useful information on the source of sulphur and the physico-chemical environment of deposition. Furthermore, S-isotopes can indicate the extent of metamorphic homogenisation on the

local or deposit scale as well as helping to identify patterns of re-equilibration brought about by metamorphic remobilisation.

Sulphur isotope signatures of regionally metamorphosed VMS deposits have been studied by various authors (e.g. Gehrisch et al., 1975; Geen et al., 1981; von Gehlen et



al., 1983; Willan & Coleman, 1983; Gregory & Robinson, 1984); Seccombe et al., 1985; Kräutner et al., 1992; Crowe, 1994). Local metamorphic re-equilibration between sulphides was recognised, but large-scale homogenisation was not identified. Original S-isotope patterns, which frequently display lithostratigraphic control were found to be generally preserved, even at metamorphic conditions as high as 670°C, 5 kbar (von Gehlen et al., 1983). Only in limited areas of the deposits substantial modifications to the S-isotope signature were observed; for example in zones where large-scale inflow of fluids from outside the system occurred. The present author reached similar conclusions in a study of S-isotope distributions in VMS deposits in the Norwegian Caledonides (Cook et al., under review) and showed evidence for the preservation of primary patterns within deposits metamorphosed at facies ranging from lower greenschist to upper amphibolite.

A study of S-isotope signatures in the Bălan orefield in the southern part of the East Carpathians gave comparable results (Kräutner et al., 1992). However, this study showed a distinct homogeneity with respect to $\delta^{34}\text{S}$ contents in pyrites and other sulphides. This was interpreted as due to differing local deposition environments, and to conditions in which reduction of seawater sulphur was the chief sulphur source. Furthermore, bacterial activity may have played an important role during genesis. A shallow environment of deposition is favoured for the Carpathian deposits, based on the presence of graphitic schists and carbonates within the sequence.

The present study is intended to add to the existing data base on S-isotope distributions in VMS deposits of the East Carpathians, of which the Baia Borşa orefield accounts for the largest part of base metal reserves. The investigation of S-isotope distributions at Baia Borşa aimed to show the source of sulphur in the deposits, to help to identify conditions of ore formation, to characterise

the degree of metamorphic homogenisation, if any, to permit a comparison with the data from Bălan and other massive sulphide deposits in the East Carpathians and to determine if the S-isotope signature of pyrite and/or other sulphides are a panacea for discriminating between primary, remobilised and epigenetic phases of mineralisation.

Geological Setting

The Baia Borşa orefield in the East Carpathians, at the easternmost margin of the Maramureş County is host to a number of sizable massive sulphide lenses. These represent the largest of the four main clusters of VMS deposits in the East Carpathian belt (Fig. 1a). Essentially pyritic, the lenses contain variable amounts of base metal sulphides, together with minor Ag and Au. The deposits are hosted within the dominantly rhyolitic volcano-sedimentary Tulgeş Tg₃ Formation of Lower Cambrian age. The regionally metamorphosed sequence is represented by a sequence of keratophyres, quartz-keratophyres, feldspathic, quartz-feldspar, quartz-muscovite, muscovite, chlorite and graphite-bearing schists. Together with their host rocks, the ore bodies underwent regional metamorphism during at least two orogenic events. Apart from very minor barite in a single sample from Colbu (Radu, pers. comm.), sulphates are not known from the massive syngenetic deposits. The Toroiaga sub-volcanic complex of Miocene age, composed of Pontian andesites, quartz-andesites and diorites, intrudes the sequence, displaying contact relationships with the host sequence and with the massive sulphide deposits. The Toroiaga massif is host to extensive polymetallic hydrothermal vein mineralisation (Borcoş, 1967; Borcoş et al., 1982). Fuller details of geological setting and field relationships in the Baia Borşa area have been given by Szoke & Steclaci (1962), Zincenco



(1971), Zincenco et al. (1973), Cook (1995) and thicknesses from 2 to 30 m. In this study, samples were collected from four of the

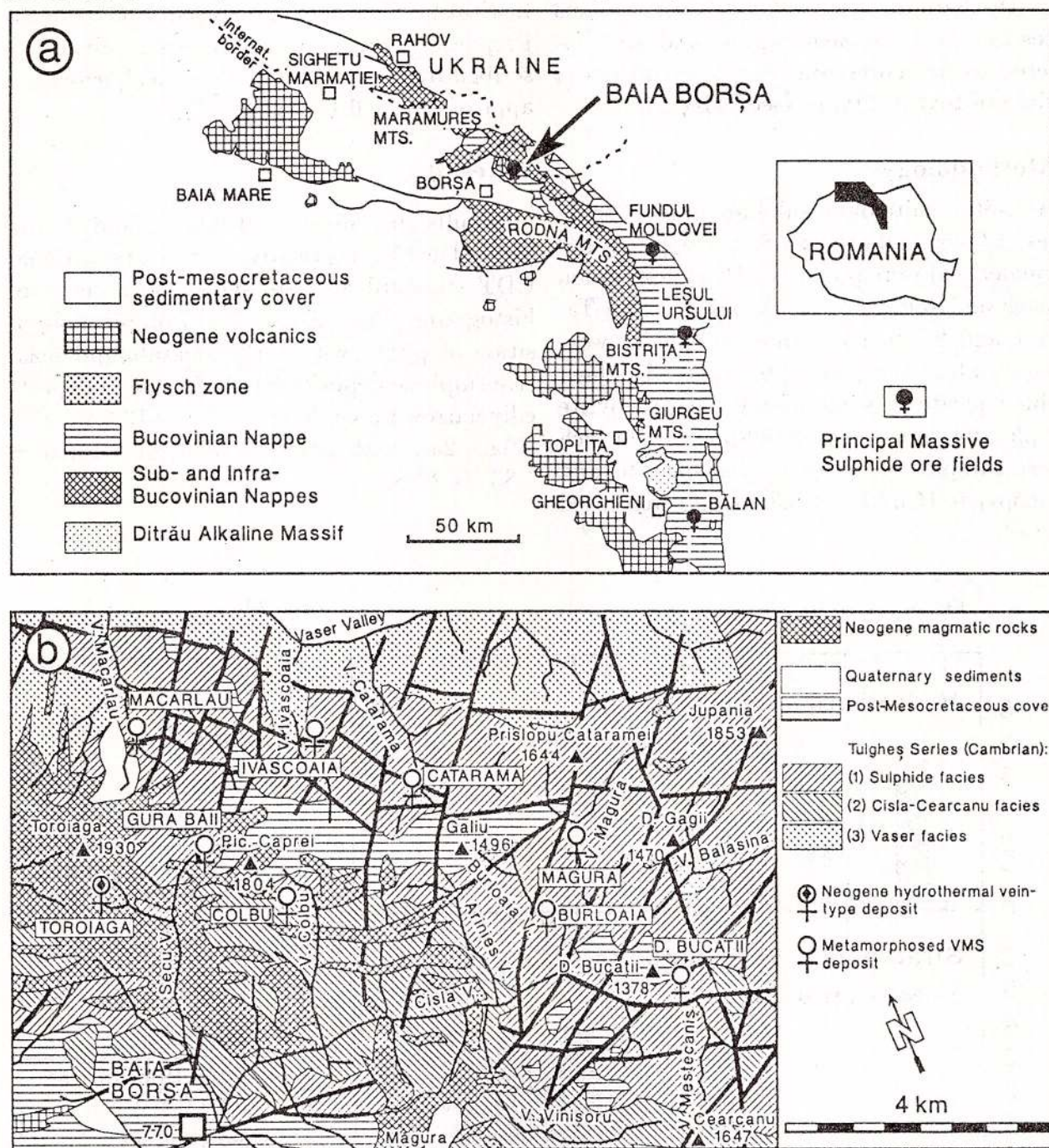


Fig. 1 – a) Geological sketch map of the East Carpathians, showing location of the Baia Borşa orefield. b) Geological map of the central part of the Baia Borşa ore-field, showing location of sulphide deposits sampled in this study.

The ore deposits lie at three distinct levels in the stratigraphy; each is sheet or less-syngenetic pyritic deposits (Colbu, Măcârlău, Ivășcoia and Dealul Bucății Est). A reference suite of samples was collected from the hy-



drothermal vein mineralisation in the Toroiaga mine. Locations of the deposits are shown on Fig. 1b. Samples were collected from various accessible parts of each deposit and are considered to be representative. They include a variety of textural types (see Table 1).

Methodology

An initial suite of 50 sulphide mineral separates (32 pyrite, 6 galenas, 8 chalcopyrites and 4 sphalerites) were prepared. Brief description of each and sample locations are given in Tables 1 and 2. In most cases, sulphides were separated by hand-picking of grains. The fine-grained pyrite in some of the massive pyrite samples does not permit hand-picking. In such cases, samples with minimal sphalerite and chalcopyrite ($\text{Cu} + \text{Zn} < 0.3 \text{ wt. } \%$) were used instead.

All S-isotope analyses were carried out on a Finnegan MAT-251 gas spectrometer at the Institut für Geochemie, Universität Göttingen. Preparation procedures were essentially as described by Rieke (1964). Analytical errors are approximately $0.1 - 0.2 \text{ } \delta^{34}\text{S}$.

Results

Results are given in Tables 1 and 2, expressed as $\delta^{34}\text{S}$ ‰ relative to the international CDT standard and are shown on a series of histograms (Figs. 2a,b). The isotopic composition of pyrite within the stratabound massive sulphide deposits fall within an unexpectedly narrow range, from $+7.9$ to $+13.6 \text{ } \delta^{34}\text{S}$ (Fig. 2a), with a mean value of $+11.16 \pm 1.83 \text{ } \delta^{34}\text{S}$.

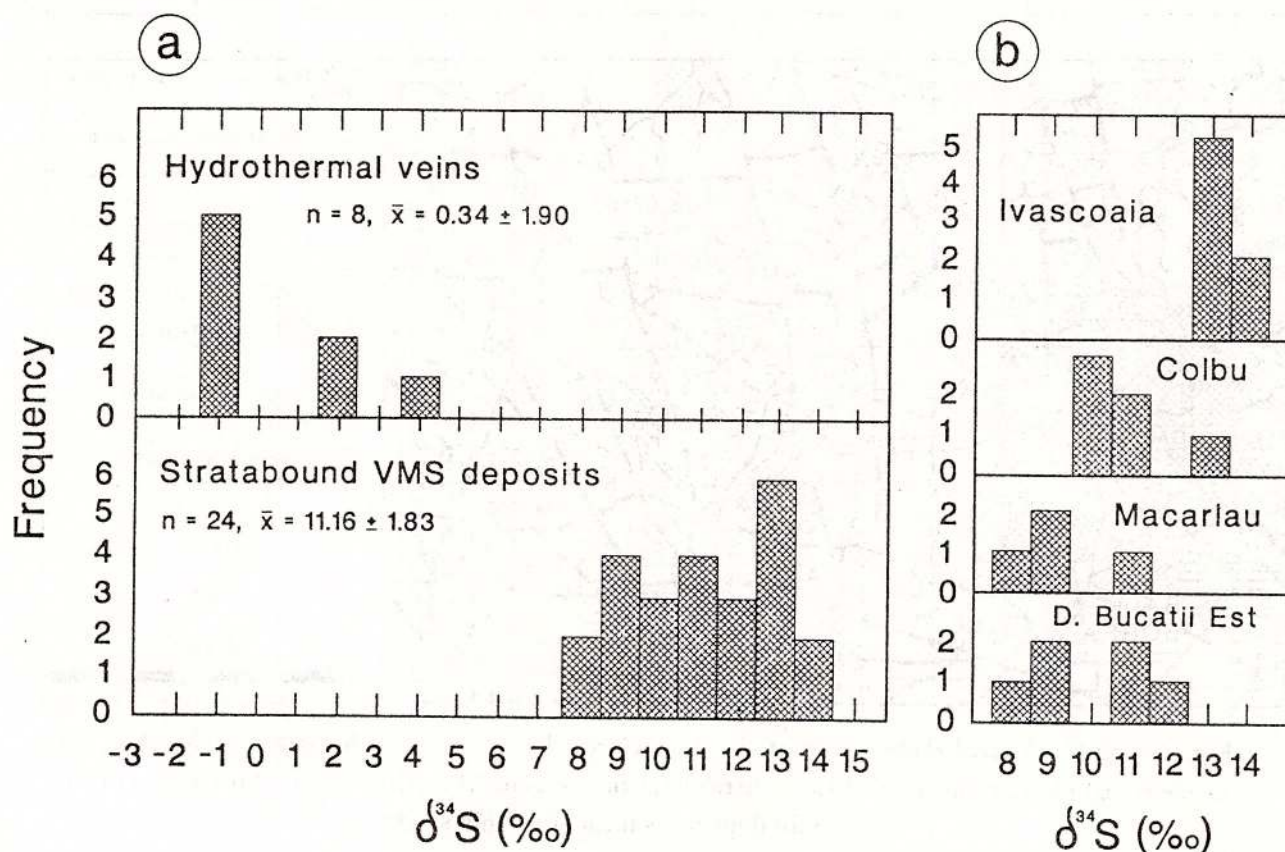


Fig. 2 – a) Histogram of S-isotope distribution in pyrite from syngenetic massive stratabound lenses and in hydrothermal vein-type mineralisation. b) S-isotope distribution in the syngenetic stratabound group broken down by deposit.

Table 1

Analysed sulphides from syngenetic deposits at Baia Borşa, location, brief description and results of sulphur isotope analysis

Sample	Mineral	Location	Description	^{34}S ‰
COLBU				
BB 120	Pyrite	gal. 10215.500	Massive pyrite ore	+9.98
BB 122	Pyrite	gal. 10215.500	Semi-massive pyrite ore	+9.98
BB 128	Pyrite	gal. 10215.400	Massive pyrite ore	+9.56
BB 199	Galena	(unknown)	In mineralised vein	+1.29
BB 375	Pyrite	gal. 10215/2a	Massive pyrite ore	+13.23
BBC-4	Pyrite	gal. 10215.500	Massive pyrite ore	+11.20
BBC-7	Pyrite	gal. 1000.2160	Massive pyrite ore	+11.21
	Galena		veined by galena	+9.92
BB 372	Sphalerite	gal. 1000.2160	Mineralised vein in fault	+4.37
BBC-8	Sphalerite	gal. 1000.2160	at andesite-ore contact	+4.52
MĂCĂRLĂU				
BB 160	Pyrite	+1250, gal. 138	Gn-Sp rich massive ore	+11.50
BB 168	Pyrite	+1250, gal. 130	Gn-Sp rich massive ore	+9.31
BB 170a	Pyrite	+1250, gal. 121	Cp-rich massive ore	+9.16
BBN-1	Pyrite	(unknown)	Massive Py cut by Gn vein	+8.35
	Galena			+0.76
BBM-2	Chalcopyrite	(unknown)	Clot of Cp in quartz matrix	+13.18
DEALUL BUCĂȚII EST				
BB 174	Chalcopyrite	gal. 208	Disseminated Cp in schist	+9.92
BB 178	Pyrite	gal. 208	Massive pyritic ore	+12.41
BB 184	Pyrite	gal. 208	Py-Cp mass in quartz lens	+10.76
BB 330	Pyrite	(dump)	Py-Cp mass in quartz lens	+8.63
	Chalcopyrite			+13.18
BB 331	Pyrite	(dump)	Banded ore, Py-Po-Sp	+7.89
BB 403	Pyrite	1135, gal. 403	Disseminated ore	+9.33
BB 408	Pyrite	1135, gal. 403	Disseminated ore	+10.65
IVĂȘCOAIA				
BB 145	Pyrite	1120, gal. 105	Massive py ore	+12.62
BB 146	Pyrite	1120, gal. 105	Disseminated ore	+13.83
BB 149	Pyrite	1120, gal. 105	Pyrite band in schist	+12.97
BB 150	Chalcopyrite	1120, gal. 105	Massive py-cpy ore	+11.39
BB 152	Pyrite	1120, gal. 105	Massive py-sph ore	+13.12
BB 155	Pyrite	(dump)	Py-Cp mass in quartz	+13.30
	Chalcopyrite			+12.99
BB 156	Pyrite	(dump)	Brecciated ore	+13.36
BB 158	Pyrite	(dump)	Py-Cp mass in quartz	+13.54
	Chalcopyrite			+14.39
BB 159a	Chalcopyrite	(dump)	Py-Cp mass in quartz	+13.10
GURA BĂII				
BB 277a	Galena	(unknown)	Fracture filling in chloritic schist	+2.11
MĂGURA				
BB 213	Pyrite	Open pit	Semi-massive Py ore	+12.10

Py: pyrite, Cp: chalcopyrite, Sp: sphalerite, Gn: galena, Po: pyrrhotite



Tab. 2 – Analysed sulphides from hydrothermal vein-type deposits, location, brief description and results of sulphur isotope analysis

Sample	Mineral	Location	Description	$\delta^{34}\text{S} \text{ ‰}$
TOROIAGA MINE				
BB 189	Pyrite	Vein X, 920 level	Py-Cpy-Qz	+1.86
BB 190	Pyrite	Vein X, 920 level	Py-Gn-Cpy-Qz	-1.12
BB 191	Pyrite	Orania vein, 1330	Rich Py-Cpy-Sp-Gn ore	-1.05
	Chalcopyrite			-1.76
	Sphalerite			-1.45
BB 192	Pyrite	Katerina, level 3	Pyrite, little Bms	-1.17
BB 194	Pyrite	Katerina, level 3	Py-Cp-Gn-Sp-SS	-0.65
	Galena			-2.80
BB 196	Pyrite	Katerina, 1330	Py-Gn ore	-1.30
	Galena			-3.08
	Sphalerite			-2.30
OTHER NEOGENE VEINS				
BB 303	Pyrite	Secu valley	Vein at fault between ande-site & hornfels, Py-Cp-Sp	+2.18
BB 304	Pyrite	(near Gura Băii)		+3.97

Py: pyrite, Cp: chalcopyrite, Sp: sphalerite, Gn: galena, SS: Pb-sulphosalts, Bms: base metal sulphides

Within the individual ore lenses investigated (Colbu, Ivășcoia, Dealul Bucății Est, Măcârlău), the range is even narrower, with pyrite from lens having a characteristic isotopic composition (Fig. 2b). These are, as follows: Măcârlău, $n=4$, mean $+9.58 \pm 1.17 \text{ ‰ } \delta^{34}\text{S}$; D. Bucății Est $n=6$, mean $+9.95 \text{ ‰ } \delta^{34}\text{S}$; Colbu, $n=6$, mean $+9.95 \text{ ‰ } \delta^{34}\text{S}$; Colbu, $n=6$, mean $+10.84 \pm 1.25 \text{ ‰ } \delta^{34}\text{S}$, Ivășcoia, $n=7$, mean $+13.25 \text{ ‰ } \delta^{34}\text{S}$.

There is no noticeable difference in the $\delta^{34}\text{S}$ signature of pyrite from massive ore from those in disseminated ores. However, on the basis of rather limited data (only 3 disseminated ores are represented), it is impossible to state if this is statistically valid. Kräutner et al. (1992) reported a marked difference between the two ore types in the Bălan study.

Isotopic compositions of chalcopyrite and galena within the stratabound ores, are, as expected, similar to those of the pyrite. Chalcopyrite ($n=7$, $x=12.13 \pm 1.61 \text{ ‰ } \delta^{34}\text{S}$) is 0.8 ‰ heavier than pyrite in two samples and 0.3 ‰ lighter in one sample in which the minerals

coexist. Such apparent lack of equilibrium can be attributed to isotopic fractionation in chalcopyrite during metamorphic recrystallisation.

The $\delta^{34}\text{S}$ -enriched pyrite in the stratabound deposits is in sharp contrast with the isotopic composition of pyrite from hydrothermal veins of the Toroiaga complex, which are characterised by compositions closely clustered around zero permil (Table 2; Fig. 2a). Other sulphide minerals from the vein-type mineralisation have compositions close to that of pyrite and differences between co-existing sulphides conform to the general rules of S-isotope fractionation; pyrite > sphalerite > chalcopyrite > galena (Sakai, 1968). Two pyrite samples from a narrow mineralised vein outcropping on the Secu Valley had more positive $\delta^{34}\text{S}$ values ($+2.18$ and $+3.97 \text{ ‰ } \delta^{34}\text{S}$). An explanation for this discrepancy may be sought in the setting of this vein which follows a fault between intrusive and hornfelsed crystalline rocks and is thus probably younger than other veins. It is possible that the hydrothermal fluids may have become more fractionated



with respect to $\delta^{34}\text{S}$ over time.

Clots of chalcopyrite associated with quartz in the ores of Măcărâu and Ivășcoia have an isotopic signature comparable with chalcopyrite from the massive ores. Such sulphide segregations have been regarded as remobilised ores by Cook (1995). Typically, they are composed of syngenetic sulphide minerals, chiefly chalcopyrite and other ductile sulphides, which were subsequently mobilised and reconcentrated, presumably during regional metamorphism and accompanying tectonic deformation. They are emplaced within zones exhibiting substantial structural control, often cross-cutting massive pyrite which itself did not undergo mobilisation. The isotopic signature of the chalcopyrite clots strongly supports a mobilisation of pre-existing stratabound chalcopyrite.

Similarly, galena from a sample from Colbu (BBC-7), which appears as veins cutting cataclastically deformed massive pyrite has a distinctly stratiform isotopic character supportive of origin through mobilisation. This contrasts with another galena sample (BB 199) from the same deposit, filling fractures which have an isotopic signature ($+1.29\text{‰ } \delta^{34}\text{S}$), comparable with the epigenetic ores of the Toroiaga hydrothermal system. One sample from the Măcărâu deposit (BBN-1), in which massive pyrite is cut by a vein of massive galena, indicates that the galena is of much later origin ($+0.76\text{‰ } \delta^{34}\text{S}$) than the pyrite ($+8.35\text{‰ } \delta^{34}\text{S}$). Two sphalerite from mineralised veins along faults in Colbu have $\delta^{34}\text{S}$ values of $+4.37$ and $+4.52\text{‰}$. These values can be interpreted as due to the circulation of late epigenetic fluids, in the same way as the mineralised veins on the Secu Valley (above).

Discussion

The ^{34}S -rich isotopic composition of pyrite and other sulphides in the stratabound ores at Baia Borșa is in full agreement with an origin involving convective circulation of heated

seawater through the volcano-sedimentary pile and exhalation onto the seafloor surface. The data indicate that source of sulphur in the deposits is likely to be a mixture of reduced seawater sulphate and sulphide sulphur leached from the volcanic host rocks during convective circulation. The composition of the Baia Borșa sulphides is about $15 - 20\text{‰ } \delta^{34}\text{S}$ lower than estimates for Cambrian seawater.

The limited compositional range in S-isotope compositions indicates either a significant degree of metamorphic homogenisation or rather uniform physico-chemical conditions of primary exhalative deposition within each deposit. Given the weight of evidence suggesting homogenisation of isotopic abundances not to be attained during metamorphism (see above references), this can be effectively ruled out as a mechanism. The majority of patterns observed are attributed to preservation of primary patterns. The slight differences in $\delta^{34}\text{S}$ between individual massive sulphide lenses can best be attributed to localised fluctuations in these parameters (e.g. Eh, pH) as a function of local seafloor environment. Pyrite from disseminated ores within the Ivășcoia deposit contain the heaviest sulphur; this may be regarded as evidence in support of the argument that this deposit may actually represent a zone of stringer or stockwork mineralisation in an environment somewhat different to the other deposits. The Cu-rich (i.e. Zn-Pb poor) chemistry of the ores and relationships between ore and wallrock, in which one grades into the other, and the wallrock contains abundant disseminations of sulphides without sharp contacts are also possible evidence in support of such a concept. Higher fraction of ^{34}S into pyrite may take place as a response to reduced temperatures, enhanced $f\text{O}_2$ and other parameters.

The substantial differences in S-isotope composition between the syngenetic and epigenetic types of mineralisation can form the basis discrimination of discrete generations of sulphides. Although this can normally be carried



out by simple observation based on structural criteria, the method has application to discrimination of remobilised ores from those of epigenetic origin. Such segregations can often appear similar to mineralisation introduced epigenetically during Neogene times. Cook (1995) has shown how the substantial differences in the chemical composition of galena and sphalerite can also be used to distinguish syngenetic, mobilised and epigenetic ores.

The isotopic abundance in sulphides from Baia Borşa show broad similarities with those at Bălan (Kräutner et al., 1992), which would be expected given the similar age and setting of the deposits. However, the Bălan data not only show a far greater spread than those at Baia Borşa, but average values are also significantly enriched in ^{34}S . However, the majority of samples studied were examples of disseminated ore, in which ‰ $\delta^{34}\text{S}$ values are higher (e.g. for pyrite $\times 17.11$ ‰ $\delta^{34}\text{S}$). Pyrite from the massive ores have isotopic abundances identical to those at Baia Borşa ($n=2$, $\times 11.99$ ‰ $\delta^{34}\text{S}$). Kräutner et al. explained the deviation in $\delta^{34}\text{S}$ between massive and disseminated ores in terms of slow precipitation of pyrite at higher pH and lower temperature conditions, leading to higher fractionation between FeS_2 and fluid. The present author would agree with this interpretation as well as the suggestion that a greater contribution of seawater sulphate may be involved in disseminated ores precipitated at the margins of the system. Both interpretations are fully commensurate with his own observations in the Norwegian Caledonides (Cook and Hoefs, under review).

The sulphur source for the Toroiaga vein system is entirely magmatic, as would be expected. Geothermometry, based on the S-isotope compositions of pyrite-galena, pyrite-sphalerite and pyrite-chalcopryrite pairs from Toroiaga, using the calibration of Ohmoto & Rye (1979) give a wide range of temperature: py-gal $484 \pm 50^\circ$ and $416 \pm 50^\circ\text{C}$; py-sph $277 \pm 95^\circ$, $597 \pm 124^\circ\text{C}$; py-cp $522 \pm 102^\circ\text{C}$, respectively. The mean of these temperatures

is considerably higher than those suggested ($< 300^\circ\text{C}$) by the earlier fluid-inclusion studies of Borcoş (1967). It can be reasonably assumed from this spread in temperatures that all or some of the co-existing phases are not in isotopic equilibrium, although all appear to be equilibrium parageneses. Further interpretation and evaluation of a larger data set are necessary in order to suggest definitive explanations for this discrepancy.

Aknowledgements

The assistance of Radu Daniel and many other geologists from Cuart S.A., Baia Mare, during the authors, field visits to Baia Borşa is much appreciated. Prof. J. Hoefs, Göttingen is thanked for the sulphur isotope analyses. Financial support from the Deutsche Forschungsgemeinschaft for these analyses is gratefully acknowledged.

References

- Borcoş, M. (1967) Studiul geotermometric al mineralizației din masivul subvulcanic neogen Toroiaga-Tiğănuț (Maramureș). *D.S. Inst. Geol.*, 53/2, p. 219–240, București.
- , Andăr, P., Andăr, A., Berza, T. (1982) Geochimia mineralizațiilor polimetallice din cîmpul minier Toroiaga. *D.S. Inst. Geol. Geofiz.*, 67/2, p. 55–82, București.
- Cook, N.J. (1995) Polymetallic massive sulphide deposits at Baia Borşa, Romania. Extended abstract for 3rd SGA Meeting, Prague, 1995. Balkena, Rotterdam.
- , Hoefs, J. (under review) Sulphur isotope characteristics of metamorphosed volcanogenic massive sulphide deposits in the Norwegian Caledonides. *Chemical Geology*.
- Crowe, D.E. (1994) Preservation of original hydrothermal $\delta^{34}\text{S}$ values in greenschist to upper amphibolite volcanogenic massive sulfide deposits. *Geology*, 22, p. 873–876.
- Gehrisch, W., Maucher, A., Nielsen, H. (1975) Sulfur-isotope and trace element analyses from the Sulitjelma ore bodies, Northern Norway. *Mineralium Deposita*, 10, p. 57–69.



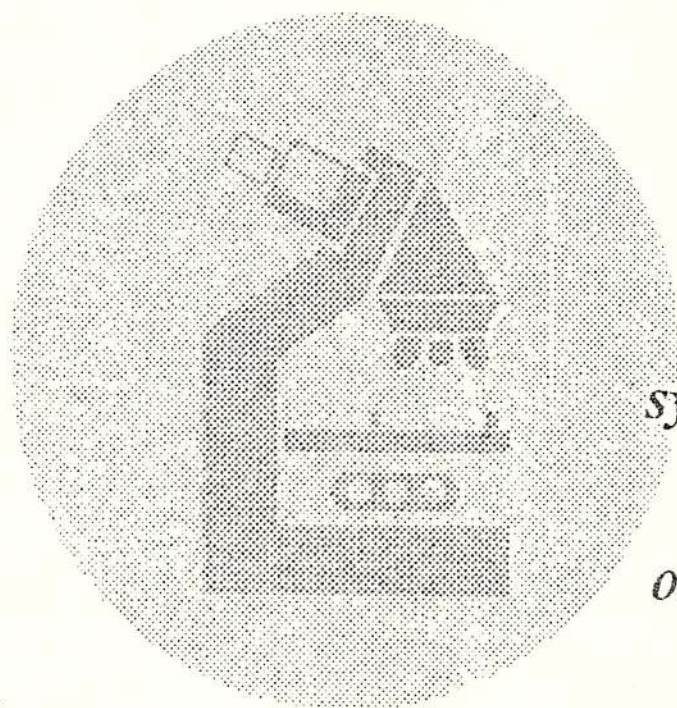
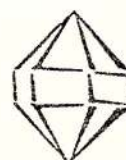
- Green, G.R., Solomon, M., Walshe, J.L. (1981) The formation of the volcanic-hosted massive sulfide deposit at Roseberry, Tasmania. *Economic Geology*, 76, p. 304-338.
- Gregory, P. W., Robinson, B. W. (1984) Sulphur isotope studies of the Mt. Molloy, Di-anne and O.K. stratiform sulphide deposits, Hodgkinson Province, North Queensland, Australia. *Mineralium Deposita*, 19, p. 36-43.
- Kräutner, H.G., Udrescu, C., Gaftoi, F. (1992) Sulfur isotopes and trace elements in copper ores and pyritic schists from Bălan (East Carpathians). *Rom. J. Mineral Deposits*, 75, p. 1-29, Bucureşti.
- Ohmoto, H., Rye, R.O. (1979) Isotopes of sulfur and carbon. In: *Geochemistry of Hydrothermal Ore Deposits* (H.J. Barnes, ed.), J. Wiley & Sons, p. 509-567, New York.
- Radu, D., Cook, N.J. (1995) The stratiform pyrite and base metal ore deposits hosted within the Tulgheş Series in the Baia Borşa area, Maramureş Mountains. In: *3rd Mineralogical Symposium, Excursion Guides* (G. Udubaşa ed.), *Rom. J. Mineralogy*, 77, Suppl. 2, p. 79-97, Bucureşti.
- Ricke, W. (1964) Präparation von Schwefeldioxyd zur massenspektrometrischen Bestimmung des Schwefel-Isotopen-Verhältnisses $^{32}\text{S}/^{34}\text{S}$ in natürlichen Schwefelverbindungen. *Z. Anal. Chem.*, 199, p. 401-413.
- Sakai, H. (1968) Isotopic properties of sulfur compounds in hydrothermal processes. *Geochemical Journal*, 2, p. 29-49.
- Seccombe, P.K., Spry, P.G., Both, R.A., Jones, M.T., Schiller, J.C. (1985) Base metal mineralization in the Kanmantoo Group, South Australia: A regional sulfur isotope study. *Economic Geology*, 80, p. 1824-1841.
- Szoke, A., Steclaci, L. (1962) Regiunea Toroiaga - Baia Borşa. *Studiu Geologic, Petrografic, Mineralogic şi Geochimic*. Editura Academiei Republicii Populare Române, 240p., Bucureşti.
- von Gehlen, K., Nielsen, H., Chunnett, I., Rozendaal, A. (1983) Sulphur isotopes in metamorphosed Precambrian Fe-Pb-Zn-Cu sulphides and barite at Aggeneys and Gamsberg, South Africa. *Mineralogical Magazine*, 47, p. 481-486.
- Willan, R.C.R., Coleman, M.L. (1983) Sulfur isotope study of the Aberfeldy barite, zinc, lead deposit and minor sulfide mineralization in the Dalradian metamorphic terrain, Scotland. *Economic Geology*, 78, p. 1619-1656.
- Zincenco, D. (1971) Stratigrafia seriei de Tulgheş în Bazinul Văilor Cislă şi Vaser (Versantul Stîng) - Maramureş. *Stud. Cerc. Geol., Geof., Geogr., seria Geologie*, 16, p. 387-396, Bucureşti.
- , Andăr, P., Andăr, A., Volanschi, E. (1973) Studiul geochimic al mineralizaţiilor stratiforme de sulfuri polimetalice din zăcămintul Burloia - Carpaţii Orientali. *Stud. Cerc. Geol. Geof. Geogr., Seria Geologie*, 18/1, 41-65, Bucureşti.

Received: November, 1995



SECOND CIRCULAR

April 1997



4th

symposium

on

MINERALOGY

3 - 8 October 1997

Iasi, Romania

Organised by:

Mineralogical Society of Romania

Geological Institute of Romania

University 'Al. I. Cuza', Iasi

Geomold S.A, Campulung Moldovenesc



Institutul Geologic al României



GEOETHERMOBAROMETRY OF METAPELITIC ROCKS FROM THE WESTERN PART OF THE PRELUCA CRYSTALLINE COMPLEX, MARAMUREŞ

Daniel M. RADU

S.C. CUART S.A., Str. Victoriei 146, RO-4800 Baia Mare, Romania

Andreas MAIS, Nigel J. COOK

Mineralogisches Institut der Universität Würzburg, Am Hubland, D-97074 Würzburg, Germany



Key words: Preluca Crystalline Complex. Micaschists. Geothermobarometry. Garnet. Staurolite. Biotite. Muscovite. Chlorite. Kyanite.

Abstract: The Preluca Massif is an island of Upper Precambrian crystalline rocks within Upper Cretaceous – Sarmatian sedimentary rocks in NW Transylvania. In the western part of the massif, a series of micaschist characterised by the paragenesis garnet-biotite-staurolite-muscovite-quartz is the dominant lithology. Electron probe microanalyses of garnet, biotite, staurolite, muscovite and chlorite were carried out. The results, including profiles across zoned garnet, confirm the belief that these parageneses formed as a result of prograde regional metamorphism. This paragenesis was subsequently overprinted by reactions taking place under retrograde conditions. Using the compositions of the silicate phases, it was possible to constrain the conditions of metamorphism using a variety of geothermometric techniques. Garnet-biotite and garnet-staurolite pairs gave temperature estimates between 520 and 530° C. The program THERMOCALC 1.1 gave values of $600 \pm 65^\circ$ C for the garnet-biotite-staurolite-muscovite assemblage. Pressures are constrained at 8 ± 0.5 kbar using the garnet-rutile-aluminosilicate-ilmenite-quartz (GRAIL) geobarometer. These T and P estimates are interpreted to correspond to conditions of peak metamorphism. Garnet-chlorite geothermometry suggested temperatures of about 480° C for the retrograde event (520 – 525° C using THERMOCALC). Such estimates are consistent with the stability fields of the component minerals and correspond to the staurolite zone of the amphibolite facies. No evidence for differences in peak metamorphic conditions between the various samples in the investigated part of the Preluca complex were identified.

Introduction

The Preluca Massif, situated about 30 km south of Baia Mare, is the largest of several Upper Precambrian crystalline windows

within Upper Cretaceous – Sarmatian sedimentary rocks (Fig. 1). The complex is some 140 km² in area and forms a horst structure, in which the dominant tectonic element is the Preluca Fault, situated on the north-



ern margin. The metamorphic units are represented by orthogneisses, micaceous quartzites and micaschists, with amphibolites, amphibole gneisses, pyroxenites, black quartzites and leptinites. Crystalline lime- and dolostones occur in the core of an anticline structure in the central part of the massif. Amphibolites are abundant in the western half of the Preluca massif. The complex is host to the large Mn-Fe deposit of Răzoare (Kalmar & Lelkes-Felvari, 1991; Udubaşa et al., in press). An improved understanding of the metamorphic evolution of host lithologies is crucial for the interpretation of the genetic history of the deposit.

Stratigraphic investigations (Balintoni, 1982) showed that the Massif consists of four formations: the Răzoare (Lower Terrigene) Formation, the Măgureni Carbonate Formation, the Preluca Nouă Formation (including amphibolites, paragneisses, amphibolite gneisses, pyroxenites, leptinites, black quartzites as well as the dominant garnet-micaschists, and the Valea Cavnicului (Upper Terrigene) Formation. Kalmar (1994a) also divided the massif into four formations, in which the Răzoare Formation was renamed the Răzoare Gneiss Formation, the Valea Cavnicului Formation is included in the Preluca Nouă Formation, and only a small part of the Preluca Nouă Formation (*sensu* Balintoni, 1982) is considered to belong to the Țicău Formation (Fig. 1). All display evidence of amphibolite facies metamorphism of Barrovian type. Kalmar (1994a) concluded this to correspond to the Hercynian orogenesis. Pb-Pb dating on the Răzoare gneisses gave 1300 ± 300 Ma, suggesting an earlier metamorphism in the Middle Algonkian. Subsequent overprinting at greenschist facies is evident. K-Ar dating of micas and amphiboles gave ages of 84 to 110 Ma and can be correlated with Middle Cretaceous Alpine orogenesis. Cocis et al. (1995) have recently summarised previous studies within the Preluca Massif.

In the extreme western part of the massif

(Fig. 1), the Upper Terrigene (Valea Cavnicului or Țicău) Formation is represented by a series of rocks in which micaschists are the predominant lithology. These units are characterised by the mineral paragenesis garnet-staurolite-biotite-muscovite-quartz. Kyanite and chloritoid appear sporadically, and together with retrograde chlorite define the units mineralogically. This paper addresses the metamorphic evolution of the micaschists and phase relationships between minerals, as determined from preliminary studies on micaschists samples from the Grajdului Valley (PM-1, -2). These data are augmented by additional data on micaschists samples from the Lăpuș gorge (PM-64), an outcrop near the Răzoare mine (PM-8b) and from a locality northwest of the mine (PM-58), shown on Figure 1. Determination of mineral compositions by electron probe microanalysis has permitted the application of various geothermometric techniques, in an attempt to deduce at least part of the metamorphic evolution of the investigated part of the massif.

Petrography

The micaschists are characterised by porphyroblastic garnet and staurolite, both ranging in size from 2 to 20 mm in diameter, within a matrix composed of biotite, muscovite, plagioclase feldspar (An_{20-27}) and quartz (Pl., Fig. a). Inclusions of muscovite, biotite, plagioclase, rutile, ilmenite, staurolite, kyanite are widespread in the poikiloblastic varieties. Chlorite overgrows the garnet rims at the expense of biotite. Kyanite is restricted to a small number of thin section and is only rarely observed in hand specimen. More common is a fine-grained kyanite. In some samples, fibrous sillimanite is observed to overgrow kyanite (Pl., Fig. b). Accessory minerals are tourmaline, apatite, rutile and ilmenite. Chloritoid has not been observed in samples from Preluca, but is observed in sections from the Țicău



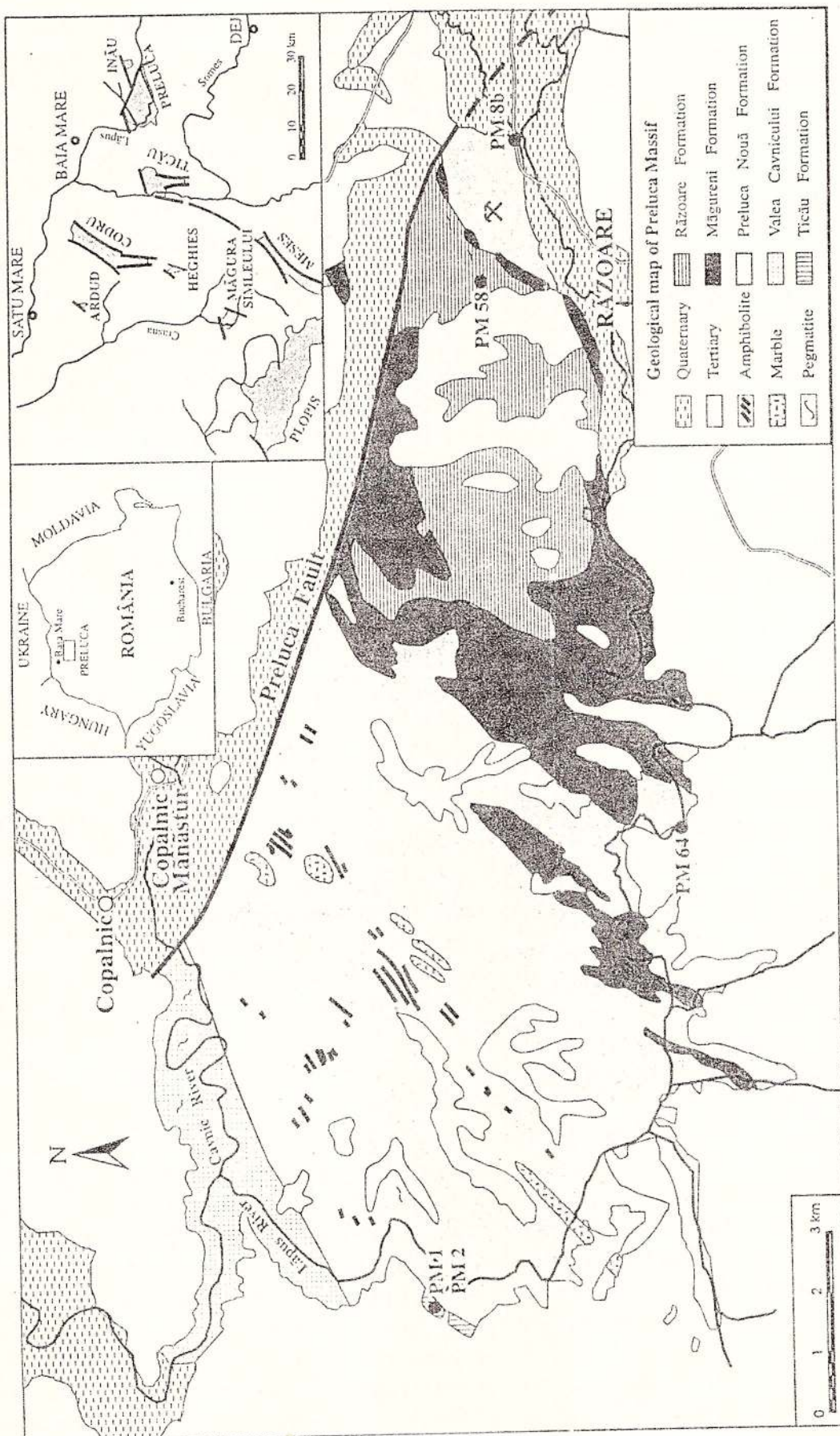


Fig. 1 –Geological sketch map of the western part of the Preluca Massif, indicating the location of samples. Inset shows the location of the Preluca Massif and other crystalline islands in NW Romania.

massif to the west. Further details of petrography, together with whole-rock geochemical data on relevant micaschists, have been given by Mais (1996).

Analytical Methods

All electron probe microanalyses were carried out on the CAMECA SX-50 instrument in Würzburg. Natural mineral standards were used. Elements not reported in the table were not detected. A beam current of 15 nA and an accelerating voltage of 15 kV were used. At least six analyses were carried out on each mineral grain and several grains from each sample were analysed to assess compositional homogeneity. Profile scans were carried out on zoned minerals, using a spacing of 200 μm throughout.

Mineral Compositions

Garnet

Microprobe analyses revealed comparable patterns in all analysed grains, although the extent of zoning is more extensive in some grains compared to others. A homogeneous core is surrounded by a zoned region, in which the proportions of almandine and pyrope increase and spessartine and grossular decrease, towards a plateau-like rim, in which the grossular and spessartine components are close to zero. A decrease in $\text{Fe}/(\text{Fe}+\text{Mg})$ from core to rim from 0.95 to approx. 0.80 is noted. Composition evolution (Table 1, Fig. 2) can be correlated to an increase in the proportions of molecular almandine and pyrope (Alm, Py) contents during garnet growth, in equilibrium with staurolite, followed by a decrease in Alm and Py as the garnet begins to react, suggesting resorption of garnet under retrograde conditions.

Spessartine and grossular components behave antipathetically to Alm and Py. The

low Mn contents in the garnet rims may suggest that the retrograde effects were limited, although bulk compositions may have also played a role. The relatively high Ca contents in the garnet cores and near absence of other Ca minerals in the micaschists suggest that Ca was preferentially partitioned into the garnet lattice at the onset of regional metamorphism.

Staurolite

All analysed staurolite grains had similar compositions (Table 1). Profiles across staurolites revealed no zonation, which is interpreted as indicating staurolite growth to have taken place during only a single event, under conditions close to peak metamorphism. Contents of Mn, Ti and Zr are low but detectable, consistent with comparable metamorphic assemblages.

Biotite

Analysed biotite compositions (Table 1) varied little between samples. Octahedral Al contents were around 0.9 atoms p.f.u. and $\text{Mg}/(\text{Mg}+\text{Fe})$ ratios were about 0.5. When plotted on the ideal biotite plane, they cluster in the field characterising muscovite-bearing pelitic schists metamorphosed at amphibolite facies. Using the compositional variation in biotite as a function of metamorphic grade after Guidotti (1984), the analysed biotites correspond to the lower and upper staurolite zone (IV-V).

Muscovite

Only a single white mica was identified. Composition variation is limited (Table 1), characterised by Si contents of 6.0 to 6.2 atoms p.f.u., enhanced Na (up to 40 mol. % paragonite), $\text{Mg}/(\text{Mg}+\text{Fe})$ ratios of 0.4 to 0.6 and low Ca contents (Figs. 3a and b). The high paragonite and low celadonite content can be correlated with continuous reactions between muscovite and co-existing phases during prograde metamorphism. Many of these reactions



involve a Tschermak exchange between muscovite and coexisting minerals, leading to progressive enrichment in Na (Guidotti, 1984).

Chlorite

Compositions of the retrograde chlorite, occurring on the margins of porphyroblastic

Table 1
Representative mineral compositions in cations per mineral formula

Garnet normalized to 24 O atoms				
sample	PM-1(core)	PM-1(rim)	PM-2(core)	PM-2(rim)
Si	5.863	5.866	5.905	5.861
Al	4.062	4.058	4.012	4.060
Mg	0.400	0.870	0.439	0.678
Fe ²⁺	5.008	5.042	5.053	5.237
Fe ³⁺	0.113	0.119	0.103	0.123
Mn	0.209	0.010	0.103	0.010
Ca	0.385	0.078	0.407	0.080
Oxide sum	99.87	99.97	100.06	100.23
Fe/(Fe+Mg)	0.93	0.85	0.92	0.89

Staurolite normalized to 23 O atoms			Biotite normalized to 22 O atoms		
sample	PM-1	PM-2	sample	PM-1	PM-2
Si	3.807	3.794	Si	5.422	5.394
Al	8.846	8.881	Al	3.439	3.471
Ti	0.060	0.069	Ti	0.168	0.170
Mg	0.347	0.315	Mg	2.517	2.368
Fe ²⁺	1.590	1.581	Fe ²⁺	2.296	2.45
Mn	0.003	0.003	Mn	0.002	0.001
Zn	0.058	0.053	Ca	n.d.	0.001
Oxide sum	97.53	97.27	Na	0.197	0.116
Fe/(Fe+Mg)	0.82	0.83	K	1.587	1.553
			Oxide sum	94.38	94.36
			Fe/(Fe+Mg)	0.477	0.509

Muscovite normalized to 22 O atoms			Chlorite normalized to 28 O atoms	
sample	PM-1	PM-2	sample	PM-1
Si	6.100	6.049	Si	5.240
Al	5.696	5.754	Al	5.614
Ti	0.029	0.030	Ti	0.015
Mg	0.103	0.152	Mg	4.452
Fe ²⁺	0.097	0.104	Fe ²⁺	4.513
Mn	0.001	0.001	Fe ³⁺	0.065
Ca	n.d.	n.d.	Mn	0.006
Ba	0.008	0.008	Ca	0.008
Na	0.497	0.545	Na	0.029
K	1.366	1.346	K	0.037
Oxide sum	95.69	94.87	Oxide sum	87.28
Fe/(Fe+Mg)	0.39	0.41	Fe/(Fe+Mg)	0.503



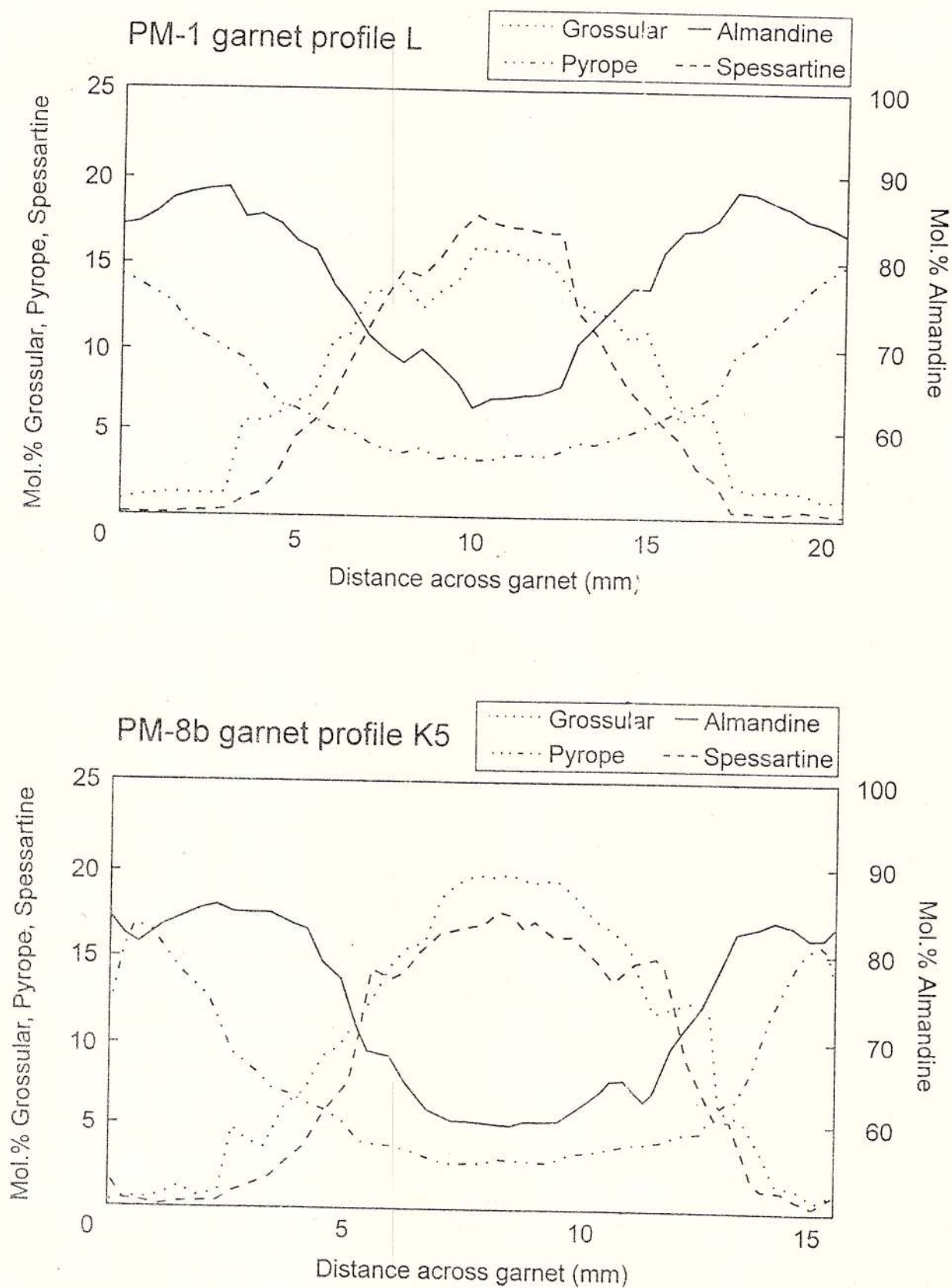


Fig. 2 – Representative profiles across zoned garnet in samples PM-1 and PM-8b.

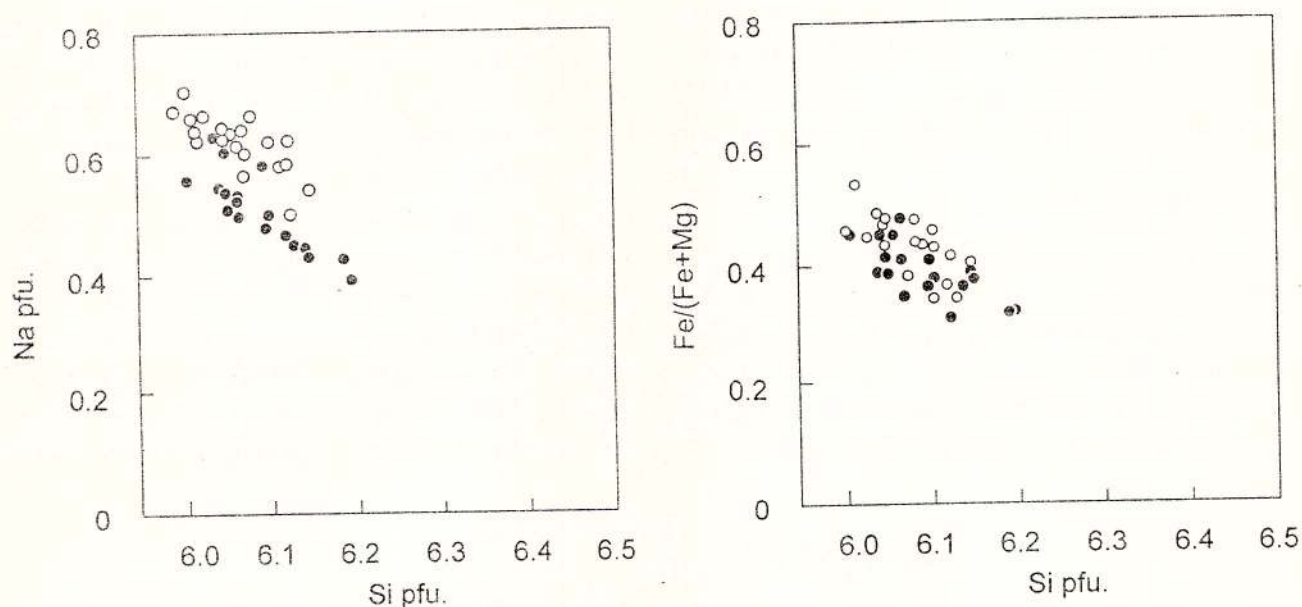


Fig. 3 - Variation in muscovite composition in analysed micaschists. a) Diagram of Si (atoms p.f.u.) vs Fe/(Fe+Mg) (atom. props.). b) Diagram of Si vs Na (both atoms p.f.u.), showing the relatively high paragonite content of the muscovites. Filled circles: samples PM1, PM2. Open circles: sample PM-8b.

Table 2
Geothermometric calculations

Sample	PM-1	PM-2	PM-64	PM-50	PM-58
(i) Conventional geothermometers at P (est.) = 5 kbar					
garnet + biotite (Perchuk & Lavrenta, 1983)	522 ± 16° C	529 ± 7° C	588 ± 18° C	565 ± 20° C	581 ± 18° C
garnet + staurolite (Hodges & Spear, 1982)	531 ± 11° C	533 ± 9° C			
garnet + chlorite (Ghent et al., 1987)	480 ± 13° C				
(ii) THERMOCALC 1.1 (Powell & Holland, 1988) at P(est.) = 6 kbar					
Prograde assemblage	600 ± 65°	603 ± 64° C			
Retrograde assemblage	523 ± 20°	520 ± 19° C			
(iv) Pressure estimates					
GRAIL geobarometer (Bohlen et al., 1983; Berman, 1988)			7.6 ± 0.3 kb	7.0 ± 0.3 kb	6.5 ± 0.3 kb

garnet (Table 1) plot in the field of Ferri-dolite, using the $Al^{(iv)}-Fe^{(vi)}$ diagram of Töger (1967). The high Fe contents may be correlated with chlorite formation after garnet.

Geothermobarometry

Using the compositions of the silicate phases described above, a number of geothermometric techniques were applied. Only the compositions of co-existing equilibrium assemblages were used. Results are summarised in Table 2, and plotted on P-T diagram in Figure 4.

ternally consistent thermodynamic data sets. These differences are not considered to be statistically significant in view of the relatively large errors associated with such methods.

Estimates of metamorphic pressure are permitted by the assemblage garnet-rutile-aluminosilicate-ilmenite-quartz, the GRAIL geobarometer (Bohlen et al., 1983; Berman, 1988). Estimates of 6 to 8 ± 0.5 kbar were obtained. The estimates of peak metamorphism of $530-600^\circ\text{C}$ and $6-8$ kbar are consistent with the stability fields of component minerals and

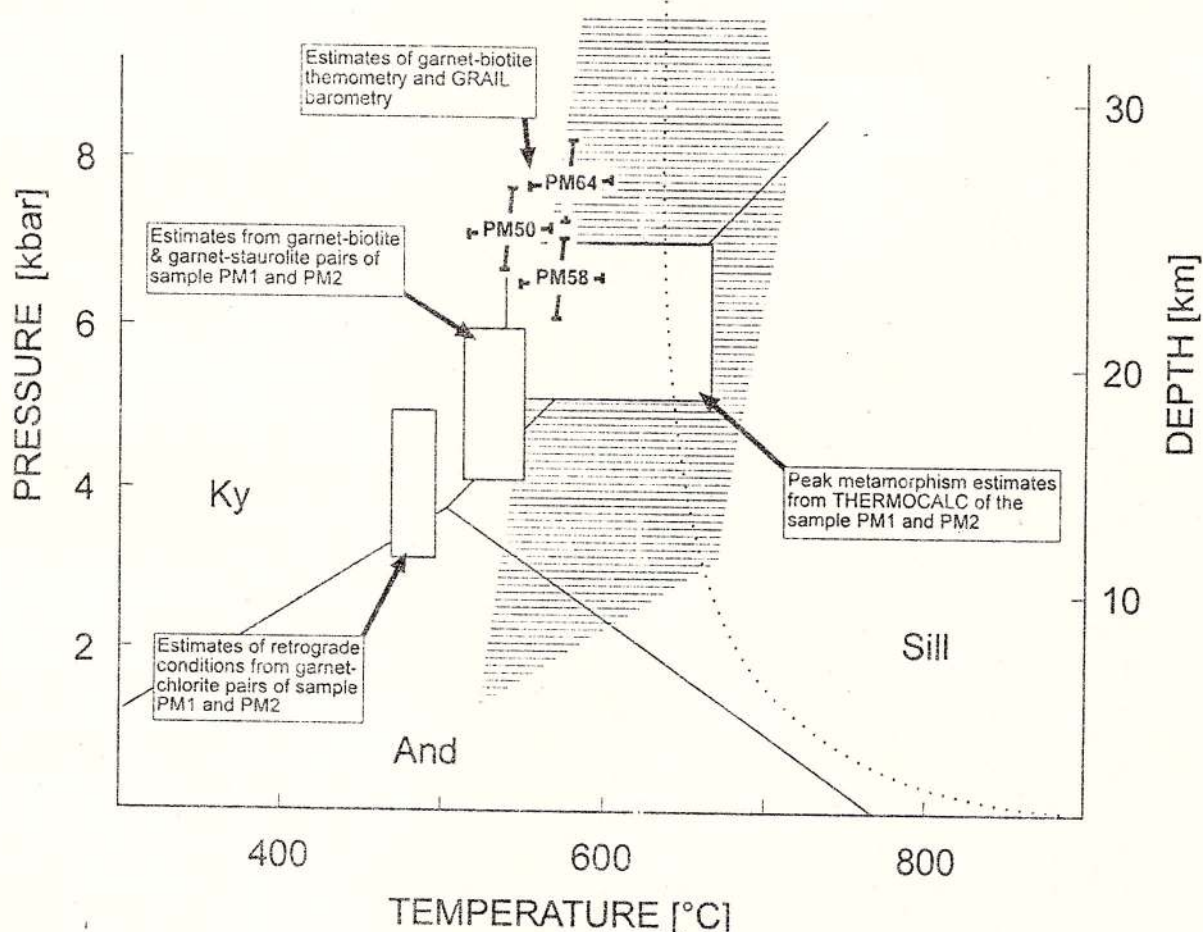


Fig. 4 – P-T diagram indicating the results of the geothermometric calculations. Boxes indicate the results of geothermobarometry on samples PM-1 and PM-2. The crosses indicate estimates, with errors, from samples PM-8b, PM-58 and PM-64. The shaded area shows the stability field of quartz-staurolite paragenesis.

Slightly different estimates are obtained from different methods and as a result of using different calibrations, notably between individual mineral pairs and that calculated using in-

correspond to the staurolite isograd of the amphibolite facies. No evidence of metamorphism at higher grades was recognised.

Temperature from samples which contained



kyanite gave comparable results, which approach 600° C for the peak metamorphism at pressures of 7 kbar. The presence of kyanite in some of the studied mica schists indicates that P-T conditions were above the kyanite-sillimanite invariant curve (Fig. 4) and are concordant with observation of an initial granitic migmatitic melting. The erratic occurrence of both kyanite and chloritoid is attributed to bulk rock chemistry. The observed fibroblastic sillimanite overgrowing kyanite permit reconstruction of the post-peak path, which most probably ran in a clockwise direction.

The co-existence of staurolite with quartz places indicates that the peak metamorphic conditions lay below the stability field of this paragenesis, indicated on Figure 4, after Bucher and Frey (1994). The staurolite+quartz assemblage was formed by the reactions:

muscovite + chlorite = staurolite + biotite + quartz + vapour

chlorite + muscovite + garnet = staurolite + biotite + quartz + vapour

Comparable temperature estimates were reported by Kalmar and Kovacs-Palfy (1993), using mineral assemblages from the Țicău Hill. They concluded the main metamorphic event to have taken place at temperatures between 500 and 600° C and pressures of 4 to 6 kbar, with the greenschists facies retrograde event corresponding to about 450° C and 3 kbar. More recently, Kalmar (1994b) obtained the following results for the Măgura Șimleului crystalline island using garnet-biotite methods: 542–579° C and 6.3–7.2 kbar (peak metamorphism); 505–535° C and 5.6–6.5 kbar (retrograde event).

Taken together with the data of Kalmar and Kovacs-Palfy (1993) and Kalmar (1994b), the results given in the present paper confirm that most of the crystalline islands in NW Transylvania underwent metamorphism under similar P–T conditions and show comparable paths of metamorphic evolution.

Continuing work is aimed at defining the relative roles of bulk rock composition and variable metamorphic conditions in determining paragenetic relationships within the micaschists, amphibolites and other rock units in the massif. Additionally, it is hoped to assess if reconstruction of local metamorphic evolutionary patterns and/or evidence for polyphase metamorphism is permitted through additional geothermobarometric and fluid-inclusion data.

References

- Balintoni, I. (1982) Formațiuni cristaline. Report, Arch. I.G.R., București.
- Berman, R.G. (1988) Internally-consistent thermodynamic data for minerals in the system $K_2O-Na_2O-CaO-MgO-FeO-Fe_2O_3-Al_2O_3-TiO_2-H_2O-CO_2$. *Journal Petrology*, 29, p. 445–522.
- Boheler, S.R., Wall, V.J., Boettcher, A.L. (1983) Experimental investigations and geological applications of equilibria in the system $FeO-TiO_2-Al_2O_3-SiO_2-H_2O$. *Am. Miner.*, 68, p. 1049–1058, Washington.
- Bucher, K., Frey, M. (1994) Petrogenesis of metamorphic rocks. Springer, 318 p., New York.
- Cocis, D., Udubașă, G., Hârtoșanu, P., Radu, D. (1995) Excursion D. Medium grade metamorphic rocks of the Preluca massif and the Răzoare Mn-Fe deposit. In: Excursion guides, 3rd Symposium on Mineralogy, Baia Mare, August 1995. *Rom. J. Mineralogy*, 77, Suppl. 2, p. 99–112, București.
- Ghent, E.D., Stout, M.Z., Black, P.M., Brothers, R.N. (1987) Chloritoid-bearing rocks associated with blueschists and eclogites, northern New Caledonia. *Journal of Metamorphic Geology*, 5, p. 239–254, Great Britain.
- Guidotti, G.V. (1984) Micas in Metamorphic Rocks. In: Micas (S.W. Bailey ed.). *Mineralogical Society of America Reviews in Mineralogy*, 13, p. 357–467.
- Hodges, K.V., Spear, F.S. (1984) Geothermometry, geobarometry and the Al_2SiO_5 triple



- point at Mt. Moosilauke, New Hampshire. *Am. Miner.*, 67, p. 1118-1134, Washington.
- Kalmar, J. (1972)** Stratigrafia terenurilor metamorfice și sedimentare din insulele cristaline Inău, Preluca și Țicău. Unpub. Ph.D. Thesis, Faculty of Geology and Geophysics, 409 p., București.
- (1994a) Studii mineralogice și petrologice pe rocile metamorfice din insulele cristaline din NV Transilvaniei. Summary of the lecture for Cand. Title in Geol. Sci., Budapest.
 - (1994b) Garnet-biotite in metamorphic rocks of the Măgura Șimleului, Romania. Jubilee Geological Symposium, Cluj-Napoca, Abstract Vol. p. 37-38.
 - , Kovacs-Palfy, P. (1993) Geological structure of Țicău Hill (NW Transilvania). Third Geological Symposium, Baia Mare, Abstract Vol., p. 24-25.
 - , Leikes-Felvari, G. (1991) The metamorphic Mn ore deposit of Răzoare (Romania) and its geological setting. *Mineralia Slovaca*, 23 p. 413-419.
- Mais, A. (1996)** Geochemische Untersuchungen an metamorphen Gesteinen der kristallinen Komplexe Preluca, Inău und Țicău, NW-Rumänien. Unpub. Diploma Thesis, Mineralogisches Institut der Universität Würzburg, 100p.
- Perchuk, L.L., Lavrent'eva, J.V. (1983)** Experimental investigation of exchange equilibria in the system cordierite-garnet-biotite. In: *Kinetics and Equilibria in Mineral Reactions* (ed. S.K. Saxena), Springer, p. 119-239.
- Powell, R., Holland, T.J.B. (1988)** An internally consistent thermodynamic data set with uncertainties and correlations. II. Application methods, worked examples and a computer program. *Journal of Metamorphic Geology*, 6, p. 171-204, Great Britain.
- Tröger, W.E. (1967)** Optische Bestimmung der gesteinsbildenden Minerale. Teil 2, Textband. Schweizerbart'sche Verlagsbuchhandlung, 822 p., Stuttgart.
- Udubaș, G., Hârtoșanu, P., Ilincă, G., Valdiman, S. (1997)** The regionally metamorphosed Mn-Fe deposit at Răzoare, Preluca Mts, Romania. *Rom. J. Mineral Deposits*, 77, p. 3-19, București.

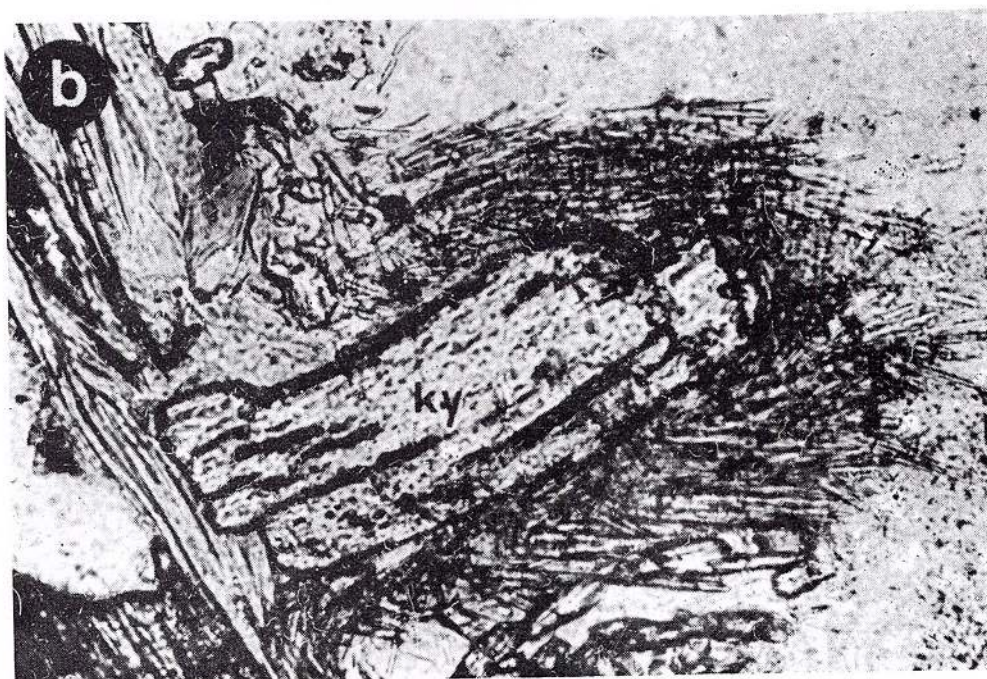
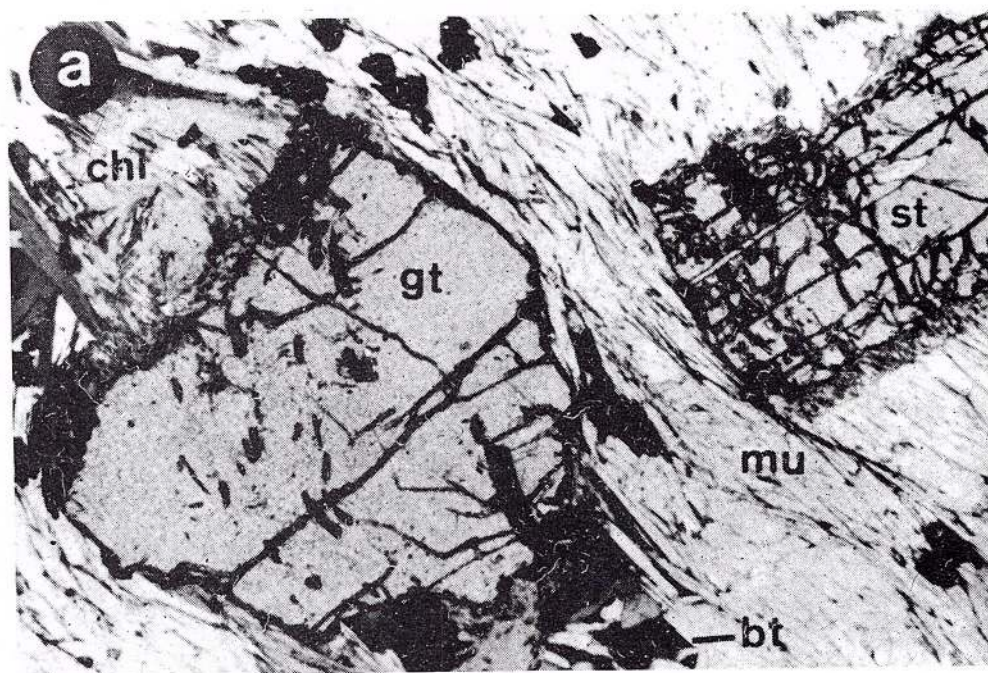
Received: April 4, 1996

Plate

Photomicrographs of micaschists in transmitted light

- a. Typical mineral paragenesis in the micaschists. gt: biotite, st: staurolite, mu: muscovite, qz: quartz, corresponding to peak metamorphic conditions, and retrograde development of chlorite (chl). Sample: PM-8b. Width of photo: 64 mm.
- b. Kyanite porphyroblast (ky) overgrown by fibrous sillimanite. Sample: PM-50. Width of photo: 480 μ m.

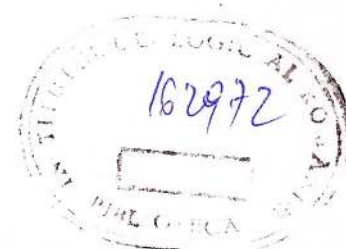




Rom. J. Mineralogy, vol. 78, București, 1997



Institutul Geologic al României



GEOCHEMICAL STUDIES OF GOLD–SILVER–TELLURIUM MINERALIZATION IN THE VICINITY OF SĂCĂRÂMB, SOUTHERN APUSENI MOUNTAINS, ROMANIA: SOME PRELIMINARY RESULTS

D.H.M. ALDERTON

Department of Geology, Royal Holloway (London University), Egham, Surrey TW20 0EX, UK

G. SIMON

Department of Geological Sciences, University of Michigan, Ann Arbor, Michigan 48109–1063, USA

M. IOAN

S.C. Prospekțiuni S.A., Str. Caransebeș nr. 1, RO–78344 București–32

I. PANAZAN, E. ORLANDEA, I. CSIBI

Minexfor S.A., Str. Minerului nr. 2, 2700 Deva, Romania



Key words: Gold–Silver–Tellurium mineralization. Geochemical studies. Major elements. X-ray fluorescence. Fluid inclusions. Stable isotopes (O,C). Radiogenic isotopes (Sr). Săcărâmb. Apuseni Mts.

Abstract: Mineralized veins in the Săcărâmb region of western Romania are hosted by Neogene hornblende (\pm quartz, biotite, pyroxene) andesites (stocks and lava flows) with a characteristic island-arc geochemistry. In the vicinity of the mineralized veins the andesites are heavily altered; zoned sericitic and argillic assemblages are the most abundant. These are associated with marked influxes of K, Rb, and CO_2 , and large losses in Na and Mg. The veins show the following mineral paragenesis: early pyrite > sphalerite and galena > sulphosalts and Au/Ag tellurides > rhodochrosite and calcite. Fluid inclusions in vein quartz hosting the mineralization are 2 phase aqueous in character. Temperatures of homogenization have a mean value around 260–300°C, and the salinity is low (less than 5 wt % NaCl equivalents). Evidence of boiling does not appear to be common. Stable isotopic analyses have produced the following results: Vein quartz $\delta^{18}\text{O} = 13.5$ to 16.5 (‰ SMOW); calcite in host andesite $\delta^{13}\text{C} = -12.3$ (‰ PDB); vein calcite and rhodochrosite $\delta^{18}\text{O} = -14.6$ to -16.5 (‰ SMOW) and $\delta^{13}\text{C} = -5$ to -7 (‰ PDB). Quartz and calcite are clearly not in isotopic equilibrium, indicating that either they were deposited at different temperatures, or from fluids with different compositions. At 300°C, fluids precipitating quartz would have an isotopic composition of $\delta^{18}\text{O} = 7$ to 9 ‰ SMOW; this value is close to a magmatic value and not indicative of major component of (unexchanged) meteoric fluids. The later carbonates appear to have been deposited from meteoric fluids. The characteristics of the mineralization, alteration, and host rocks point to an island-arc setting similar to that seen today in the epithermal gold deposits of the western Pacific region. However, the magmatic characteristics of the hydrothermal fluids, the lack of boiling phenomena, and the high temperatures, indicate that at least some parts of the mineralization are not typically epithermal, and probably formed at deeper (and therefore hotter) levels.



Introduction

The renowned gold-silver-tellurium vein deposits in the Săcărâmb region of western Romania have in the past been subjected to many detailed mineralogical studies, but relatively little is known of their genesis and evolution. A detailed, multidisciplinary, geochemical study of this mineralization is currently being undertaken with a view to determining the source of the fluids and the ore components, and the conditions of mineral formation. Hopefully the results of this study will help to establish the geological controls to the mineralization, and thus be an aid to future exploration in the region. Preliminary results of this study are presented here.

Techniques

Geochemical analyses of rocks were obtained by X-ray fluorescence using a Philips PW1400 spectrometer. Major elements were determined on fusion discs and trace elements were determined on pressed powder pellets using the major element concentrations for calculation of matrix corrections. Two-sigma precision of the trace element data is generally better than 1% or 1ppm, whichever is the higher value.

For the fluid inclusion study, samples of quartz were prepared as doubly-polished sections, approximately 300 μm in thickness. These were examined using a standard petrographic microscope. The thermometric behaviour of the fluid inclusions was studied using a Linkam TH600 microscope heating-freezing stage. This was calibrated using synthetic H_2O - and CO_2 -rich fluid inclusions in quartz; the accuracy of the resulting data is approximately 0.1°C at temperatures below -20°C , $\pm 0.2^\circ\text{C}$ in the range -20 to $+50^\circ\text{C}$, and $\pm 0.5^\circ\text{C}$ in the range $+50$ to 220°C . Salinities of the fluids were derived from the last melting temperatures of ice, using the relationship of

Bodnar (1993).

Minerals were analysed for O- and C-isotopic compositions in the stable isotope laboratories at Royal Holloway. CO_2 was released from carbonates by reaction with phosphoric acid. Quartz was mixed with an olivine standard and attacked by laser fluorination using ClF_3 , and the oxygen released converted to CO_2 by reaction with heated graphite (Mattey & Macpherson, 1993). Isotope ratios were measured on a VG Prism mass spectrometer. Mineral-water oxygen isotopic fractionation relationships were obtained from Zheng (1993) for quartz, and the compilation of Longstaffe (1989) for carbonates.

For the radiogenic isotope analysis, the Sr was separated by conventional ion exchange techniques and analysed on a VG354 mass spectrometer using multidynamic data collection.

Local Geology

The host rocks to the mineralized veins in the Săcărâmb region are dominated by Neogene andesites and lesser amounts of Neogene sediments (sandstones and shales) (Ghițulescu, Socolescu, 1941). The local basement rocks consist of Mesozoic sediments and ophiolitic assemblages. Previous geological studies have interpreted the igneous rocks as intrusive stocks and extrusive lava flows, but in the field it is often difficult to determine their precise form, particularly where the rocks have been altered close to the mineralized vein. All the igneous host rocks are porphyritic and contain abundant hornblende; in addition they may contain phenocrysts of quartz and biotite and relict pyroxene. Some are hydrothermally altered, with the production of sericite, calcite, epidote, and Fe oxides; these *propylitic* alteration assemblages occur in large (at least several tens of meters) zones around the mineralized regions.

The chemical composition of the unaltered



igneous rocks (Table) is typically calc-alkaline and places them in the field of normal andesites. Their low Nb contents on a 'spidergram' highlight their island arc affinity (see Figure 1; see Thirlwall, 1988).

Mineralization and Hydrothermal Alteration

More than 230 mineralized veins have been found in the deposit; these occur in an area of c. 1 km² and to a depth of about 600 m. The length of the veins is typically about 500–600 m, with a thickness varying from a few mm to 2 m (average around 0.3 m).

Ghițulescu, Socolescu (1941) and Udubașa et al. (1992) have summarised the dominant mineral assemblages in the main vein groups of Săcărâmb:

- quartz, rhodochrosite, nagyagite, and abundant base metal sulphides, in the Magdalena vein group (SE part of the mine).
- quartz, barite, rhodochrosite, sylvanite, krennerite, gold, and subordinate base metal sulphides, in the Longin vein group (NE part of the mine).
- calcite, petzite, and alabandite, in the Nepomuc vein group (SW part of the mine).

Many parts of the mine are now no longer accessible but access is still possible in the upper levels via some exploration or old, maintained levels, and many of the important veins can still be examined here. The mineralized veins sampled during this study show the following paragenesis:

Early pyrite > sphalerite and galena (with quartz) > sulphosalts and Au/Ag tellurides > calcite and rhodochrosite. Open-space, cavity fill textures are common, but evidence of extensive reactivation and brecciation of the veins are also apparent.

Adjacent to the mineralized veins the host rocks are intensely altered. These wallrock alteration selvages are typically up to 1–2 m in width, and are dominated by sericitic assemblages containing quartz, sericite, calcite, and

pyrite. Argillic assemblages containing kaolinite are also present, but appear to be of restricted occurrence. It has been suggested that the mine lies in a large adularia-sericite zone of alteration, but as yet this study has not been able to confirm the presence of adularia. The sericitic assemblages are dominated by enrichments in K, Rb, and CO₂, and marked depletions in Na, Mg, and Sr (due to replacement of plagioclase, biotite, and amphibole by sericitic white mica and calcite (Fig. 1).

Fluid Inclusions

Fluid inclusions occur sporadically in the mineralized vein quartz; some samples appear devoid of fluid inclusions whilst others contain large populations. The inclusions often occur in planes which are parallel to the crystallographic zones of the host quartz, and thus a clear primary origin shows. Most of the quartz samples so far studied have been associated with the early (precious metal) base phase of mineralization.

The fluid inclusions are two-phase and aqueous in character. On heating, homogenization is almost always to the liquid phase. T_h values have a mean value of 260–300°C. The salinity of these fluids is low (1–4 wt% NaCl equivalents). Evidence of boiling is present in some samples but tends to be rare.

Stable Isotopes (O,C)

The isotopic analysis of quartz and carbonates from the mineralized area has given the following results;

Vein quartz $\delta^{18}\text{O} = 13.5$ to 16.0 ‰ SMOW
 Vein calcite, Mn-calcite, and rhodochrosite $\delta^{18}\text{O} = -14.6$ to -16.5 ‰ SMOW, $\delta^{13}\text{C} = -5.4$ to -7.2 ‰ PDB.

Calcite in host andesite $\delta^{13}\text{C} = -12.3$ ‰ PDB.

Quartz and calcite in the veins are clearly not in isotopic equilibrium, indicating that



Table

Chemical composition of andesites and ore alteration assemblage from Săcărâmb. Major elements in weight %, 'trace' constituents in ppm (both on a volatile-free basis). Total Fe expressed as Fe_2O_3 . Analyses were carried out by XRF on ignited samples; also given is the 'loss on ignition' value (LOI) ($=\text{H}_2\text{O}$, CO_2 , S, etc.). Localities: (Fresh andesites) RO94-1 Calvaria; RO94-2 Zuckerhut; RO94-3 Sarcau; RO94-4 Haitau; (Sericitic assemblage) RO94-16 Karthause vein, IPRG level.

	RO94-1	RO94-2	RO94-3	RO94-4	RO94-16
SiO_2	59.70	62.15	59.60	61.88	60.18
Al_2O_3	17.55	17.34	17.22	17.37	16.33
Fe_2O_3	6.12	5.29	5.80	5.35	4.54
MgO	2.48	2.48	2.87	2.55	1.12
CaO	7.43	6.16	6.43	5.24	7.22
Na_2O	3.20	3.52	3.32	3.62	0.00
K_2O	1.90	1.86	1.79	2.31	5.89
TiO_2	0.71	0.55	0.59	0.55	0.58
MnO	0.16	0.14	0.11	0.16	0.48
P_2O_5	0.36	0.22	0.22	0.25	0.24
Total	99.61	99.71	97.95	99.28	96.53
LOI	2.10	0.84	1.18	1.23	7.71
Ni	9.1	11.3	9.9	9.2	16.8
Cr	23.1	23.8	18.6	28.0	26.0
V	147.0	141.0	168.9	151.8	126.4
Sc	21.4	17.4	22.3	19.0	13.7
Cu	33.2	45.9	57.0	45.5	27.8
Zn	77.8	62.9	61.7	62.9	78.0
Ga	17.9	17.1	16.6	16.5	16.5
Pb	22.0	21.0	17.7	18.6	40.8
Sr	909.1	801.5	799.1	756.4	344.9
Rb	45.3	52.2	47.3	78.8	209.2
Ba	1143.0	1440.5	1353.5	1506.4	2788.4
Zr	146.3	103.8	96.1	104.4	142.1
Nb	11.3	10.9	9.9	10.6	13.1
Th	9.9	8.7	8.0	8.8	12.0
Y	28.5	17.3	20.1	19.3	20.8
La	37.3	26.5	28.2	27.6	39.4
Ce	71.2	51.3	52.9	51.0	80.7
Nd	29.1	21.0	22.2	21.2	30.7



SPIDERGRAM - SĂCĂRÂMB

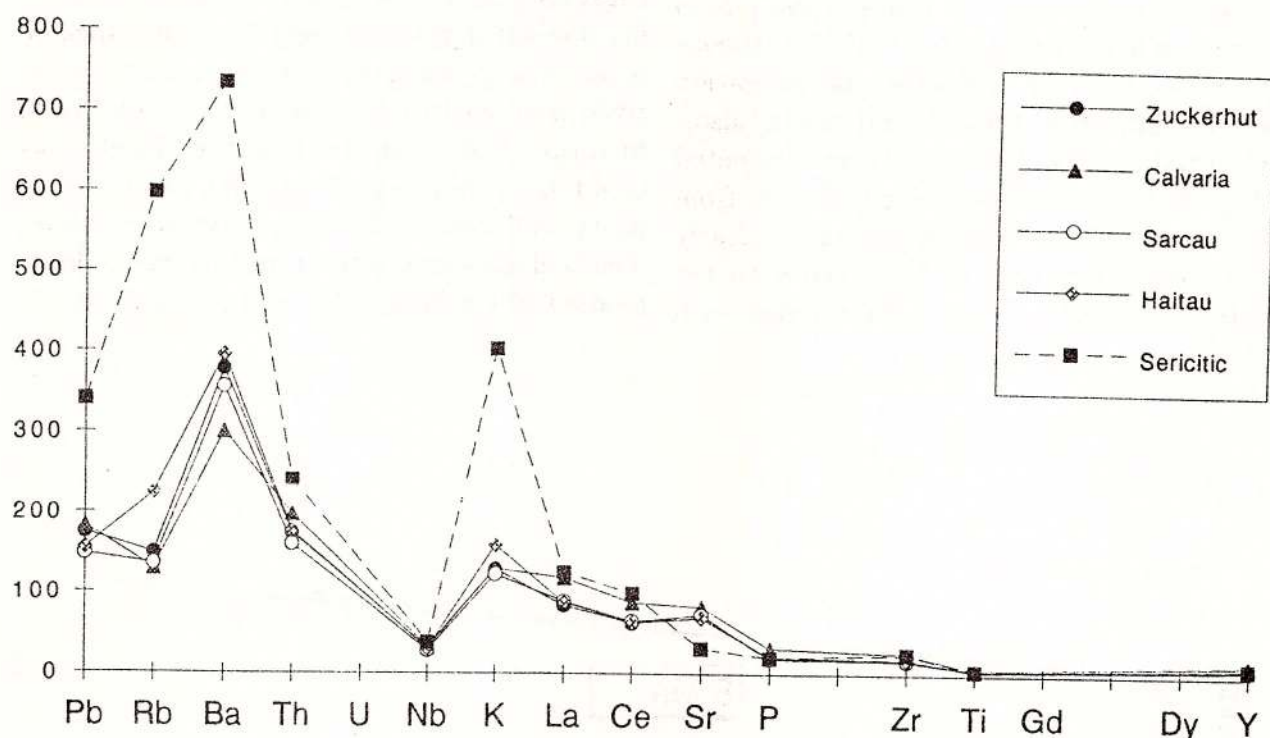


Fig. 1 - Chondrite-normalized incompatible element diagram for fresh and hydrothermally altered andesites from Săcărâmb. Normalising factors after Sun (1980)

they were either deposited at different temperatures or from fluids with different isotopic compositions. This is not entirely unexpected considering that the calcite occurs much later in the paragenesis than does the quartz.

At 300°C the fluids precipitating quartz would have had isotopic compositions of $\delta^{18}\text{O} = 7$ to 9 ‰ SMOW; this value is close to a hypothetical magmatic value and is not indicative of a major component of (unexchanged) meteoric fluids being present in the hydrothermal system (Sheppard, 1986). In contrast, waters which precipitated the calcite would have had much lower $\delta^{18}\text{O}$ contents, e.g. +4.1‰ SMOW at 300°C, 0‰ at 200°C, and -2.9‰ at 140°C. This data suggests that the later calcite was formed from fluids with a high component

of low ^{18}O water, possibly a meteoric fluid of local derivation. The quartz and calcite analyses thus indicate that there was a change in hydrothermal fluid source during the vein paragenesis, possibly from an early phase dominated by magmatic waters, to a later phase dominated by meteoric waters.

The $\delta^{13}\text{C}$ composition of the carbonate is not particularly informative because the large uncertainties in temperature and unknown pH and $f\text{O}_2$ do not allow a calculation of the fluid composition (Ohmoto, 1972). However, the values are typical of magmatic-hosted vein carbonates associated with epithermal precious metal mineralization (Field and Fikarek, 1985).

Radiogenic Isotopes (Sr)

The main aim of the Sr isotopic study is to provide an accurate date for both the igneous host rocks and the hydrothermal alteration (and by inference the mineralization also). The initial results of this study are presented in Figure 2. The altered (sericitic) rocks from the margins of the mineralized veins clearly show their enrichment in Rb relative to the unaltered andesites. The limited data avail-

pretation). The isochron for the unaltered andesites intersects at a $^{87}\text{Sr}/^{86}\text{Sr}$ value of about 0.7045, whilst the isochron for the alteration intersects at a value of about 0.7060. This suggests that the Sr in the hydrothermal fluids was not derived entirely from the volcanic rocks; a large component must have been derived from rocks with a relatively high initial Sr ratio. (Note that the Sr in the altered rocks could be a mixture of original Sr from the hosts, and new Sr introduced to the system. The hydrothermal alteration involved a large amount of leaching of Sr, and the amount of

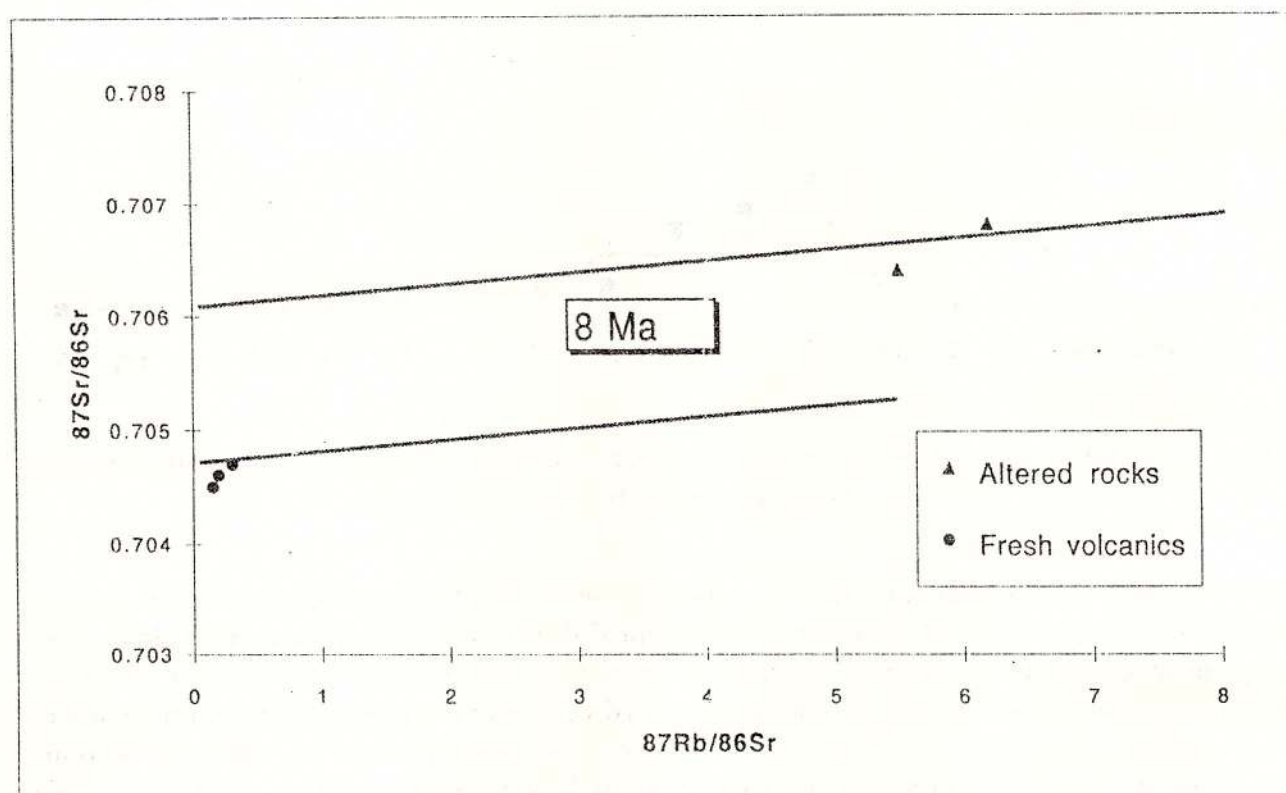


Fig. 2 – Rb–Sr isotopic diagram showing analyses of fresh and hydrothermally altered andesites from Săcărâmb. Note that the 8my isochron represents an arbitrary choice based on stratigraphic information, and is not derived from this data.

able also indicate a different source for the Sr in both rock types. If an approximate age of 8 My is assumed for the igneous rocks and the mineralization then the resulting isochrons intersect the Sr ratio axis at quite different values. (Note that the exact age chosen for these isochrons does not affect the following inter-

added Sr must have been small in volume. Thus the Sr ratio of the 'new' Sr could be much larger). The most likely rock types with this Sr ratio would be those with a continental character. If so, this would mean that the hydrothermal fluids had interacted with, and leached Sr from, basement rocks with a continental char-

acter surrounding the volcanic centres. Presumably this means that the gold and other metals in the mineralized veins could also have been derived from continental basement.

Conclusions

The characteristics of the mineralization (polymetallic, polyphase, Au-Ag-Te in veins), hydrothermal alteration (sericitic +/- argillic), and host rocks (andesites) point to a classic epithermal precious metal, island-arc type of setting, as seen today in the western Pacific region (Mitchell, 1992).

Although there are some hydrothermal breccias in close association with the mineralized veins, there is a general lack of features indicative of high level boiling. This observation coupled with the relatively high temperatures and stable isotopic signatures of the (earlier) mineralization are perhaps indicative of a relatively deep-seated (rather than true epithermal) environment. It could be that the mineralization at Săcărâmb contains more of a magmatic component than is usually envisaged for a typical epithermal vein system. The later carbonate-rich paragenesis seems more typical of a large low T, meteoric input to the system.

Acknowledgements

This work is funded by a grant from the natural Environmental research Council (NERC) of the UK. Chemical and isotopic analysis has been assisted by Giz Marriner, Joel Baker, Liz Whittaker and Wayne Cox.

References

- Bodnar, R.J. (1993) Revised equation and table for determining the freezing point depression of H₂O-NaCl solutions. *Geochim. Cosmochim. Acta*, 57, p. 683-684.
- Field, C.V., Ficarek, R.H. (1985) Light stable-isotope systematics in the epithermal environment. In: Berger, B.R. & Bethke, P.M. (eds.) *Geology and Geochemistry of epithermal system, Reviews in Economic Geology*, 2, p. 99-128.
- Ghițulescu, T.P., Socolescu, M. (1941) *Edude géologique et minière des Monts Métalifères. An. Inst. Geol. Roum.*, XXI, p. 181-463, Bucharest.
- Longstaffe, F.J. (1989) Stable isotopes as traces in clastic diagenesis, In: Hutcheon, I.E (ed.), *Short course in burial diagenesis, Mineralogical Society of Canada Short course Series*, 15, p. 201-277.
- Mattey, D., Mac Pherson, C. (1993) High-precision oxygen isotope microanalysis of ferromagnesian minerals by laser-fluorination. *Chem. Geol.*, 105, p. 305-318.
- Mitchell, A.H.G. (1992) Andesitic arcs, epithermal gold and porphyry-type mineralization in the western Pacific and eastern Europe. *Trans. Instn. Min. Metall.*, 101, p. B125-B138.
- Ohmoto, H. (1972) Systematics of sulfur and carbon isotopes in hydrothermal ore deposits. *Econ. Geol.*, 67, p. 551-578.
- Roedder, E. (1984) Fluid inclusions. *Reviews in Mineralogy*, 12, Mineralogical Society of America.
- Sheppard, S.M.F. (1986) Characterization and isotopic variations in natural waters. In: J.W. Valley, H.P. Taylor & J.R. O'Neil (eds), *Stable isotope in high temperature geological processes, Reviews in Mineralogy*, 16, Mineralogical Society of America, p. 165-180.
- Sun, S-S. (1980) Lead isotopic study of young volcanic rocks from mid-ocean ridges, ocean island and island arcs. *Phil. Trans. Roy. Soc. London*, A297, p. 409-445.



- Thirlwall, M.F. (1988)** Wenlock to mid-Devonian volcanism of the Caledonian-Appalachian orogen. In: Harris, A.L. & Fettes, D.J. (eds) *The Caledonian-Appalachian Orogen, Geol. Soc. London Special Publication*, 38, p. 415-428.
- Udubaşa, G., Strusievicz, R.O., Dafin, E., Verdes, G. (1992)** Mineral occurrences in the Metaliferi Mts, Romania (Excursion Guide). *Rom. Journ. Mineral.*, 75 (2), 35 p.
- Zheng, Y-F. (1993)** Calculation of oxygen isotope fractionation in anhydrous silicate minerals. *Geochim. Cosmochim. Acta*, 57, p. 1079-1091.

Received: December, 1995



MINERALOGIE DES TOPAZES DU HOGGAR CENTRAL

Youcef CHALAL et Mokrane KESRAOUI

Université des Sciences et de la Technologie Houari Boumediene.

Institut des Sciences de la Terre. BP 32 El Alia. 16111

Key words: Topaz. Analysis. RX. Central Hoggar.

Abstract: Mineralogy of topaz from central Hoggar. A specific magmatism in central Hoggar is represented by an albite and topaz granite belonging to the late Panafrikan blocks. This particular granite, unknown in the Panafrikan belt, has a constant mineralogical composition: quartz, albite, potash feldspar, lithian micas (zinnwaldite) and topaz. The presence of this last mineral marks both the aluminous character and the abundance of fluorine of this formation. The mineralogical study (chemistry and structure) allows to make a distinction between the magmatic topaz and the hydrothermal one. The magmatic topaz links to the albite and topaz granite in both regions of Tamanrasset and Laouni. The hydrothermal topaz is from the veins of quartz-greisen, greisen and Hananere' samples pegmatite. The minerals were analysed with an electron microprobe. The results show clearly that the magmatic topaz has a high silica and fluorine content as compared to the hydrothermal one which is richer in the alumina. The powder X-ray diffraction shows that the hydrothermal topaz is relatively richer in OH-ion than in fluorine.

1 – Structural formula of magmatic topaz: $\text{Al}_{1.98}\text{SiO}_4\cdot\text{F}_{2.01}$

2 – Structural formula of hydrothermal topaz: $\text{Al}_{2.12}\text{Si}_{1.05}\text{O}_4(\text{O}_{0.61}\text{F}_{1.39})$

Introduction

Le magmatisme spécifique conduisant à la formation d'un granite albite-topaze connu dans le Hoggar central est intimement associé aux gisements et aux indices Sn-W.

L'une des principales caractéristiques de ce type de magmatisme consiste en l'expression minéralogique remarquable sous forme de

topaze en particulier, de son caractère alumineux et fluoré; d'où l'intérêt de l'étude de ce minéral-clé.

Localisation des gisements étudiés

Les échantillons étudiés ont été prélevés de deux régions (Fig. 1):



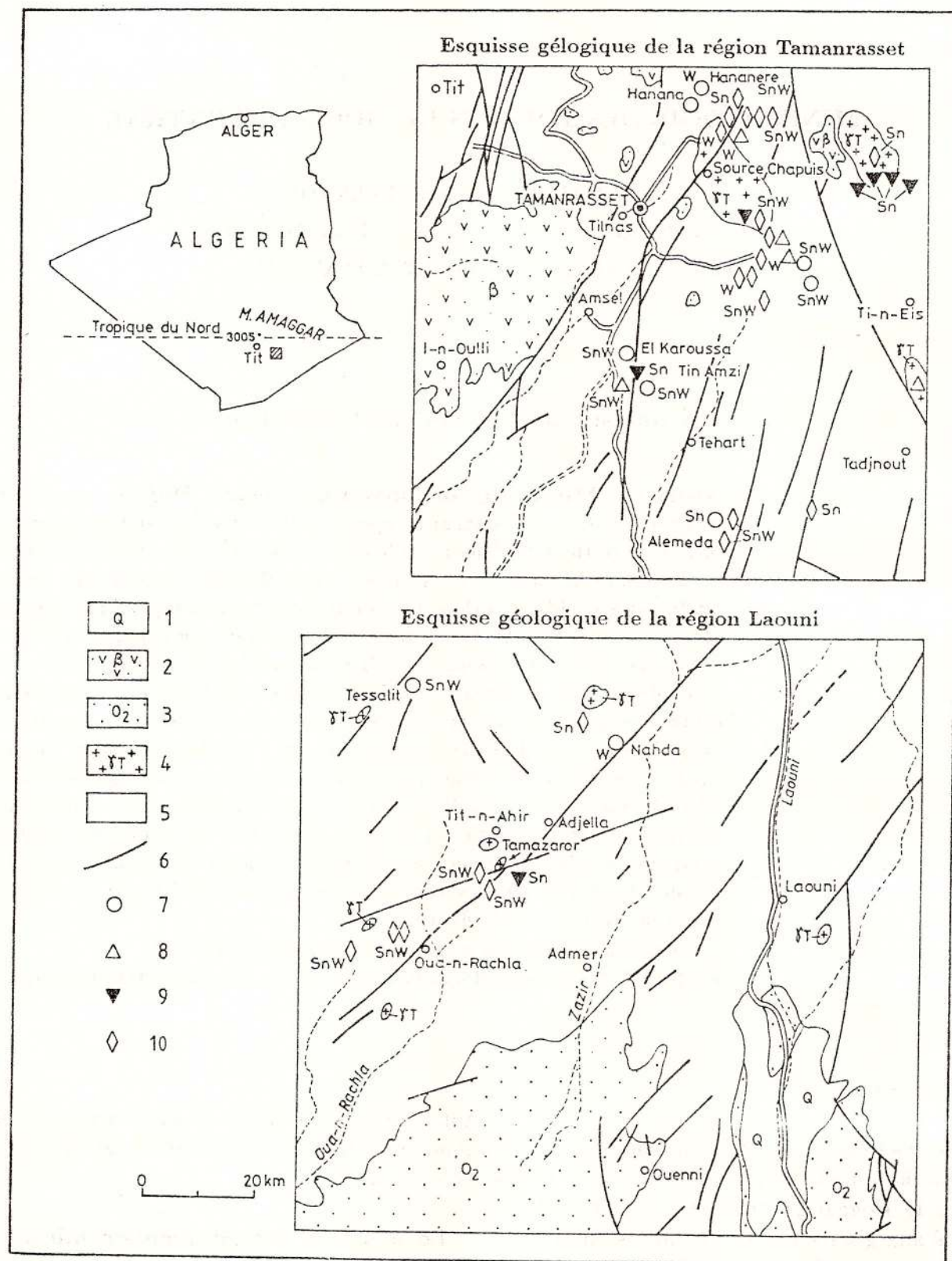


Fig. 1 - Localisation des régions étudiées (Extraits de la carte géologique et gîtologique du Hoggar, au 1:1.000.000, Alger, 1977). Légende: 1, Quaternaire; 2, Basaltes et volcanisme récent; 3, Ordovicien; 4, Granites "Taourirt" (Eocambrien); 5, Roches métamorphiques protérozoïques; 6, Failles. Gisements et indices Sn W: 7, Filon; 8, Stratiform; 9, Placer; 10, Indeterminée.

1. Région de Tamarasset

Cette région est caractérisée par de nombreux pointements de granites albite-topaz intrus dans des formations granito-gneissiques régionales (Tessibent, Hanana, Hananère....) ou les dans massifs panafricains tardifs d'Intounine et de d'Aheleheg. Le gisement de Tin Amzi (M. Kesraoui, 1990) à l'étain-wolfram nous a fourni l'essentiel des échantillons de topazes étudiés.

2. Région de Laouni

Cette région comporte plusieurs massifs granitiques panafricains tardifs. Les échantillons proviennent du massif de Tamazaror, caractérisé par la présence d'un granite à l'albite-topaze associé à des filons minéralisés en wolframite (Y. Chalal 1989).

Minéralogie des topazes

Dans la région de Tin Amzi, la topaze des granites et microgranites n'est observable qu'au microscope. Dans les granites, ses sections montrent des formes prismatiques avec des clivages nets selon 001; dans les microgranites elles sont plus trapues et la forme la plus fréquente est celle d'un losange (Fig. 2a).

Au niveau du granite de Tamazaror, la topaze se présente sous forme de grands cristaux automorphes aux clivage nets et montrant des inclusions d'albite (Fig. 3).

Dans les greisens de Tin Amzi, associés aux filons de quartz minéralisés, les topazes sont plus accessibles à l'étude macroscopique. Elles sont presque isométriques avec une prépondérance des formes {021} et {102} (Fig. 2b), s'agglutinant en agrégats, transformant le greisen en véritable topazite. Les topazes de couleur blanche sont translucides; elles montrent des formes allongées pouvant atteindre 3 à 4 cm de longueur. De tels cristaux ont été décrits dans les pegmatites d'Oural, où ils sont associés à des lépidolites (Talansev, 1988).

Dans les filons de quartz à wolframite, les

cristaux de topaze ont un faciès prismatique allongé; leurs dimensions peuvent atteindre 1 cm. Les formes observées dans ces cristaux sont {110}, {101}, et {021}. On note un développement assez important des faces (120) et (021) (Fig. 2c). Les faces du prisme {110} sont finement striées en longuer. Ces cristaux sont transparents et ont des couleurs variant du jaune clair au brun-rougeâtre; cette couleur serait due à des hydroxydes de fer s'infiltrant entre les zones de croissance et les cassures. G.G.Lemlein (1973) explique les variations de couleur des topazes par la présence de traces de fer à différents états de valence.

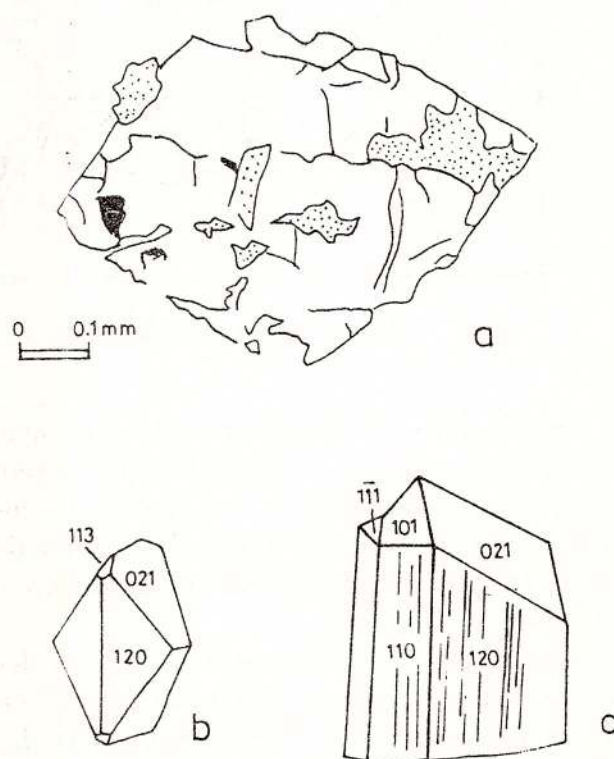


Fig. 2 - a, Aspect macroscopique d'une topaze de Tin Amzi; formes de cristaux: b, dans la topazite; c, dans les filons de quartz à wolframite.

Analyses des topazes à la microsonde

La topaze constitue une solution solide entre le terme fluor-topaze ($\text{Al}_2 \text{SiO}_4 \text{F}_2$) et le terme tout à fait théorique hydroxyle-topaze ($\text{Al}_2 \text{SiO}_4 \text{OH}_2$).

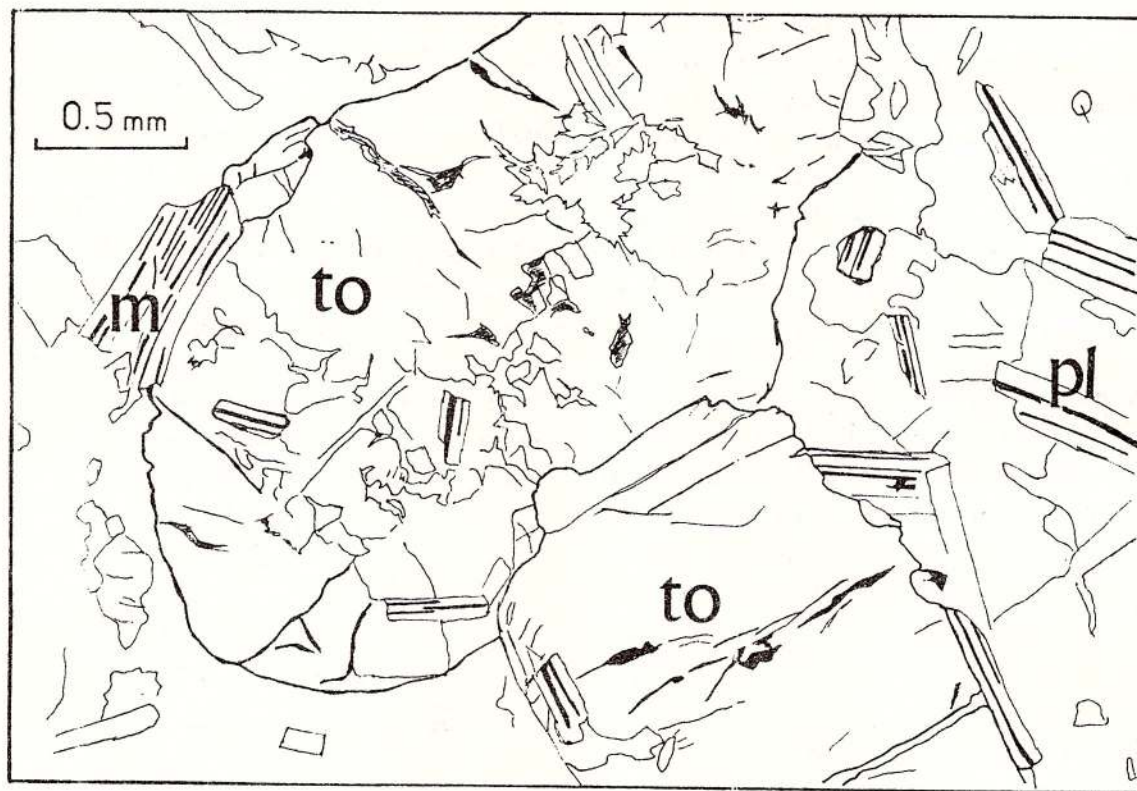


Fig. 3 – Inclusions d'albite dans les cristaux de topaze du granite de Tamazaror.

Les résultats de l'analyse à la microsonde (Tab. 1) montrent une tendance à une légère surestimation des teneurs en fluor, en raison de l'inexistence des standards (l'atome de fluor étant trop léger pour être déterminé avec précision).

Nous distinguons clairement les topazes des granites par leur enrichissement relatif en fluor. Les topazes des filons de quartz et des greisens montrent par contre un déficit en fluor et un enrichissement en alumine.

Étude aux rayons X

Deux échantillons de topaze prélevés d'une topazite (Xoc e TOH1) et deux autres d'un filon de quartz minéralisé (HT1) et de la

pegmatite de Hananere (HR33, HR61, HR62) ont été soumis à l'analyse par diffraction des RX. Les paramètres de maille ont été calculés par la méthode des moindres carrés, en introduisant les angles 2θ de toutes les réflexions obtenues dans les diffractogrammes. Les résultats obtenus sont donnés dans le tableau 2 ci-joint:

Le paramètre b_0 est le plus sensible au remplacement du Fluor par l'hydroxyle OH dans la structure de la topaze. En effet, les atomes de Fluor remplacés par OH se situent dans les couches perpendiculaires à b_0 (P.E. Rosenberg, 1967). Le paramètre b_0 est d'environ 8.789 Å pour les fluor-topazes, il augmente progressivement avec la substitution du F^- par OH^- .

Tableau 1
Résultats des analyses à la microsonde

Tin Amzi								
Lame Point	T2H 1	TH2 2	TH2 3	Z223 1	Z223 2	Z223 3	Z141 1	Z141 2
SiO ₂	31.73	32.13	31.50	31.87	32.42	32.35	32.83	32.67
TiO ₂	0.01	0.01	0.07	0	0	0	0	0.07
Al ₂ O ₃	52.05	52.30	52.50	55.52	56.02	55.91	56.35	55.97
FeO	0	0	0.01	0	0.06	0.05	0.05	0.10
MnO	0.04	0	0	0	0	0.01	0.02	0.08
CaO	0.02	0	0	0.05	0.01	0	0.02	0
Na ₂ O	0.02	0.04	0.04	0.01	0.05	0	0.02	0
K ₂ O	0	0	0.01	0.02	0	0.01	0.01	0
F	21.12	19.66	19.86	14.08	15.68	14.63	13.81	13.34
Total	104.99	104.14	103.99	101.55	104.24	102.96	103.11	102.23
F=O	8.89	8.27	8.36	5.93	6.60	6.16	5.81	5.61
Total	96.10	95.87	95.63	95.62	97.64	96.80	97.30	96.62
FORMULE STRUCTURALE SUR LA BASE DE 6 OXYGENES								
Points	1	2	3	4	5	6	7	8
Si	1.003	1.025	1.006	1.03	1.02	1.038	1.04	1.05
Al	1.938	1.969	1.977	2.11	2.13	2.10	2.12	2.09
F	2.10	1.98	2.00	1.39	1.36	1.53	1.44	1.57
OH		0.02		0.61	0.64	0.47	0.66	0.33
Lame GQS 10 (Tamazaror)								
Points	1	2	3	4	5	6	7	
SiO ₂	31.60	31.48	28.73	31.93	32.09	32.02	32.03	
Al ₂ O ₃	55.55	55.23	52.90	53.83	52.92	53.04	53.15	
F	20.51	21.27	21.39	19.12	20.76	19.57	19.13	
FORMULE STRUCTURALE SUR LA BASE DE 6 OXYGENES								
Si	0.97	0.97	1.00	0.97	1.01	1.02	1.02	
AlVI	2.00	2.00	2.00	2.00	1.96	1.98	1.99	
AlIV	0.02	—	—	0.01	—	—	—	
F	1.99	2.05	1.90	2.05	2.06	1.96	1.92	

Conclusions générales

Cette étude confirme l'existence de deux populations de topazes génétiquement différentes grâce à des critères cristallographiques et chimiques;

1 – Magmatique, elle est associée au granite et/ou microgranite avec une grande richesse en Fluor: $\text{Al}_{1.98}\text{Si}_{1.00}\text{O}_4\text{F}_{2.01}$

2 – Hydrothermale, associée aux filons de quartz ou de greisens, plus riche en hydroxyle-topaze: $\text{Al}_{2.12}\text{Si}_{1.05}\text{O}_4\cdot(\text{OH}_{0.61}\text{F}_{1.39})$



Tableau 2

No. éch.	a _o	b _o	c _o	V(Å ³)	Origine
XOC	*4.650	8.793	8.385	342.84	Topazite Tin Amzi
TOH1	*4.653	8.794	8.380	342.90	Topazite Tin Amzi
HT1	*4.644	8.792	8.377	341.25	Filon de Quartz Tin Amzi
HR33	+4.647	8.802	8.391	343.22	Pegmatite Hananère
HR61	+4.649	8.798	8.391	343.21	- // -
HR62	+4.656	8.804	8.405	344.53	- // -
1	4.652	8.789	8.394	343.20	Durango, Mexique
2	4.648	8.792	8.394	342.99	Topaz Mountain Utah
3	4.662	8.826	8.399	345.59	Minas Gerais, Brasil

1,2,3 Données Rosenberg (1967).

* Kesraoui (1990).

+ Rabehi et Sabaou (1992).

Les cristaux de topazes d'origine hydrothermale sont plus allongés que les cristaux magmatiques plutôt prismatiques, ce qui correspond à la variation du paramètre b_o très sensible au remplacement du fluor par OH dans la structure de la topaze.

Bibliographie

- Armines, A. (1977) Inventaire et prospective des ressources minérales du Hoggar. Inédit. 294 p.
- Chalal, Y. (1989) Contribution à l'étude de la greisénisation et des minéralisations wolframifères associées au granite de Tamazaror et de Sédis. Laoni, Hoggar central. Caractérisations pétrologiques, géochimiques et implications métallogéniques. Thèse de magister. IST/USTHB. Alger, 252 p.
- Kesraoui, M. (1990) Greisénisation et minéralisations W-Sn à Tin Amzi (Hoggar central). Typomorphisme des minéraux et aspects géochimiques. Thèse de magister. IST/USTHB. Alger, 180 p.
- Lemlein, G.G. (1993) Couleurs des cristaux de topazes. In: Morphologie et genèse des cristaux. Ed. Nauka. Moscou, p. 141-149, Russe.
- Rabehi, S., Sabaou, N. (1992) La coupole greisée de Hananère (Hoggar Central). Pegmatite et minéralisations W-Sn associées. *Mémoire d'ingénieur IST/USTHB*, 143 p.
- Rosenberg, P.E. (1967) Variations in the unit-cell dimensions of topaz and their significance. *Am. Mineralogist*, 52, p. 1890-1895.
- Talantsev, A.S. (1988) Les pegmatites d'Oural. Ed. Nauka, Moscou. 143 p. En russe.

Received: August, 1995



ON THE PRESENCE OF GARNET-SPESSARTINE-CALDERITE IN THE DELINEȘTI Mn-Fe DEPOSIT

Paulina HÂRTOPANU, Iulian VANGHELIE, Gabriela STELEA

Institutul Geologic al României. Str. Caransebeș nr.1, 79678, București, 32

Erna CĂLINESCU "Prospecțiuni" S.A. Str. Caransebeș nr. 1, 78344 București, 32



Key words: Semenik Mts. Delinești ore deposit. Spessartine-calderite. Hybrid ore (koduritic). Hematite. Acmite. Rhodochrosite. Pyrophanite. IR spectrum. Rx analysis. Gonditic ore. Metasomatoses. Oxidation. Static metamorphism.

Abstract: Spessartine-calderite occurs in the hybrid ore of the Delinești Mn-Fe ore deposit as small, idiomorphic (newly formed), clean, transparent grains, yellow or orange in colour. It is associated with sodic alkali pyroxenes of acmite type, pyrophanite, hematite, magnetite, phlogopite, rhodonite, pyroxmangite, rhodochrosite, dannemorite. The values of the parameter a_0 for garnets from the ore are ranging from 11.6 to 11.794 Å, intermediary values between spessartine and calderite. The chemical analyses pointed out the presence in these garnets of a relatively high percentage in Fe_2O_3 versus FeO . The main components of garnet in the Delinești ore deposit are, as follows: 40-45 % spessartine, 45-60 % calderite, 0-5 % almandine. Spessartine-calderite was formed by metasomatoses with Fe^{3+} on the metamorphic older spessartine garnet.

The Delinești Mn-Fe ore deposit constituted the object of several mineralogical studies since the last century. Detailed studies were carried out by Savu (1962) who determined several minerals, such as: rhodonite, pyroxmangite, dannemorite, spessartine, tephroite, schefferite, pistacite, magnetite, jacobsonite, rhodochrosite, piemontite, orthite. Giuscă (1962) identified in the Delinești ore deposit stilpnomelane associated with rhodochrosite and in the secondary ore he mentioned canbyite and its amorphous equivalent hisingerite. Dimitrescu and Popa (1973) pointed out in this ore deposit some parageneses and the

crystallochemical formulae of the main minerals consisting the ore deposit: rhodonite-pyroxmangite, rhodochrosite, dannemorite, spessartine. The petrographic, mineralogical and genetic data on the Delinești Mn-Fe ore deposit were completed by the researches effected by Hârtopanu and Hârtopanu (1993).

Several new minerals for this ore deposit were identified by the authors of this paper: alkali pyroxene of acmite type, spessartine-calderite, yellow alkali amphiboles, phlogopite, Mn-humite, pyrophanite, monasite, Mn-anthophyllite, Mn-tremolite, Mn-actinolite, huebnerite, dravite, barium feldspars, albite,



microcline, maganite, manganiferous calcite, baryte, bemmentite, neotocite, manganiferous brown chlorite, manganiferous stilpomelane, grossular. The last one is found in the adjacent rock.

Spessartine-calderite and calderite are known in few occurrences in the world because of the restrictive formation conditions. Among them mention should be made of: (1) calderite in the Wabush metamorphosed ferri-ferrous formation in SW Labrador where it is found in association with acmite, rhodonite, hematite (Klein, 1966); (2) in the state of Michigan (USA) in the Champion mine in the Marquette ore deposit in association with rhodochrosite, kutnohorite, spessartine, jacobsonite, dannemorite (Babcock, 1968); (3) in the Otjosundu ore deposit in Namibia, SW Africa, in association with braunite, jacobsonite, "vredenburgite", rhodonite, diopside, acmite, bixbyite, hyalophane, celsian, quartz (De Villiers, 1951). In Romania spessartine-calderite was described at Dealul Negru in the Lotrului Mts, in association with braunite bixbyite (Bălan, 1978) and in the Dealul Rusului and Dadu ore deposit in the Bistrița Mts (Hârtopanu *et al.*, 1993).

The Delinești Mn-Fe ore deposit is situated in the northern part of the Semenik Mts in the Precambrian metamorphites of the Sebeș-Lotru Series metamorphosed in the almandine amphibolite facies. These rocks are penetrated by granitic acid intrusions, veins of alkali pegmatites and hydrothermal quartz – which determined a modification of the baric and thermal parameters in the manganese ore, reflected in the modification of the mineralogical composition of the ore. Thus, the Delinești ore belongs to three major types (Hârtopanu *et al.* 1993a): (1) spessartitic (=gonditic) consisting mainly of spessartine, quartz, \pm dannemorite; (2) carbonatic (=queluzitic) formed of rhodochrosite, rhodonite, pyroxmangite, \pm tephroite; (3) hybrid (=koduritic) resulting from the spessartitic and carbonatic types thermally, metaso-

matically and hydrothermally altered. These modifications are shown by the occurrence of new minerals (Hârtopanu *et al.*, 1993 b). Spessartine and spessartine-calderite are the most widely spread minerals of the ore deposit; spessartine is specific to the gonditic petrographic type, and spessartine-calderite is characteristic of the hybrid petrographic type. The major occurrences, approximately from north to south, are: Ohabîța, Valea Fierului, Tâlva Bobului, Măgura Mică, Măgura Mare, Dealul Socului and Poiana Finetului. Other Mn-Fe occurrences bearing calderite-spessartine are found at Rugi and Dealul Mare. The spessartine-calderite-bearing ore is yellow or orange in colour. Apparently the texture of the ore is massive; under the microscope the texture is banded because of the alternation between spessartine and spessartine-calderite, acmite and spessartine-calderite, hematite and spessartine-calderite, etc. The wiping of the banding was observed in case of the spessartine-calderite association with acmite or monasite. The spessartine-calderite garnet occurs as small grains, idiomorphous, clean, transparent, yellow or orange in colour. The grains seem to be unaffected by metamorphism and penetrated by minerals previously formed: schlieren of spessartine-calderite penetrate rhodonite, pyroxmangite, phlogopite, spessartine as well as other minerals formed previously. Taking into account all these features spessartine-calderite can easily be differentiated from old spessartine garnet. This is so affected by metamorphism that the limits between the grains are no longer visible, it looking like a spessartine mass with a conchoidal breaking. The grains are broken, turbid and translucent; it is brown, locally orange, when it shows a tendency to pass to spessartine-calderite, indicated by the decrease of the FeO content and the increase of the Fe_2O_3 content.

The main associations for spessartine-calderite are, as follows: spessartine-calderite, quartz, magnetite (Pl. I, Fig. 1); spessartine-calderite, quartz, dannemorite; spessartine-



calderite, acmite, monasite, pyrophanite; spessartine-calderite, acmite, yellow alkali amphiboles, hematite (Pl.I, Fig.5); spessartine-calderite, acmite, phlogopite, microcline, albite, pyrophanite in the gonditic hybrid, and spessartine-calderite, hematite, rhodochrosite (Pl.I, Fig.2); spessartine-calderite, pyroxmangite, dannemorite, rhodochrosite; spessartine-calderite, pyroxmangite, dannemorite, rhodochrosite; spessartine-calderite, huebnerite (Pl.II, Fig.3); spessartine-calderite, rhodonite, rhodochrosite, acmite, hematite, pyrophanite, yellow alkali amphiboles in the carbonatic hybrid ore.

Rx Study of the Spessartine-Calderite

Table 1 presents the values of the primary cell parameter (a_o) for garnets from the

Table 1
Primary cell parameter (a_o) for garnets from the Delinești manganese ore

No	Sample no	$a_o(\text{\AA})$
1	Spessartine ASTM	11.60
2	D-20	11.61
3	D-48	11.62
4	D-55	11.62
5	D-75A	11.63
6	D-14A	11.65
7	D-15A	11.65
8	D-52	11.65
9	D-62A	11.65
10	D-4A a	11.65
11	D-94	11.66
11	D-8B 6	11.66
13	D-91	11.67
14	10 B 1	11.67
15	D-16A	11.68
16	D-8A a	11.69
17	D-47	11.73
18	D-90A	11.79
19	Calderite ASTM	11.82

Delinești manganese ore in comparison with the a_o parameters for spessartine (ASTM: 20992) and calderite (ASTM: 10-367).

The mathematic ratio between different values d_i , indices h_i , k_i , l_i and parameter a_o is, as follows:

$$(h_i^2 + k_i^2 + l_i^2)A = Q_i \quad (1)$$

$$\text{where } A = 1/a_o^2, \quad Q_i = 1/d_i^2$$

$$\text{and } i = 1, 2, 3, \dots, n$$

According to the least squares method the best value for coefficient A is obtained providing that:

$$\sum_{i=1}^n [(h_i^2 + k_i^2 + l_i^2)A - Q_i]^2 = \min \quad (2)$$

Condition (2) is true if the derivate of the first grade versus the coefficient A of ratio (2) is zero. Therefore:

$$\frac{\partial}{\partial A} \sum_{i=1}^n [(h_i^2 + k_i^2 + l_i^2)A - Q_i]^2 = 0$$

Effectuating the calculations, one obtains:

$$A \sum_{i=1}^n (h_i^2 + k_i^2 + l_i^2)^2 = \sum_{i=1}^n (h_i^2 + k_i^2 + l_i^2)Q_i \quad (3)$$

The solving of equation (3) in relation to A was based on our own calculation programme in BASIC system. From the value of coefficient A we calculated the value of parameter a_o :

$$a_o = \frac{1}{\sqrt{A}}$$

The values of the parameter a_o for garnets from the Delinești manganese ore studied by us are ranging from 11.61 Å to 11.79 Å, they representing intermediary values between the values of parameter a_o for spessartine and calderite.

Chemical Composition of Spessartine-Calderite

23 spessartine and spessartine-calderite samples have been analysed. The results are presented in Table 2. The quite small sizes of the garnet made impossible the complete elimination of the associated quartz, which explains the high SiO₂ percentage. The other oxides belong to the analysed mineral; in most



Table 2
Chemical composition of the Delnești spessartines and spessartine-caldarites

Sample	SiO ₂	TiO ₂	Al ₂ O ₃	Fe ₂ O ₃	FeO	MnO	MgO	CaO	K ₂ O	Na ₂ O	Oxygen correction	Total	Fe ₂ O ₃ total
D 20	47.99	0.54	15.23	2.14	6.91	21.97	0.87	1.76	0.00	0.00	2.31	99.98	9.82
D 49II	43.22	0.69	15.32	3.06	6.91	22.97	2.02	3.03	0.04	0.00	2.37	99.97	10.75
D 55	36.16	0.25	12.87	5.15	9.54	19.88	1.75	5.67	0.00	0.00	2.45	99.92	15.75
D 75a	42.83	0.17	16.09	1.77	0.00	32.57	2.03	1.63	0.16	0.03	2.28	99.72	1.77
D 14A	37.51	0.45	16.43	4.84	3.51	31.18	0.80	2.60	0.03	0.00	2.57	100.09	8.73
D 15A	36.86	0.50	16.73	3.52	0.19	33.96	1.82	4.30	0.04	0.05	2.37	100.50	3.73
D 52	35.45	0.28	17.98	6.86	2.60	32.20	0.61	3.46	0.00	0.00	-	99.56	9.75
D 62A	40.37	0.28	15.11	5.24	3.87	29.54	0.40	3.03	0.05	0.00	2.49	100.66	9.54
D 4Aa	47.44	0.70	14.40	2.85	0.00	27.03	0.97	3.42	0.13	0.32	1.88	99.99	2.84
D 94	35.10	0.21	17.13	5.31	0.16	36.11	0.68	2.59	0.04	0.00	2.52	100.01	5.48
D 8B6	43.16	0.80	13.07	5.97	0.16	27.69	1.23	5.31	0.00	0.13	1.93	99.97	6.15
D 91	35.93	0.55	17.97	4.30	0.00	32.67	1.49	4.48	0.00	0.00	2.28	99.83	4.30
10 B1	35.69	0.56	16.86	4.45	0.23	34.07	1.46	4.44	0.03	0.00	2.38	100.30	4.70
D 16A	37.21	0.60	16.51	4.87	0.17	32.66	1.41	4.38	0.03	0.05	2.28	100.34	5.06
D 8Aa	40.23	0.60	9.50	10.37	0.00	26.93	2.06	7.29	0.04	0.62	1.88	99.97	10.37
D 47	33.46	0.45	10.86	12.98	0.45	35.20	0.36	4.88	-	0.01	0.76	99.15	13.48
D 90A	41.05	0.25	6.89	14.73	0.00	25.87	1.56	6.61	0.09	0.49	1.81	99.52	14.73
D 94A	35.57	0.23	16.44	5.36	0.00	37.85	0.80	2.75	0.01	0.00	-	100.09	5.36
D 90II	43.15	0.23	7.13	14.31	0.00	23.65	2.18	6.63	0.05	0.86	1.65	100.02	14.31
D 98	35.63	0.42	15.58	7.29	1.36	34.87	0.65	3.56	0.02	0.15	-	99.96	8.80
D 63B	35.81	0.18	18.60	3.55	5.17	31.33	0.77	3.54	0.01	0.00	-	99.65	9.29
D 3	53.90	0.00	10.00	7.21	0.00	27.35	0.00	5.80	0.00	0.00	-	99.85	-
D 9	59.57	0.00	17.29	5.68	0.00M	15.68	0.00	1.30	0.00	0.00	-	99.44	-

of the analysed samples $\text{FeO} = 0$ or it occurs in very small amounts; the Al_2O_3 percentage is low but not absent and consequently we call it spessartine-calderite, not calderite. It is to note the calcium presence and the lack or presence in small amounts of magnesium. When the FeO content is higher than the Fe_2O_3 content it is a spessartine-calderite, as in case of samples D-55, D-56A, D-63B. In order to avoid any doubt as regards the accuracy of the results obtained using the classical method of chemical analysis all the samples presented in Table 2 have been reanalysed using the plasma spectrometer. The results are similar. On the basis of the chemical analyses the important

cations in basis 12 oxygen (Table 3) have been calculated and among them Fe^{3+} , Fe^{2+} and Mn^{2+} have been taken into account. On the basis of these parameters the major components of the Delinești garnet have been calculated: spessartinic (Mn^{2+} , Fe^{2+}), calderitic (Mn^{2+} , Fe^{3+}) and almandinic (Fe^{2+}). Most of the samples contain 40–45 % spessartine, 45–60 % calderite and 0–5 % almandine. The data have been plotted on the spess-cal-alm ternary diagram (Fig. 1); a concentration of the data on the spess-cal line, approximately in the middle, slightly towards the calderitic field, can be noticed.

Table 3
Cations calculus for the Delinești spessartine and spessartine-calderite

Sample no.	CATIONS									
	Si^{4+}	Ti^{4+}	Al^{3+}	Fe^{3+}	Fe^{2+}	Mn^{2+}	Mg^{2+}	Ca^{2+}	K^{1+}	Na^{1+}
D 75a	3.453	0.010	1.529	0.107	0	2.224	0.344	0.141	0.016	0.005
D 15A	3.064	0.031	1.639	0.220	0.013	2.391	0.226	0.383	0.004	0.008
D 16A	3.086	0.037	1.614	0.304	0.012	2.295	0.174	0.389	0.003	0.008
D 94	2.980	0.013	1.714	0.339	0.011	2.597	0.086	0.236	0.004	0
D 91	2.994	0.034	1.765	0.270	0	2.306	0.185	0.400	0	0
D 62A	3.320	0.017	1.464	0.324	0.266	2.058	0.049	0.267	0.005	0
D 90A	3.442	0.016	0.681	0.929	0	1.837	0.195	0.594	0.010	0.080
D 90II	3.531	0.014	0.688	0.881	0	1.639	0.266	0.581	0.005	0.136
10 B1	2.99A	0.035	1.667	0.281	0.016	2.421	0.183	0.399	0.003	0
D 14A	3.136	0.028	1.619	0.304	0.245	2.208	0.100	0.233	0.003	0
D 49II	3.468	0.042	1.449	0.185	0.464	1.561	0.242	0.261	0.004	0
D 8Aa	3.348	0.038	0.932	0.649	0	1.898	0.256	0.650	0.004	0.100
D 20	3.747	0.032	1.401	0.126	0.451	1.453	0.101	0.147	0	0
D 8B6	3.485	0.049	1.244	0.363	0.011	1.894	0.148	0.459	0	0.020
D 4Aa	3.721	0.041	1.331	0.168	0	1.796	0.113	0.287	0.013	0.049
D 55	3.218	0.017	1.351	0.345	0.711	1.500	0.232	0.541	0	0
D 47	2.922	0.030	1.118	0.853	0.033	2.604	0.047	0.457	0	0.002
D 52	2.936	0.017	1.755	0.427	0.180	2.258	0.075	0.307	0	0
D 94A	3.034	0.015	1.653	0.344	0	2.736	0.102	0.068	0.001	0
D 98	3.000	0.027	1.546	0.462	0.096	2.487	0.082	0.258	0.002	0.024
D 63B	2.994	0.011	1.833	0.223	0.362	2.219	0.096	0.227	0.001	0
D 3	4.049	0	0.932	0.408	0	1.422	0	0.472	0	0
D 9	4.187	0	1.432	0.300	0	0.929	0	0.098	0	0



Infrared Analysis

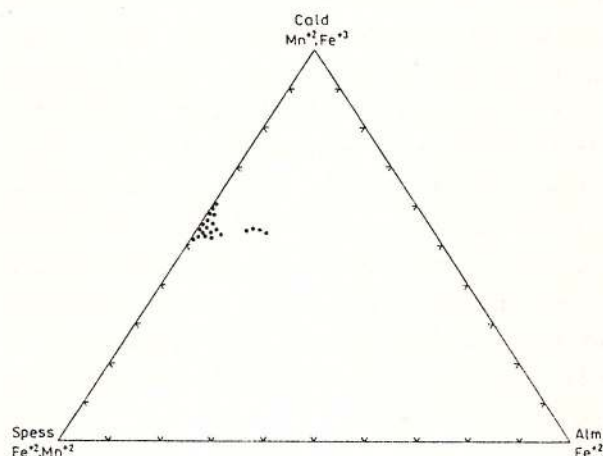


Fig. 1 - Spessartine-calderite plotting on the spess-cald-alm diagram (% cations).

The infrared analysis of the Delinești garnets rendered evident the presence of spessartine (sample 20) and of a component similar with the grossular (sample D-90A), which indicates the existence of the intermediary term - calderite (highlighted by the Rx diffraction and chemically, for which no IR standard spectra are available). The gradual substitution of Fe^{2+} by Fe^{3+} determines the shifting of the bands towards smaller wave numbers (Fig. 2 and Tab. 4).

The 632 cm^{-1} band, typical of spessartine, occurs in all the three spectra. The analysed samples contain small quartz impurities which produce specific bands (Q).

Table 4
IR analyses for the Delinești spessartine and spessartine-calderite

Spessartine Moenke catalogue	Spessartine (D 20)	Grossular Moenke catalogue	Calderite (D 90A)	Spessartine- Calderite (D 10)
Brooken Hill Australia	Delinești	Oravița România	Delinești	Delinești
452	452	450	456	450
472	476	470	470	470
525	520	—	—	—
562	564	540	532	556
—	—	618	618	624
632	632	—	632S	630S
870	872	840	840	860
892	894	860	862	880
995	958	915	928	944
980	980	960	962	970
1070	1080	1080	1075	1080S
			1085S	

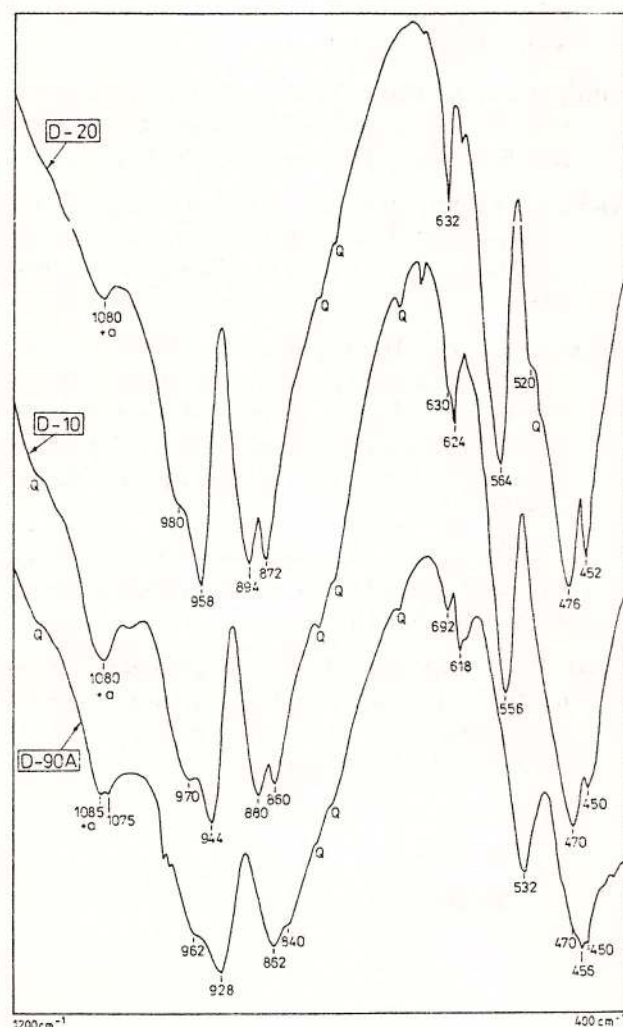


Fig. 2 – IR spectra of the Delinești garnets between 400 and 1200 cm^{-1} (Samples D20, D10, D90A).

Spessartine-Calderite Formation

The old spessartine, described above, is a metamorphic mineral, formed from an initially sedimentary material. Spessartine-calderite is a metasomatic mineral. It was formed by metasomatism with Fe^{3+} on the old spessartine. This hypothesis is based on three arguments: (1) garnet zonation, which displays a colourless central zone, belonging to the old spessartine, and a yellow zone, yellow being specific to the calderitic garnet (Pl. II, Fig. 6); in other cases the marginal zone is constituted

of a lot of small yellow idiomorphic grains of spessartine-calderite; (2) the close association of the spessartine-calderite with minerals that include Fe^{3+} , such as acmite, hematite; (3) spessartine-calderite forms veinlets within the old spessartine (Pl. I, Fig. 4).

The intimate process took probably place by the destruction of the crystalline network of the old spessartine and the appearance of a multitude of small idiomorphic crystals of spessartine-calderite or calderite. In this way can be explained the orientation of the latter, taken over from the first metamorphosed old garnet. These transformations took place because of the appearance of a strong oxidizing environment in the Delinești ore deposit (after the first major phase of metamorphism), when the almandinic component of the old spessartine garnet is removed almost entirely by the iron oxidation.

Figure 3 shows a fold formed of an idiomorphic spessartine-calderite (black/ and white quartz); after the main metamorphic

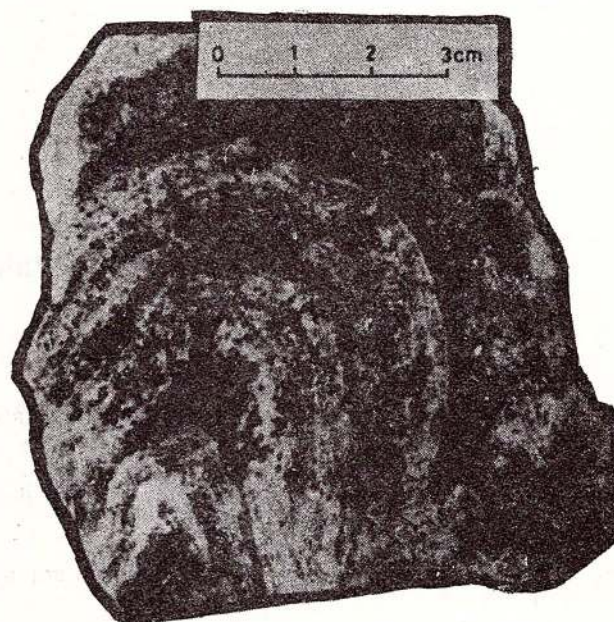


Fig. 3 – Fold formed in spessartine-calderite (black) and quartz (white).

stage which determined the formation of the old spessartine and after the ore folding, it reached the static metamorphism stage. This

metamorphism is characterized by the presence of strong oxidation conditions under which the initial spessartine became unstable and was altered into spessartine-calderite by the substitution of Fe^{2+} by Fe^{3+} .

After the spessartine-calderite formation, the Fe-Mn ore at Delinești underwent some hydrothermal alterations materialized into several veinlets filled with: baryte, barium feldspars, albite, bemmentite, neotocite, manganese brown chlorite, rhodochrosite, Mn-calcite (Pl. I, Fig. 6; Pl. II, Fig. 5).

References

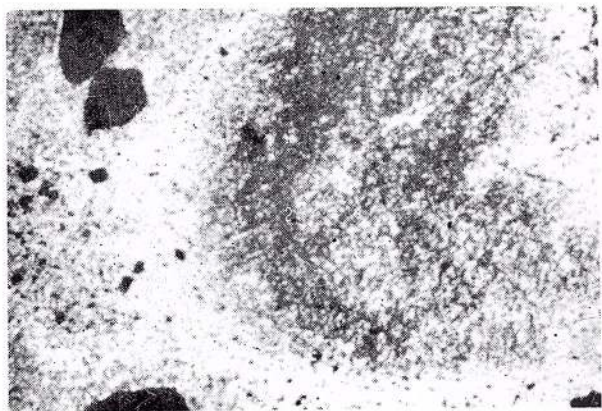
- Babcock, L.L. (1968) Manganese minerals from Champion Mines, Marquette County, Michigan. *The Compass*, 45, p. 162-170.
- Bălan, M. David, M. (1978) Date mineralogice privind parageniza cu piemontit de la Delul Negru (Munții Lotrului). *Stud. Cerc. Geol. Geofiz. Geogr., Geologie*, 23/2, p. 215-229, București.
- De Villiers, C.E. (1951) The manganese ores of Otjosunui South-West Africa. *Trans. Geol. South Africa*, 54, 89.
- Dimitrescu, R., Popa, Gh. (1973) Asupra mineurilor manganifere din zăcămintul Delinești. *An. Șt. Univ. "Al.I.Cuza" Iași*, XIX, p. 11
- Klein, C. (1966) Mineralogy and petrology of the metamorphosed Wabush Iron Formation Southwestern Labrador. *Journ. Petrol.*, 7, p. 246-305.
- Hârtopan, P., Hârtopan, I., Cristea, C. (1993a) Mineralogy and genesis of the Delinești Mn-Fe ores. *Roum. Journ. Mineralogy. Second symposium on Mineralogy 5-11 July 1993, Timișoara. Abstracts volume*, 77, p. 19-20, București.
- , Hârtopan, I., Mosonyi, E., Cristea, C., Stelea, G., Udrescu, C. (1993b) Report. Arch. IGR, Bucharest.
- Savu, H. (1959) Contribuții la cunoașterea zăcămintelor de mangan din regiunea Delinești (Munții Semenic). *D.S. Inst. Geol.*, XLVI (1958-1959), p. 147-157, București.

Received: June, 1995

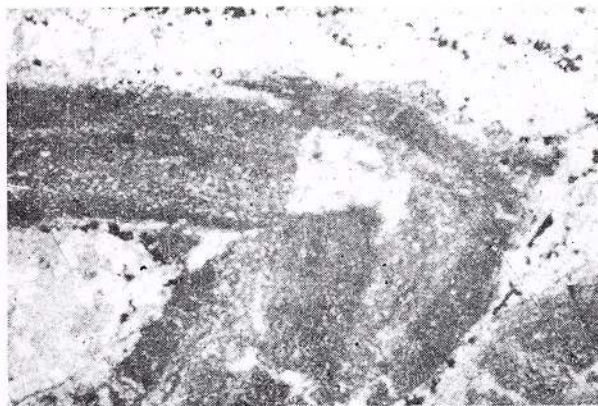
Plate I

- Fig. 1 - Fold in spessartine-calderite ore; black large grains = magnetite. Sample D 6. Waste dump of gallery 1, N +, x 40.
- Fig. 2 - Folded spessartine-calderite ore; metallic black = hematite. Sample D 85. Waste dump of gallery 1, N +, x 40.
- Fig. 3 - Old (blackish grey) spessartine "pocket" included in a pyroxmangite mass. Sample D 94. Waste dump of gallery 2, N ||, x 40.
- Fig. 4 - Spessartine-calderite + quartz vein in gonditic ore. Sample D22a. Waste dump of gallery 1, N ||, x 40.
- Fig. 5 - Vein with spessartine-calderite, acmite, yellow alkali amphiboles penetrating the gonditic ore. Sample D 7(1). Waste dump of gallery 1, N ||, x 40.
- Fig. 6 - Fissures in gonditic ore filled with hydrothermal minerals: Baryte, ba feldspars, rhodochrosite. Sample D 41. Waste dump of gallery 1, N ||, x 40.

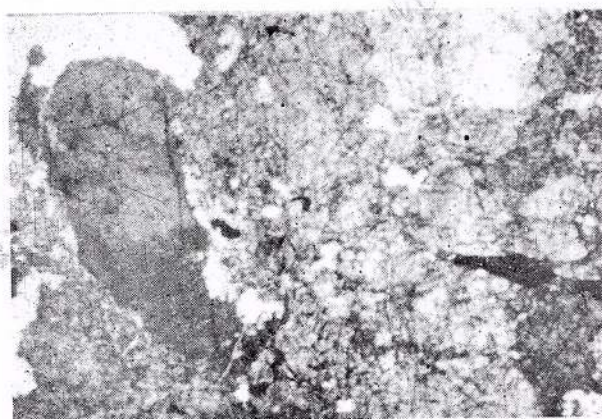




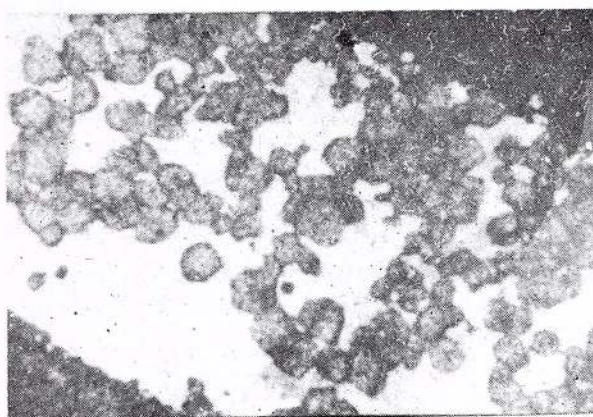
1



2



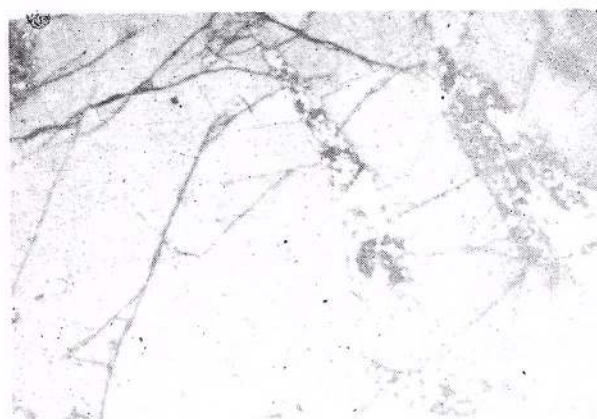
3



4



5

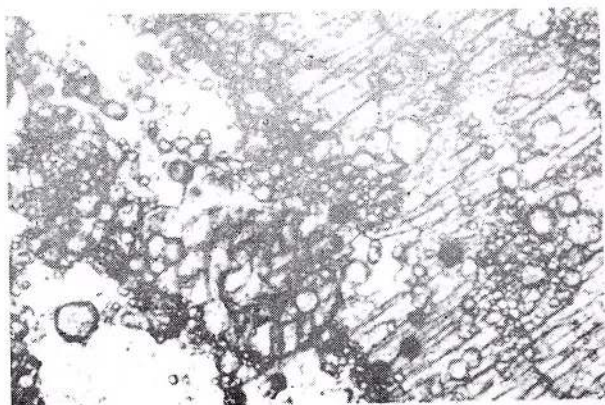


6

Plate II

- Figs. 1,2** – Spessartine-calderite with rhodonite association (black in N+, fine-grained, large-grained, with cleavage) pyroxmangite (small, with two cleavage directions) and microcline (white, left-hand bottom, in N|| and grey-blackish in N+). Sample 24. Waste dump of gallery 1, N|| (Fig. 1) and N+ (Fig. 2), x 60.
- Fig. 3** – Spessartine-calderite association (black in N+ with huebnerite (two directions of digging). Sample D 82. Waste dump of gallery 2, N+, x 40.
- Fig. 4** – Spessartine-calderite association (small grains with high relief) with rhodonite (white, with cleavage) and hematite (black). Sample D 47. Waste dump of gallery 1, N||, x 40.
- Fig. 5** – Old spessartine penetrated by veinlets and cracks filled with baryte (white), neotocite (black), rhodochrosite (grey). Sample D 94. Waste dump of gallery 1, N||, x 40.

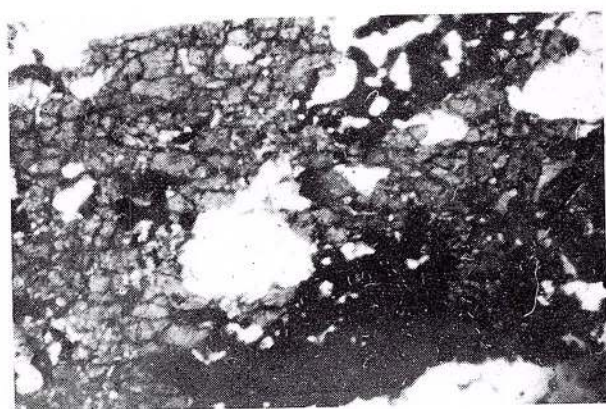




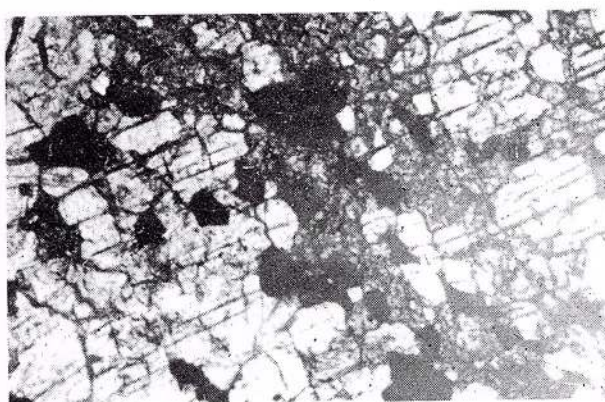
1



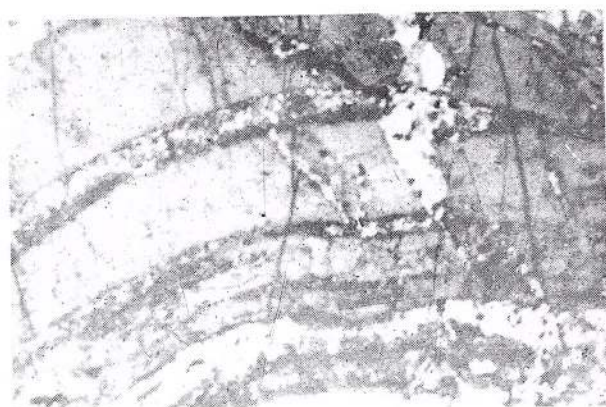
2



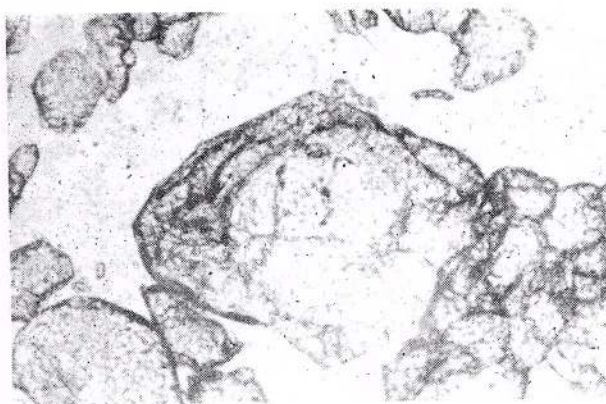
3



4



5



6

Rom. J. Mineralogy, vol. 78, București, 1997



Institutul Geologic al României



MINOR ELEMENTS IN QUARTZ: HYDROTHERMAL VS METAMORPHIC

Gheorghe UDUBAŞA, Paulina HÂRTOPANU, Şerban ANASTASE, Ana ŞERBĂNESCU

Institutul Geologic al României. Str. Caransebeş nr.1, 79678, Bucureşti, 32

Key words: Quartz. Minor Elements. Emission Spectrography. Radiochemical Neutron Activation. Hydrothermal Processes. Metamorphic Processes.

Abstract: About 150 quartz samples of different origins have been analysed by emission spectrography and radiochemical neutron activation (RNAA) in order to find out if possibilities do exist to distinguish the quartz produced by hydrothermal, metamorphic or other processes. The hydrothermal quartz is generally richer in minor elements (especially in Al, Fe, Ti) and contains fluid inclusions of rather complex composition as compared with the metamorphic quartz. Some data on synthetic quartz are also given (minor elements in different growth zones) as a supplementary tool for estimating temperature conditions of hydrothermal quartz.

1. Introduction

Widely distributed in a large variety of geological environments the quartz may furnish significant information in deciphering the conditions under which the associated minerals and the quartz itself have formed. In this respect, the crystal morphology and the minor element contents seem to be useful features that are also easily to be obtained. The purpose of this paper is to find out if any possibility exists to distinguish the quartz of different origins by using the minor element contents and also to depict the gold and aluminium distribution trends. The analysed material includes quartz from hydrothermal (postmagmatic) veins, metamorphic quartz, quartz from magmatic rocks and from metamorphic pegmatites as well as well developed crystals from sedimentary rocks. The analytical methods used were emission spectro-

graphy, radiochemical neutron activation analysis (RNAA) and for some samples inductively coupled plasma spectrometry. X-Ray diffraction analysis was also currently used in order to test if silica polymorphs other than alpha-quartz were present in the samples. Purity of quartz samples has been verified by thin section examination and by handpicking under the binocular microscope.

2. Minor elements distribution

2.1. Gold and Aluminium Contents versus Crystal Morphology

Quartz crystals of different habit and origins were analysed by RNAA for gold and by emission spectrography for aluminium and the remaining elements. In the case of quartz crystals of hydrothermal origin the increase of gold content by decreasing formation temperature is obvious. The crystal habit does not show



significant changes except, however, the ratio of $r + z : m$ faces. The quartz phenocrysts from the Neogene rhyodacites from Roşia Montană, Metaliferi Mts (bearing important stockwork and vein type gold deposits) show the typical habit of beta-quartz which is now completely inverted to alpha-quartz (X-Ray tested). The sedimentary quartz of grey-blackish colour was collected from the so-called "Salt Breccia" of Badenian age (locality Ruşavăţ, on Buzău Valley) and exhibits habit changes from the Cumberland-type (r and m faces) to flattened crystals (tabular along y and z axes); such crystals are quite typical of the "Maramureş diamonds" occurring in sedimentary rocks in the northern part

of Romania. Figure 1 contains also the representation of results for massive quartz samples of metamorphic origin, for which the same trend seems to exist, i.e. increase of gold content by decreasing formation temperature, from metamorphic pegmatites to shear-zone related quartz bodies.

The relationship between aluminium content and formation temperature is shown in Figure 2. In the case of hydrothermal quartz the dependence is similar to that of gold, i.e. the aluminium content increases with decreasing temperature except the quartz phenocrysts in the rhyodacites. The sedimentary quartz is also relatively rich in aluminium.

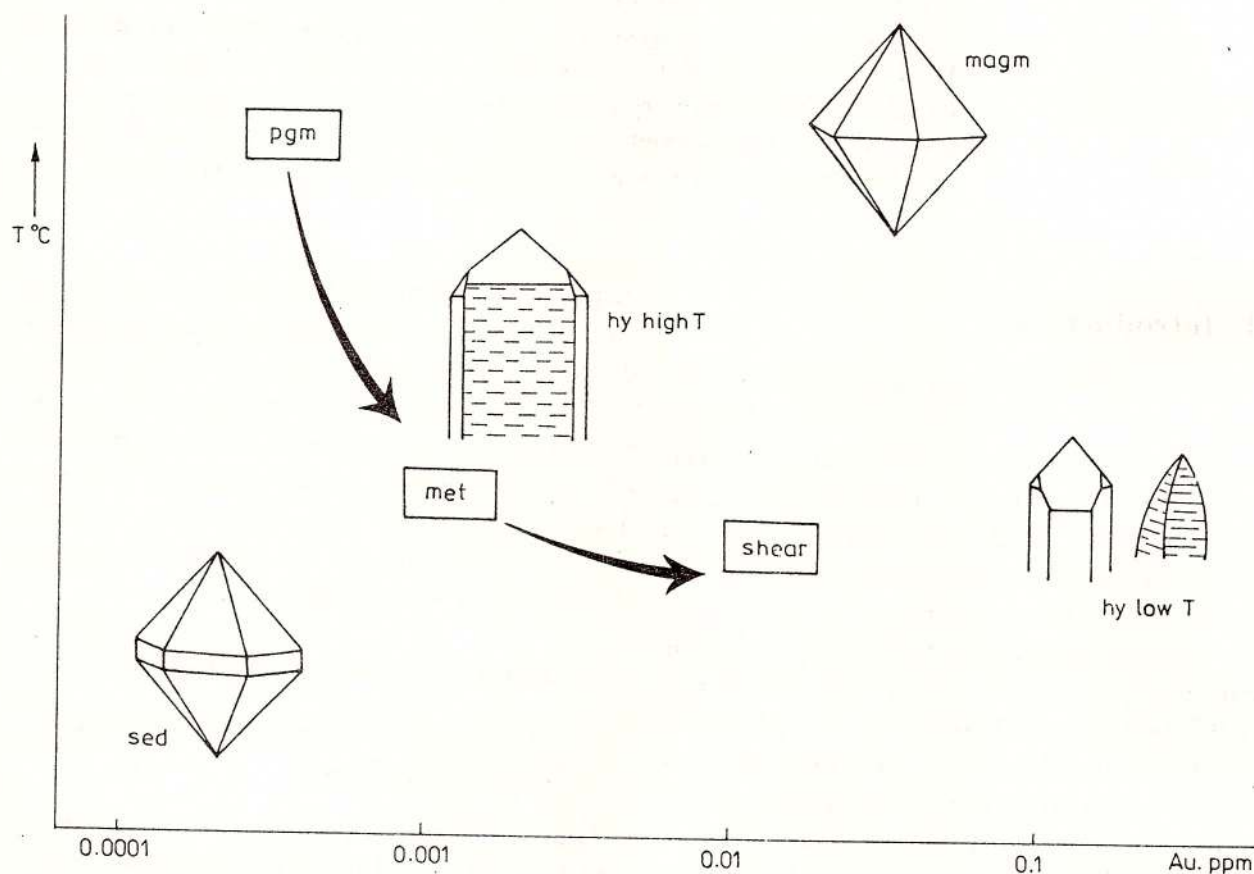


Fig. 1 – Gold content versus formation temperature for hydrothermal quartz (hy), high- and low temperature – Borşa-Săcărâmb base metal deposit and Hondol gold deposit (Metaliferi Mts); phenocrysts in Neogene rhyodacites from Roşia Montană (magm); sedimentary quartz in the "Salt Breccia" of Badenian age (Ruşavăţ, Buzău Valley). The same trend shows the quartz occurring in various metamorphic environments, i.e. in metamorphic pegmatites from Voineasa (pgm), in different metamorphic series in the South Carpathians as lenses or short veins (met) and in sheared metamorphics in the same area (shear). See also Table 1 for details.

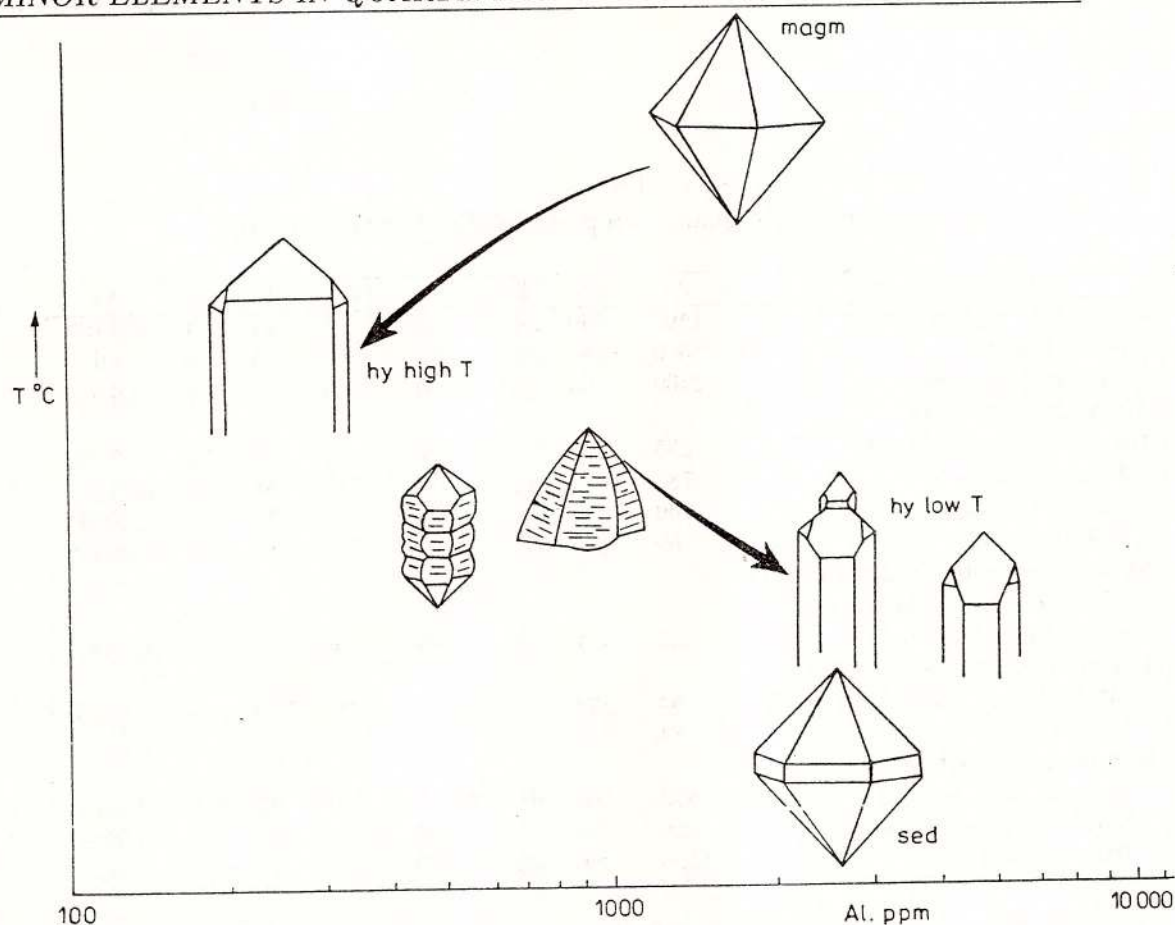


Fig. 2 - Aluminium content versus formation temperature for magmatic (magn), hydrothermal (hy) and sedimentary (sed) quartz. The magmatic and sedimentary quartz samples are the same as in Figure 1. The hydrothermal quartz crystals come either from high-temperature base metal deposits (from left to right) at Bocşa-Săcărâmb, Herja, Rodna (metasomatic replacement in metamorphic limestones) or from lower-temperature base metal deposits such as Ruschiţa (vugs in the metamorphic host rocks, lacking other minerals, near the ore bodies) as well as from the low-temperature gold veins at Hondol; this is the estimated order of decreasing temperature.

2.2 Metamorphic Quartz

It occurs everywhere in the metamorphic rocks as lenses or short veins.

The genesis of quartz in metamorphic rocks has been hypothesized by Schultz et al. (1986) in the following manner: there exist quartz bodies related to retrogressed metamorphics, i.e. they are (mainly) pressure-related (model A) and quartz bodies linked to metamorphic sequences in areas with thermal domes, i.e. they are (mainly) temperature-related (model B). The size is somewhat different, the quartz bodies of model B being greater but the quartz is less pure. The pressure-related quartz bodies in strongly retrogressed metamorphics may

have metallogenic significance; under adequate conditions (existence of protore, position of the shear plane in relation to that of the protore) such shear-zone related quartz bodies may concentrate metals (especially gold and copper). The data presented in the Table 1 confirm such an assumption; the shear-zone related quartz bodies of Valea lui Stan type (Udubaşa and Hann, 1988) show higher contents of minor elements when compared with the barren quartz bodies located in metamorphic terrains not or only gently affected by retrogression but showing effects of thermal domes.

By direct comparison the metamorphic quartz is definitely purer than most quartz

Table 1
Minor elements in quartz samples of different origin (ppm)

Occurrence type	Al	Fe	Ti	Ca	Mg	Mn	Cu	Au
Rhyodacite phenocrysts	1400	150	57	160	70	11	1	0.0311
Albești granites	8300	280	81	360	79	5	4	nd
Voineasa pegmatites	2400	23	15	70	5	–	1.5	0.0009
Metamorphic quartz								
Big barren bodies (n=26)	295	611	–	50	82	42	23	0.0023
– Uricani (n=7)	780	1054	14	146	187	56	17	0.0024*
– Buchin (n=6)	160	697	–	101	21	70	9	0.0023*
– Hobița (n=13)	69	249	–	9	15	14	43	0.0021*
Shear zone related bodies (n=10) (Valea lui Stan, Ghimbav Valley-Leaota Mts etc.)	355	152	2	1360	26	34	19	0.0141
Barren nests, lenses and veins								
– Sibîșel Series, South Carp. (n=5)	54	124	7	172	26	3	–	0.0080
– Leaota Group (n=7)	84	159	–	211	16	3	–	nd
Sedimentary quartz								
– Rușavăț (Salt Breccia)	2800	1100	65	3000+	520	22	2.5	0.0007
– Sârbi (Cret. sandstone)++	600	1750	–	5000	2100	46	34	0.0093
– Brad (Chert)+++	1500	5200	15	900	155	17	15	nd

* = Single value; + = More than figure indicated; ++ = Crystals in vugs; chalcopryrite present; +++ = Intensely colored (grey, red, yellow); lenses in volcanic pyroclastics; the material contains also cristobalite and finely dispersed iron hydroxides.

Note: If n is not given the indicated value represents single analyses carried out on big, good homogenized samples.

samples of hydrothermal origin. The metamorphic quartz is massive, rather fine grained, translucent and contains small amounts of fluid inclusions as well as minute inclusions of feldspars, tourmaline, micas etc. Some metamorphic occurrences contain quartz of optical grade with Al contents down to 100 ppm and negligible amounts of Fe, Ti, Ca, Mg, Mn and Cu (Tab. 1). The purest samples of metamorphic quartz are those from the Hobița deposit, Petreanu Mts.

The Al content seems to have an inverse correlation to the intensity of retrograde changes (Fig. 3). The same trend is obtained if the sum of the analysed elements is used. In fact, this diagram may be interpreted as indicating a positive correlation between the Al content (or sum of the elements) and the metamorphic

grade as well; at least the samples labelled U, B and C are from metamorphic terrains not involved in shearing and the quartz bodies have formed under conditions of model B. Anyhow, this may be given as an example of convergence, a feature typical of many geological phenomena. A supplementary tool in distinguishing the productive quartz bodies as against the barren ones is represented by the fluid inclusions in quartz.

The CO₂-rich inclusions are characteristic of the quartz formed during progressive metamorphism and/or conditions of thermal domes. Aqueous inclusions of moderate salinity (maximum 20 weight percent NaCl equiv.) commonly occur in the ore-bearing quartz bodies related to shear, such as the Valea lui Stan gold-quartz deposit.



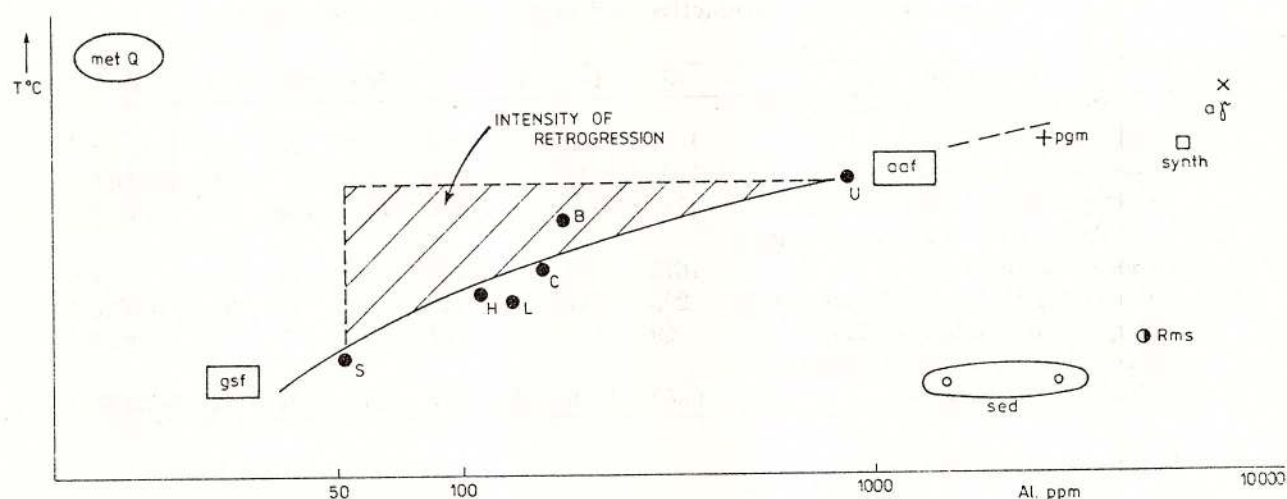


Fig. 3 - Aluminium content versus metamorphic grade from green facies (gsf) up to almandine amphibolite facies (aaf). Included are also plottings of quartz samples from granites (aγ), pegmatites (pegm), synthetic quartz (synth), quartz beds or veins in Middle Devonian shales from Ramsbeck Pb-Zn ore deposit, Germany (Rms) and sedimentary quartz (sed). The "metamorphic line" includes samples of quartz from Uricani (U), Buchin (B), Costești, Căpățâna Mts (C), Leaota Mts (L), Hobița, Petreanu Mts (H) and from the Sibișel Series (strongly retrogressed) in the South Carpathians (S). See Table 2 for details.

Coexistence of the two types of fluid inclusions suggests that the quartz bodies are polygenetic in character as is the case of the Costești (Căpățâna Mts) and Jidoștița (Mehedinți Mts) quartz bodies, that are mineralized with gold and iron and copper sulfides. For the first type inclusions (i.e. CO₂ rich) Pintea (in Hârtoapanu et al., 1991) has estimated pressures of 1.8 to 3.8 kbar and temperatures of 460° to 520° C (Costești gold-quartz occurrence). Within the shear zones the quartz is commonly strongly fissured and contained few (and small) inclusions.

3. Natural versus synthetic quartz

Synthetic quartz crystals produced in Romania (Plate) and Japan have been analysed also for minor elements (Tabs. 2,3). There is a striking resemblance between the inner zone (high-temperature) of the synthetic quartz crystals and the higher-temperature

natural quartz crystals of hydrothermal nature and between the outer zone (lower-temperature) of the synthetic quartz crystals and the low-temperature natural crystals. However, significant differences occur especially in the case of aluminium; in the synthetic quartz crystals this element is 50 times richer in Al as compared with the core zones. Less evident is such a trend for the elements Fe, Ti and Mn. Lower mobility of elements within the rapidly cooled marginal parts of the synthetic quartz and in the low-temperature natural quartz is responsible for the relative enrichment in some minor elements.

Discussion

The present paper contains only a part of the available data concerning the quartz typomorphysm. Other data are still incomplete or do not have satisfactory explanation yet. An interesting, but incompletely solved feature is



Table 2
Minor elements in productive and barren quartz bodies (ppm)

Occurrence type	Al	Fe	Ti	Ca	Mg	Mn	Cu	Au
Productive – gold-bearing								
Valea lui Stan (n=3)	1675	166	–	2630	45	76	12	0.0053*
Ghimbav Valley (n=3)	1263	48	–	1108	63	–	8	0.0246*
Costeşti Valley (n=6)	2110	470	–	2000	306	150	–	0.1497*
Productive – Pb-Zn-As-bearing								
Cioclovina (n=2)	1675	28	–	1380	14	11	–	nd
Barren-big bodies (n=26, see Tab.1)	295	611	–	50	82	42	23	0.0023
Barren-small bodies (n=12)	69	141	–	192	21	3	–	0.0080
Hydrothermal Gold-bearing veins (Hondol, Săsar) (n=4)	6350	1310	65	932	253	364	13	0.5359*

* = Single values for gold

Table 3
Minor elements in synthetic and natural quartz (ppm)

Zone in synthetic quartz								
Deposit type	Al	Fe	Ti	Ca	Mg	Mn	Cu	Sum
Inner zones (n=3)	122	47	–	33	19	–	7	333
High T deposit (n=4)	371	37	–	101	17	2	1	512
Outer zones (n=3)*	6400	46	–	42	29	8	9	6512
Outer zones (n=2)**	4700	1550	46	265	110	–	2	5683
Low T deposit (n=4)	5500	567	46	430	124	120	3	6741

* = Romanian synthetic quartz

** = Japanese synthetic quartz

the appearance of the IR absorption bands at 3400^{-1} , which has been interpreted by Dolomanova *et al.* (1972) as being due to the presence of beta-quartz slabs within the dominant alpha-quartz structure; the channels typical of the beta-quartz structure enable water to be present, a fact in accordance with increasing intensity of IR absorption bands by decreasing temperature of quartz. Color centres, thermoluminescence, REE distribution etc. may have also typomorph significance in quartz (Pavlishin, 1983; Novgorodova, 1984; Petrovskaya *et al.*, 1986; Traoré *et al.* 1986; Wünsch, 1990 and many others).

No claim of completeness is invoked by the present paper. Our genetic listing of quartz types is by far not complete and many data and information furnished by more sophisti-

cated methods represent tasks of future research. However, the attempt made and the results already obtained so far show interesting features involving quartz typomorphism.

The data presented here do not fit the quartz geothermometer curve proposed by Dennen *et al.* (1970) but increase of Al content with increasing formation temperature of quartz can be generally assumed. The Al content seems not to be directly related to temperature, as it may be affected by the presence of other elements (Scotford, 1970) and probably also by kinetical aspects of crystal growth.

The data presented above show that the hydrothermal quartz is richer in minor elements as compared with the metamorphic quartz, a fact due primarily to a greater element availability in the postmagmatic hydrothermal flu-



ids. The abundance of fluid inclusions, which seem to contain a greater part of the elements usually analysed (Novgorodova et al., 1984; Petrovskaja, 1985), is also a characteristic feature of the hydrothermal quartz.

Analyses of synthetic and natural quartz samples indicate similar distribution patterns of minor elements. In this respect it is interesting to note the discrete, but persistent presence of Ti in both outer zones of the synthetic quartz crystals and in the low-temperature gold-bearing vein quartz; the same is true if the same discrete, but persistent presence of rutile in the low-temperature gold-bearing veins is considered. This last feature has been many times suggested by Udubaşa (1978, 1982).

The two models of quartz genesis in metamorphic rocks proposed by Schultz et al. (1986) fit well the observed relationships in the metamorphics of the South Carpathians. The productive and barren quartz bodies in metamorphic environments may primarily be distinguished by their settings, i.e. in areas with thermal domes (generally producing barren quartz bodies) and in areas with well expressed shear zones (as a rule giving productive quartz bodies, if an adequate protore is present). The two quartz types contain minor elements at different concentration levels; the most promising as discriminatory ones are seemingly Al and Ca (Tab. 2), which are constantly higher in the productive bodies. In addition, the fluid inclusions rich in CO_2 are typical of the temperature-related bodies whereas inclusions of moderate salinity (about 20 percent NaCl equiv.) seem to occur mostly in pressure-related quartz bodies such as those located in the shear zones.

As regards the initial stages of gold-bearing quartz bodies in areas with supposed thermal domes relevant observations have been obtained in the Semenik Mts. At Gărâna (eastwards of the known Văliug gold deposit of shear-zone related type) there were observed

both main schistosity-conformable lenses and veins of limited size. The distribution of gold is quite different in the two types of quartz. The intersection of lenses with veins are the most favourable sites for gold enrichment (Fig. 4). The area does not show significant retrograde changes and the quartz-gold concentration evolved under conditions of a presumed thermal dome.

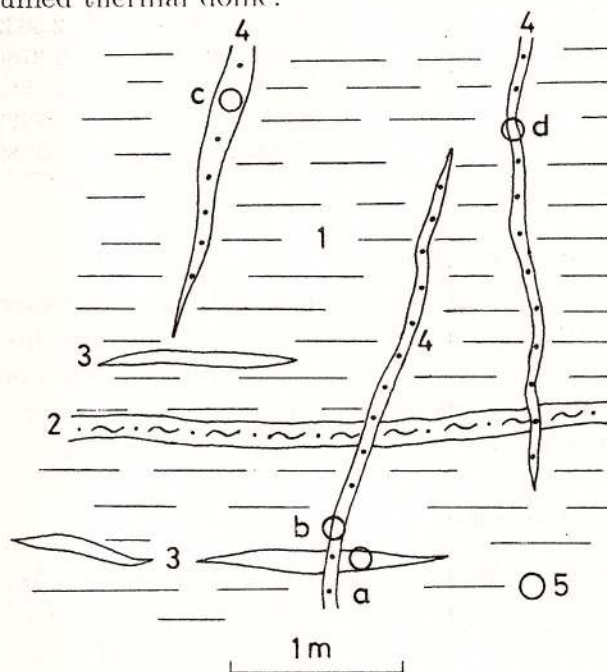


Fig. 4 - Initial stages of gold-quartz concentration (Gărâna, Semenik Mts). 1, micaschists; 2, quartz-rich micaschist; 3, quartz lenses (without sulphides); 4, quartz veins with pyrite; 5, sample location.

If a shear zone would have acted on such a structure then an extended gold concentration had occurred. This seems to be the case of the nearby situated Văliug gold deposit. Finally, a last feature of gold distribution among co-existing minerals including quartz is shown in Table 4. Generally, other minerals than quartz preferentially concentrate gold; however, the gold content in quartz is much higher than in the barren bodies (see Tab. 1). As usually, exceptions are present as is the case of the last mineral pair in Table 4.

Table 4
Gold Content of Coexisting Minerals (ppm)

Minerals	Au	Sample location
Arsenopyrite	19.0401	Costeşti, Căpăţâna Mts
Pyrite	4.8080	Hârtopan et al., 1991)
Quartz	0.1497	
Arsenopyrite	18.1635	Ditto
Quartz	0.0230	
Spessartine	2.5632	Sadu Valley, Cibin Mts (lenses in
Titanian hematite	2.2780	kyanite-bearing micaschists)
Quartz	1.9583	
Quartz	2.7422	Semenic Mts (nests or lenses in
Titanian hematite	1.7689	kyanite-bearing micaschists)

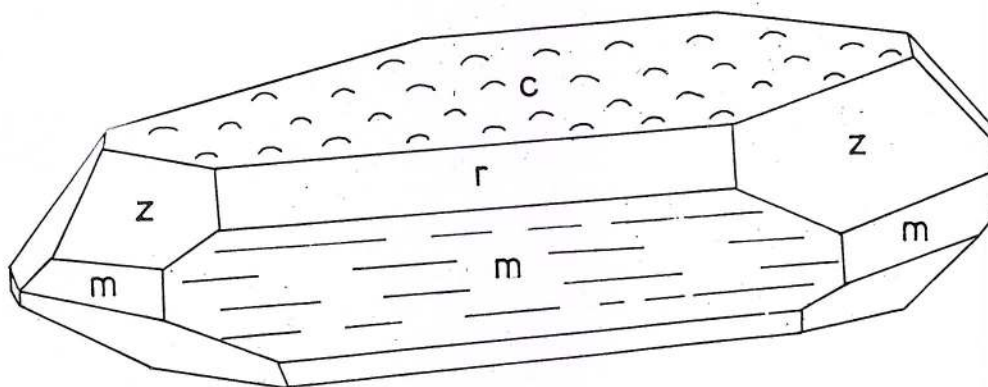
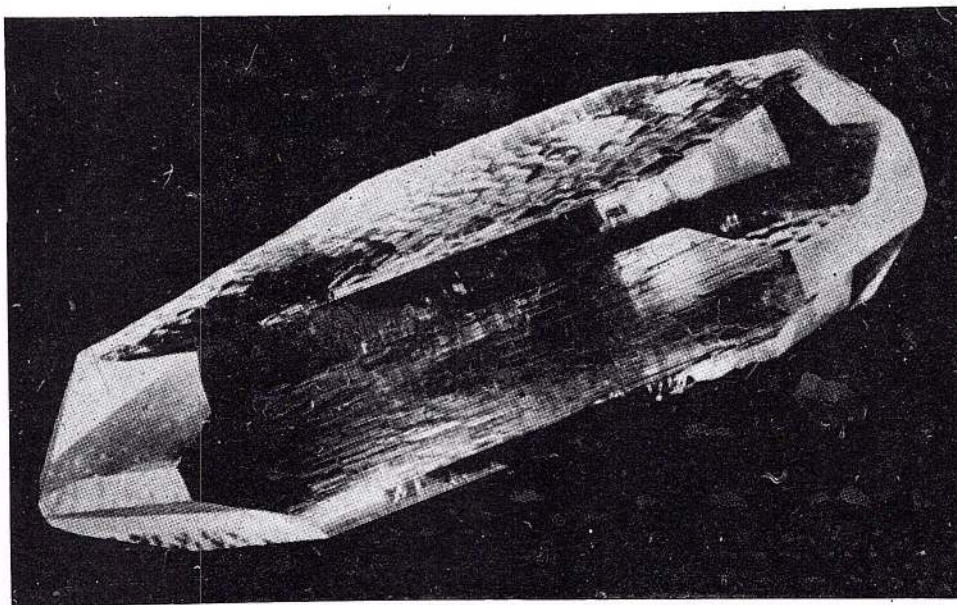
Acknowledgements

The authors express their gratitude to I. Pintea (GIR Cluj-Napoca Branch) for giving the permission to use in this paper the preliminary data on fluid inclusions in the shear-zone related quartz bodies.

References

- Dennen, W.S., Blackburn, W.H. (1970) Aluminium in quartz as a geothermometer. *Contr. Miner. Petr.*, 27, p. 332-342, Heidelberg.
- Dolomanova, E.I., Gasoian, M.S., Korolev, N.V., Rudnitkaia, E.S., Tiutneva, G.K., Uspanskaia, A.B., Elinson, M.M. (1972) Tipomorfniie osobennosti gidrotermalnogo kvartsa. In: Tipomorfizm mineralov i ego prakticheskoe znachenie. Nedra Publ. House, p. 138-148, Moscow.
- Fronde, C. (1962) Dana's system of Mineralogy. III. Silica Minerals, Wiley & Sons, New York, 334 p.
- Hârtopan, I., Udubaşa, G., Dinică, I., Pintea, I., Hârtopan, P. et al. (1991) Unpublished Report, Arch. GIR, Bucharest.
- Novgorodova, M. I., Veretennikov, V. M., Boiavskaia, R.V., Drînkîn, V.I. (1984) Gheohimia elementov-primesei v zolotonosnom kvartse. *Gheohimia*, 3, p. 370-383, Moskva.
- Pavlishin, V.I. (1983) Tipomorfizm kvartsa, sludi i polevii spatov v endogennih obrazovaniiah. Haukova Dumka Publ. House, 232 p., Kiev.
- Petrovskaia, N. V., Novgorodova, M. I., Natrikhev, V.D., Drînkîn, V.I., Voinkov, D.M. (1985) Primesi redkih elementov v kvartse kak indikator istocinika rudnogo veshstva. *Gheol. Rudn. Mestor.*, 3, p. 66-74, Moskva.
- Schultz, H., Beyer, W., Thomas, R. (1986) Zur Bildung von Quarzkörpern in den Metamorphiten der erzgebirgischen Antiklinalzone. *Z. angew. Geol.*, 32, p. 117-120, Berlin.
- Scotford, D.M. (1975) A test of aluminium in quartz as a geothermometer. *Amer. Miner.*, 60, p. 139-142, Washington.
- Traoré, I., Schrön, W., Baumann, L. (1986) Geochemische Untersuchungen an goldführenden Gangquartzen. *Z. geol. Wiss.*, 14, p. 297-305, Berlin.
- Udubaşa, G. (1978) Hydrothermal rutile in the Barza-Carpen gold-bearing ore deposits, Metaliferi Mts. *D.S. Inst. Geol. Geofiz.*, LXIV/1, p. 43-51, Bucureşti.
- (1982) Rutile of postmagmatic mineral formation. In: Amstutz et al. (eds.) Ore genesis. The state of the art. Springer, Berlin - Heidelberg - New York, p. 784-793.
- , Hann, H.P. (1988) A shear-zone related Cu-Au ore occurrence Valea lui Stan, South Carpathians. *D.S. Inst. Geol. Geofiz.*, 72-73/2, p. 259-282, Bucureşti.
- Wünsch, K. (1990) Zur Mineralassoziation und Spurenelementgeochemie metamorphogener Quarzkörper im Südteil der DDR. *Z. angew. Geol.*, 36, p. 54-59, Berlin.





Plate

Synthetic crystal of quartz, grown hydrothermally, produced in Romania. The crystal is 18 cm in length and weighs 1.010 kg. The uncommon form and the roughness of the *c* and *m* faces are due to special growth conditions (see, Frondel, 1962, for details).

ÉTUDE GÉOCHIMIQUE SUR LES MUSCOVITES DES PEGMATITES DE CRIŞENI – MUNTELE RECE (MONTS APUSENI)

Dan STUMBEA

Universitatea "Al.I.Cuza", Catedra de Mineralogie-Geochimie

Bd. Copou nr. 20A, 6600, Iaşi



Key words: Muscovite. Pegmatite. Microprobe Analysis. Geochemistry. Crişeni–Muntele Rece. Apuseni Mountains.

Abstract: Muscovite-class pegmatite from Crişeni-Muntele Rece seems to be generated by an anatectic-granitization process, at 7–8 to 10–11 km depth level, under ultrametamorphic conditions. The muscovites are characterized by an alkali-deficiency in the X sites of crystallochemical formula and a substitution of Al^{IV} by Mg, Fe^{2+} and Mn; they formed under substantial aluminium excess. These muscovites show the following types of substitution: alkali-deficient, Tschermak, phengite and dioctahedral-trioctahedral substitutions. Within these muscovites an important participation of "muscovite" and "ferrophengite" terms (almost equal – 34 %) as well as a slight one of "ferrimuscovite" (17 %) and "picrophengite" (11 %) terms were observed. The muscovite-paragonite geothermometer gave temperatures of 340° – 380° C showing that muscovite formed in the final stage of pegmatite-pneumatolitic process and at the beginning of the hydrothermal one. The muscovites from Crişeni-Muntele Rece present some common features with the tourmalines from the same area: they formed under aluminium excess conditions and they show Tschermak and alkali-deficient substitutions.

1. Introduction

Cet ouvrage essaie de faire une caractérisation géochimique des muscovites associées avec du quartz, qui remplissent les fissures traversant des cristaux de tourmaline dans les corps pegmatitiques de Crişeni – Muntele Rece (Monts Apuseni).

A point de vue géographique, le périmètre des pegmatites étudiées est situé au nord-est des Monts Apuseni, environ 25 – 30 km à de la ville de Cluj – Napoca (Fig. 1);

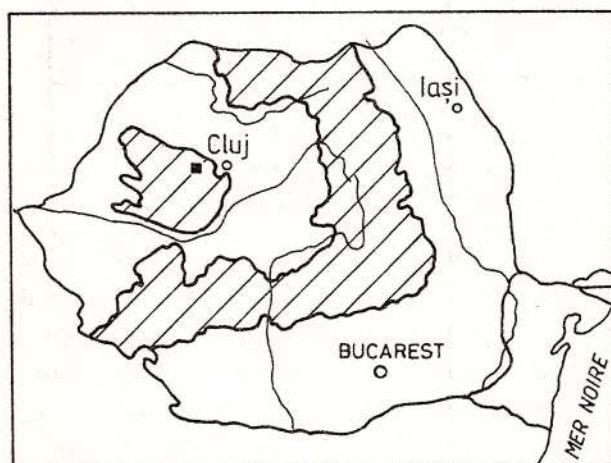


Fig. 1 – Localisation du périmètre étudié dans la province pegmatitique carpatique.



il est encadré vers le sud-est par la vallée de la Iara et vers le nord-ouest par celle du Someșul Rece. Les corps pegmatitiques sont situés sur le versant gauche de la vallée Rîșca – affluent sud de la vallée Someșul Rece.

Au point de vue géologie, les pegmatites de Crișeni – Muntele Rece appartiennent à la sous-province pegmatitique Gilău – Muntele Mare, qui fait partie de la Province pegmatitique carpatique. Les pegmatites sont cantonnées dans les roches mésométamorphiques de la série de Someș (Fig. 2), remarquée par la prédominance des gneiss sur les micaschistes, par le développement plus important des mica (muscovite) et par la concentration maximum des migmatites. Les roches métamorphiques sont représentées par des gneiss, micaschistes à l'almandin et disthène, plus rarement par des amphibolites et quartzites.

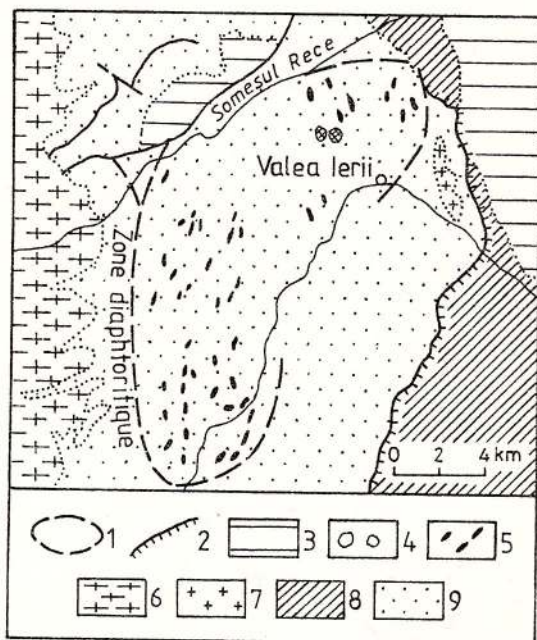


Fig. 2 – Disposition des pegmatites de Crișeni-Muntele Rece dans la série mésométamorphique de Someș. 1, sous-province Gilău-Muntele Mare; 2, charriage; 3, couverture sédimentaire; 4, pegmatites de Crișeni-Muntele Rece; 5, occurrences de pegmatites; 6, granitoïdes; 7, granitoïd de Codru; 8, schistes épimetamorphiques de la série de Biharia, série de Muncel et série d' Arada; 9, schistes mésométamorphiques de la série de Someș et de la série de Baia de Arieș (d'après Mârza, 1980).

Les paragenèses de ces roches correspondent au faciès almandin-amphibolitique. Dans le cadre de la série de Someș il y a deux faciès, avec un développement spatial à peu près égal: le faciès des gneiss et celui des micaschistes. Les apparitions de pegmatites dans cette série – pas seulement celles de Crișeni – Muntele Rece – se trouvent presque entièrement encadrées dans faciès des gneiss. Dans la sous-province Gilău – Muntele Mare, il y a deux districts pegmatitiques: Someșul Rece – vallée de la Iara – dans la série de Someș et le district Geamăna-Măzăraru – dans la série de Baia de Arieș. Les pegmatites étudiés par nous appartiennent au premier district.

Les pegmatites sont des corps épigénétiques par rapport aux schistes cristallins, ayant des limites tranchantes. Près de ces pegmatites filoniens de sécrétion on rencontre localement, dans la masse des gneiss migmatiques, des gneiss pegmatoïdes et des pegmatites muscovitiques, sous forme de corps irréguliers à transition graduée vers les roches encaissantes, ce qui marque l'existence des pegmatites de recristallisation et des pegmatites metasomatiques (Mârza, 1980).

Les composants minéralogiques principaux de ces pegmatites sont les feldspaths alcalins (orthose, microcline, albite, oligoclase), quartz et muscovite, subordonnement tourmaline et grenats. Cette composition indique des pegmatites simples ou céramiques, ce qui représente un argument en faveur de l'origine métamorphique des pegmatites du cristallin de Gilău; cette hypothèse est en accord avec la classification des pegmatites envisagée par Ginsburg et al. (1979), qui situe les pegmatites céramiques d'origine anatectique à une profondeur d'environ 11 km. Mârza (1980) considère d'ailleurs que, dans le cas des Monts Gilău, les granites (granite de Muntele Mare), les pegmatites et les migmatites sont les produits d'un processus unitaire d'anatexie-granitisation (ultramétamorphique) développés en étapes; ils ont résulté par le mécanisme de différenciation

magmatique – quand la fusion a été complète (magma régénérée) et par une différenciation métamorphique – quand la fusion a été partielle (migma).

Les recherches de Norton (1973, 1981) ont montré que certains pegmatites aux éléments rares (ex. Li) peuvent être générés par des processus métamorphiques.

A présent, les pegmatites de Muntele Rece font l'objet de l'exploitation en carrière dans le but d'extraire le feldspath, utilisé dans l'industrie céramique.

2. Méthodes d'investigation

L'étude géochimique des pegmatites de Crișeni – Muntele Rece a été précédée par des observations microscopiques. Ces observations nous ont permis de mettre en évidence les grains microscopiques – généralement idiomorphes – de muscovite et la façon dont ils sont associés avec le quartz, dans les veinules qui traversent des cristaux cataclasés de tourmaline.

Les résultats analytiques utilisés dans la caractérisation géochimique ont été obtenus à l'aide d'une microsonde électronique marque CAMECA SX 50 et l'interprétation de ces données a été entamée en partant du calcul des paramètres cristallochimiques conformément à 22 atomes d'oxygène. Ces valeurs ont permis l'utilisation de certains diagrammes de corrélation, le calcul de la composition normative, ainsi que l'utilisation de certains diagrammes diagnostiques (ex. Foster, 1960; Salye, 1975; Bailey, 1984) qui offrent des informations sur les conditions génétiques de formation de cette muscovite.

3. Caractéristique géochimique

Les résultats analytiques des muscovites de Crișeni – Muntele Rece – résultats présentés dans le Tableau 1 pour certains échantillons analysés par nous – indiquent une teneur en silice qui varie entre 44,703 et 48,031 %, se tandis que la participation de l'alumine

se place dans l'intervalle 32,143 – 35,277 %. Ces valeurs sont en accord avec celles publiées dans la littérature géologique concernant les pegmatites de Roumanie; il faut pourtant mentionner la participation relativement supérieure de l'alumine.

Les formules cristallochimiques des muscovites (Tab. 2) mettent en évidence la double disposition de l'aluminium – dans les sites tétraédriques (Al^{IV}) et, respectivement, octaédriques (Al^{VI}). Du plus, les paramètres cristallochimiques (Tab. 1) montrent aussi l'existence d'un excès important en aluminium, avec des valeurs comprises entre 0,126 et 0,394. Les formules structurales mettent en évidence aussi le fait que la présence du fer, du magnésium et manganèse est le résultat de la substitution de l'aluminium dans les sites octaédriques; ainsi, les diagrammes ($Fe^{2+} + Fe^{3+}$) : Al^{VI} (Fig. 3) et $Mg:Al^{VI}$ (Fig. 4) montrent des corrélations négatives entre ces paires de valeurs, ce qui justifie la présence de ces trois éléments dans les positions octaédrique des formules cristallochimiques.

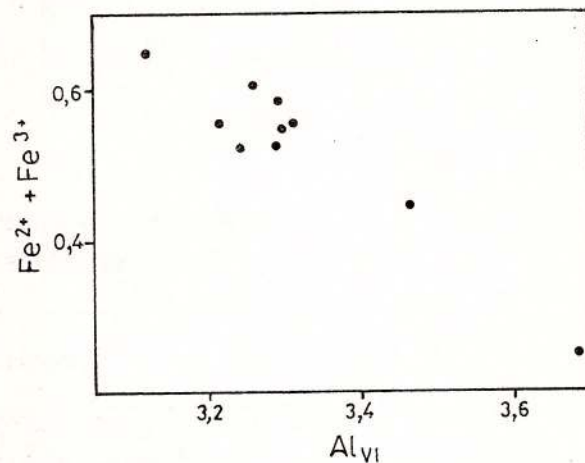


Fig. 3 – Le diagramme de corrélation ($Fe^{2+} + Fe^{3+}$) : Al^{VI}

Les analyses des muscovites étudiées par nous mettent en évidence la participation réduite du manganèse (tout au plus 0,111 %). Les teneurs en sodium sont en accord avec les données expérimentales; ainsi, la limite de solubilité de la paragonite en muscovite, calculée

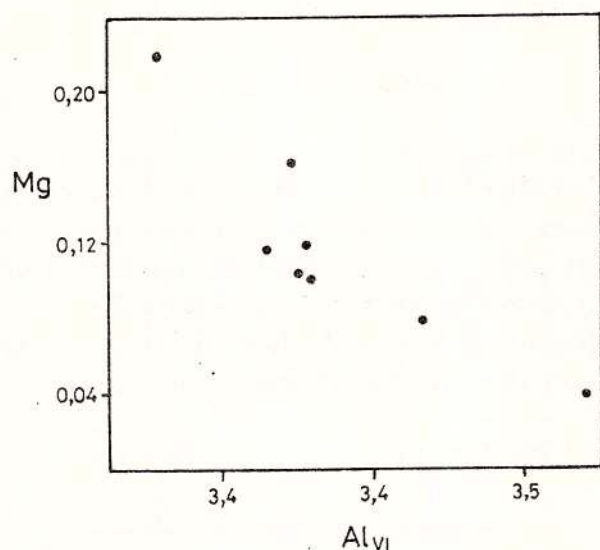
Tableau 1
Les teneurs et les paramètres cristallochimiques de quelques muscovites
des pegmatites de Crişeni-Muntele Rece

	M 7.1	M 7.2	M 4.17	M 11.23	M 11.32	M 16.48
SiO ₂	47,040	47,330	46,065	48,031	46,926	44,703
TiO ₂	0,094	0,034	0,000	0,052	0,033	0,009
Al ₂ O ₃	33,412	32,143	32,817	33,428	33,491	35,277
Fe ₂ O ₃	1,910	2,938	1,807	3,158	2,578	0,669
FeO	2,996	3,139	4,400	2,865	2,669	1,624
MnO	0,111	0,000	0,006	0,068	0,004	0,073
CaO	0,001	0,025	0,006	0,000	0,000	0,056
MgO	0,819	1,100	0,101	0,568	0,522	0,201
K ₂ O	10,050	10,532	10,515	10,213	10,038	10,212
Na ₂ O	0,355	0,253	0,158	0,400	0,380	0,511
Paramètres cristallochimiques						
Si	6,317	6,397	6,301	6,387	6,339	6,126
Al _{IV}	1,683	1,603	1,699	1,613	1,661	1,874
Al _{VI}	3,207	3,122	3,290	3,238	3,330	3,695
Ti	0,009	0,003	0,000	0,005	0,003	0,001
Fe ³⁺	0,193	0,299	0,186	0,316	0,262	0,069
Fe ²⁺	0,336	0,355	0,503	0,318	0,301	0,186
Mn	0,012	0,000	0,001	0,007	0,000	0,008
Ca	0,000	0,003	0,001	0,000	0,000	0,008
Mg	0,163	0,221	0,020	0,116	0,104	0,041
K	1,721	1,815	1,834	1,731	1,728	1,784
Na	0,091	0,066	0,041	0,102	0,099	0,135
Al	0,316	0,394	0,300	0,387	0,399	0,126

Tableau 2
Les formules cristallochimiques de quelques muscovites
des pegmatites de Crişeni-Muntele Rece

Formules cristallochimiques	
M 7.1	$(K_{1,721}Na_{0,091}Ca_{0,000})_{1,812}(Al_{3,287}^{VI}Fe_{0,193}^{3+}Fe_{0,336}^{2+}Mg_{0,163}Mn_{0,012}Ti_{0,009})_4(Si_{6,317}Al_{1,683}^{IV})_8O_{20}(OH, F)_4$
M 7.2	$(K_{1,815}Na_{0,066}Ca_{0,003})_{1,884}(Al_{3,122}^{VI}Fe_{0,299}^{3+}Fe_{0,355}^{2+}Mg_{0,221}Mn_{0,000}Ti_{0,003})_4(Si_{6,397}Al_{1,603}^{IV})_8O_{20}(OH, F)_4$
M 14.17	$(K_{1,834}Na_{0,041}Ca_{0,001})_{1,876}(Al_{3,290}^{VI}Fe_{0,186}^{3+}Fe_{0,503}^{2+}Mg_{0,020}Mn_{0,001}Ti_{0,000})_4(Si_{6,301}Al_{1,699}^{IV})_8O_{20}(OH, F)_4$
M 11.23	$(K_{1,731}Na_{0,102}Ca_{0,000})_{1,833}(Al_{3,238}^{VI}Fe_{0,316}^{3+}Fe_{0,318}^{2+}Mg_{0,116}Mn_{0,007}Ti_{0,005})_4(Si_{6,387}Al_{1,613}^{IV})_8O_{20}(OH, F)_4$
M 11.32	$(K_{1,728}Na_{0,099}Ca_{0,000})_{1,827}(Al_{3,330}^{VI}Fe_{0,262}^{3+}Fe_{0,301}^{2+}Mg_{0,104}Mn_{0,000}Ti_{0,003})_4(Si_{6,339}Al_{1,661}^{IV})_8O_{20}(OH, F)_4$
M 16.48	$(K_{1,784}Na_{0,091}Ca_{0,008})_{1,927}(Al_{3,695}^{VI}Fe_{0,069}^{3+}Fe_{0,186}^{2+}Mg_{0,041}Mn_{0,008}Ti_{0,001})_4(Si_{6,126}Al_{1,874}^{IV})_8O_{20}(OH, F)_4$



Fig. 4 - Le diagramme de corrélation Mg : Al_{VI}

lée par nous est - tel le cas des données expérimentales - 24 % molécule-gramme (c'est à dire 2 % de poids Na₂O).

Le diagramme Fe²⁺ : Ti (Fig. 5) montre une corrélation légèrement positive entre ces deux éléments, pendant que la corrélation entre Na et K soit négative (Fig. 6), ce que signifie la substitution de ces deux éléments alcalins entre eux; le diagramme Ti : Al^{VI} (Fig. 7) ne met pas en évidence l'existence de quelque corrélation entre les deux éléments. D'autre part, le diagramme Al^{VI} : Al^{IV} (Fig. 8) montre une corrélation positive nette entre les deux types d'aluminium, ce qui semble surprenant à la première vue. Pourtant, en corrélant cette observation avec les résultats obtenus dans le cadre de l'étude des tourmalines provenant des mêmes corps pegmatitiques (Stumbea, in press), on peut tirer deux conclusions: (a) les muscovites se sont formées dans les conditions d'un apport substantiel d'aluminium; (b) ce trait caractéristique du processus d'engendrement se retrouve aussi chez les tourmalines dont les muscovites semblent être en relation épigénétique.

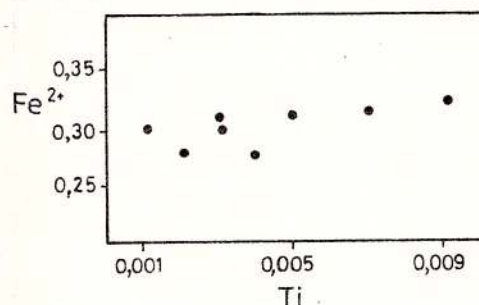
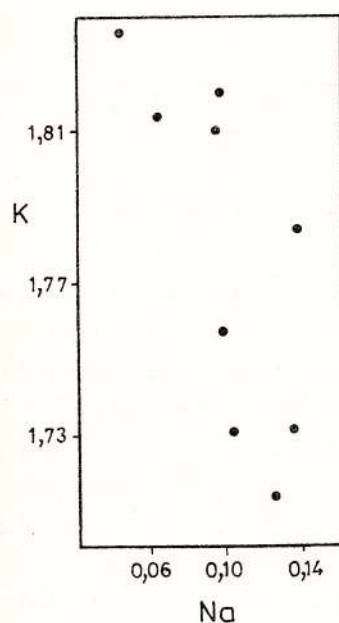
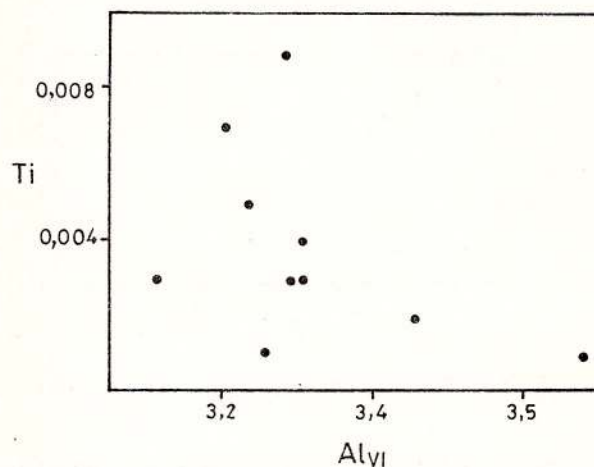
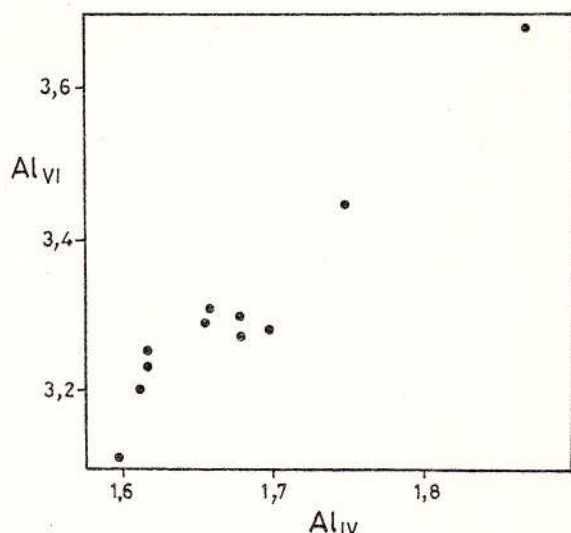
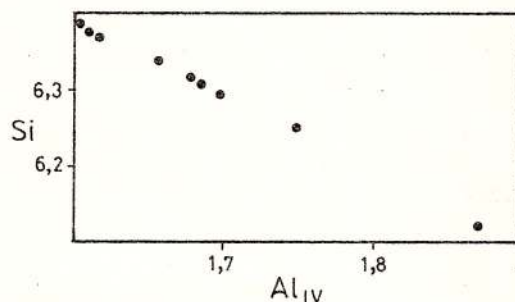
Fig. 5 - Le diagramme de corrélation Fe²⁺ : Ti

Fig. 6 - Le diagramme de corrélation K : Na

Fig. 7 - Le diagramme de corrélation Ti : Al_{VI}

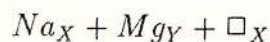
Fig. 8 - Le diagramme de corrélation $Al_{VI} : Al_{IV}$

La substitution du Si^{4+} par Al_{IV}^{3+} dans les sites tétraédriques - c'est pas étonnant - est évidente, fait démontré par la corrélation négative entre les deux éléments (Fig. 9). Le rapport quantitatif $Si^{4+} : Al_{IV}^{3+}$ dans ces sites a été calculé à l'aide du paramètre a_{Si} qui varie entre 20,03 et 23,42 %; ces valeurs sont caractéristiques pour les muscovites des pegmatites et elles sont en accord avec les données publiées par Murariu (1979) pour les pegmatites de Monts Rodnei.

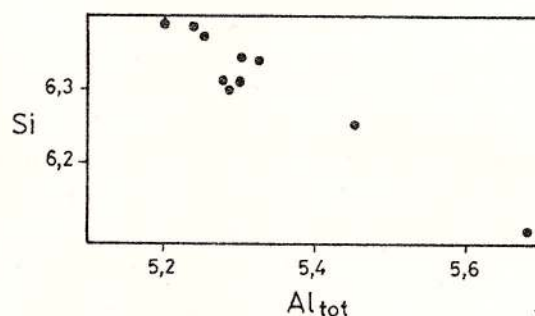
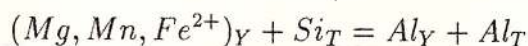
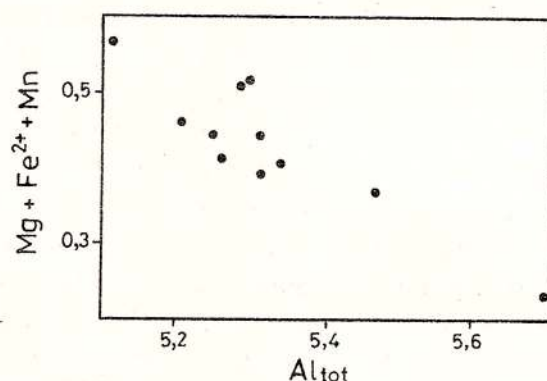
Fig. 9 - Le diagramme de corrélation $Si : Al_{IV}$

Les formules cristallographiques montrent une participation importante des alcali dans les sites X (1,812-1,927). Pourtant, on peut observer un déficit dans ces positions, ce qui se trouve en corrélation avec l'excès en aluminium dans les sites Y et correspond à un

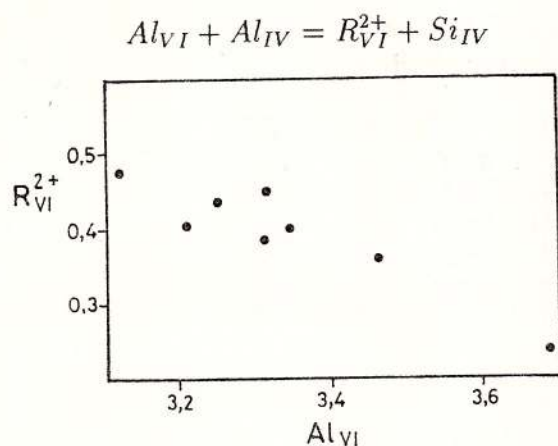
cas typique de substitution au déficit en alcali (Henry et Guidotti, 1985):



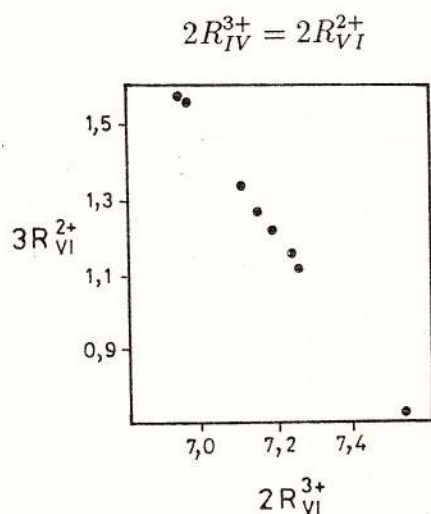
Les diagrammes $Si : Al_{tot}$ (Fig. 10) et $(Mg+Mn+Fe^{2+}):Al_{tot}$ (Fig. 11) mettent en évidence une corrélation négative entre les deux paires de valeurs, ce qui représente un argument en faveur de la manifestation d'une substitution de type Tschermak; cette substitution a lieu par le mécanisme suivant:

Fig. 10 - Le diagramme de corrélation $Si : Al_{tot}$ Fig. 11 - Le diagramme de corrélation $(Mg + Fe^{2+} + Mn) : Al_{tot}$

Un autre type de substitution qui se manifeste dans les muscovites étudiées par nous, est la substitution phengitique; cette manifestation est prouvée par les corrélations négatives mises en évidence dans les diagrammes $Si : Al_{IV}$ (Fig. 9) et $R_{VI}^{2+} : Al_{IV}$ (Fig. 12) et a lieu par le mécanisme:

Fig. 12 - Le diagramme de corrélation $R_{VI}^{2+} : Al_{VI}$

Enfin, la corrélation négative montrée par le diagramme $3R_{VI}^{2+} : 2R_{VI}^{3+}$ (Fig. 13) relève la substitution dioctaédrique-trioctaédrique qui se manifeste dans les échantillons analysés par nous:

Fig. 13 - Le diagramme de corrélation $3R_{VI}^{2+} : 2R_{VI}^{3+}$

Les muscovites des pegmatites de Crișeni - Muntele Rece sont caractérisées par la participation des termes "muscovite", "ferri-muscovite", "picrophengite" et "ferrophengite". La projection des valeurs correspondant aux muscovites étudiées par nous dans les diagrammes des figures 14 et 15 met en évidence

la disposition des points dans les champs situés entre les termes "muscovite" et "phengite".

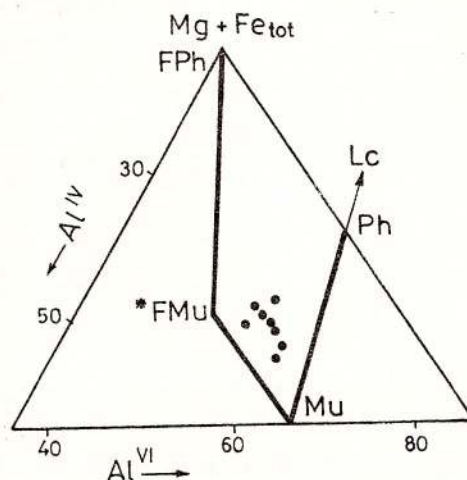


Fig. 14 - Le diagramme $(Mg + Fe_{tot}) : Al_{IV} : Al_{VI}$. FMu-ferrimuscovite; *FMu-ferrimuscovite de Kanehir et Banno (1960()); Mu-muscovite; Ph-phengite; FPh-ferriphengite; Lc-leucophyllite; Cd-céladonite.

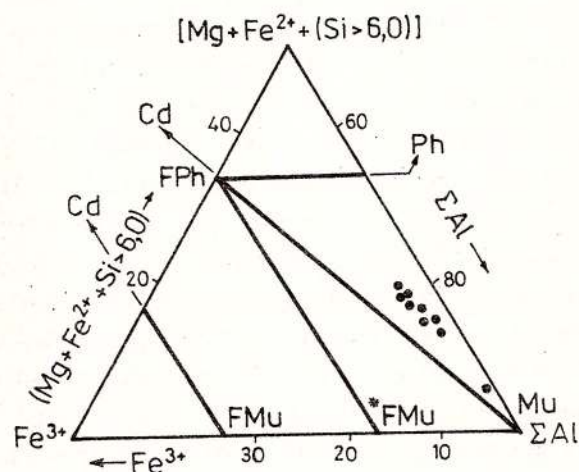


Fig. 15 - Le diagramme $[Mg + Fe^{2+} + (Si > 6,0)] : Fe^{3+} : Al_{tot}$. Les symboles sont les mêmes que dans la Figure 14.

Ces deux diagrammes offrent seulement une information qualitative sur la participation des divers termes de la muscovite. Pour obtenir des informations qualitatives, on a calculé la composition normative de ces muscovites (Tab. 3).

Tableau 3
La composition normative de quelques muscovites
des pegmatites de Crişeni-Muntele Rece

	M 7.1	M 7.2	M 14.17	M 11.23	M 11.32	M 16.48
Muscovite	28,21	20,05	37,65	29,30	35,22	69,53
Ferrimuscovite	18,37	16,47	9,41	24,18	20,47	5,43
Picrophengite	17,52	24,35	2,02	12,43	11,37	4,52
Ferrophengite	35,89	39,12	50,91	34,07	32,93	20,51

A partir de ces résultats on a construit les diagrammes de la figure 16; le diagramme de la figure 16a présente l'intervalle de variation de la participation des quatre termes, pendant que le diagramme de la figure 16b montre la moyenne de leur participation. On peut observer une participation égale des termes "muscovite" (34,09 %) et "ferrophengite" (34,77 %) et une participation moins importante des termes "ferrimuscovite" (17,50 %) et "picrophengite" (11,59 %). La participation réduite par rapport aux données publiées dans les ouvrages géologiques roumains (Murariu, 1979) peut être mise au crédit du déficit en alcali dans les sites X; ça, au cas échéant que ce déficit ne soit pas seulement apparent (dans la situation où une certaine participation du lithium dans les sites Y mettrait disponible une quantité de magnésium, fer bivalent et manganèse qui peuvent ainsi pénétrer les position X).

Le diagramme $Al^{VI} : Al^{IV}$ (Černý, 1982) (Fig. 17) montre la disposition des points correspondant aux muscovites étudiées par nous, au voisinage et même dans le champ des pegmatites à muscovite. Ce résultat semble confirmer l'hypothèse de la genèse métamorphique des pegmatites de Crişeni - Muntele Rece, mais déplace leur profondeur d'engendrement entre 7-8 et 10-11 km (Ginsburg et al., 1979).

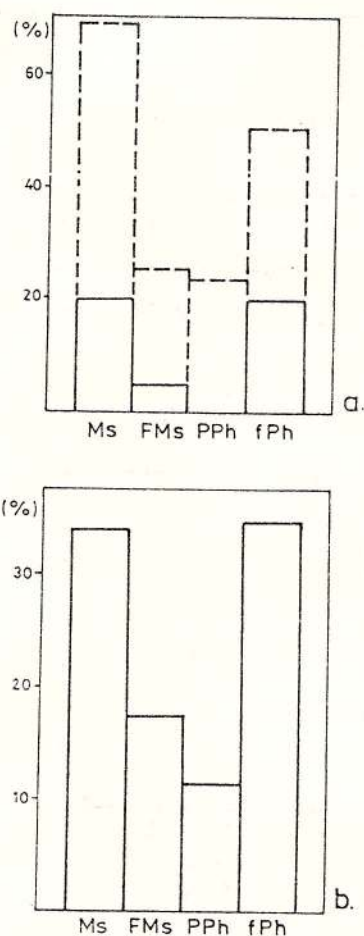


Fig. 16 - Diagrammes avec la composition normative des muscovites de Crişeni-Muntele Rece. a- la variation de la participation des termes: 1-valeurs maximum, 2-valeurs minimum; b-la moyenne de la participation des termes. Mu-muscovite; FM-ferrimuscovite; PPh-picrophengite; fPh-ferrophengite.

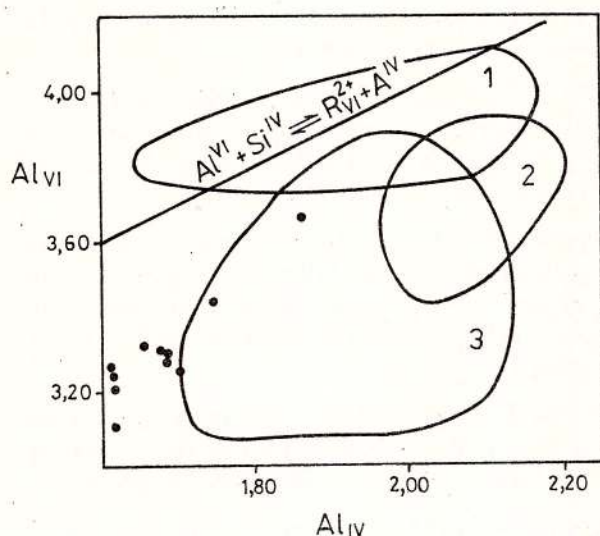


Fig. 17 - Les substitutions octaédriques-tétraédriques dans les muscovites des pegmatites (1) à éléments rares; à éléments rares jusqu'à muscovites; (3) à muscovites.

Le diagramme de Foster (1960) (cité par Bailey, 1984) (Fig. 18) vient confirmer les conclusions tirées auparavant.

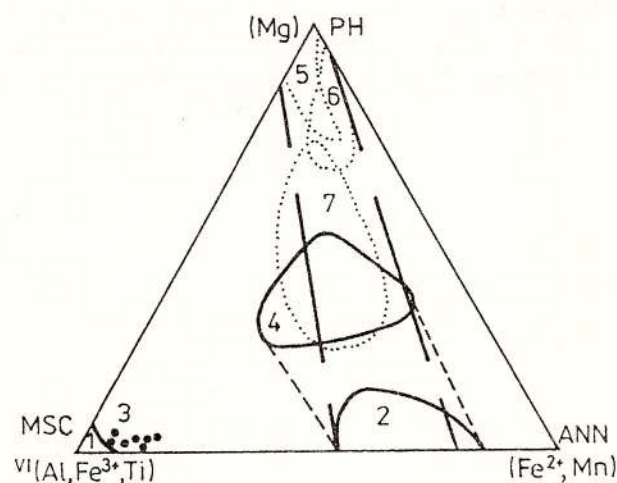


Fig. 18 - La composition de quelques muscovites des pegmatites dans le diagramme ternaire Mg : (Al + Fe³⁺ + Ti)_{VI} : (Fe²⁺ + Mn) (Foster, 1960). 1, muscovite et 2, biotite des pegmatites à éléments rares; 3, muscovite et 4, biotite des pegmatites à muscovites; 5, phlogopite d'exo-contact (marbres); 6, phlogopite d'exo-contact (roches ultramaphiques); 7, mica ferromagnésien à alcali rares.

Finalement, on va présenter le domaine des températures d'engendrement pour les muscovites de corps pegmatitiques étudiées. En utilisant le diagramme de phase au domaine sous-solidus pour le système muscovite-paragonite (Eugster et Yoder; cités par Pomârleanu, 1971), on a obtenu pour les muscovites de Crișeni - Muntele Rece, un intervalle de température compris entre 340° et 380° C. Ce domaine est caractéristique plutôt au début du stade hydrothermal d'évolution, ce qui nous fait penser que les muscovites des veinules microscopiques qui traversent les cristaux de tourmaline se sont formées pendant le stade final du processus pegmatitique-pneumatolytique, en passant vers le stade hydrothermal. D'autre part, cet intervalle s'encadre dans le domaine de température 280°-580° C, spécifique aux muscovites d'un grand nombre de pegmatites granitiques du monde.

4. Conclusions

L'étude géochimique sur les muscovites des corps pegmatitiques de Crișeni - Muntele Rece nous a permis de tirer les conclusions suivantes:

- les pegmatites appartiennent aux types céramique et muscovitique; elles ont pris naissance à des profondeurs comprises entre 7-8 et 10-11 km, probablement par des processus d'anatexie-granitisation, dans des conditions ultramétamorphiques;
- les teneurs en silice et alumine correspondent aux intervalles de valeurs publiées pour les muscovites des pegmatites de Roumanie;
- les formules cristallographiques et le calcul des compositions normatives nous ont montré que les muscovites se sont formées dans les conditions d'un apport substantiel en aluminium;
- le magnésium, le fer et le manganèse peuvent remplacer l'aluminium dans les sites octaédriques, pendant que le titane substitue faiblement le fer bivalent et ne remplace pas

l'aluminium dans les mêmes sites;

– les éléments alcalins peuvent se substituer entre eux dans les sites X; il y a un certain déficit dans ces positions;

– on a mis en évidence quatre types de substitution au sein de ces muscovites: substitution au déficit en alcali, Tschermak, phengitique et substitution dioctaédrique-trioctaédrique;

– la composition normative montre la participation égale des termes "muscovite" et "ferrophengite" et une participation plus réduite des termes "ferrimuscovite" et "picrophengite";

– le domaine de température pour l'engendrement des muscovites étudiées est compris entre 340⁰ et 380⁰ C, ce qui signifie que ces minéraux se sont formés à la fin du stade pegmatitique-pneumatolytique et au début du stade hydrothermal;

– les muscovites et les tourmalines dont elles s'associent, présentent quelques caractéristiques communes: ces minéraux se sont formés dans les conditions d'un excès en aluminium et de la manifestation des substitutions Tschermak et au déficit en alcali.

Ginsburg, A.E., Timofeev, I.N., Feldman, L.G. (1979) Principles of geology of the granitic pegmatites. Nedra, 296 p.

Henry, D.J., Guidotti, C.V. (1985) Tourmaline as a petrogenetic indicator mineral: An example from the staurolite-grade metapelites of NW Maine. *Am. Mineral.*, 70, p. 1–15.

Mârza, I. (1980) Considérations génétiques sur les pegmatites du cristallin du Gilău (Monts Apuseni) et la province pegmatitique carpatique. *An. Inst. Geol. Geofiz.*, LVII, p. 423–431, București.

Murariu, T. (1979) Studiul mineralogic, geochemic și structural al pegmatitelor din Munții Rodnei. *St. tehn. econ.*, Ser. I, 15, 264 p., București.

Norton, J.J. (1973) Lithium, Cesium and Rubidium – the rare alkali metals. *U.S. Geol. Surv. Prof. Pap.*, 820, p. 365–378.

– (1983) Origin of lithium-rich pegmatitic magmas, southern Black Hills, South Dakota. *Geol. Soc. Am., Rocky Mt. Sect.*, 34 Ann. Meeting Rapid City, Abstr. Progr., 221 p.

Pomârleanu, V.V. (1971) Geotermometria și aplicarea ei la unele minerale din România. Ed. Acad. Rom., 158 p., București.

Stumbea, D. (in press) L'étude de la tourmaline des pegmatites de Crișeni-Muntele Rece (Monts Apuseni). *Anall. Univ. "Al.I.Cuza" Iași*.

Bibliographie

Bailey, S.W. (1984) *Micas. Rev. Mineral.*, 13, 584 p., Chelsea-Michigan.

Černý, P. (1982) In: Černý, P. (ed.), *Mac Course Handbook*, 8, Min. Assoc. of Canada, 555 p., Winnipeg.

Received: December 10, 1995



GLAUCONITIC MINERALS FROM THE TRANSYLVANIA BASIN. NEW MINERALOGICAL DATA

Dana POP, Ioan BEDELEAN

Catedra de Mineralogie-Petrometalogenie Univ. "Babeş-Bolyai"

Str. M. Kogălniceanu 1, 3400, Cluj-Napoca

Key words: Glauconitic minerals. "Glaucanie". Density. Refractive index. Optical microscopy. SEM. XRD. Eocene. Miocene. Transylvania Basin.

Abstract: The presence of the glauconitic minerals in the Transylvania Basin was registered a long time ago (Hauer & Stache, 1863; Koch, 1900) but they were considered mainly as a lithologic-stratigraphic marker: the glauconitic level from the Căpuş Beds (Upper Lutetian, Eocene) or the limit between the Coruş/Chechiş Beds (Eggenburgian, Miocene). The samples were optically examined (in thin sections) and then submitted to a granulometric and electromagnetic separation; the density, the refractive index, the SEM and XRD behaviour of the hand-picked green grains were analyzed. The conclusions on the above-mentioned analytical methods are, as follows: - the structure consists of an irregular interlayering of a ferriferous mica ("illite"-type) and expandable layers ("smectite"-type), showing the 1M, 1Md and <1Md polytypes; - Eocene "glaucanites" (15 % exp.) are more evolved than the Miocene ones (25 % exp.); - the lithofacies control upon the maturity degree seems to be proved for the Eocene "glaucanites".

Introduction

Green silicatic sedimentary grains have been studied by many specialists, since the 60's and 70's (Burst, 1958; Toler & Hower, 1959; Odin, 1972, 1975; Odin & Matter, 1981), as the XRD and SEM techniques became usual and the mineralogical heterogeneity became certain. In 1978 the AIPEA Nomenclature Commission proposed the classifying criteria and redefined the mineral varieties of the glauconitic minerals (Odom, 1984).

The glauconite s.s., or the "ordered glauconite" is described as a potassium and iron (Fe^{3+})-rich with an ordered structure (less

than 10 % expandable layers) and the 1m polytype (layer stacking sequence).

"Disordered glauconites" are mineral mixtures containing an iron-rich mica ("illitic"-type) and 10 to 20 % expandable layers ("smectitic"-type). The polytype is generally 1Md.

"Interstratified glauconite/smectite" (G/S, 10 - 14s) is characterized by a minimum potassium content, an extremely disordered structure (1Md or < polytype) caused by the common random mixed-layering and a participation of the expandable layers between 20-60 %.



Compositional, structural and morphological characteristics reflect the glauconitization evolutionary stage reached by the organic or mineral substratum undergoing authigenous crystal growth, the direction of evolution being from the mixed-layer, opened, disordered mineral to the closed, ordered one.

The term "*glauconie*" (in Greek meaning bluish or pale green) was first used by Brogniart (1823). Keferstein (1828) proposed "*glauconite*", without any specification about the mineralogical or morphological meaning of this word (Odom, 1984).

"*Glaucony*" (Odin & Matter, 1981) (pl. "*glauconies*") is used here as a morphological, faciesal term, therefore it should not be confused with the above-mentioned mineral species (AIPEA classification).

Celadonite (proposed by Glocker, 1847 from the French word "*celadon*", meaning pale or sea green; in Odom, 1984) is a dioctahedral mica, very similar to glauconitic minerals, associated with igneous rocks, mainly basalts. It has a lower tetrahedral charge, an increased crystallinity (sharp peaks on diffractograms), usually of 1M polytype. From a chemical point of view, celadonites possess more K in the interlayer, Mg in the octahedral sheet and Si in the tetrahedral one (Odom, 1984). The different modes of occurrence usually serve to differentiate the two minerals.

Stratigraphical control

"*Glauconie*" occurrences in the Transylvania Basin have been recorded a long time ago (Hauer & Stache, 1863; the Eocene level). This macroscopically easy detectable mineral particularly helped much in the lithological-stratigraphical correlation.

Two stratigraphical levels with dominant glauconitic minerals are almost continuous on large areas in the north-western part of the Transylvania Basin.

The glauconitic level enclosed by the Căpuș Beds (Eocene, Upper Lutetian) may be ob-

served in the Gilău - Luna de Sus - Săvădisla - Lita area (Stoicovici & Mureșan, 1964; Mureșan & Tătărim, 1967) associated, in the Căpuș area, with the ferruginous oolitic formation. However, isolated occurrences are known westwards, in the Huedin-Călățele area (Hauer & Stache, 1863; Răileanu & Saulea, 1956; Mureșan & Stoicovici, 1987), the extreme northern outcropping point being Răpaosului Valley (Ortelec) (Rusu, 1967; 1987). Such a distribution leads to the idea of a continuous (autochthonous ?) sequence with distinct facies significance along the whole western basin border.

The second level in which the predominance of the glauconitic minerals is diagnostic is that at the Coruș/Chechiș Beds boundary (Miocene, Eggenburgian), characterized by a lithological uniformity and a remarkable extension (Șuraru, 1967) between Coruș, in the south, and Surduc - Cristolțel, in the north (about 70 km in length and 0.5 - 3 m in thickness). This level has been a stratigraphical bench mark even in the first bibliographical records (Koch, 1900) (Fig. 1).

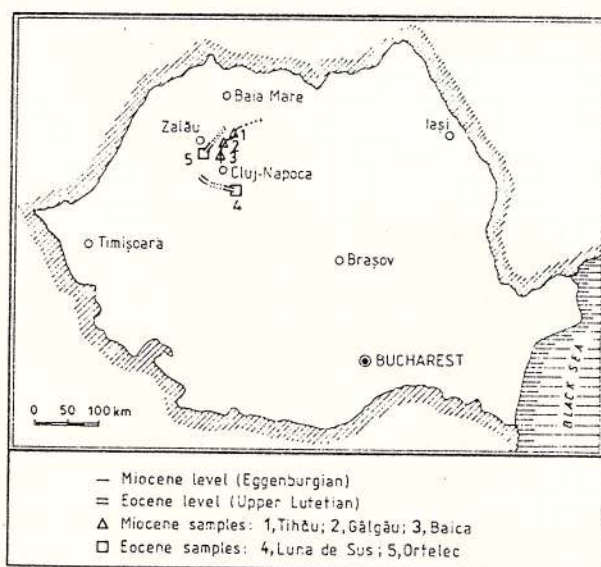


Fig. 1 - Repartition of the "*glauconie*" occurrences

Other "*glauconie*" occurrences in the Transylvania Basin are mentioned in the Creta-

ceous period (Bielz, 1889; Mareş & Todiriță-Mihăilescu), as well as in the Oligocene deposits (A. Rusu, personal communication).

The samples were collected from several formations of various petrographical compositions and they include only a part of the outcropping areas of the Eocene and Miocene sequences (Tab. 1). The profiles in the Dâmbu Rotund Hill (Luna de Sus, Cluj distr.), for the Eocene deposits, and that at Corbul Cornilor (Tihău, Sălaj distr.), for the Miocene ones, are represented in Figures 2, 3.

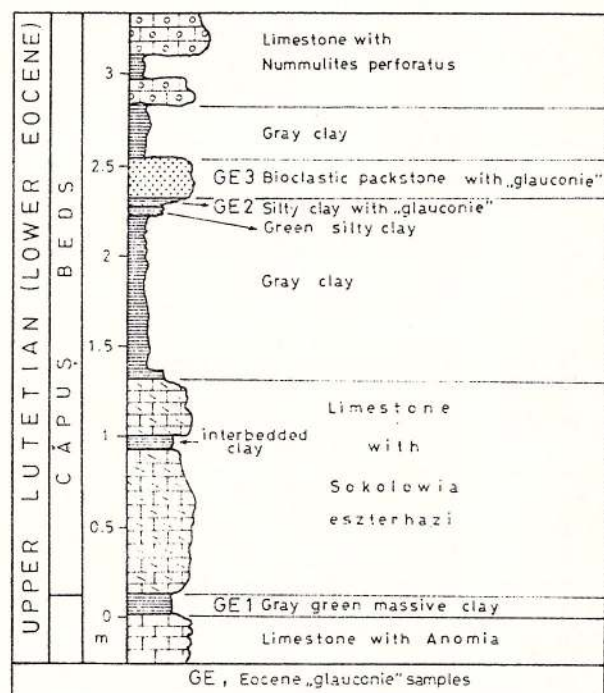


Fig. 2 – Profile in the dâmbu Rotund Hill (Luna de Sus, Cluj distr.)

The separation method of glauconitic grains

The method suggested by Odin (1969) was used, with slight changes determined by the devices employed (Fig. 4).

Electromagnetic separation (in the absence of a Frantz isodynamic separator) allowed to obtain a magmatic fraction, a non-magmatic one respectively, whose compositions and characteristics are rendered in Table 2.

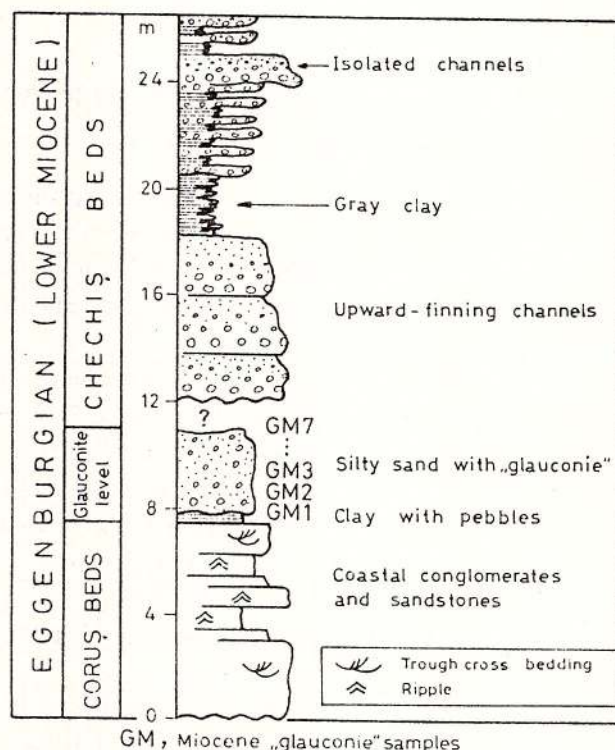


Fig. 3 – Profile at Corbul Cornilor Hill (Tihău, Sălaj distr.)

The green grains hand-picked under the binocular were submitted to an examination by X-rays diffraction (in oriented samples and powder mounts) and an optical one (in thin sections and by SEM).

Density determination

Density is an important physical parameter in determining the mineralogical type of "glauconite". A positive correlation exists between the density index and the colour intensity of the grains (Odin, 1975; Odin & Matter, 1981), as well as the amount of iron (Cimbalnikova, 1970a) or of potassium and, respectively, a negative one with the extent of expandable layers within the interstratified structures G/S, and the water amount in the interlayer region (Odin, 1975).

All these variables of the glauconitogenesis define, by certain limits reached at different

Table 1
Occurrences and petrographic description of samples

No. of sampl.	Macro- and microscopic petrographical characteristics	Occurrence
GE	Plastic, massive grey-greenish clay + subangular quartz clasts, poorly sorted (30 %)	Dâmbu Rotund Hill, Luna de Sus (Cluj distr.)
GE 2	Argillaceous silt with "glaucanie" + quartz, muscovite clasts and carbonatic bioclasts	Dâmbu Rotund Hill, Luna de Sus (Cluj distr.)
GE 3	Bioclastic packstone + quartz clasts with green films on fissures; microsparitic cement	Dâmbu Rotund Hill, Luna de Sus (Cluj distr.)
GE 4	Glaucinitic silty clay + quartz clasts; medium sorted	Răpaosului Valley, Ortelec (Sălaj distr.)
GM 1	Clay with pebbles + quartzite lithoclasts and quartz crystalloclasts	Corbul Cornilor Hill, Tihău (Sălaj distr.)
GM 2	Glaucinitic silty sand + argillaceous matrix, quartzite lithoclasts; poorly sorted	Corbul Cornilor Hill, Tihău (Sălaj distr.)
GM 3	Glaucinitic silty sand; uneven, poorly sorted; bioturbation traces	Corbul Cornilor Hill, Tihău (Sălaj distr.)
GM 4	Glaucinitic silty sand; uneven, poorly sorted; bioturbation traces	Corbul Cornilor Hill, Tihău (Sălaj distr.)
	Glaucinitic silty sand; poorly sorted, with traces of settlement/compaction	Corbul Cornilor Hill, Tihă (Sălaj distr.)
GM 6	Glaucinitic silty sand (Gl=75%) + opaque minerals (10%) in argillaceous matrix	Corbul Cornilor Hill, Tihău (Sălaj distr.)
GM 7	Laminated sandy silt + opaque minerals in argillaceous matrix	Corbul Cornilor Hill, Tihău (Sălaj distr.)
GM 11*	Glaucinitic silty sand; poorly sorted	Baica (Sălaj distr.)
GM 19*	Glaucinitic silty sand	Dosurior Creek, Gâgău (Sălaj distr.)

(*) – samples from prof. Șuraru



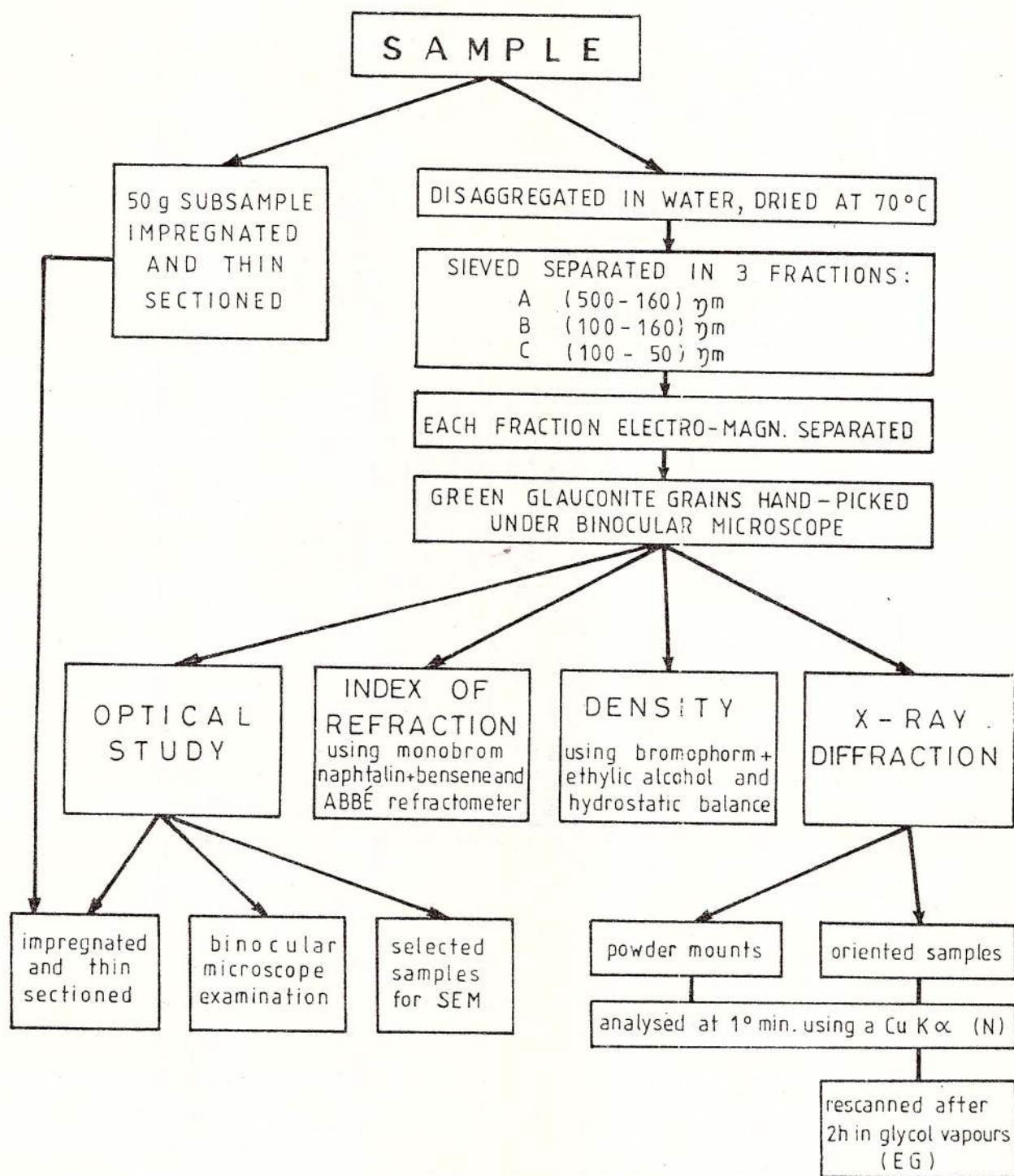


Fig. 4 – Flow-chart of methods of sample analysis

evolutionary stages, distinct mineralogical and genetic types.

According to various authors, values of "glauconies" density range between 2.2 and 2.9 g/cm³, though exceptional values of 3.1 g/cm³ were also mentioned (Odin & Matter, 1981).

In order to determine the density of the analysed samples we used several bromophorm and ethylic alcohol miscible mixtures.

The A granulometric fractions (the purest ones) of samples GE 2 and GM 2 have been used and, in each case, a different behaviour

Table 2
Macroscopical characteristics of magnetic and non-magnetic fractions

Sample	Granulometric fraction	Magnetic fraction				Non-magnetic fraction	
		"Glaucanie"		Other minerals			
		Frequency	Colour		Surface of grains		Morphological types and frequencies
GE 2	A	90 %	Dark green to black	Smooth glossy; cracks filled with a light green mineral (immature "glaucanie")	Fragmentary - 34% Spheroidal - 30% Lobate - 20% Ovoidal - 10% Fossil casts, molds - 5% light green grains - 1%	ferruginized organic fragments (sponge spicules, etc.) 5% - "limonitic" aggregates	Quartz(80%);angular to subangular, transparent, pink, white or affected by "verdissement", Calcedony-red colour, angular Calcite-crystaloclasts and organic (mollusc fragments, sponge spicules) Feldspar-prismatic, altered, mat Muscovite-lamellae Gypsum, Apatite (subordonately)
	B	75 %	-/-	-/-	Fragmentary - 40% Spheroidal - 35% Lobate - 10% Ovoidal - 10% Light green grains - 5% Fragmentary 90% Spheroidal - 10%	Quartz (25%): subangular, white, pink, smoky, yellow, frequently affected by "verdissement" process	-/-
	C	45 %	-/-	-/-		Quartz - (45%) coated with iron oxy-hydroxides Muscovite, Biotite lamellae (10%), Amphiboles, Rutile, Zircon	-/-
GM 2	A	99 %	Bluish-green to light green	Mat, coarse; on lobate grains, cracks filled with light green mineral	Fragmentary - 80% Lobate - 5% (largest in size) Spheroidal - 5% (all are smaller than the similar fraction in the Eocene sample)	Chlorite, Muscovite, Biotite, lamellae Quartz, subangular, transparent, "Limonite", Amphiboles, Rutile	"Glaucanie" pelloids (25%) Quartz (65%) angular to subangular, transparent, white frequently affected by "verdissement" Chlorite, Muscovite, (Biotite) lamellae Polymneral aggregates in "limonitic" cement, Feldspars
	B	85 %	Light green to yellowish green	-/-	Fragmentary -90% Spheroidal - 10%	-/-	-/-
	C	60%	-/-	-/-	Fragmentary 100 %	-/-	-/-



of the glauconitic grains, due to different densities, was noticed.

For the Eocene "glauconies" (GE 2-A), the extreme values 2.7 and 2.9 g/cm³ were recorded but the density of the grains deposited at the liquid bottom – owing to the lack of corresponding heavy liquids – could not be quantified. We assume that the high density of some of the Eocene glauconitic grains may be related to an oxidation process which is obvious in the Căpuș area.

The density of Miocene "glauconies" proved to vary within more narrow limits, ranging between 2.50 and 2.54 g/cm³.

Density difference between the two samples as well as colour variation leads to a first supposition concerning the mineralogical types. Thus, we may consider that Eocene "glauconies" are characterized by more ordered and evolved structures than the Miocene ones; the latter are more immature, containing crystallites with less ordered structures.

Refractive index determination

For this determination, A granulometric fractions of the same samples GE 2 and GM 2 were used in order to give the opportunity

to compare the optical parameters of the glauconitic grains of different ages. It is already well known the positive correlation between refractive index (n) and iron content as well as the structural order degree of the glauconitic minerals. There is a reverse correlation between n and the number of expandable layers (Odin & Matter, 1981).

The method of miscible liquids was employed, i.e. monobromnaphthalen ($n = 1.6571$) and benzene ($n = 1.500$), according to the variation limits of "glaucony" refractive index. The following values were obtained;

GE 2-A (Eocene) $\alpha = 1.594$; $\beta = \gamma = 1.604$

GM 2-A (Miocene) $\alpha = 1.582$; $\beta = \gamma = 1.604$

Depending on the average refractive index ($n = (\alpha + \beta)/2$), the two samples were represented in the Toler & Hower (1959) diagram, which expresses the relationship between the refractive index and the extent of expandable layers (Fig. 5). According to this diagram, a content of about 25 % expandable layers in the Eocene glauconitic minerals and about 28 % in the Miocene ones can be estimated, therefore in both cases the optical parameters indicate disordered interstratified varieties of G/S type.

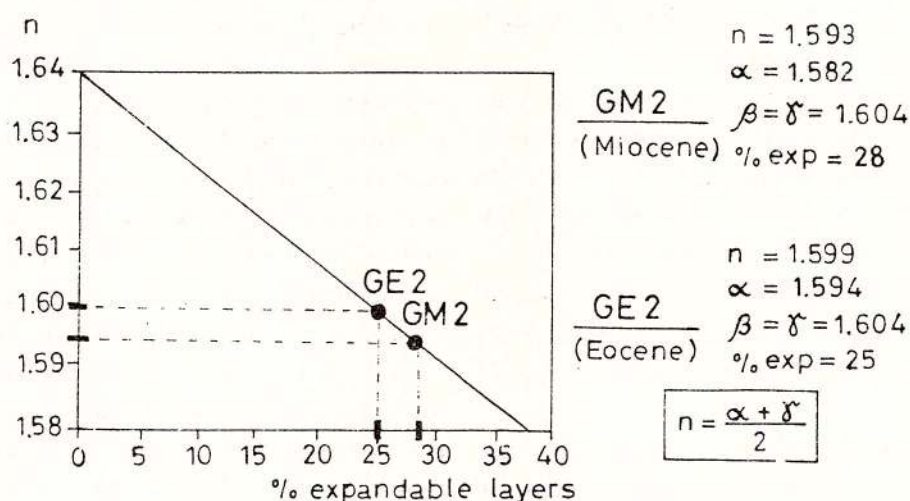


Fig. 5 – Relation between refractive index and per cent expandable layers (after Toler & Hower, 1959)



Optical microscopy

Petrographical characteristics (composition and fabric) of the host rocks (Table 1) and, especially, the microstructural aspects of the glauconitic grains were studied in thin sections, under plane polarized light.

The morphological types are given according to Triplehorn's (1966) classification, revised after Odin (1975), Odin & Matter (1981).

The granular type (Odin & Matter, 1981) is predominant in the studied samples, "peloids" (*sensu* Pettijohn, 1975 and Fischer, 1987) being generally ovoidal, spheroidal shaped, subrounded (Pl. I, Figs. 1, 2).

Lobate, mammilate peloids suggesting their formation by the substitution of foraminiferal internal molds or by the incomplete fragmentation of the initial grains (after opening some surface cracks in the process of crystal growth) in samples GE 3, GM 3, GM 7, GM 11 (Pl. I, Fig. 2) appear subordinately.

Light-greenish vermicular peloids consisting of quasiparallel or fan-like crystalline (Pl. I, Fig. 5), slightly pleochroic and with a typical extinction can also be found in samples GM 3 and GM 11. In this case, a micaceous substratum may be supposed, arguments being offered by the SEM study (see the "according" type, *sensu* Odin, 1972).

As far as sample GE 3 is concerned, we may notice in some cases the existence of green-yellowish fillings of the nummulites chambers (abundant in the rock), the mineralogical nature of which could not be determined.

Also, an authigenous, light-greenish mineral develops on cracks of quartz crystalloclasts and quartzite lithoclasts in samples GE 3, GM 3 and GM 7.

For these two situations we may only suppose a poorly developed glauconitic mineral, of the green film (pelicular) type described by Odin & Matter (1981), without any clear mineralogical arguments. SEM images (Pl. III, Fig. 6) prove the existence of the lamellar, automorphic development of this mineral.

Microphotographs of the analyzed samples are representative especially of the internal "fabric" of the glauconitic peloids (*acc.* to Mc Conchie & Lewis, 1980).

Random microcrystalline internal textures, the most usual and implying the existence of a homogeneous material as a substratum of glauconitization, are predominant (Pl. I, Figs. 1, 4, 5).

In Figure 1, Plate I a fibro-radial rim, with a higher birefringence, surrounds peloids with random internal texture, but it cannot be specified if it is the tangential layer "c" of the "corona" structure, as it was described by Zumpe (1971).

Micaceous internal textures are characteristic of the glauconitic peloids which seem to have a 2:1 phyllosilicate mineral as substratum (Pl. I, Fig. 5).

Oriented microcrystalline internal textures, of "zebra" type (Odin, 1975) which point to a previous calcareous organic precursor (Pl. II, Figs. 1, 3) affected by the glauconitization process and surrounded by a random granular mass are also visible. On the detailed image (Pl. II, Fig. 2) the existence of concentric layers, caught in the microcrystalline aggregate ("fossilized"), can also be noticed. This "coating" type internal structure (according to Zumpe, 1971) illustrates successive episodes of sediment reworking – each of them followed by glauconitic accretion processes. These elements point to an autochthonous, probably perigenous origin, *sensu* Lewis, 1964 (accumulation within the same sedimentation basin, after a short distance transport) of the Miocene "glauconies" from sample GM 11.

Within the same Miocene samples we may notice the accidental predominance of composite glauconitic grains, with quartz inclusions (Pl. I, Figs. 5, 6). According to Harder (1980), a SiO_2 content of the iron hydroxide precipitate higher than necessary (about 6 ppm SiO_2) for the "glauconie" synthesis could be invoked in such cases.

The processes of crystal growth may be con-



sidered responsible for the formation of radial and concentric cracks (Pl. I, Figs. 1, 3), also visible on the SEM images (Pl. III, Fig. 2; Pl. IV, Figs. 2, 5).

Diagenetic compaction processes led to the formation of an argillaceous film, sometimes of thin muscovite lamellae coating glauconitic pelloids (Pl. I, Fig. 4; Pl. II, Fig. 4), or to the deformation of some elastic crystalloclasts (Pl. I, Fig. 4). Other times diagenesis proceed itself chemically, by filling cracks inside the grains and cementing them in amicrosparitic, carbonate mass (Pl. II, Fig. 5).

Scanning electron microscopy (SEM)

Scanning electron microscopy (SEM) was employed by several authors as an important classification criterion for differentiating glauconitic morphologic types and for identification of the substratum (mineral or organic), as well as of the stage reached by the process of glauconitization.

For the SEM study, grains ranging between 160–500 μm (A fraction) and 100–160 μm (B fraction) of the GE 2, GM 2 and GM 7 samples were chosen under the binocular, as they emphasize more clearly the glauconitic nanostructure.

The following substratum types could be outlined in the analyzed samples: foraminiferal molds (GE 2) (Pl. III, Fig. 1); lobate pelloids with an organomorph aspect (GE 2) (Pl. III, Fig. 3); fecal pellets with a characteristic longitudinal development and symmetrical and parallel microfissures (GE 2) (Pl. III, Fig. 4); micaceous lamellae ("accordion"-like) produced by expansion of the stratified structure due to the authigenic growth of glauconitic minerals between (001) planes (GM 2) (Pl. III, Fig. 5); quartz grains with "glauconie" (?) lamellae set on the fissures (GM 7) (Pl. III, Fig. 6).

This variety of substrata illustrates almost all the possibilities described by previous authors and accepted today as distinct, but similar

glauconitization ways. A single exception can be mentioned – that is organic lamellibranchiate remains, visible in thin sections (Pl. II, Figs. 1, 3).

The identification of the substratum may be of help to match the classification of morphological types described by McConchie & Lewis (1980). Thus, we can speak about ovoidal sphroidal pelloids (Pl. III, Figs. 1, 4), lobate pelloids (Pl. III, Fig. 3), vermicular grains (Pl. III, Fig. 5).

In sample GE 2 we can identify a peculiar morphological type, first described by McConchie & Lewis (1980), more exactly a "spongy glauconie", characterized by a porous earthy surface (Pl. IV, Fig. 1). The grain shown in Plate IV, Figure 2 is considered to be the closest to the serrulate subtype, having distinctly and sharply serrated protuberances and pores.

According to the SEM aspects, correlated with the XRD data, Odin (1975) depicted several evolutive stages of the crystallites, corresponding to the increase of ordering degree, from an expandable "smectite"-type to an "illitic"-type, potassium-enriched one.

In our samples, these stages are illustrated by the following nanostructural aspects:

a) "nascent", incipient stage – in case of the "spongy glauconie", on whose porous surface we can notice rounded protuberances of globular type (GE 2) (Pl. IV, Fig. 1);

b) slightly evolved stage – characterized by the crystallization of automorphic, small-sized 1–2 μm network-like spangles (GE 2) (Pl. IV, Fig. 3);

c) evolved stage – less frequently represented in the analyzed samples, suggested by lamellae networks and some rosettes of "glauconie" in the sample GM 2 (Pl. IV, Fig. 4).

On most grains, cracks ("croute de plain") generated by the increase of the volume of the polycrystalline aggregate (inner authigenous growth) can be noticed. On the walls of these cracks, typical evolved glauconitic lamellae develop (Pl. III, Fig. 2; Pl. IV, Figs. 2, 5).



The roundness degree of the "glaucanie" grains (mostly in case of the more fragile lobate type, Pl. III, Fig. 3), the "friction lenses" (Pl. IV, Fig. 6) and the impact "craters" from their surface (Pl. III, Fig. 1; Pl. IV, Fig. 5) represent indices of the autochthony/allochthony of the green grains in the host rock.

The X-ray diffraction (XRD) analysis

X-ray diffraction analyses have been carried out on samples GE 2-A and GE-B, as well as GM 2-A and GM 2-B (belonging to the same sample but to distinct granulometric fractions), GE 3-A and GE 4-A from Eocene deposits in different occurrences and from samples GM 2-A to GM 7-A at various levels of the same Miocene deposits.

The diffractograms obtained on a DRON diffractometer with a Cu anticathode are shown in Figure 6. The d/n and I values recorded by Warshaw (1957) (cf. Odom, 1984)

were used.

First of all, the presence of specific peaks of glauconitic minerals is obvious, on the left side of (020) peak: $(11\bar{1})$, for all the samples, excepting GE 2-B and GM 7-A (in which the splitting of the (020) peak is noteworthy), and (021) in the samples GE 3-A. These peaks, as well as (002), of low intensity, are diagnostic in differentiating glauconitic minerals versus illite.

For estimating the "opening" degree of the glauconitic minerals (that is the extent of expandable layers), the (001) peak shift toward small 2θ angles and the (003) peak decrease (Odin, 1975) were taken into consideration. The most "opened" glauconitic minerals are in samples GM 7-A and GM 2-A, all the others having a certain opening degree. Therefore, none of the samples contain perfectly closed glauconitic micas proper, but G/S interstratifications.

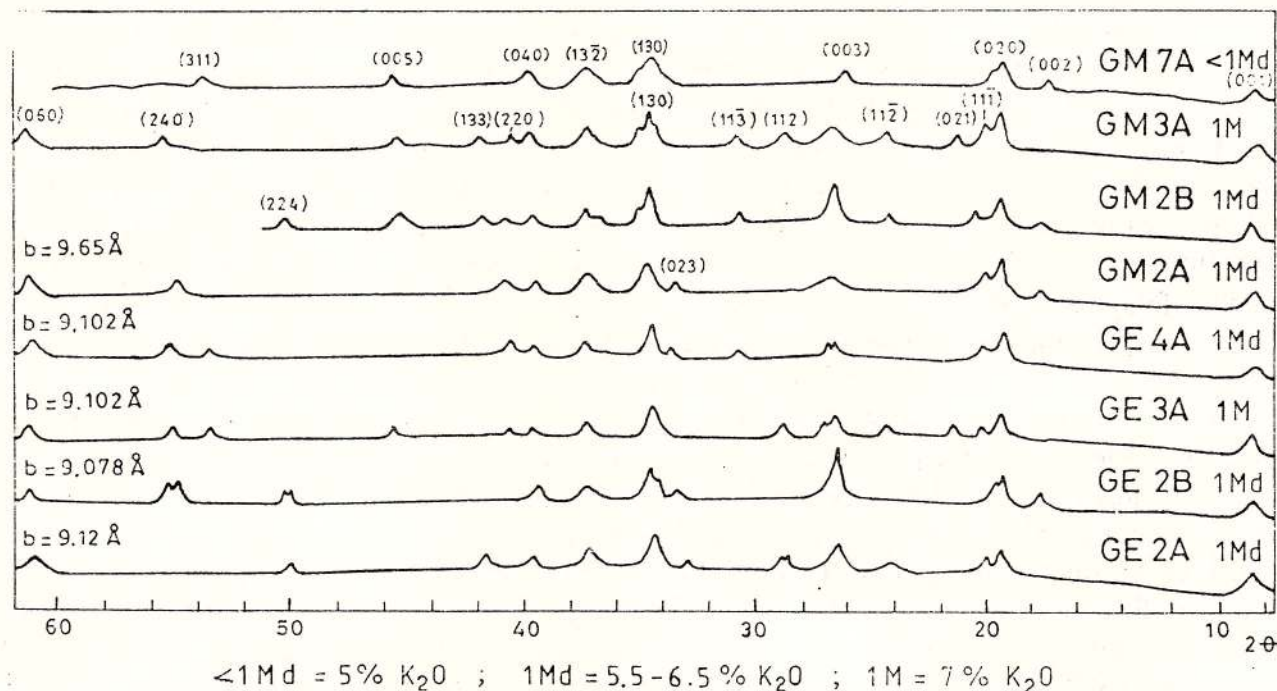


Fig. 6 - X-ray diffractograms (powder mounts) on "glaucanie" grains; GE 1 - GE 3: Eocene "glaucanie" from Dâmbu Rotund Hill; GE 4: Eocene "glaucanie" from Ortelec; GM 2 - GM 7: Miocene "glaucanie" from Corbul Cornilor Hill. Granulometric fractions: A = 160-500 μm ; B = 100-160 μm .

The layer-stacking sequence of expandable layers ("smectitic"-type) with the non-expandable ones ("illitic"-type) may be estimated by comparing the relative intensities of the group of peaks $(11\bar{2})$, (003) and (112) (Odin, 1975).

Approximately equal intensities of these peaks emphasize a more advanced degree of structural order (samples GE 3-A and GM 3-A). Lower values of the intensities of the $(11\bar{2})$ and (112) peaks, compared to the (003) peak intensity (GE 2-A), as well as the order of intensity decrease of the two symmetrical peaks against (003) (GM 2-B) – or their absence (GE 2-B, GE 4-A, GM 2-A, GM 7-A) – are a consequence of a lower structural order degree.

The (060) peak is located for all samples around the value $d = 1.51 \text{ \AA}$, a typical dioctahedral feature. As a consequence of the rather significant amount of iron, these glauconitic minerals have a mixed character, i.e. di- and trioctahedral (Odin, 1975).

Starting from the same (060) peak and using the calculation of b parameter: $b = d(060) \times 6 \text{ (\AA)}$ (Holtzapffel, 1975), values ranging between 9.08 and 9.65 \AA (Fig. 6) were obtained. They are higher than that recorded by Warshaw ($b = 9.066 \text{ \AA}$).

It is obvious that GE and GM 3-A samples consist of a glauconitic mineral which is closest to the micaceous structure 1M (glauconite s.s.). Both Eocene "glauconies" GE 2 (A, B) and GE 4-A, as well as the Miocene GM 2 (A, B) ones represent the 1Md polytype. Sample GM 7-A may be taken as an open, disordered mineral, with a layer stacking sequence resemblance, by distinct from that of the 1Md polytype. Therefore it has been included in the <1Md type (Fig. 6).

These polytypes are generally characteristic of the trioctahedral micas (Bailey ed., 1984) but in case of glauconitic minerals there is a mixed behaviour, as already shown.

Because the chemical data concerning the studied samples are absent, we employed the Odin's (1975) diagrams that relate the K_2O

content to some diffractograms features.

A content of about 5 % K_2O for sample GM7-A (<1Md), about 5.5 – 6.5 % K_2O for the samples with 1Md polytype (GE 2-A,B, GE 4-A, GM 2-A,B) and a content of about 7 % K_2O in the samples with the most evolved structure, 1M (GE 3-A, GM 3-A) (Fig. 6) can thus be estimated.

In order to determine the extent of expandable layers, some diffractograms on oriented samples (untreated and ethylene glycolated) from samples GE 2-A and GM 2-A (Fig. 7) were obtained.

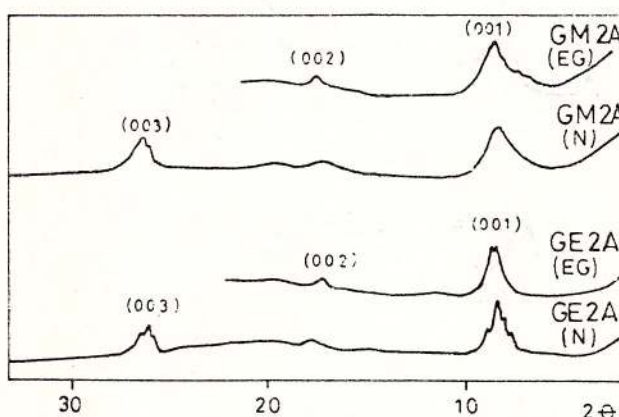


Fig. 7 – X-ray diffractograms (oriented samples): air dried (N) and glycolated (EG) on Eocene (GE 2-A) and Miocene (GM 2-A) samples.

On the ethylene glycolated samples, we used (001) peaks and compared the relative intensities of unmodified peaks ("illite" – type) with those shifted towards lower 2θ angles ("smectite" – type). The values were compared also with those given by Cimbalnikova (1970 b). About 15 % expandable layers for the Eocene "glauconies" (GE 2-A) and about 25 % expandable layers for the Eocene "glauconies" (GE 2-A) and about 25 % expandable layers for the Miocene (GM 2-A) ones were determined. These contents are lower than those obtained by using the refractive indices (Fig. 5).

According to these values, GE 2-A may be included within the G/S interstratifications, as far as the AIPEA classification is concerned.

Using the same diffractograms, the follow-

ing geometric indices were calculated: crystallinity index K_l (Kubler, Segonzac), complexity index I_c (Esquevin, White), sharpness ratio I_T (Weaver) and the opening index E_o (mellières, Perez-Nieto), currently employed for illite (Rocha & Gomes, 1990) (Fig. 8).

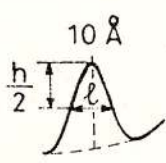
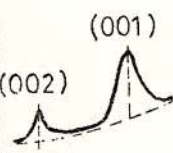
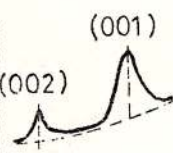
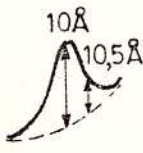
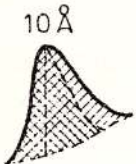

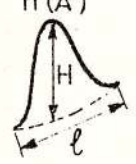
	GE 2-A (Eocene)	GM 2-A (Miocene)
 10 Å % expandable layers	15	25
 (001) (002) Crystallinity index (mm) K_l (Kubler, Segonzac)	8	19
 (001) (002) Complexity index (Esquevin, White) $I_c = \frac{I(001)}{I(002)}$	5.4 N.B. The ferriferous character compared with illite	8.23
 10 Å 10.5 Å Sharpness ratio (Weaver) $I_t = \frac{I(10 \text{ Å})}{I(10.5 \text{ Å})}$	2.08	1.32
 10 Å Opening index (Mellières, Perez Nieto) $E_o = 100 \times \frac{St - Si}{St}$ 	25	9.14
 $n(\text{Å})$ "Glaucanie" opening index* (Odin) $\phi = \frac{H}{l} \times (14 - n)$ (* powder mounts)	3.78	3.76
Polymorphs	1 Md	1 Md
CRYSTALLOGRAPHIC VARIETY	a) Mc Conchie, Lewis(1980) < 40 % exp.	DISORDERED GLAUCONITE A. Moderately B. Extremely
	b) Odin (1975)	DISORDERED OPEN GLAUCONITE $d(001) \in (10-11) \text{ Å}$
	c) Hower(1961)	DISORDERED GLAUCONITE 10-20 % exp. (RANDOMLY) INTERSTRATIFIED G/S > 20 % exp.

Fig. 8 – Crystallinity indices and conclusions on the XRD study (oriented samples and powder mounts).

The absolute values of these indices do not provide accurate structural data but, by comparison, we can estimate that Eocene glauconitic minerals (GE 2-A) are characterized by a relatively more evolved structure than the Miocene ones (GM 2-A).

These indices are completed by a specific parameter, showing the opening degree of the glauconitic minerals, that is the Φ coefficient (glauconite opening index) (Odin, 1975). For both samples very close values (GE 2-A: $\Phi = 3.78$; GM 2-A: $\Phi = 3.76$) were obtained. They are situated between the values given by the same author for a closed and ordered glauconite ($\Phi = 7.5$) and an opened, disordered glauconitic mineral ($\Phi = 1.5$).

After summing up the X-ray diffraction data and considering the crystallographic classifications given by various authors (Hower, 1961; Odin, 1975; McConchie & Lewis, 1980), we may conclude that the glauconitic minerals in the studied samples represent irregular interstratifications (mixed-layers G/S, or 10-14s), with variable degrees of structural ordering (Fig. 8).

Some other aspects can be emphasized:

- vertical variations in profiles within the same stratigraphical level are obvious (polytypes <1Md for GM 7-M, 1Md for Gm 2-A, B and 1M for GM 3-A), connected probably with the burial diagenesis;

- there are arguments which support the idea of a more evolved structure in case of the Eocene "glauconies", compared to the Miocene ones, but in both cases, the mineralogical types are disordered glauconite and interstratified G/S (AiPEA classification);

- there is a correlation between the petrographical composition of the host-rock and the evolution stage reached by the glauconitic minerals (Odin, 1975); in our case, glauconite with a micaceous-type structure (1M) - from sample Ge 3-A - is hosted by a bioclastic packstone, respectively, a more opened, less evolved

glauconitic mineral (1Md) - sample GE 2-A - was separated from a glauconitic silty-clay. Both samples belong to the same Eocene profile from Dâmbu Rotund Hill, Luna de Sus. The significance of this fact is, of course, sedimentological, being related to the bathymetric, energetic and probably eustatic conditions existing during sedimentation for each lithological sequence.

Conclusions

The present paper is only a beginning in an attempt to elucidate the complex mineralogical and sedimentological problems concerning glauconitic minerals and the glauconitization process in Romania.

The following main conclusions can be drawn:

- the green grains under study are monophasic (they contain only species of the group of glauconitic minerals);

- the structural opening and ordering degree is variable, but considering these parameters, both the Eocene and Miocene "glauconies" may be included into the glauconitic mixtures, consisting of an irregular interstratification between ferriferous mica layers and "smectitic"-type expandable layers;

- a relative increase of the structural order degree may be noticed in the Eocene samples, which implies their higher maturity, as compared to the Miocene ones (suggested, by start, by the difference in colour);

- the evolutionary trends are also connected to the lithological facies in which "glauconies" develop: for the rocks formed under conditions of low sedimentation rate and a medium - to high energy environments (coarser, siliciclastic rocks, bioclastic packstone) conditions are more favourable for the glauconitogenesis: a longer contact of the substrata with the sea - water and the sea-floor and winnowing, that favour intense cationic exchanges.



References

- Bailey, S. W (1984) Classification and Structures of the Micas. In: Bailey S.W. (ed.) *Micas. Rev. Miner.*, 13, p. 1-12, Chelsea, Michigan.
- Bielz, E.A. (1889) Die Gesteine Siebenbürgens. Eine systematische Aufzählung der in diesen Lande vorkommenden Mineralien und Fels arten mit ihren Fundorten und ihrem Vorkommen. 2 Auflage, Separatbuch, 82 p., Hermannstadt.
- Burst, J.F. (1958) Mineral heterogeneity in glauconite pellets. *Am. Mineral.*, 43, 5-6, p. 481-497, Menasha, Wisconsin.
- Cimbalnikova, A. (1970 a) Index of refraction and density of glauconites. *Cas. Mineral. Geol. Ceskosl.*, 15, 4, p. 335-345, Praha.
- (1970 b) Type, extent and mode of 10Å/14Å interlayering in glauconites. *Acta Univ. Carolinae, Geologica*, 4, p. 253-266, Praha.
- Fischer, H. (1987) Excess K-Ar ages of glauconite from the Upper Marine Molasse and evidence for glauconitization of mica. *Geol. Rundschau*, 76, p. 885-902, Stuttgart.
- Harder, H. (1980) Syntheses of glauconite at surface temperatures. *Clay & Clay Minerals*, 28, 3, p. 217-222, London.
- Hauer, Fr.R.V., Stache, G. (1863) *Geologie Siebenbürgens*. 636 p., Wien.
- Holtzapffel, T. (1985) Les minéraux argileux. Préparation. Analyse diffractométrique et détermination. *Soc. Géol. du Nord*, 12, 136 p., Villeneuve D'Ascq.
- Hower, J. (1961) Some factors concerning the nature and origin of glauconite. *Am. Mineral.*, 46, 3-4, p. 313-334, Menasha, Wisconsin.
- Koch, A. (1900) Die tertiärbildungen des Beckens der Siebenbürgischen Landestheile. II. Neogene Abtheilung, Budapest.
- Lewis, D.W. (1964) "Perigenic"; a new term. *J. Sed. Petrol.*, 34, p. 875-876, Tulsa.
- Mareş, I., Tătărîm, N. (1967) Studiul glauconitului din depozitele eocene din regiunea Cluj (Luna de sus - Lita). *Anal. Univ. Buc., Geol. Geogr.*, XVI, 2, p. 25-48, Bucureşti.
- , Todiriţă-Mihăilescu, V. (1970) Asupra prezenţei glauconitului în depozitele neocretace din regiunea Sebeşel - Săsciori. *Anal. Univ. Buc., Geol.*, 19, p. 61-68, Bucureşti.
- McConchie, D.M., Lewis, D.W. (1980) Varieties of glauconite in late Cretaceous and early Tertiary rock of the South Island of New Zealand, and new proposals for classification. *New Zealand J. Geol. Geoph.*, 23, 4, p. 413-437, Wellington.
- Mureşan, I., Stoicovici, E. (1987) Contributions à la caractérisation des accumulations de fer dans les formations éocènes de la bordure nord-ouest du Bassin de la Transylvanie. In: Petrescu, I. (ed. in-chief) *The Eocene from the Transylvanian Basin*. p. 269-284, Cluj- Napoca.
- Odin, G.S. (1969) Méthode de séparation des grains de glauconie. Intérêt de leur étude morphologique et structurale. *Rev. Géogr. phys. Géol. dyn.* (2), 11, 2, p. 171-176, Paris.
- (1972) Observations nouvelles sur la structure de la glauconie en accordeon ("vermicular pellets"); description du processus de genèse de ces granules par neoformation. *Sedimentology*, 19, p. 285-294, Amsterdam.
- (1975) De glauconarium: constitutione, origine, aetateque. Thèse Doct. État, Univ. P & M. Curie, 280 p., Paris.
- , Matter, A. (1981) De glauconarium origine. *Sedimentology*, 28, p. 611-641, Amsterdam.
- Odom, E.I. (1984) Glauconite and Celadonite Minerals. In: Bailey, S.W. (ed.) *Micas. Rev. Miner.*, 13, p. 545-572, Chelsea, Michigan.
- Pettijohn, E.J. (1975) *Sedimentary rocks*. III edition, Harper International Edition, 628 p., New York, Evanston, San Francisco, London.
- Răileanu, Gr., Saulea, E. (1956) Paleogenul din regiunea Cluj şi Jibou (NV-ul Bazinului Transilvaniei). *An. Com. Geol.*, XXIX, p. 271-308, Bucureşti.
- Rusu, A. (1967) Studiul geologic al regiunii Moigrad (NV-ul Bazinului Transilvaniei). *D.S. Com. Stat. Geol.*, LIII, 1, (1965-1966), p. 427-455, Bucureşti.
- (1987) Ostrenia biohorizons in the Eocene of the NW Transylvania (Romania). In: Petrescu, I. (ed. in chief) *The Eocene from the Transylvanian Basin*, p. 175-182, Cluj-Napoca.
- Rocha, F.T., Gomes, C.S.F. (1990) Determinação da cristalinidade de minerais argilosos por DRX. Aplicações práticas a problemas de lithostratigrafia. *Geociências*, 5, 2, p. 37-50, Aveiro.



- Stoicovici, E., Mureșan, I. (1964)** Studiul zăcămintului de limonit oolitic și de glauconit din formațiunile eocene ale Bazinului Transilvaniei (1,2). *Studia Univ. B.B., Ser. Geol. Geogr.*, 1, p. 7-16; 2, p. 17-29, Cluj-Napoca.
- Șuraru, N. (1967)** Beiträge zur Kenntnis des Burdigals im nord-westlichen Teil des Siebenbürger Beckens zwischen Cluj und Surduc (Rumänien). *N. Jb. Geol. Paläont., Mhf.*, 8, p. 489-497, Stuttgart.
- Toler, L.G., Hower, J. (1959)** Determination of mixed layering in glauconites by index of refraction. *Am. Miner.*, 44, 11-12, p. 1314-1318, Menasha, Wisconsin.
- Triplehorn, D.M. (1966)** Morphology, internal structure and origin of glauconite pellets. *Sedimentology*, 6, p. 247-266, Amsterdam.
- Zumpe, H.H. (1971)** Microstructure in Cenomanian glauconite from the Isle of Wight, England. *Mineral. Mag.*, 38, p. 215-224, London.

Received: September, 1994

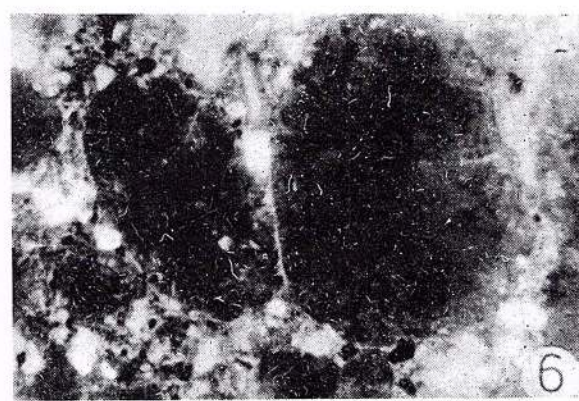
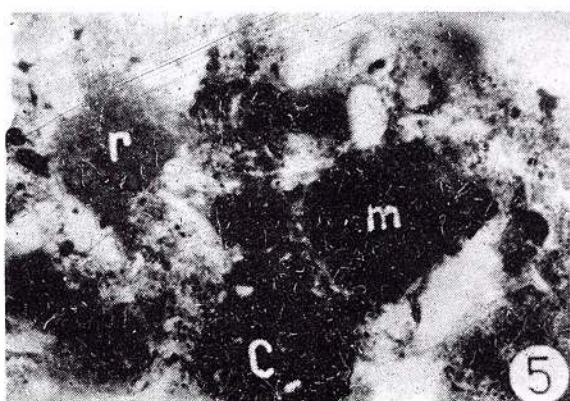
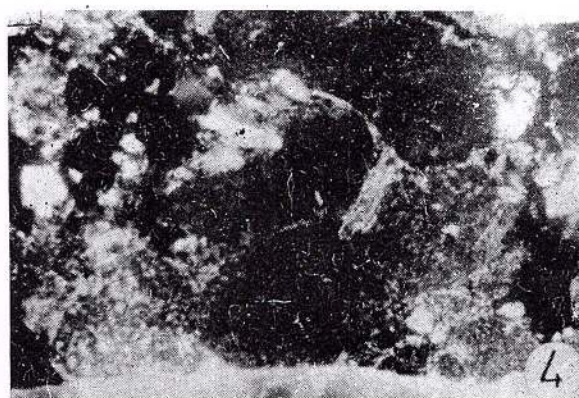
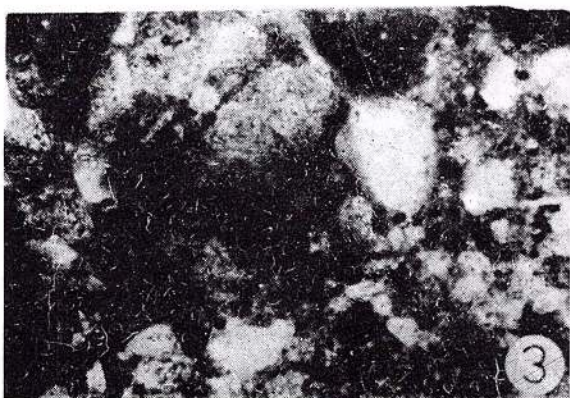
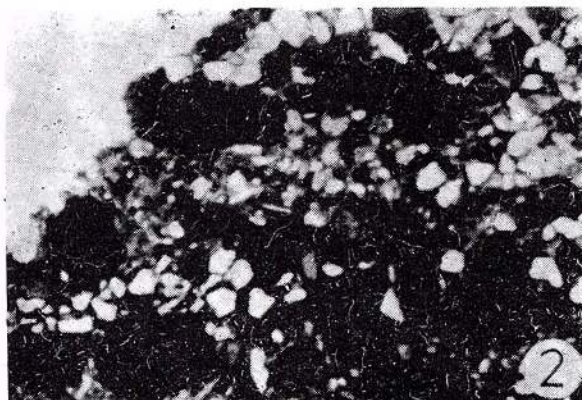
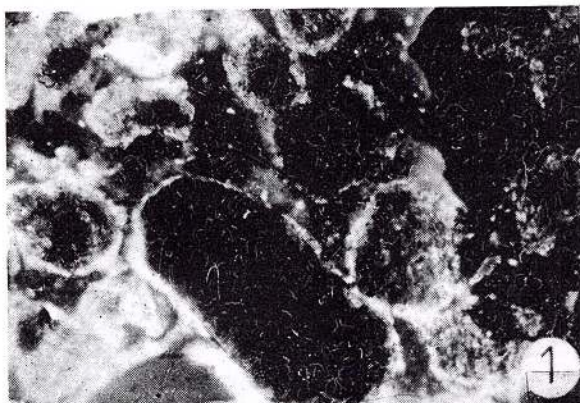
Accepted: November, 1994



Plate I

- Fig. 1** – Ovoidal and spheroidal glauconitic grains, with random microcrystalline internal textures, fibro-radial rims (higher birefringence) and concentric and radial cracks (GM 2-A, loose magnetic fraction, N+, 12.5X);
- Fig. 2** – Weakly silty sandstone, with angular to subrounded glauconitic grains and quartz clasts; signs of bioturbation are present (GM 3, 1N, 56X);
- Fig. 3** – Supposed foraminiferal mold as a substratum of glauconitization; internal radial cracks as indices of crystal growth (GM 11, 1N, 98X);
- Fig. 4** – Random microcrystalline glauconitic grains bordered by a micaceous rim and a biotite lamella, showing traces of diagenetic pressure (GM 5, N+, 98X);
- Fig. 5** – Different types of internal microstructures; (m) – micaceous, (r) – random microcrystalline, (c) – composite grain (with quartz inclusions) (GM 11, 1N, 160X);
- Fig. 6** – Brown-coloured relic (biotite?) in the centre of a glauconitic grain (right) and composite grain (left), with quartz and carbonate inclusions (GM 11, 1N, 98X).





Rom. J. Mineralogy, vol. 78, Bucureşti, 1997



Institutul Geologic al României



Plate II

Fig. 1 – Green shell fragment with internal "zebra" texture preserved in a random microcrystalline glauconitic grain (GM 11, 1N, 160X);

Fig. 2 – Detail of Fig. 1: internal "fossilized" concentric layers (C1) (coatings) illustrating several episodes of sediment reworking, each succeeded by glauconitic accretion (1N, 320X);

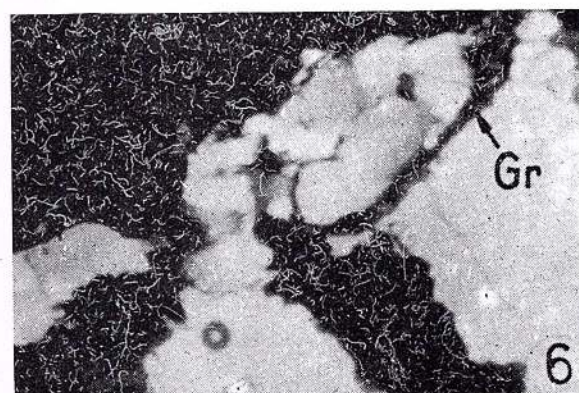
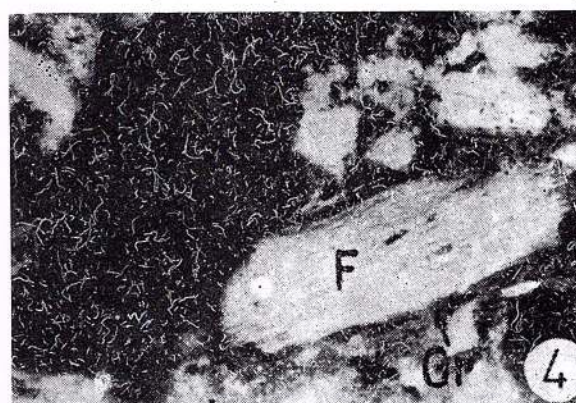
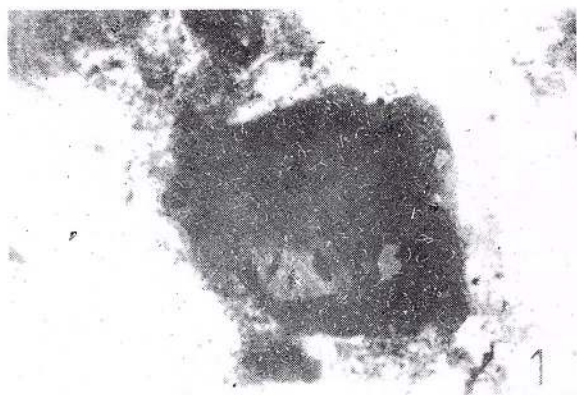
Fig. 3 – Organic precursor of "glauconie" still visible; oriented microcrystalline internal texture (GM 11, 1N, 160X);

Fig. 4 – Glauconitic grain with a biotite lamella molding it; argillized feldspar crystalloclast (F), surrounded by a green (glauconitic ?) coating (Gr) (Gm 11, 1N, 160X);

Fig. 5 – Glauconitic grains filled on the cracks and surrounded by a carbonatic cement (GM 19, 1N, 160X);

Fig. 6 – Green mineral (Gr) ("glauconie" ?) on the fissures of quartzitic lithoclasts (GM 3, N+, 12.5X)





Rom. J. Mineralogy, vol. 78, Bucureşti, 1997



Institutul Geologic al României

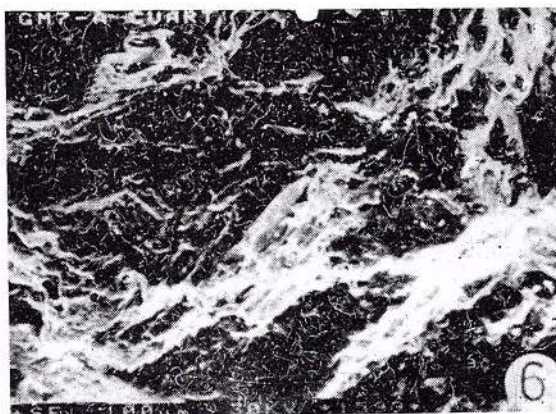
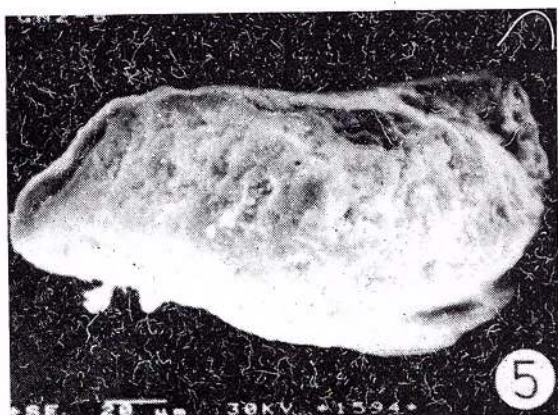
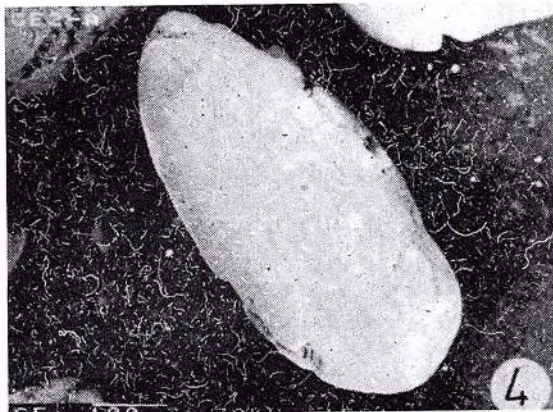
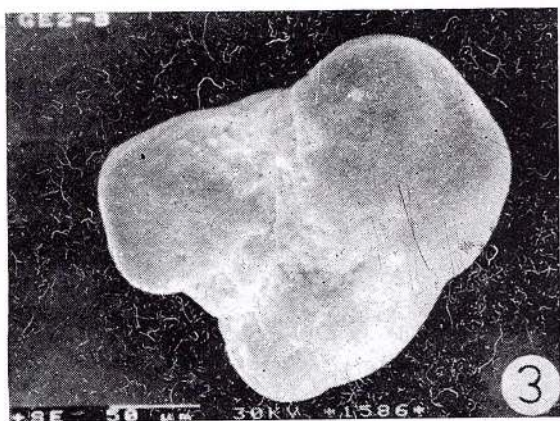
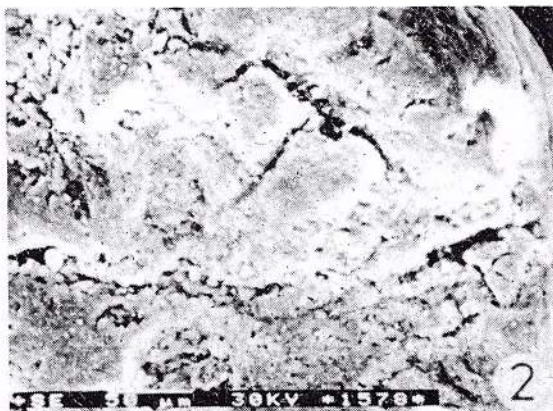


Plate III

SEM images of different substrata and morphological types

- Fig. 1** – "Glaucanie" replacing foraminiferal molds, with "croute de pain" cracks and impact "craters" (GE 2-A);
- Fig. 2** – Detail of Fig. 1; the cracks, being protected from erosion, preserve the original nannos-structure;
- Fig. 3** – Lobate pelloid, probably of organic nature (GE 2-B);
- Fig. 4** – Ovoid pelloid, with smooth and polished surface, suggesting a fecal pellet substratum (GE 2-A);
- Fig. 5** – A possible micaceous substratum is suggested by the erosion of the surface of the green grain following parallel planes (GM 2-B);
- Fig. 6** – Quartz grain (black, massive), with a lamellar green mineral ("glaucanie" ?) on the fissure (GM 7-A).





Rom. J. Mineralogy, vol. 78, București, 1997



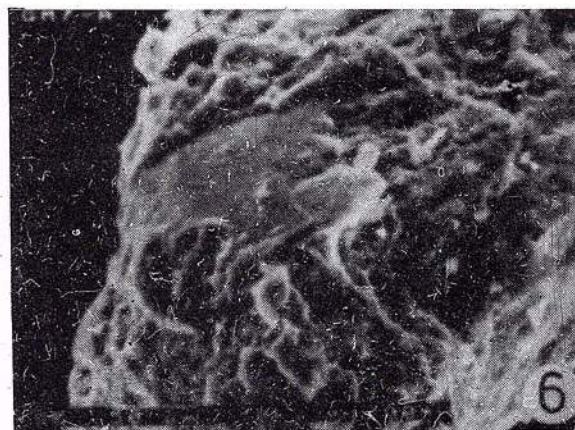
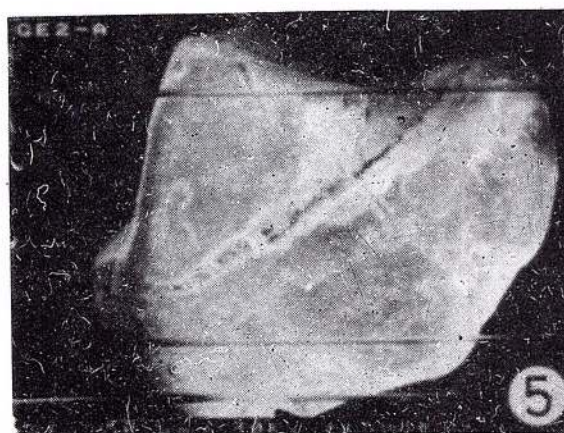
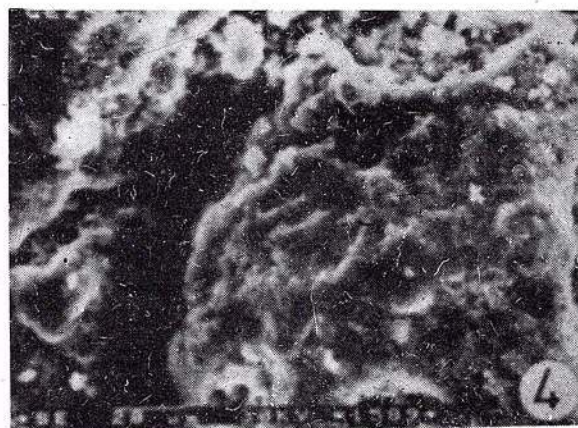
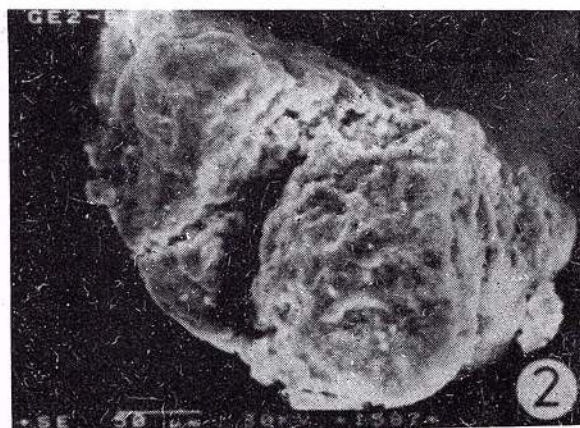
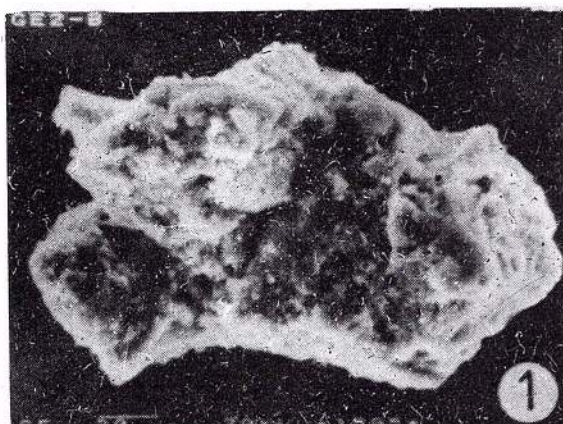
Institutul Geologic al României



Plate IV

Morphological types and evolutionary stages (SEM)

- Fig. 1** – Porous earthy surface of a "spongy glauconie";
- Fig. 2** – Green grain with features of the "serrulate" subclass of the "spongy" type; in the right side, a boxwork of small lamellae of evolved "glauconie" (GE 2-B);
- Fig. 3** – Microgeodes and small dissolution pits which contain small lamellae of slightly evolved "glauconie" (GE 2-B);
- Fig. 4** – Automorphic rosette-like lamellae (3 – 5 μm) indicating the evolved stage of glauconitization; diagenetic carbonates (white) cover them (GE 2-B; detail of Fig. 2);
- Fig. 5** – Typical cracked grain, with impact "craters" and diagenetic carbonate (white, platy) developed in the fissure (GE 2-A);
- Fig. 6** – Signs of movement on the glauconitic grain; scratches (right) and "friction lens" (left) suggesting a perigenous or detrital origin (GM 7-A).



om. J. Mineralogy, vol. 78, București, 1997



Institutul Geologic al României



PALYGORSKITE IN MAGNESIAN SKARNS FROM BĂIȚA BIHOR (RÉZBANYA): A SECOND ROMANIAN OCCURRENCE AND A REVIEW

Ştefan MARINCEA, Magda CIULAVU, Iulian VANGHELIE

Institutul Geologic al României, Str. Caransebeş nr. 1, 78344, Bucureşti



Key words: Magnesian skarns. Physical properties. Microprobe data. SEM study. X-ray data. Infrared spectrum. Băița Bihor - Apuseni Mountains - Romania.

Abstract: A new find of palygorskite in the unusual context of skarn areas rises to two the number of the occurrences of this mineral in Romania. As at Ocna de Fier, the locality of its first Romanian mention, the palygorskite from Băița Bihor occurs as cavity infillings in a coarse-grained dolomite enclosed in the skarn mass. Palygorskite fibres, up to 2 mm in length, overcoat scalenohedral calcite. Physical constants are: $n_{mean} = 1.55(2)$, $D_{meas} = 2.25(2)$, $D_{calc} = 2.342(2)$. Microprobe analyses gave as average composition: $SiO_2 = 51.93\%$, $Al_2O_3 = 12.26\%$, $Fe_2O_3 = 0.25\%$, $MgO = 13.39\%$, $CaO = 0.63\%$, $K_2O = 0.05\%$, H_2O (theoretical) = 19.60% . The main IR-absorption bands recorded in the frequency range between 4000 and 250 cm^{-1} are located at 3692 , 3624 , 3588 , 3520 cm^{-1} (OH stretchings), 1626 , 910 , 875 cm^{-1} (OH bendings), 1190 , 1130 cm^{-1} (bridged Si-O-Si vibrations), 1090 , 1024 , 998 cm^{-1} (Si-O stretchings), 632 , 580 , 520 cm^{-1} (Si-O bendings), 626 cm^{-1} (Al-O stretching), 485 , 445 , 415 , 390 and 268 cm^{-1} (essentially cation-oxygen vibrations). Both palygorskite from Băița Bihor and Ocna de Fier were found to be orthorhombic. Refined cell dimensions are: $a = 5.218\text{ Å}$, $b = 17.907\text{ Å}$, $c = 12.7185\text{ Å}$ for the Băița Bihor palygorskite and $a = 5.183\text{ Å}$, $b = 18.046\text{ Å}$, $c = 12.31\text{ Å}$ for the Ocna de Fier one. Some chemical peculiarities of the palygorskite in skarn areas (i.e. higher contents of Al and Ca) can explain their stability during epithermalism and weathering.

1. Introduction

Quite widespread in some other regions of the world (Jones, Galan, 1988), palygorskite ($Si_8Mg_5O_{20}(OH)_2(OH_2)_4 \cdot 4H_2O$) is an enough rare mineral in Romania. Only one mention, that in skarns at Ocna de Fier, benefits by reliable data given by Kissling (1967). Two other ones, in more common environments, as

clay constituent in bentonites at Alba Iulia (Neacșu, 1969) or in Pannonian clays in the Transylvanian Basin (Matei, 1983) are not well substantiated.

The recently found occurrence, that one at Băița Bihor, rises to two the number of palygorskite occurrences in the unusual context of skarn areas. As at Ocna de Fier, the palygorskite at Băița Bihor occurs as filling of



some vugs in the magnesian skarn mass. In fact, the mineral appears to be not wholly unexpected in such type of occurrences. A number of palygorskite mentions on fissures or in (karst) cavities of dolomitic marbles (Demangeon, Salvayre, 1969) or dolomitic limestones (Zaritsky, Orlov, 1973; Müller-Vonmoos, Schindler, 1973 e. a.) show that the mineral can easily precipitate from an epigenetic or hydrothermal solution in magnesian systems.

Last but not least it is to be noted that the description of palygorskite at Băița Bihor rises to 135 the number of mineral species described by various authors (see Stoici, 1983 and Udubașa et. al. 1992 for references) in this world-wide famous occurrence.

This paper aims therefore to bring new and more accurate data on this phyllosilicate of special interest for the Romanian mineralogy.

2. Geological setting

As the majority of Romanian skarn areas, including the one at Ocna de Fier, the skarns at Băița Bihor are developed in the contact aureole of an important body of "banatites" (a major granite-granodiorite intrusion of Late Cretaceous - Paleogene age). The banatites at Băița Bihor belong to an extended pluton (the Southern Bihor batholith) and were ascribed by Ștefan et al. (1988) to the second cycle of the Iaramian magmatism in the Apuseni Mountains (Danian-Ypresian in age). Calcic and magnesian skarns largely develop within the contact aureole. They have as protolite Mesozoic sedimentary formations belonging to some structural units individualised as the Codru Nappes System (the Vetre, Următ and Vălani Units) and the Bihor Autochthon (the Bihor Unit): Bordea, Bordea (1973).

As a peculiarity, the magnesian skarns at Băița Bihor materialise metasomatic columns described as bodies by Stoici (1974) or by Cioffica et al. (1977). They are preferentially hosted by some areas of dolomitic marbles or

magnesian hornfels resulting from the thermal metamorphism of the dolostones in the Vetre Unit (the Frăsinel dolosparite, of Carnian - Norian age) and in the Vălani Unit (the Obârșia Izbuc Formation, of Anisian - Carnian age). Magnesian skarn bodies were described by Stoici (1974) at Baia Roșie, Bolfu - Tony, Hoanca Moțului, Antoniu, Sturzu and Martha.

From the mineralogical point of view, the magnesian skarn assemblages consist of forsterite, spinel, clinohumite, humite, chondrodite, diopside, phlogopite, tremolite, dolomite, calcite, with superposed talc, serpentines, and brucite. They show strong disequilibria with scarce or no paragenetical intergrown phases. Mineralizations of iron oxides, magnesian borates, base-metal sulphides and Bi-sulphosalts were recognised to overlap on the

magnesian skarn areas (Cioffica, Vlad, 1968; Stoici, 1974; Cioffica et al. 1977)

3. Occurrence

Taking into account that subsequent hydrothermal alteration products of the initial skarn assemblages are widely spread at Băița Bihor as well as at Ocna de Fier, these two occurrences of palygorskite are not unexpected.

At Băița Bihor the mineral was found as filling of some cavities individualised in a mass of coarse-grained dolomite from Baia Roșie. The relation host dolomite - skarn is more obvious than at Ocna de Fier, the carbonate mass being practically enclosed in the inner zone of the metasomatic body at Baia Roșie. Palygorskite from both occurrences overcoats scalenohedral calcite and fills up the gaps between calcite crystals. It occurs as a mass of randomly oriented crystals of fibrous habit. At Băița Bihor the length of the fibres does not exceed 2 millimetres. They clearly differ from the unusually large crystals reported by Kissling (1967) at Ocna de Fier (up to 1 cm in length), which seem to be in reality bunches of shorter intergrown fibres.



At Băița Bihor palygorskite is not associated with hydrothermal quartz, as at Ocna de Fier, but with calcite.

As proved by the position of the (10 $\bar{1}$ 4) spacing on the X-ray diffraction pattern, the associated calcite is nearly stoichiometric. This spacing was recorded at $d = 3.033 \text{ \AA}$ and gives, by using the Goldsmiths X-ray determinative method as indicated by Marincea (1993), a content of only 0.68% magnesite in solid solution.

4. Physical properties

The megascopic colour of the palygorskite at Băița Bihor is white, with yellowish tints given by some supergene iron-rich alteration products which are easy to remove by etching with acetic acid.

A mean refractive index of 1.55 was measured by oil immersion techniques at 20° C. Taking into account that the determination was made on a direction perpendicular to the fibre elongation by using the Schröder method, this index practically corresponds to n_p or n_m . It is coincident with the one reported by Kissling (1967) for the palygorskite at Ocna de Fier ($n=1.55$).

The specific gravity of the palygorskite from Băița Bihor was measured by using the flotation method. A value of 2.25(2) was obtained by sink-float of isolated crystals in bromoform-toluene solutions. This value, as is to be expected taking into account the extent of the specific surface and the sorptive properties of palygorskite (Jones, Galan, 1988), is lower than the calculated specific gravity of 2.342 (see below).

5. Chemical composition

Because the material available was in small quantity, the chemical analysis of palygorskite from Băița Bihor was carried out using a Phillips 515 electron microprobe hosted by METAV S.A., Bucharest. Operating conditions were 15 kV as accelerating voltage and

20 nA as sample current on brass. To minimise sample degradation and compositional change due to electron bombardment, a slightly defocused beam was used over a counting time of 100 seconds.

The average composition determined as mean of 3-5 single spot analyses on four separate grains is: $\text{SiO}_2 = 51.93\%$ (50.70 - 53.03%), $\text{Al}_2\text{O}_3 = 12.26\%$ (11.82 - 12.70%), $\text{Fe}_2\text{O}_3 = 0.25\%$ (0.00 - 0.57%), $\text{MgO} = 13.39\%$ (12.59 - 13.85%), $\text{K}_2\text{O} = 0.05\%$ (0.00 - 0.17%) and $\text{CaO} = 0.63\%$ (0.22 - 1.01%). The variation limits are given in parentheses. As shown by Jones and Galan (1988), most of the iron in palygorskite is in the trivalent state of oxidation. Consequently, the total iron content is assumed to be ferric iron. The remainder of the analysis was assumed to represent H_2O . As the gravimetric determination of the water according to Penfield method was impossible because of the small quantity of the material available, the theoretical values given by Hirsiger and Müller-Vonmoos (1975) may be assumed to complete compositional data. These values are 8.5% for the zeolitic water, 9.0% for the bounded water and 2.1% for the water in hydroxyl, the analysis total reaching thus a satisfactory value of 98.11%.

Based on the structural model given by Drits and Sokolova (1971) and using the chemical data presented before, the average structural formula of the Băița Bihor palygorskite is: $(\text{Mg}_{2.862}\text{Al}_{1.516}\text{Fe}_{0.027}^{3+}\square_{0.595})(\text{Si}_{7.445}\text{Al}_{0.555})\text{O}_{20}(\text{OH})_2\text{Ca}_{0.097}\text{K}_{0.009}(\text{OH})_4 \cdot 4\text{H}_2\text{O}$. Taking into account that neither water nor hydroxyl were determined, the formula was based on 21 oxygen atoms in the anhydrous compound, as indicated by Smith and Norem (1986).

The structural formula shows that sites occupancies are in accordance with the average data given for palygorskite by Newman and Brown (1987); thus, Al in the four-fold coordinated sites does not exceed the maximal limit of 0.66 and the sum of the cations in six-fold coordinated sites (4.415) lies within the reported limits (3.76 - 4.64). The average



structural formula leads to a molecular mass of 838.413, which was used to calculate the specific gravity.

6. SEM examination

The morphology of the palygorskite from Băița Bihor was examined by standard secondary electron imaging techniques, using a PHILLIPS 515 SEM apparatus. In order to eliminate the problems related to the static charging, samples were two times covered with graphite under vacuum. Typical images of the characteristic fibrous habit are shown on Plate. The composite nature of the fibres, with a ribbed appearance, was also observed by Smith and Norem (1986). Curved crystals are frequent. Impurities are scarce, consisting of scalenoedra of calcite. Palygorskite fibres may reach 10 μm in diameter.

7. X-ray powder diffraction data

The X-ray powder diffraction pattern of the Băița Bihor palygorskite was performed with a DRON 3 diffractometer using Ni-filtered $\text{CuK}\alpha$ radiation and pure CaF_2 as an internal standard. The record was made using a scanning speed of $1^\circ 2\theta/\text{min}$ and a time constant 2.5 sec, with setting 35 kV and 20 mA, within the 2θ range of 8° – 60° . Constants are 1.5405 Å for the wavelength of $\text{CuK}\alpha$ radiation and 5.4626 Å for the cell edge of fluorite at 20°C .

The obtained X-ray powder data are given in Table 1, together with similar data given by Kissling (1967) for the palygorskite from Ocna de Fier. The two patterns were recorded in different conditions and show some variations in the d-values which probably corresponds to differences in chemical composition. The indexing of the reflections was based on the structural determinations of Christ *et al.* (1969), which was also accepted by Jones and Galan (1988) who proposed a normal axes inversion. This reversed notation was preferred and is given in Table 1.

Since both monoclinic and orthorhombic

polymorphs of palygorskite were described (Gard, Follet, 1968; Christ *et al.*, 1969; Drits, Sokolova, 1971; Hirsiger *et al.*, 1975; Jones, Galan, 1988) it is important to distinguish between these two polymorphic types using powder data alone if possible. Although powder data for both polymorphs are available (Christ *et al.*, 1969), they are difficult to correlate since the natural samples measured have different compositions. Under ideal conditions monoclinic palygorskite may be readily distinguished from the orthorhombic one due to the splitting of the (121) and (161) reflections at about 20° and $35^\circ 2\theta$, respectively (Christ *et al.*, 1969). As in our pattern these reflections are unsplit, the palygorskite polymorph of Băița Bihor is presumed to be the orthorhombic one.

A supplementary attempt to ascertain which polymorph is present was undertaken after the calculation of the cell dimensions in both hypotheses of symmetry. Accordingly, unit-cell parameters were determined by least-squares refinement of the data in Table 1. Both an unpublished computer program written for G.I.R. by Vanghelie (P.A.V., 1994) and the classical program written by Appleman and Evans (1973) revised for microcomputer use by Benoit (1986) were used for the refinements. The obtained cell dimensions and space group information are given in Table 2, together with similar data for comparison.

A recalculation of the d-values based on the obtained cell parameters showed that the differences between calculated and observed d-spacings (Table 1) are smaller in the orthorhombic variant of symmetry. Consequently, the assumption that the Băița Bihor palygorskite has an orthorhombic cell (probably Pn) seems justified.

As a last remark it is to be noted that the cell volume determined from the refined constants in Table 2 is of 1188.4 Å³. This value, correlated with the molecular mass deduced on the basis of the chemical data gives, for $Z = 2$, a calculated specific gravity of 2.342, which



Table 1
X-ray powder diffraction data for palygorskite from Romanian skarns

No	Băița Bihor						Ocna de Fier				(hkl)
	d(obs)	d calc ortho	d calc mono	d calc ortho	d calc mono	I/I ₀	d (obs)	d calc ortho	d calc mono	I obs	ortho
	(1)	(2)	(3)	(4)	(5)	(6)	(7)	(8)	(9)	(10)	(11)
1	10.455	10.371	10.369	10.369	10.363	100					(011)
2	6.366	6.362	6.368	6.359	6.358	25					(002)
3	5.400	5.403	5.393	5.404	5.397	20					(031)
4	4.480	4.476	4.465	4.477	4.470	45					(040)
5	4.257	4.251	4.240	4.249	4.247	40	4.34	4.222	4.214	s	(121)
6	4.111	4.127	4.130	4.125	4.125	30					(013)
7	3.660	3.679	3.669	3.678	3.676	20	3.66	3.63	3.594	v.s	(122)
8	3.336	3.343	3.334	3.342	3.340	45	3.30	3.310	3.282	v.s	(132)
9	3.184	3.181	3.184	3.180	3.179	40	3.10	3.078	3.081	w	(004)
10	2.596	2.593	2.592	2.592	2.591	30					(044)
11	2.596	2.591	2.585	2.591	2.588	30					(160)
12	2.533	2.531	2.526	2.530	2.530	35	2.55	2.511	2.527	v.w	(211)
13	2.533	2.539	2.532	2.539	2.536	35	2.55	2.545	2.539	v.w	(161)
14							2.40	2.368	2.364	v.w	(212)
15							2.24	2.309	2.305	w.	(222)
16							2.05	2.052	2.054	v.w	(006)

- (1) derived from 2θ values;
- (2) refined for an orthorhombic cell with $a=5.221 \text{ \AA}$, $b=17.904 \text{ \AA}$ and $c=12.723 \text{ \AA}$ using the PAV program;
- (3) refined for a monoclinic cell with $a=5.215 \text{ \AA}$, $b=17.858 \text{ \AA}$, $c=12.74 \text{ \AA}$ and $\beta=90.27^\circ$, using the orthorhombic indexing with ($\bar{1}21$) and ($\bar{1}61$) reflections added, and the PAV program;
- (4) refined for an orthorhombic cell with $a = 5.218 \text{ \AA}$, $b = 17.907 \text{ \AA}$ and $c = 12.7185 \text{ \AA}$, using the computer program of Appelman and Evans (1973) as given by Benoit (1986);
- (5) refined for a monoclinic cell with $a = 5.220 \text{ \AA}$, $b = 17.88 \text{ \AA}$, $c = 12.717 \text{ \AA}$ and $\beta = 90.00^\circ$, using the computer program of Appelman and Evans (1973) as given by Benoit (1986);
- (7), (10) as given by Kissling (1967), reflections at 1.692 \AA (v.w.), 1.582 \AA (s), 1.499 \AA (s), 1.44 \AA (s) and 1.283 \AA (v.s.) also given (Mn filtered $\text{FeK}\alpha$ radiation, setting 30 kV, 10 mA);
- (8) refined for an orthorhombic cell with $a=5.183 \text{ \AA}$, $b=18.046 \text{ \AA}$, $c=12.31 \text{ \AA}$ and $\beta=92.50^\circ$, using the PAV program;
- (9) refined for a monoclinic cell with $a=5.272 \text{ \AA}$, $b=18.00 \text{ \AA}$, $c=12.34 \text{ \AA}$ and $\beta = 92.500^\circ$, using the PAV program.

agrees well with the values reported for palygorskite by Jones and Galan (1988):

$$G = 2.29 - 2.36.$$

On the other hand, it should be emphasized that the analysis by the same approaches of the diffraction data provided by Kissling (1967) for the palygorskite at Ocna de Fier (Table 1) also indicates the orthorhombic

symmetry. The refined cell dimensions are given in Table 2 and the two sets of tentatively calculated d-spacings (for monoclinic and orthorhombic unit cell) in Table 1. However, because many of the diffraction peaks given by Kissling (1967) are not indexed, cell parameters have been estimated only on the basis of the first nine spacings given in Table 1.



Table 2
Comparative crystallographic data for palygorskite from various occurrences

Polymorph	Space group	Sample location	Cell parameter				Source of information
			a(Å)	b(Å)	c(Å)	β	
monoclinic	A2/m	Attapulgis	5.200	18.000	12.900	?	Bradley (1940) fide Jones, Galan (1988)
orthorhombic	(?)	Brazil	5.207	17.857	12.690		Huggins et al. (1962) fide Christ et al. (1969)
monoclinic	P2/a	unknown locality	5.22	18.06	12.75	95°50'	Zvyagin et al. (1963)*
orthorhombic	Pbmn	Palygorskaya	5.26	17.9	12.65		Preisinger (1965)*
orthorhombic	Pn	Sapillo (New Mexico)	5.242	17.872	12.725		Christ et al. (1969)*
orthorhombic	Pn	Zaachila (Mexico)	5.199	17.885	12.781		Christ et al. (1969)*
orthorhombic	Pn	Attapulgis	5.199	17.925	12.823		Christ et al. (1969)*
monoclinic	P2/a	Glasgow (Virginia)	5.127	17.864	12.681	92°14'	Christ et al. (1969)*
monoclinic	P2/a	Metaline (Washington)	5.24	17.83	12.78	95°46'	Christ et al. (1969)*
monoclinic	C2/m	Dzhezdy (Kazakhstan)	5.15	17.85	13.14	107°	Christ et al. (1969)*
orthorhombic	Pn	Băița Bihor	5.218	17.907	12.718		This paper
orthorhombic	Pn	Ocna de Fier	5.183	18.046	12.31		This paper

* The axes inversion proposed by Jones and Galan (1988) was accepted. Consequently the original a parameter transforms into c.

8. Infrared absorption data

An infrared absorption spectrum of a palygorskite sample from Băița Bihor was recorded in the 4000 to 250 cm^{-1} region using a SPECORD M-80 spectrometer. The sample was prepared as compressed disk of powdered palygorskite and KBr (2.5 weight%) to minimise polarisation effects. To avoid the effect of absorbed water, the KBr was dehydrated at 150° C for 24 hours prior to analysis. The KBr disk was prepared using 800 mg of mechanically ground powder compacted under 2300 N/cm^2 pressure.

The spectrum is given in Figure and shows as a main feature the well pronounced band complex in the OH stretching vibration region, between 4000 and 3000 cm^{-1} . It can be explained by the variability of the structural positions of water in palygorskite, which contains, beside the hydroxyl groups associated with the octahedral sheets, three kinds of structural water: hygroscopically adsorbed, zeolitic (present in the structural channels)

and bound to six-fold coordinated cations, on the edges of octahedral sheet (Caillère and Henin, 1961; Hayashi et al. 1969; Prost, 1975; Rautureau and Mifsund, 1975; Serna et al., 1977; Van Scoyoc et al., 1979). Consequently, the bands in the 4000-3000 cm^{-1} region can be assumed as follows:

1 - the band at 3692 cm^{-1} is due to the structural hydroxyl and can be assumed to a Si-OH stretching (Serna et al., 1977);

2 - the sharp band at 3624 cm^{-1} is due to the structural OH coordinated to the octahedral ion pair Al-Al (Serna et al., 1977; Van Scoyoc et al., 1979) or to a fundamental OH stretching of the unperturbed OH in the bound water (Hayashi et al., 1969; Serna et al., 1977);

3 - the weak band at 3588 cm^{-1} materialises another stretching of the structural hydroxyl, the (Al, Fe^{3+}), (Fe^{2+} , Mg) - OH one (Serna et al., 1977). This vibrational mode is normally split into two distinct bands corresponding to the Al, (Fe^{2+} , Mg) - OH vibrations, recorded by Serna et al. (1977) at 3595 and 3560 cm^{-1} , respectively. The fact that in our spectrum the



band at lower frequency, assigned by Serna et al. (1977) to the $\text{Fe}^{3+}, (\text{Fe}^{2+}, \text{Mg}) - \text{OH}$ vibration, is missing, agrees well with the low content of iron in the sample;

Rozenzon, 1981).

The other main and striking feature of the infrared spectrum in Figure 1 is the presence of a well pronounced series of absorption bands

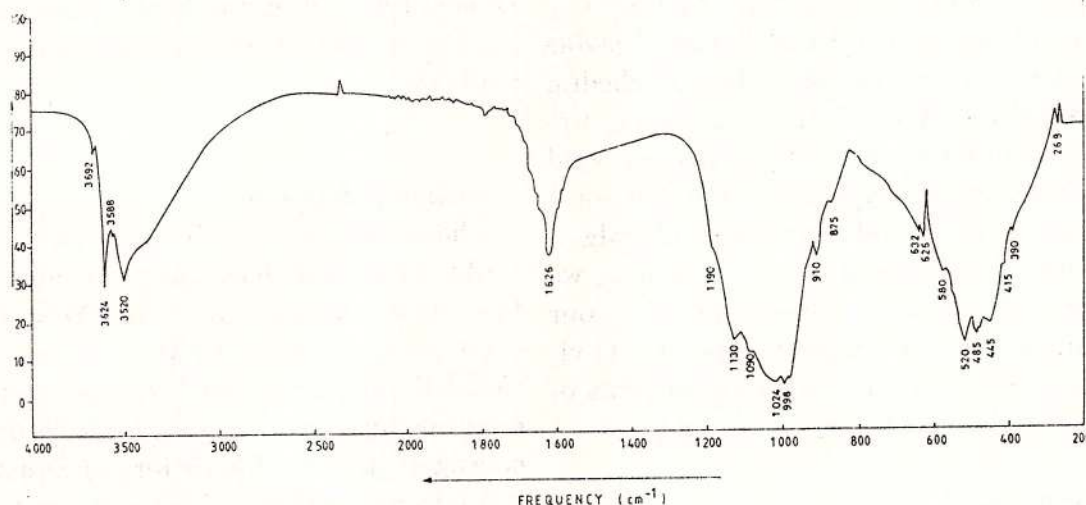


Fig. Infrared absorption spectrum recorded for a sample of palygorskite from Băița Bihor.

4 - the band at 3520 cm^{-1} may be ascribed to the zeolitic water (Hayashi et al., 1969) and represents a classical O-H stretching of a hydrogen-bounded hydroxyl (Serna et al., 1977). Work on hydroxyl-bounded compounds has shown that the O-H stretching frequency is an almost linear function of the O-H ... O bond distance (Nakamoto et al., 1955). Our band, recorded at 3520 cm^{-1} , is slightly less energetic than the characteristic free O-H frequency at about 3700 cm^{-1} and indicates a weak hydrogen bond, consonant with the band assumption.

The corresponding OH bending vibrations occur in a larger frequency range, between $1700\text{--}1600 \text{ cm}^{-1}$ and $950\text{--}850 \text{ cm}^{-1}$, respectively. The fundamental OH bending, assigned to either bound or zeolitic water (Hayashi et al., 1969; Serna et al., 1977), was recorded at 1626 cm^{-1} . Two other bendings were recorded at 910 cm^{-1} and 875 cm^{-1} and represent Al-OH-Al (Gupta, Malik, 1969; Farmer, 1979; Heller-Kallai, Rozenzon, 1981) and, Mg(Fe)-OH-Al vibrations respectively (Heller-Kallai,

on a broad complex, at $1200\text{--}950 \text{ cm}^{-1}$. These bands, recorded at $1190, 1130, 1090, 1024$ and 998 cm^{-1} , were found by Moenke (1966) at $1200, 1125, 1090, 1035$ and 1000 cm^{-1} , and can be assumed to classical stretching vibrations of the (SiO_4) tetrahedra (bands at $1090, 1024$ and 998 cm^{-1}) and to vibrations of Si-O-Si groups which serve as bridges between alternating aluminosilicate ribbons (bands at 1190 and 1130 cm^{-1}): Yariv (1986).

The ν_4 bending motion of the (SiO_4) groups is expected to lie between 650 and 500 cm^{-1} , as in orthosilicates (Farmer, 1972). Theoretically, this vibrational mode of tetrahedral ions is triply degenerate and gives rise to either one, two or three vibrational bands depending upon the symmetry configuration of the ion and its surrounding field. Consequently, only three of the bands in the $650\text{--}500 \text{ cm}^{-1}$ region can be assigned to the (SiO_4) bending vibration. More probably these bands are those at 580 cm^{-1} , 520 cm^{-1} and one of the bands at 632 or 626 cm^{-1} . The fourth band in the region is clearly due to a vibration involving the

(AlO_6) octahedra, as found by Stubican and Roy (1961) in some other layer silicates.

Likewise, the absorption bands below 500 cm^{-1} are essentially related to the vibrations supposing the participation of the (AlO_6), (FeO_6) and (MgO_6) octahedra. At least one of the bands at 485 cm^{-1} and 445 cm^{-1} is due to another vibration of the (AlO_6) octahedra. As theoretically proved the vibrational frequencies should decrease with increasing bond length, the bands at 415 cm^{-1} and 390 cm^{-1} may express Fe-O and more probably Mg-O vibrations. Following the same reasoning we suppose that the weak band recorded in our spectrum at 268 cm^{-1} materializes a Ca-O vibrational mode, due to the minor amounts of six-fold coordinated Ca in the sample.

Conclusions

This second occurrence of palygorskite in skarn areas in Romania shows that both chain-structure clays, namely sepiolite and palygorskite, are stable under conditions of weak alkalinity of the final stage of skarn evolution.

The mineralogical approaches which were used in this paper gave new and reliable data on palygorskite from skarns. It was pointed out that both palygorskite from Băița Bihor and Ocna de Fier are orthorhombic. This fact is expected taking into account that the experiments carried out by Hirsiger and Muller-Vonmoos (1975) have proved that the monoclinic polymorph converts into orthorhombic by heating. Consequently, the orthorhombic polymorph of palygorskite, which remains structurally unchanged during the slight thermal variations induced by hydrometasomatism and hydrothermalism, is suggested to be characteristic of skarn systems. The infrared spectrum of a sample from Băița Bihor distinctly contains all the bands assumable to hydroxyl groups, to hygroscopically adsorbed or zeolitic and bound water.

On the other hand, mineral chemistry investigations as well as some peculiarities of the in-

frared spectrum show that the palygorskite at Băița Bihor is more aluminous and calcic than other palygorskites. As the high aluminosity increases the mineral stability under conditions of acid leaching (Singer, 1977, fide Jones, Galan, 1988), its remarkable persistence during the epithermalism and weathering can be explained.

Acknowledgements

Thanks are due to Mr. Dan Nour (RAMR Băița Bihor) who generously provided some of the samples used for analysis. We wish to express our appreciation to Mrs Carmen Bunesco (METAV SA, Bucharest) for the electron microprobe analysis. We are also grateful to our colleague Gabriela Stelea for her assistance in the infrared analysis. Last but not least, we are sincerely grateful to Dr. George Udubașa and Gavril Sabau for critical reading and correction of the manuscript.

References

- Benoit, P.H. (1986) Indexing and least-squares powder diffraction program written by D.E. Appleman and H. T. Evans (1973) revised for microcomputer use. Lehigh University, Bethlehem, Pennsylvania.
- Bordea, S., Bordea, J. (1973) Noi date stratigrafice și structurale în nord-vestul Munților Bihor. *D. S. Inst. Geol.*, LIX, 5, p. 5-12, București.
- Caillère, S., Henin, S. (1961) Palygorskite. In G. Brown ed.: *X-ray Identification and Crystal Structures of Clay Minerals*. Mineralogical Society, London, p. 343-353.
- Christ, C.L., Hathaway, J.C., Hosteller, P.B., Shepard, A.O. (1969) Palygorskite: New X-ray data. *American Mineralogist*, 54, 1-2, p. 198-205.
- Cioffica, G., Vlad, Ș. (1968) Observații asupra skarnelor de la Băița Bihorului. *Șt. Cerc. Geol. Geofiz. Geogr., seria Geologie*, 13, p. 43-50.
- , Vlad, Ș., Volanschi, E., Stoici, S. (1977) Skarnele magneziene cu mineralizații asociate de



- la Băița Bihorului. *St. Cerc. Geol. Geofiz. Geogr., seria Geologie*, 22, p. 39-57.
- Demangeon, P., Salvayre, H. (1969)** Nouveau cas de genèse de palygorskite en milieu solide carbonaté. *Bull. Soc. franc. Minéral. Cristallogr.*, 92. 3, p. 313.
- Drits, V. A., Sokolova, G. V. (1971)** On the structure of palygorskite. *Krystallografiya*, 16, 1, p. 228-231.
- Farmer, V. C. (1972)** The infrared spectra of minerals. *Mineralogical spectra of minerals*. Mineralogical Society, London, 382 p.
- (1979) Infrared spectroscopy. In: *Data Handbook for Clay Minerals and Other Non-metallic Minerals*. H. van Olphen and J. J. Fripiat eds., Pergamon Press, Oxford, p. 285-330.
- Gard, J. A., Follet, E. A. (1968)** A structural scheme for palygorskite. *Clay Minerals*, 7, p. 367-369.
- Gupta, G. C., Malik, W. U. (1969)** Fixation of hydroxy-aluminium by montmorillonite. *American Mineralogist*, 54, 11-12, p. 1625-1634.
- Hayashi, H., Otsuka, R., Imai, N. (1969)** Infrared study of sepiolite and palygorskite on heating. *American Mineralogist*, 54, 11-12, p. 1613-1624.
- Heller-Kallai, L., Rozenson, I. (1981)** Mössbauer studies of palygorskite and some aspects of palygorskite mineralogy. *Clays and Clay Minerals*, 29, 3, p. 226-232.
- Hirsiger, W., Müller-Vonmoos, M., Wiedemann, H. G. (1975)** Thermal analysis of palygorskite. *Thermochimica Acta*, 13, p. 223-230.
- Jones, B. F., Galan, E. (1988)** Sepiolite and palygorskite. In: *Hydrous phyllosilicates (exclusive of micas)*. S. W. Bailey ed., Mineralogical Society of America, *Reviews in Mineralogy*, 19, chap. 16, p. 631-674.
- Kissling, Al. (1967)** Studii mineralogice și petrografice în zona de exoskarn de la Ocna de Fier (Banat). Academiei Ed., Bucharest, 172 p.
- Marincea, Șt. (1993)** Mineralogical data concerning the magnesian hornfels in the Pietroasa area (Bihor Mountains). *Romanian Journal of Mineralogy*, 76, 1, p. 29-41, București.
- Matei, L. (1983)** Argilele panoniene din Transilvania. Academiei Ed., Bucharest, 160 p.
- Moenke, H. (1966)** Mineralspektren, II. Akademie - Verlag, Berlin.
- Müller-Vonmoos, M., Schindler, C. (1973)** Palygorskite im helvetischen Kieselkalk des Bürgenstocks. *Schweiz. Mineral. Petr. Mitteilungen*, 53, 3, p. 395-404.
- Nakamoto, K., Margoshes, M., Rundle, R. E. (1955)** Stretching frequencies as a function of distances in hydrogen bonds. *J. Amer. Chem. Soc.*, 77, p. 6480-6486.
- Neacșu G. (1969)** Bentonitele între Alba Iulia și Ocna Mureș. Academiei Ed., Bucharest, 204 p.
- Newman, A. C., Brown, G. (1987)** The chemical constitution of clays. In: *Chemistry of Clays and Clay Minerals*. A. C. D. Newman ed., Mineralogical Society, London, p. 1 - 128.
- Preisinger, A. (1965)** Prehnit - ein neuer Schichtsilikattyp. *Tschermaks Mineral. Petrog. Mitt.*, 10, p. 491-504.
- Prost, R. (1975)** Étude de l'hydratation des argiles: interaction eau-minéral et mécanisme de la rétention de l'eau. Unpubl. Ph. D. Thesis, University of Paris VI, France.
- Rautureau, M., Mifsud, A. (1975)** Thermal analysis studies of sepiolite and palygorskite under vacuum and in normal conditions, C. R. Acad. Sci. Paris, 281, D, p. 1071-1074.
- Serna, C. J., Van Scoyoc, G.E., Ahlrichs, J.L. (1977)** Hydroxyl groups and water in palygorskite. *American Mineralogist*, 62, 7-8, p. 784-792.
- Smith, D. G. W., Norem, D. (1986)** The electron-microprobe analysis of palygorskite. *Canadian Mineralogist*, 24, 3, p. 499-511.
- Stoici, S. D. (1974)** Studiul geologic și petrografic al bazinului superior al Crișului Negru - Băița Bihor, cu privire specială asupra mineralizației de bor și a skarnelor magneziene. Șt. tehn. econ. I. G. G., seria I, 7, 199 p.
- (1983) Districtul metalogenetic Băița Bihorului. Ed. Academiei, Bucharest, 190 p.
- Ștefan, A., Lazăr, C., Berbeleac, I., Udubașa, G. (1988)** Evolution of banatitic magmatism in the Apuseni Mts. and associated metallogenesis. *D. S. Inst. Geol. Geofiz.*, 72 - 73/2, p. 195-213.
- Udubașa, G., Ilinca, G., Marincea, Șt., Săbău, G., Rădan S. (1992)** Minerals in Romania: The state of the art 1991. *Romanian Journal of Mineralogy*, 75, p. 1-51, București.



- Van Scoyoc, G. E., Serna, C. J., Ahlrichs, J. L. (1979) Structural changes in palygorskite during dehydration and dehydroxylation. *American Mineralogist*, 64, 1 - 2, p. 215-223.
- Yariv, S. (1986) Infrared evidence for the occurrence of SiO groups with double-bond character in antigorite, sepiolite and palygorskite. *Clay Minerals*, 21, 5, p. 925-936.
- Zaritsky, P. V., Orlov, O. M. (1973) Palygorskite from karst cavities of L₁ limestone of the Middle Carboniferous of the Donetz Basin. *Dokl. Akad. Nauk S.S.S.R.*, 208, 1, p. 196-199 (in Russian).

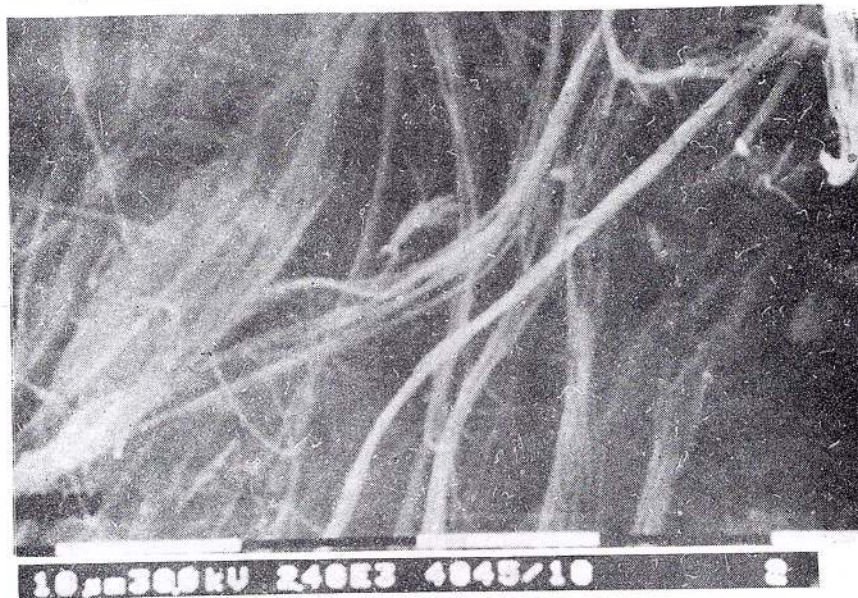
Plate

Fig. 1 - Scanning image of typical palygorskite crystals, which clearly shows the composite nature of the fibres.*

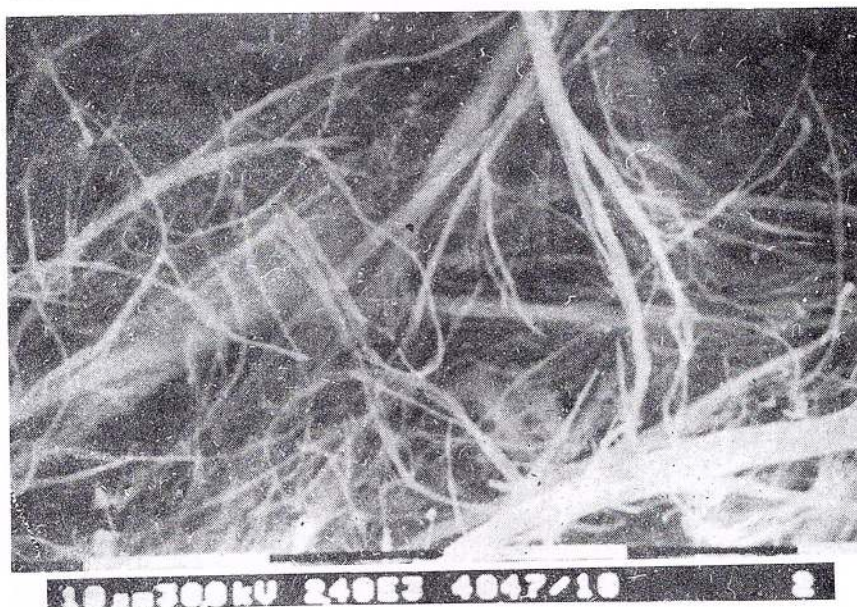
Fig. 2 - Scanning image of a palygorskite aggregate showing some calcite inclusions (clear white).*

Fig. 3 - Randomly oriented palygorskite fibres.*

* The magnification (scale bar) and instrument operating voltage are indicated immediately below each photo.



1



2



3

SEPIOLITE FROM DEALUL MĂGURENILOR – PRELUCA VECHE, MARAMUREȘ DISTRICT, ROMANIA

Ioan KALMÁR, Péter KOVÁCS-PALFFY, Mária FÖLDEVARI

Geological Institute of Hungary, 1143 Budapest XIV, Stefánua út 14



Key words: Preluca Mts. Măgureni Carbonate Formation. Dolomite. Pegmatite. Sepiolite. X-ray pattern. DTA. Chemical analyses. SEM micrographs.

Abstract: In the Măgureni Hill situated in the Preluca Mts (NW Transylvania) regionally metamorphosed carbonatic rocks (dolomitic and calcitic marbles) were intruded by several "hot" pegmatite bodies during the latest phase of the regional metamorphism. The crystallization of pegmatites was accompanied by the diopside-tremolite-phlogopite skarn formation and was followed by hydrothermal processes. The SiO_2 -bearing alkaline aqueous solutions reacted with the Mg-rich wall rock resulting in the formation of a magnesian clay mineral association. Sepiolite is the most interesting among them, both from mineralogical and from economic point of view. The sepiolite of the Măgureni Hill forms thin veins and lenses. The accompanying minerals are talc, saponite, chlorite, kaolinite, marcasite, calcite and opal. Chemical, XRD, DTA, IR and electronmicroscopic studies proved the presence of pure, magnesian sepiolite, with a very small amount of alumina and iron oxide. Mg-coordinated and free (zeolitic) water were also indicated. Finally, the experiences for extraction, enrichment and the possibility of utilisation are presented. Sepiolite, known as a fibrous clay mineral, can be formed in sedimentary and magmatic environments. In sedimentary domain, sepiolite-bearing residual clays can be formed by alteration of the Mg-rich igneous rocks (i.e. basalts, gabbros, peridotites and dunites). Sepiolite, together with dolomite, magnesite and Mg-salts can precipitate in hypersaline (bitter) lakes in desertic environments. The sepiolite content of some marine or lacustrine marls and limestones is due to the reworking of that kind of sediments (Power, 1981). Mg-carbonates and hydrated Mg-silicates, such as serpentines, chlorites, saponite, vermiculite, talc and sepiolite are formed by the hydrothermal alteration of the above-mentioned igneous rocks. In the Măgureni area, a new genetic type was found: the vein-like sepiolite, formed by the reaction between late pegmatitic solutions and metamorphosed carbonate rocks, such as dolomitic and calcitic marbles.



1. Geological setting

The Măgureni Area is situated in the NW part of Transylvania, Romania, near the cities of Baia Mare and Tg. Lăuș (Maramureș District), in the northern and central part of the Preluca Mts. The main sepiolite occurrences are located in the localities Măgureni and Preluca Veche.

The Preluca Mts is one of the seven metamorphic "islands" situated between of the Apuseni Mts and the East Carpathians. They represent the uplifted basement of the Pannonian Domain, i.e. the northeastern edge of the Tisia Great Intra-Carpathian Structural Unit.

Four stratigraphic units were separated in the Preluca Mts: the Răzoare Gneiss Formation, the Măgureni Carbonate Formation, the Preluca Nouă Micaschists and Amphibolite Formation and, in the SW corner, the Țarcu Micaschists Formation. The main structural element is a NE-SW oriented anticline, which includes in its core the Răzoare Formation. The Măgureni Carbonate Formation constitutes the wings of this anticline.

Upper Cretaceous, Paleogene and Neogene detrital and carbonate rocks from the sedimentary cover of the metamorphic basement.

2. The Măgureni Carbonate Formation

The typical succession of the Măgureni Formation is developed in the northwestern wing of the anticline, between the Măgureni and Preluca Veche localities.

In the upper part of the Răzoare Gneiss Formation few white and grey calcitic marble lenses are intercalated. The transition between the biotite-almandine-kyanite-An₃₅ plagioclase paragneiss and the marbles is sharp, but in the lower part of the carbonate rocks 1–5 m thick paragneiss and micaschists lenses or layers can be found. The Măgureni Carbonate Formation is covered by the Preluca Nouă Micaschists and Amphibole Formation, along an important stratigraphic unconformity (Kalmár, 1972a).

The Măgureni Carbonate Formation is built up of five stratigraphic subdivisions, which are, as follows: the Lower Calcitic Member, the Lower Dolomitic Member, the Main Tremolitic Level, the Upper Dolomitic Member, and the Upper Calcitic Member. Mica-bearing marbles ("cippolino"), tremolitic marbles, as well as rare micaschists and amphibolite intercalations also appear at different stratigraphic levels, which cannot be correlated one another (Angelescu *et al.*, 1978, unpubl.).

The main or rather exclusive mineral of these rocks is the coarsely developed, twinned carbonate, dolomite or/and calcite. Beside carbonates, which represent 95–99 % of the rocks, quartz, muscovite, phlogopite, tremolite, and graphite were also identified.

The MgO content of carbonate rocks varies between few percent in calcitic marbles and 18–23 % in the dolomitic ones; the chemical analyses demonstrate frequently an excess of the MgO, exceeding the theoretical value of 21.7 %.

Tremolite constitutes white, 0.2–5 mm large, tabular, euhedral, twinned prisms which are oriented parallel to the foliation of the carbonate rocks. The chemical analysis of tremolite shows a small amount of the iron and magnesium oxide.

The metamorphosed carbonate rocks are massive, oriented, banded and more rarely they show a well developed schistosity. Towards the northern Great Preluca Fault the rocks were intensively breccified, forming an incohesive, cornered auto-breccia which is exploited in several quarries as construction raw material and anti-acid mixture for melioration of the soils.

3. The pegmatites and skarn-like contact zones

A large number of pegmatite lenses and lodes are formed in the paragneisses (Răzoare Formation) as well as in the carbonatic rocks.



They form 0.3–2 m thick, 10–150 m long, tabular or irregular, frequently zoned bodies. Usually, the zonation is due to the disposition of the quartz- and muscovite-rich as well as to tourmaline-bearing separations (Kalmár 1972b).

The pegmatites consist of quartz, orthoclase, plagioclase (20–30 % An), muscovite, tourmaline and almandine forming grains up to 5–10 cm in size. Frequently, aplite and hydrothermal quartz veinlets cut the pegmatitic bodies. In the contact zone with the carbonate rocks, skarn-like, 5–20 cm thick diopside-magnetite-tremolite-phlogopite lenses were formed. This mineral association is stable at 500–650°C and 2–2.5 kb (Winkler, 1970). The sepiolite-bearing veins occur frequently in the neighbourhood of this reaction zone.

4. The occurrences of sepiolite

The main sepiolite occurrences of the Preluca Mts can be found on the northern and western slope of the Măgureni Hill (Fig. 1).

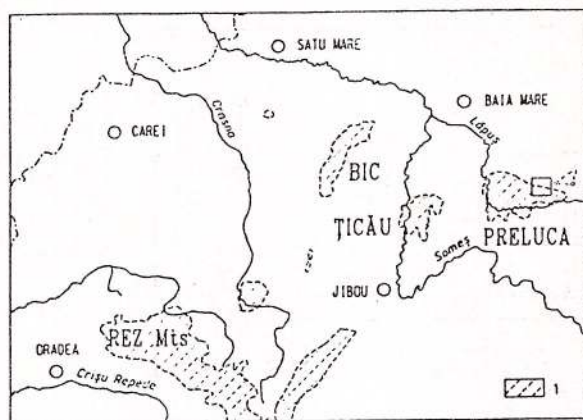


Fig. 1 – Metamorphic Island in NW Transylvania. 1, Outcropping metamorphic rocks. In frame, Măgureni area.

Sepiolite veins in marbles were also found at Răzoare (bentonite quarry), in southern Preluca (Aspra) and in the Inău Crystalline

"Island" (between the Borcut and Inău villages, as well as in deep boreholes, east of the Preluca Mts).

The sepiolite veinlets were first discovered in the mining workings made for sampling the dolomites from the Măgureni Hill. Sepiolite veins were found in No. 21 gallery on the northern slope of the Măgureni Hill (Pop & Angelescu, 1981). The strongly brecciated marble (Upper Dolomitic member) contains disrupted, lenticled veinlets, and 1–2 cm secondary sepiolite nests were found in powdery dolomite which fills the voids between the breccia elements.

A thin vein of sepiolite was found in a dolomite gravel, resulting from reworking in basal breccia of Paleogene deposits, in a little pit dugged on the southern slope of the Măgureni Hill, near the limit to the sandstones. The most interesting group of veinlets occurs in No. 25 gallery (Fig. 2). Twelve veinlet-zones were traversed here and four of them were followed directionally. They are developed in carbonate rocks, calcitic-graphitic and dolomitic marble banks (Lower Calcitic Member) which are traversed by a pegmatite lode in the left side of the gallery.

Sepiolite forming lenticular, felty or nacreous aggregates fills N–S oriented 1–5 cm thick discontinuous veins. Beside sepiolite there are some other minerals, such as steatite, talc, notronite, calcite and opal with few marcasite impregnations.

The succession of the mineral formation, based on the spatial relationship between them in sepiolite-bearing veins and lenses is presented in Figure 3.

5. Mineralogy of sepiolite occurrences

Sepiolite from the Măgureni Hill was examined by optic and electronic microscope (SEM) as well as by XRD, DTA, IR and chemical analyses.

In thin section sepiolite shows a parallel

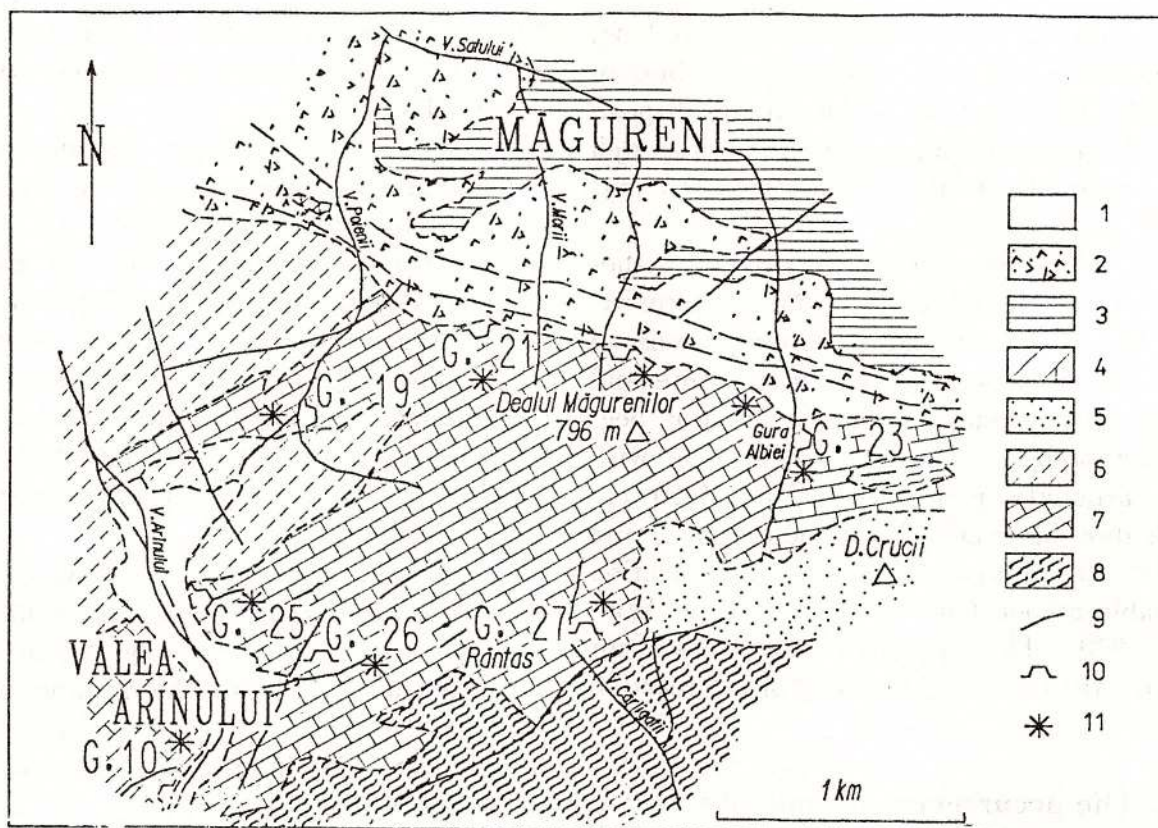


Fig. 2 – Măgureni Hill. 1, Alluvium; 2, Slope loam; 3, Upper Oligocene Buzăș Formation; 4, Upper Priabonian Cozla Limestone Formation; 5, Lower Priabonian Valea Nădașului Sandstone Formation. Crystalline Basement: 6, Preluca Nouă Micaschist Formation; 7, Măgureni Carbonate Formation; 8, Răzoare Gneiss Formation; 9, Pegmatites; 10, Galleries; 11, Sepiolite occurrences.

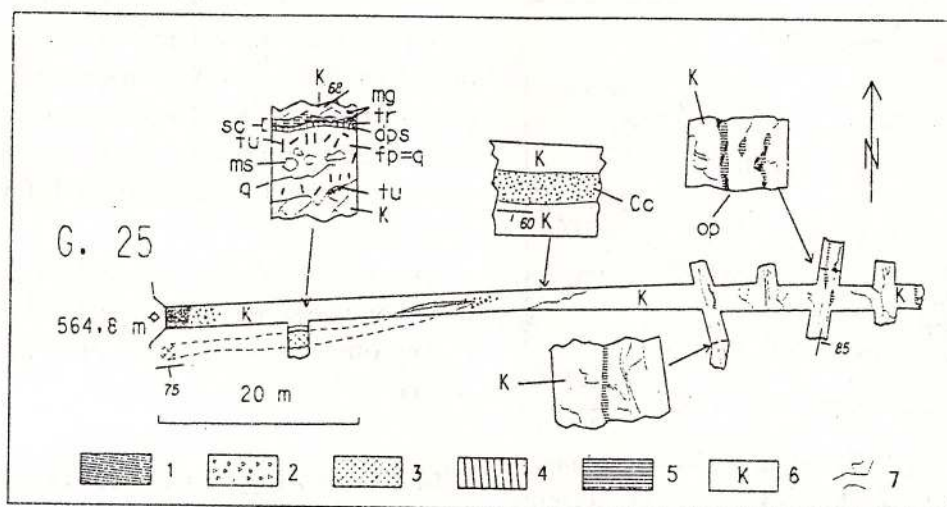


Fig. 3 – Plan of no. 25 gallery. 1, Slope loam; 2, Dolomitic breccia; Cc, Calcitic-quartzose marble; 3, Pegmatite (fp, feldspar; ms, muscovite; tu, tourmaline; q, quartz); 4, (sc), Skarn-like reaction zone (dps, diopside; mg, magnetite; tr, tremolite); 5, Sepiolite, op, opal; 6, (K), Dolomitic marble; Cc, Calcitic, quart-bearing marble; 7, thin sepiolite veins.

or irregular aggregate of thin, light green or coloured fibres, with lenticular separations of talc and clay minerals as well as with disseminated euhedral carbonate and opaque grains.

The electron-microscopic images show a hair-like aggregate of a few mm long and 0.01–0.02 mm thick threads which are composed of 0.05–0.1 μm thick sepiolite fibres. Talc, calcite, opal and other minerals occur between the threads. Most inconveniences for the chemical analyses are caused by small 0.01–0.02 μm large opal sphaerulae (Pl., Figs. 1–3).

X-ray diffractogram (Fig. 4) provided evidence of a succession of clay designed, edged peaks, which demonstrate the advanced crystallinity of this mineral. The position of these peaks is presented in Table 1.

The decomposition of sepiolite with increasing temperature was checked by analyses (Fig. 5). They proved the presence of the zeolitic as well as of the structural or crystallisation water, the dehydroxylation peak and, finally, the exothermal peak due to the formation of the enstatite.

The IR absorption spectra (Fig. 6) show the stretching of the OH-valence (3678.6 cm^{-1}), the stretching of the Mg (Fe)-coordinated structural water (3622.8 cm^{-1}) and the stretching of the free (zeolitic) water (3399.8 and 3560.5 cm^{-1}) identified by characteristic absorption bands (Hayashi, 1969).

6. Some data about the genesis of sepiolite

The above-mentioned data show a close association between the carbonate host rocks, pegmatitic lenses and sepiolite veins. In a later phase of metamorphic recrystallisation of the rocks of Preluca Mts, Si, Al and Fe-bearing hot fluids from the deeper zone ascended along the lithological discontinuities and fractures in carbonate rocks. Their reaction with carbonate host rock resulted in skarn-like rims and at progressively decreasing temperature the pegmatitic mineral aggregates were formed.

The crystallisation of minerals from pegmatitic fluids was a long process which begun by the formation of garnet, black tourmaline, oligoclase, microcline and smoky quartz, followed by muscovite, albite and milky quartz and finished by orthoclase and limpid quartz. In a later phase, the newly formed pegmatitic body was broken and the resulting cracks were infilled either by quartz-albite-orthoclase aplite, or by milky quartz.

The crystallisation of the main pegmatitic minerals did exhaust the energy of the deep sources. The ascension of the aqueous fluids continued; they moved into the fractures of carbonate rocks and reacted with them, forming the hydrothermal association, which consists of three phases: the light temperature association (talc, chlorite), the medium-temperature one (sepiolite, saponite, white calcite, sericite) and finally, the "cold" association: kaoline, limpid calcite, pyrite, marcasite and opal.

The homogenization of two-phase inclusions in the white calcite crystals occurred at $212\text{--}225^\circ\text{C}$, and in the limpid calcite at, $108\text{--}132^\circ\text{C}$.

Chemical analyses confirm the pure, iron- and aluminium-free character of sepiolite taken from the No 25 gallery (Fig. 7). The increased amount of silica is due to the presence of inseparable opal sphaerules.

The earlier sepiolite samples taken from the northern slope of the Măgureni Hill (No 1,21,22 gallery) contain 0.1–0.3 iron ions per unit cell in the octahedral position (Pop & Angelescu, 1981) (Fig. 8). Therefore, it can be suggested that the Mg/Fe ratio of sepiolite depends on the MgO content of the host rock; the increased amount of MgO facilitates the iron enrichment. This is demonstrated by experimental data (Wollast et al., 1968). Thus, one of the essential conditions of the synthesis of sepiolite is a well-defined pH-value, ranging between 8.0 and 9.2, which is assured by the presence of Ca^{++} ions as buffer.



Minerals	350°C?		212-225°C		108-132°C	
Opal						-----
Dolomite powder			-?		---	---
Marcasite					--	--
Calcite II						----
Kaolinite					-----	
Sericite			--	-----		
Calcite I				---		
Saponite			--			
Sepiolite			-----	---		
Chlorite		-----				
Steatite	---					

Fig. 4 – Succession of crystallisation in sepiolite-bearing veins.

Table 1
Diffraction pattern of sepiolite sample No 83a, No. 25 Gallery,
Măgureni Hill*

2 θ	d	I	α	2 θ	d	I	α
6.40	13.810	7	0	33.37	2.683	7	1
7.39	11.97	100	0	33.48	2.674	7	1
9.60	9.213	1	0	34.23	2.613	9	1
11.85	7.466	6	0	35.03	2.559	14	1
13.18	6.717	5	0	36.76	2.443	4	1
14.76	6.002	1	0	36.92	2.433	4	1
17.68	5.016	5	0	37.50	2.396	5	1
18.72	4.740	1	0	38.36	2.345	1	1
19.74	4.497	14	0	39.76	2.265	6	1
20.63	4.306	11	0	39.96	2.254	6	1
22.40	3.969	1	0	40.31	2.235	4	1
23.79	3.740	16	0	42.68	2.117	2	1
23.79	3.740	16	0	42.68	2.117	2	1
25.16	3.539	3	0	43.04	2.100	1	1
26.60	3.351	23	0	43.72	2.069	3	1
27.98	3.189	9	0	43.95	2.058	4	1
28.67	3.113	2	0	46.44	1.954	1	1
29.28	3.050	3	0	47.52	1.912	2	1
30.64	2.915	1	1	48.48	1.876	2	1
31.64	2.826	1	1	50.33	1.812	1	1

*Fraction <2 μ m, treated with acetic acid, 1/N.X-ray: K α . 2 θ min=2.0°; 2 θ max=66.0°;Total number of lines: 66; Error $\pm 0.2^\circ$ 

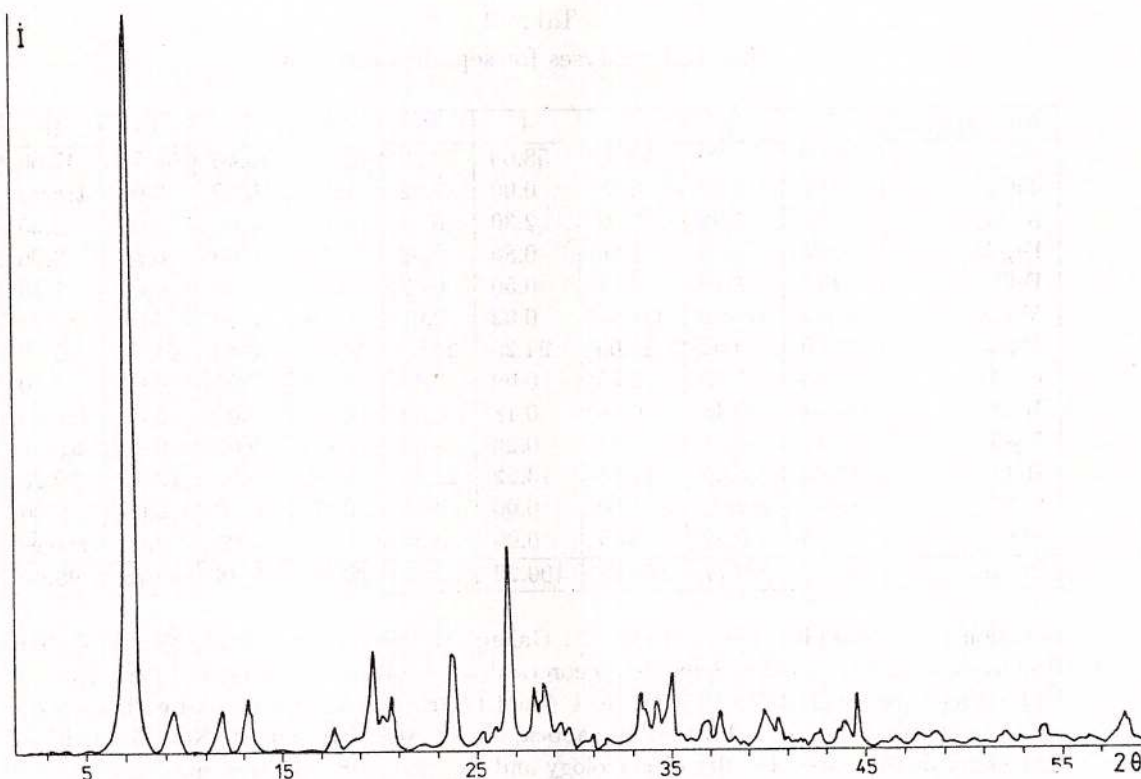


Fig. 5 - X-Ray diffractogram of sepiolite sample from the Măgureni Hill

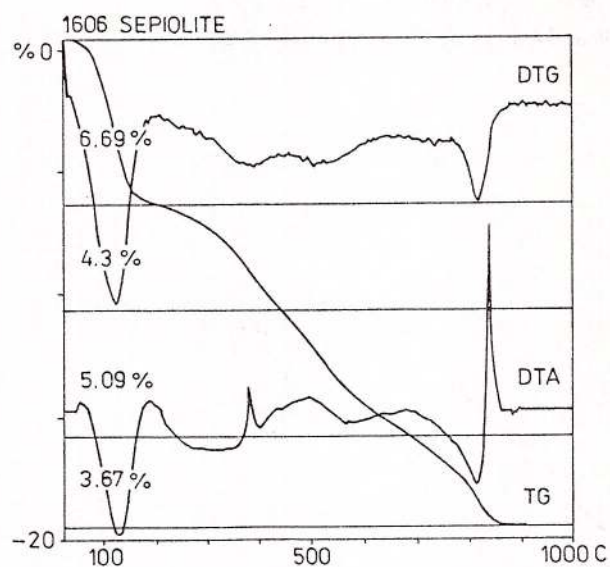


Fig. 6 - Thermal analyses of sepiolite from the Măgureni Hill

7. Utilisation of sepiolite

The technology of the enrichment of sepiolite bearing marbles was tested in 3.5 m³ samples extracted from the No. 25 gallery (Chelbea et al., 1978, unpubl.). Marbles was milled in ball and tube mill and classed in helicoidal classor linked in circuite with a hydrocyclon (Φ300 mm). The slime was flocculed with polyacrilamide and treated with HCl 1:10. The neutralised, filtered and dried sepiolite concentrate contains 80 % sepiolite, 15 % other clay minerals, 3 % quartz, and 2 % HCl-insoluble carbonats. In this way, 18-20 kg/m³ sepiolitic concentrate was extracted.

The sepiolite concentrate can be utilised for preparation of pesticides and insecticides, in pharmaceutic industry and for molecular filters.

Table 2
Chemical analyses for sepiolite samples

No. samples	1	2	3	4	12	13	14	15	16
SiO ₂	54.00	53.30	53.02	58.60	52.80	52.30	56.40	55.54	47.50
TiO ₂	0.00	0.00	0.00	0.00	0.02	0.00	0.00	0.00	traces
Al ₂ O ₃	1.78	5.92	2.03	2.30	0.18	0.00	0.00	0.00	2.35
Fe ₂ O ₃	1.24	1.75	1.96	0.86	0.32	12.50	6.50	0.00	9.96
FeO	0.75	1.19	0.81	0.50	0.02	0.00	0.00	0.00	1.18
MnO	traces	traces	traces	0.02	0.01	0.00	0.00	0.00	traces
MgO	22.00	19.09	24.00	24.20	24.30	14.27	16.43	24.89	15.10
CaO	0.65	1.55	0.58	0.09	0.44	1.39	1.05	0.00	1.40
Na ₂ O	traces	0.48	0.08	0.18	0.02	0.00	0.00	0.00	traces
K ₂ O	0.11	0.24	0.21	0.26	0.04	0.00	0.00	0.00	traces
H ₂ O ⁺	17.02	16.00	17.34	13.22	21.09	19.50	19.50	19.44	19.20
CO ₂	traces	traces	0.00	0.00	0.00	0.00	0.00	0.00	0.00
P ₂ O ₅	0.05	0.25	0.05	0.00	0.04	0.00	0.00	0.00	traces
Total	97.60	99.77	100.08	100.23	99.28	99.96	99.88	99.78	96.69

Location of the samples: No. 1-4, No. 21 Gallery Măgureni; No. 12-14, No. 25 Gallery Preluca Veche; No. 15, Mg-Sepiolite, theoretical composition (Preisinger, 1958); No. 16, Fe-bearing sepiolite (JCPDS 26-863). No 1-4 and 12, fraction <2mμ, treated with 1N acetic acid. Analyses: No. 1-4, ICPMC Cluj-Napoca; No 12, MAFI Budapest; No. 13-14, ELTE University of Budapest, Faculty of Petrology and Geochemistry, electron microprobe.

By recalculation of the chemical analyses (Table 2), the structural formula of sepiolite is, as follows:

Mg-Sepiolite $\text{Mg}_4\text{Si}_6\text{O}_{15}(\text{OH})_2 \cdot 6\text{H}_2\text{O}$ JCPDS 26-1226

Fe-Sepiolite $(\text{Mg},\text{Fe})_4\text{Si}_6(\text{OH})_2 \cdot 6\text{H}_2\text{O}$ JCPDS 29-863

Sepiolite from the Măgureni Hill (calculated on 23 O-basis, after Nemečz, 1970):

$(\text{Mg}_{3.96}\text{Fe}_{0.08}\text{Ca}_{0.02})(\text{OH})_{2.05}(\text{Si}_{8.86}\text{Al}_{0.92}\text{Fe}_{0.14})\text{O}_{14} \cdot 7\text{H}_2\text{O}$ - sample No 2

$(\text{Mg}_{4.00}\text{Fe}_{0.02}\text{Ca}_{0.02})(\text{OH})_{2.04}(\text{Si}_{7.66}\text{Al}_{0.02})\text{O}_{13.43} \cdot 7.57\text{H}_2\text{O}$ - Sample 12

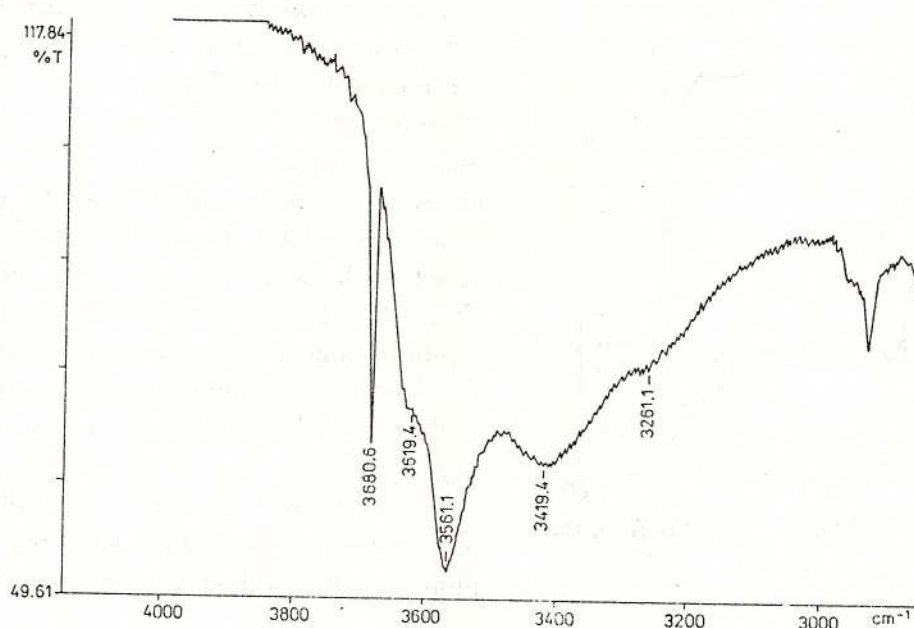


Fig. 7 - IR absorption spectrogram of sepiolite sample from the Măgureni Hill



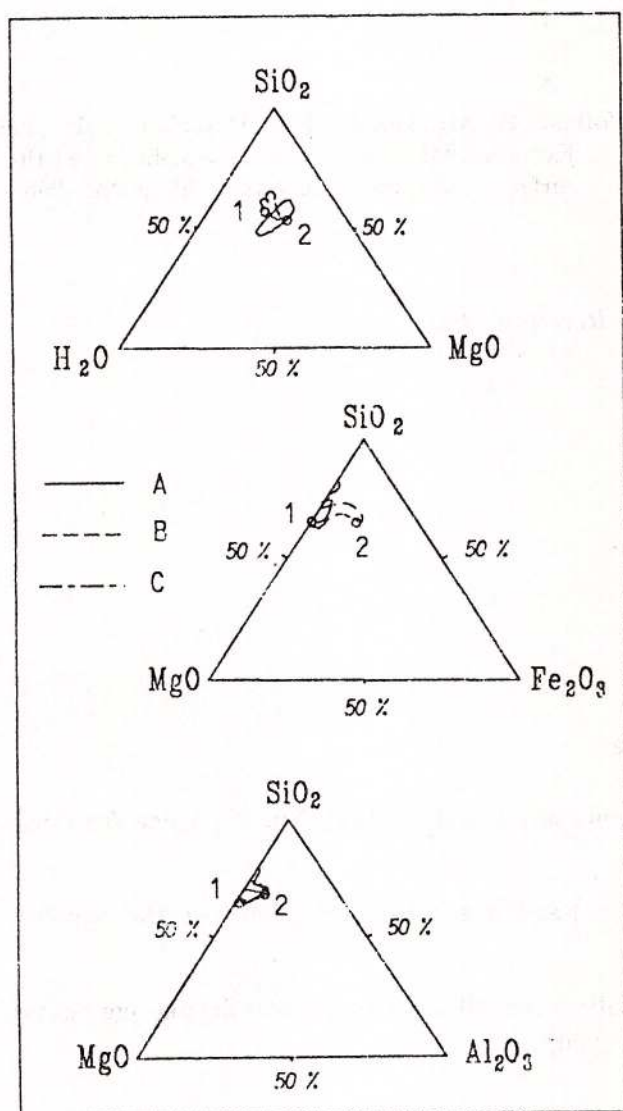


Fig. 8 – Ternary diagrams of sepiolite samples from Măgureni. A, Data from literature; B, data from gal. 21 (Pop, Angelescu, 1981); C, Data from gal. 19 and 25. 1, Mg-sepiolite (26-1226JCPDS); 2, Fe-sepiolite (26-863 JCPDS)

8. Conclusions

Sepiolite and accompanying clay and non-clay minerals were formed through the reaction of residual, neutral or alkaline, SiO_2 -bearing aqueous solutions with carbonate Mg-rich wall-rocks, related to the formation of the pegmatitic bodies. Thus, they mark one of the last stages of mineral formation which closes the metamorphic processes, preceeding the

deposition of the Mesozoic and Kainozoic sedimentary cover.

Aknowledgements

Financial support for this paper, including expenses of instrumental investigations, was provided by the Hungarian Scientific Fund OTKA, theme T 7636.

The author is indebted to dr. István Viczián and dr. Tibor Tullner for their helpful contribution to the interpretation of analytical data and in editing the English version.

The results of our research on the Romanian sepiolite were also presented in the Centenary Jubilee Session of the University of Bucharest, using the kind invitation of dr. E. Constantinescu and dr. N. Anastasiu.

References

- Hathway, J.C., Sachs, P.L. (1965) Sepiolite and clinoptilolite from Mid-Atlantic Ridge. *Amer. Miner.*, 50, p. 175–201.
- Hayashi, H., Otsuka, P., Imai, N. (1969) Infrared study of sepiolite and palygorskite on heating. *Amer. Miner.* 54, p. 206–211.
- Kalmár, I (1972a) Stratigrafia terenurilor metamorfe și sedimentare din insulele cristaline Inău, Preluca și Țicău. Ph. D. Thesis, Oil, Gase and Geology Technical University, Bucharest.
- (1972b) Pegmatitele din Munții Preluca. *D. S. Inst. Geol. Rom.*, LIX/1, p. 231–249, București.
- Nemecz, E. (1973) Agyagásványok. Akad. Kiadó, Budapest.
- Pop, N., Angelescu, I. (1981) Sepiolitul de la Măgureni-Preluca, jud. Maramureș; date mineralogice, chimice și genetice. *St. Cerc. Geol.*, 26, 1, p. 45–57, București.
- Power, R. (1981) The Sepiolite Event. *8th Congr. AIPEA, Abstr.*, p. 23–25, Pavia-Bologna.
- Preisinger, A. (1961) Sepiolite and related compounds: its stability and application. *Proc. X. Conf. Clay and Clay Minerals*, p. 365–371, Stuttgart.

Winkler, H.G.F. (1970) Abolition of metamorphic Facies. Introduction of the four divisions of Metamorphic Stage and of a classification based on Isograde in common rocks. *N. Miner. Mh.*, 5, p. 193–230, Stuttgart.

Wollast, P., Mackenzie, F.I., Briecker, O.P. (1968) Experimental precipitation of sepiolite at earth-surface conditions. *Am. Miner.*, 53, p. 222–250.

Received: June, 1995

Plate

Fig. 1 – Sepiolite, oriented thread and isolated elementary fibres. Gallery No. 25, Valea Arinului; X1000.

Fig. 2 – Steatite (st), opal sphaerules (o), calcite (cc) and iron sulphide (s) between the sepiolite threads. Gallery No. 25, Valea Arinului; X1000.

Fig. 3 – The thin fibres of the felty sepiolite from Gallery No. 19 constitute a curtain-like aggregates with calcite (cc) and small opal sphaerules (o); X2000.



1 1000 X



2 1000 X



3 2000 X

MINERAL COMPOSITION AND BLOATING EFFECT OF CLAYSHALE FROM MEŽICA Pb-Zn ORE DEPOSIT (SLOVENIA)

P. TOMŠE, B. MITRIČ

Dept. of Geology, University of Ljubljana, Aškerčeva 12, 61000 Ljubljana, Slovenia

J. KUŠEJ

Mine of Lead and Zinc Mežica, 62392 Mežica, Slovenia

Key words: Bloating effect. Expansion coefficient. Clayshale. Thermal analysis. Mežica ore deposits, Slovenia. Karavanken Mts.

Abstract: Large amounts of clayshale can be found as surroundings to layers enriched with lead and zinc ore in the Mežica ore deposit. Mineralogical investigations have been done on the representative samples in order to prove clayshale is usable as a raw material for making the expanded clay aggregate. The profile through the clayshale deposit has been made on a length of 87 m where changing clayshale layers of different thicknesses – the soft and the compact sort – can be found. Almost equal quantities of illite and chlorite have been found in all investigated samples. These are the most common minerals, therefore the name illite – chlorite clayshale can be used. Calcite has been determined quantitatively by measuring the loss of mass – on the TG curve – because of decarbonitization at the temperature interval of 743⁰–801⁰ C. Its amount is about 3 mass % and it does differ much from sample to sample. Dolomite, pyrite and microcline have been determined in traces only in the samples from the beginning of profile. In the end the plagioclases substitute the microcline. Content of quartz – determined by the X-ray diffraction – is decreasing from the beginning to the end of profile. With decreasing quartz content the expansion coefficient increases from 3.8 up to 5.8 and the bulk density inversely decreases from 0.6 up to 0.4 g/cm³. It has been stated as well that the soft type of clayshale expands less than the compact one. The soft type of clayshale has begun to expand at 1050⁰ C; at 1120⁰ C has been measured an average expansion coefficient of 4.6 and an average bulk density of 0.5 g/cm³. The compact type starts to expand at 1020⁰ C; at 1120⁰ C has been measured an average expansion coefficient (K) of 5.4 and bulk density of 0.4 g/cm³.

Introduction

Clay raw material expands during firing because of steam and gases (formed at different temperatures), which are unable to escape from the ceramic body for various reasons.

Gases arise as a consequence of subsequent reactions:

- organic components of the raw material,
- water vapour of the minerals (loss of moisture, structural water lossing),



c) steam development due to the reaction of fayalite forming,

d) steam development due to the reactions occurring between CO and iron compounds,

e) oxidation of the pyrites,

f) decomposition of the carbonate and sulphate components.

Ceramic body should have a small pore volume, dense texture and considerable pyroplastic state at the bloating temperature (Tóth, Csáky, 1989).

Expanded clay aggregate represents (Knigina, 1977) porous material with glass appearance, even distributed pores of spherical shape and bulk density up to 200 kg/m^3 . The bulk density depends on expanding coefficient of clay raw material, furthermore on method and regime of firing. Expanding efficiency measurements are represented with coefficient of expansion (Knigina, 1977) – $K = V_2/V_1$, where V_1 is the volume of ceramic body before and V_2 is the volume of ceramic body after the bloating. Different organic and inorganic materials (such as peat, filling dust,...) should be added to clay raw material in order to increase the expanding effect. Chemical, mineralogical and grain size composition of clay raw material influence on the bloating effect as many investigators (Riley, 1951, Rosenberger, 1969, pawlow, 1962) noticed.

Fastabend Ruyter (Rosenberger, 1969) determined qualitatively and quantitatively the mineral composition of clay raw material necessary for expansion. Bloating effect is greater if a great amount of mica/illite and montmorillonite is present in the raw material. Consequently, at least 25–35 mass% of smectite group minerals should be found in clay raw material in order to ensure expansion. Kaolinite plays a negative role as far as expanding effect is concerned. Kaolinite minerals have caused the clay aggregate shrinking because of structural water lossing at fast firing over the temperature 500°C . What follows is physical disintegration of fired body.

Riley and Wilson (Rosenberger, 1969) have

composed a ternary diagram to represent the expansion ability of clay minerals as function of ratios between determined oxides (Fig. 1). Area - r determines the composition, which enables the best bloating effect and minerals of smectite group fall into this area.

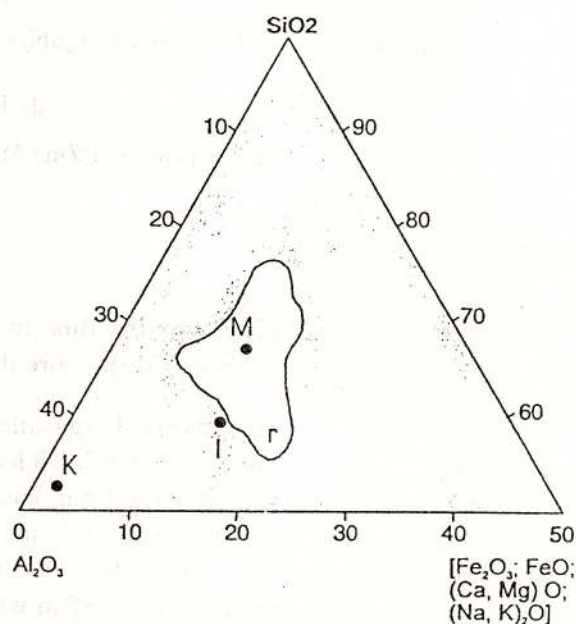
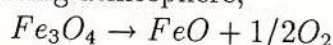


Fig. 1 – Ternary diagram after Riley and Wilson (Rosenberger, 1969). r, expansion range composition after Riley and Wilson; M, I, K, expansion points of montmorillonite, illite and kaolinite.

The kaolinite structure does not contain alkali oxides, which decreases the melting temperature, enables the bloating and shorts the time of sintering. Alkali oxides from feldspars do not influence much the clay raw material melting temperature. Alumina should be present in more than 20 mass % to give the melt a low viscosity, what enables bloating.

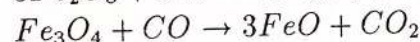
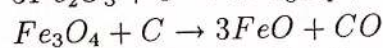
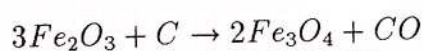
The most important reactions occurring during the clay raw material firing (gaseous phase and melt formation) are (Rosenberger, 1969):

– decomposition of magnetite in mildly reducing atmosphere,

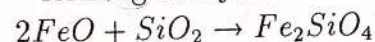


– reaction of iron oxides (hematite and magnetite) with organic matter from raw material,





– forming of fayalite.



Influence of the gaseous phases (arising during the carbonate and sulphate thermal dissociation) on the bloating effect is insignificant.

Experimental work

Upper Triassic T₃ clayshale is found as surroundings to layers enriched with lead and zinc ore in the Mežica ore deposit (Slovenia). It is composed of soft dark grey clayshale (thin layers, about some cm each) and compact dark grey clayshale. They are distributed in about some meters thick layers and arranged alternatively. The whole layer of clayshale is about 50 meters thick. The profile through the clayshale deposit has been made on a length of 87 m.

The investigated rock has a homogeneous texture and characteristic oriented structure. Quartz and mica are particularly notable grains. The matrix is finegrained and contains sericite, pyrite, carbonate minerals and organic matter (Plate, Figs. 1,2).

19 representative samples selected through the investigated profile of clayshale were used for XRD analysis. Samples were homogenised, dried up to 40° C and grinded. The analyses were carried out on non-oriented samples with an external standard. An average composition (in mass %) is, as follows: 40% of illite, 20% of chlorite, up to 20% of quartz, <5% of microcline, <5% of feldspars, <5% of calcite, <5% of pyrite.

Some representative X-ray diffractograms of soft and compact clayshale sample can be seen in Figure 2. According to the mineral composition both sorts of clayshale can be recognized as illite-chlorite clayshale (almost equal quantities of illite and chlorite have been found in all investigated samples). Dolomite, pyrite and microcline have been found in traces only

in the samples from the beginning of profile. Sample 15 has shown the highest pyrite value. Therefore we have concluded that most iron is bounded in chlorite. Plagioclases substitute the microcline in the end of profile. The content of quartz – determined by X-ray diffraction – is decreasing from the beginning to the end of profile.

Gaseous phases have been determined by thermal analysis. DTG curves peaks (Fig. 3) confirm the loss of moisture of clay minerals from investigated samples at the temperature interval from 100 up to 200° C. The minerals have lost structural water as well (between 500–600° C). Sample 1 mass loss at T<500° C is due to the thermal disintegration of pyrite. Quantitative mass lossing have been determined for all enumerated reactions (Table).

Table
Characterisitic temperatures of reactions and Δm of some representative soft clayshale samples (No 1,4,11,15) and compact clayshale samples (No 2,8,14,19)

Samp.	Temp., °C	Δ, mg	mass. %	Mineral
1	103	2.0		clay minerals
	469	1.2		pyrite
	535	3.0		clay minerals
	789	1.2	2.0	calcite
2	103	1.5		clay minerals
	545	4.1		clay minerals
	776	1.7	3.8	calcite
4	103	1.2		clay minerals
	535	4.2		clay minerals
	743	0.8	1.8	calcite
8	100	1.2		clay minerals
	530	4.4		clay minerals
	771	1.7	3.8	calcite
11	103	1.0		clay minerals
	545	4.9		clay minerals
	780	1.5	3.4	calcite
14	103	1.1		clay minerals
	540	4.3		clay minerals
	780	1.5	3.4	calcite
15	103	1.0		clay minerals
	535	4.8		clay minerals
	801	2.8	6.3	calcite
19	103	1.5		clay minerals
	535	4.6		clay minerals
	771	1.2	2.7	calcite

Calcite has been determined quantitatively by measuring the mass loss (TG curves, Fig. 4) owing to the decarbonatization at the tempe-



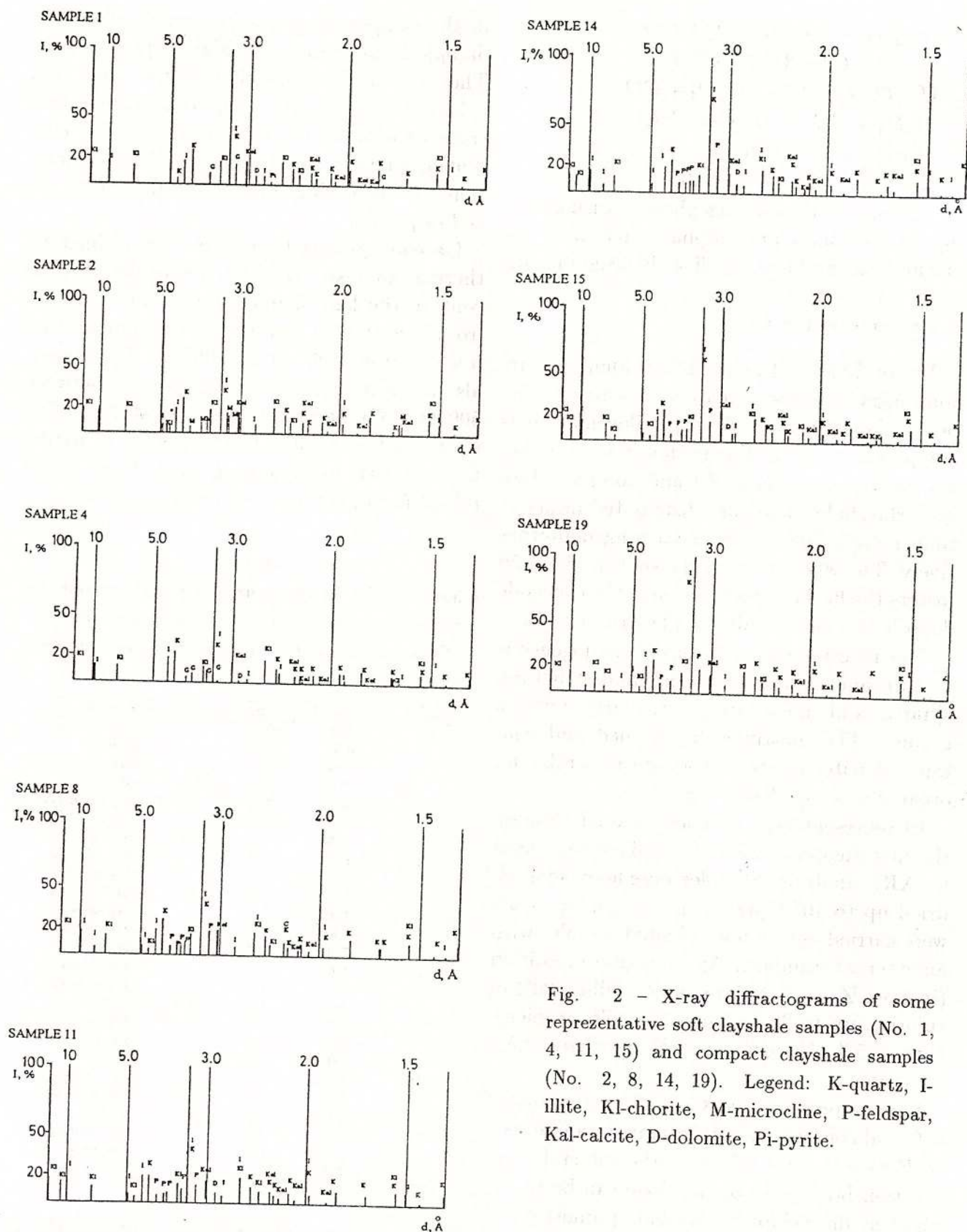


Fig. 2 - X-ray diffractograms of some representative soft clayshale samples (No. 1, 4, 11, 15) and compact clayshale samples (No. 2, 8, 14, 19). Legend: K-quartz, I-illite, Kl-chlorite, M-microcline, P-feldspar, Kal-calcite, D-dolomite, Pi-pyrite.

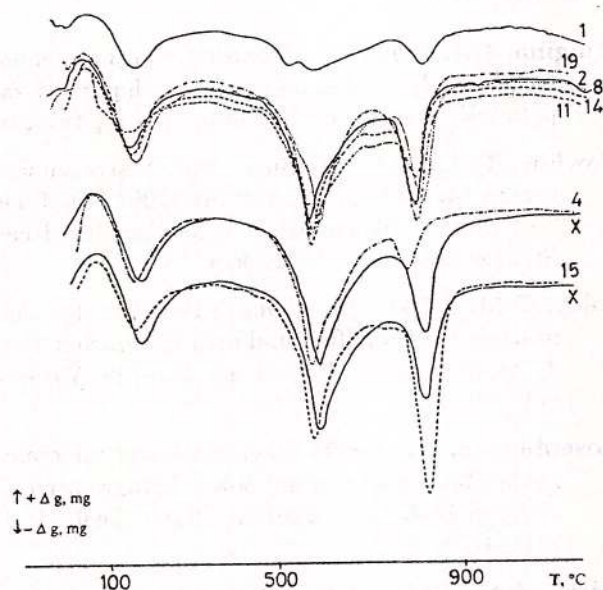


Fig. 3 - DTG curves of soft clayshale sample (No. 1,4,11,15) and compact clayshale samples (No. 2,8,14,19). X-average graphically given curve of samples 2,8,11,14,19.

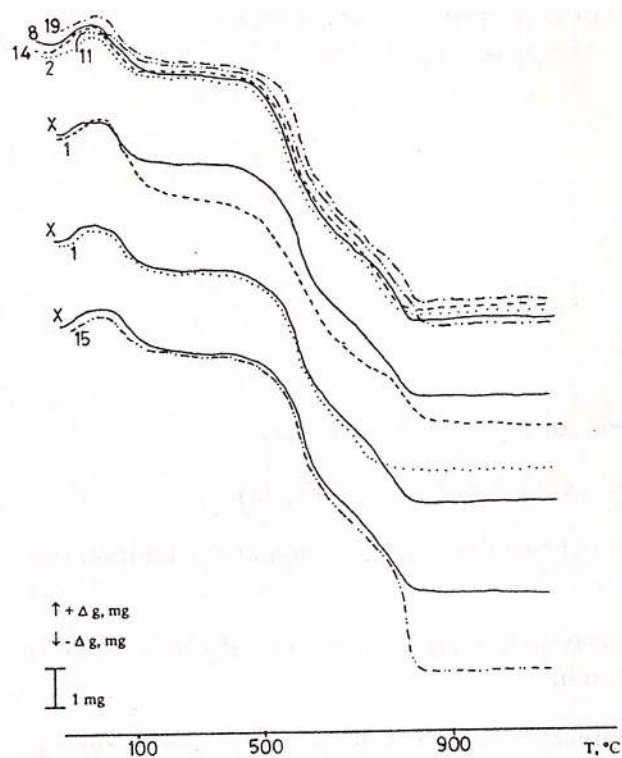


Fig. 4 - TG curves of investigated samples.
See legend of Figure 3.

temperature interval from 743°C up to 810°C. The amount (about 3 mass.%) does not differ much from sample to sample (the greatest is in sample 15, Table).

Results and discussion

Dried nonhomogenized samples aggregate have been preheated (at the temperature 200°C) and fast fired up to the temperature 1120°C in order to expand. X-ray diffraction investigations of two expanded characteristic samples (soft and compact clayshale) have shown (Fig. 5) that the expanded ceramic body consists of mullite (arisen from reaction of clay minerals with quartz), residual quartz, low tridymite, fayalite, hematite in the brown coloured surface of ceramic body and elementary iron and magnetite in the black core of aggregate (the consequence of reduction atmosphere).

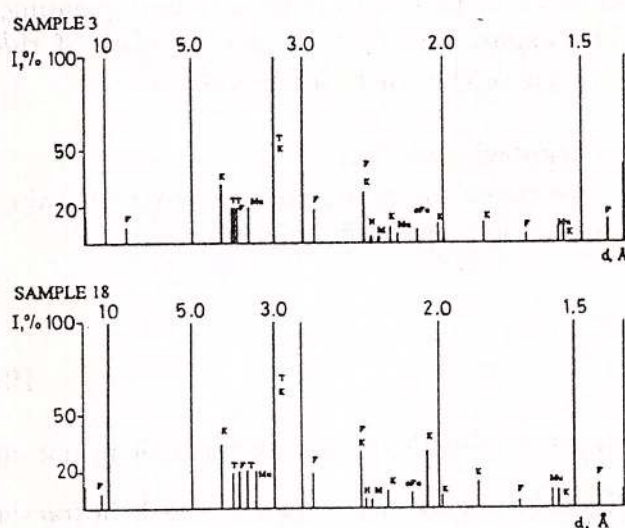


Fig. 5 - X-ray diffractograms of expanded soft clayshale (sample 3) and compact clayshale (sample 18). K-quartz; T-low tridymite; F-fayalite, Mu-mullite; α-Fe, H-hematite; M-magnetite.

It has been stated as well that the soft type of clayshale expands less than the compact one. The soft clayshale started to expand at the temperature 1050°C and the compact one at 1020°C.

With decreasing quartz content the expansion coefficient increases from 3.8 up to 5.8 and the bulk density inversely decreases from 0.6 up to 0.4 g/cm³. At the temperature 1120° C an average expansion coefficient of 4.6 and an average bulk density of 0.5 g/cm³ for soft clayshale have been measured. The compact type has an average expansion coefficient of 5.4 and a bulk density of 0.4 g/cm³ at the temperature 120° C (Plate, Fig. 3).

After grinding and homogenization of some soft and compact clayshale samples, they have been pressed and expanded at the temperature 1120° C. Differences in expansion coefficient and in average bulk density have diminished with such preparation of raw material (Plate, Figs. 4,5).

These results are in perfect coincidence with Rosenberger's and Hill-Crook's (Rosenberger, 1969) predictions on the significance of free quartz content on the expansion effect, the only factor proved to influence the expanding. The expansion effect is good in spite of the absence of the smectite minerals.

Acknowledgements

We thank an anonymous reviewer for valuable advices on finalizing the text.

References

- Knigina, G.I. (1977)** Laboratorie raboti po tehnologii stroitelnoi keramiki i iskusstvenih poristih zapolnitelei. Višaja škola Moskva, 204 p., Moskva.
- Pawlow, T. (1962)** Einfluss der Viskositätsänderung im Intervall von 800 bis 1200° C auf das Sintern und Blähen leicht schmelzender Tone. *Stenklo i keramika*, 3, Moskva.
- Riley, C.M. (1951)** Beziehungen zwischen den chemischen Eigenschaften und dem Blähen von Ton. *J. Amer. Ceram. Soc.*, 4, p. 121-128, Westerville.
- Rosenberger, H. (1969)** Chemische und mineralogische Zusammensetzung sowie korngrossenaufbau von Blähtonen. *Zeitsch. Ang. Geol.*, 5, p. 241-247, Berlin.
- Tóth, M.N., Csáky, I.B. (1989)** The role of the smectite group in the bloating process. *Ziegelin. Intl.*, 42/5, p. 246-250, Wiesbaden.

Received: October 1995

Revised form: February 1996

Accepted: August 1996

Plate

Fig. 1 – Sample of compact clayshale in transmitted light, || N, (1 cm = 35 μm).

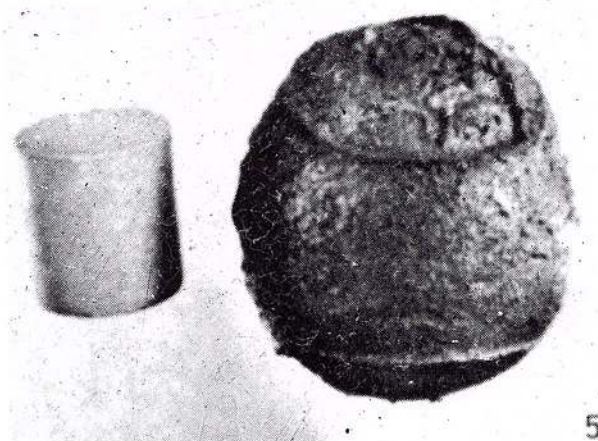
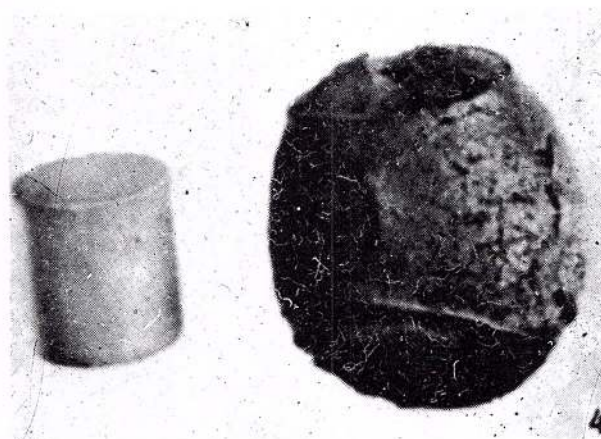
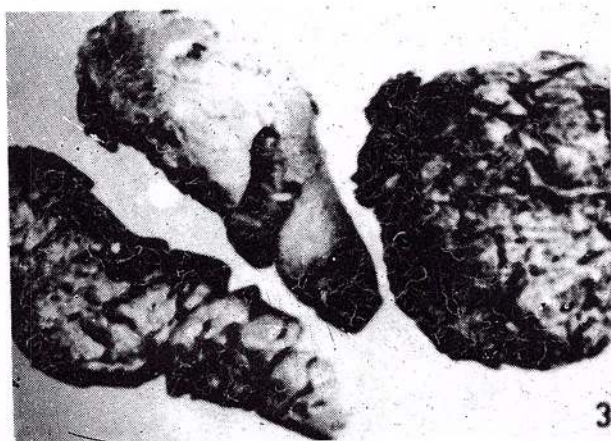
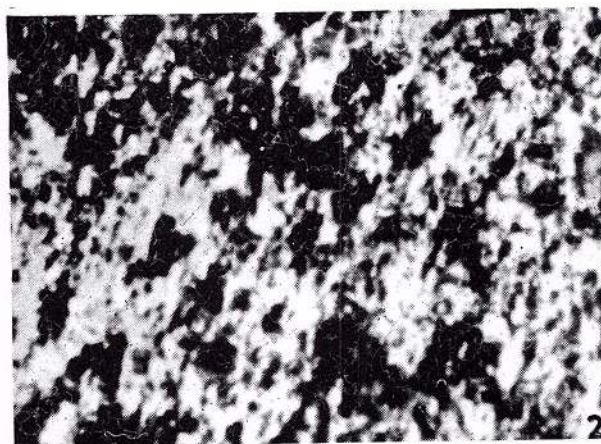
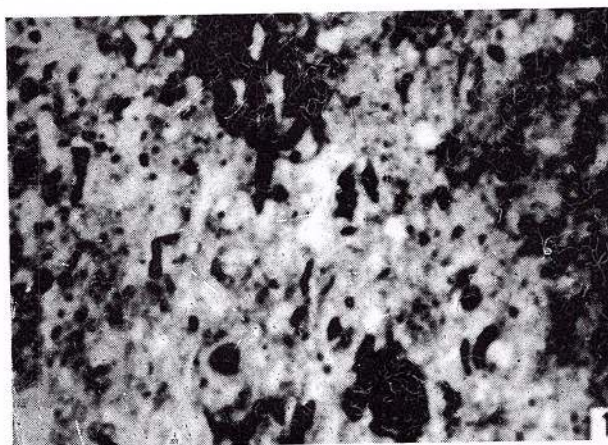
Fig. 2 – Sample of compact clayshale in transmitted light, ⊥ N, (1 cm = 35 μm).

Fig. 3 – Samples of soft (right) and compact (left) clayshale after the expansion at the temperature 1120° C (soft sample dimension is 36x44 mm).

Fig. 4 – Grinded, homogenized and compacted soft clayshale sample before and after the bloating at the temperature 1120° C (cylinder height is 16 mm).

Fig. 5 – Grinded, homogenized and compacted compact clayshale sample before and after the bloating at the temperature 1120° C (cylinder height is 16 mm).





Rom. J. Mineralogy, vol. 78, București, 1997



Institutul Geologic al României



ONCE AGAIN ON THE JOSEITE-A FROM THE SKARN DEPOSITS FROM BĂIȚA BIHOR MINE (APUSENI MOUNTAINS, ROMANIA)

Grațian CIOFLICA, Mihai LUPULESCU

Mineralogy Dept., Bucharest University, Bd. N. Bălcescu nr. 1



Key words: Joseite-A. Electron microprobe. Microhardness. Protojoseite. Chalcogenides. Sulfosalts. Sulfotellurides.

Abstract: Joseite - A from the Mo+Bi±W mineralizations hosted by Băița Bihor ore deposit has been analysed by optical, X-ray, electron microprobe and microhardness means. The empirical formula calculated on the basis of 7 total atoms is: $(\text{Bi}_{4.04}\text{Pb}_{0.02})\text{Te}_{0.9}(\text{S}_2\text{Se}_{0.02})$. Joseite-A appears in the following mineral association: cosalite, emplectite, tetradymite, bismuthinite and native bismuth. The mineralogical implication of tetradymite, native bismuth and bismuthinite in the formation of joseite-A is presented together with some considerations concerning joseite-A generation.

Introduction

Koch (1948) and Grasselly (1948) announced the first occurrence of joseite in the Mo+Bi skarn related to the Upper Cretaceous magmatic event from Băița Bihor. They described the physical properties of the mineral and presented two chemical analyses and a stoichiometric formula as Bi_3TeS . Later studies, Stoici (1974) and Cioflica, Vlad (1979), confirmed the appearance of joseite in the Băița Bihor ore deposit. The last authors, based on compositional data, gave the following formula: $\text{Bi}_3\text{Te}_{0.8}\text{S}_{1.9}$.

Our mineralogical investigations on the material sampled from the Bi-Mo-W mineralization settled on the Blidar Contact from Băița Bihor up the presence of joseite-A having $\text{Bi}_{4.04}\text{Te}_{0.9}\text{S}_2$ formula (Cioflica, Lupulescu, 1994). This paper presents new data on joseite-A for a better mineralogical characterization of the mineral.

Geological setting

The main post-magmatic events from Băița Bihor area, generating Mo+Bi±W skarns, are connected to the Upper Cretaceous - Eocene magmatic rocks, belonging to the Bihor plutons. Basalt, andesite porphyry granodiorite, aplites follow a fracture system with N-S and NW-SE direction.

The Bihor pluton, having granitoid composition, generated a large thermal and metasomatic aureole affecting the rocks from the Bihor Realm and from Codru, Arieșeni and Păiușeni Nappes system. The skarns and related mineralizations, extended in the carbonate units belonging especially to the Codru Nappes system, are between the most important products of the thermal and metasomatic phenomena. There are early skarns belonging to the magmatic stage (metamorphic skarns, sensu Kwac, 1987) and post magmatic skarns; the former are always barren, whereas the



last are often mineralized and affected by hydrothermal alteration (ore skarn, sensu Kwac, 1987).

The mineralizations are developed as impregnations veinlets, rarely as compact masses (nests, lens) on the distal skarn bodies. The following types of mineralizations are known, according to Cioflica et al. (1971, 1974, 1977):

a) $\text{Mo}+\text{Bi}\pm\text{W}$ scheelite mineralizations in calcic skarns (Blidar Contact, Secundar Contact, Fântanele Contact, Ludovica Gallery); a similar mineralization occurs in the calcic, magnesian skarns forming patches and infiltrations in the magnesian skarn from the "mantos" type bodies;

b) $\text{Cu}+\text{Bi}+\text{W}$ (scheelite) mineralizations in relation with the apo-dolostone, magnesian skarn columns (Antoniou and Sturzu);

c) $\text{Pb}+\text{Zn}+\text{Cu}+\text{B}$ mineralizations hosted by apo-dolostone, magnesian skarn columns, often with a complex morphology, due to their ramification in the upper part (Baia Roşie, Marta, Bolfu Toni, and Hoanca Motului);

d) quartz molybdenite impregnations and veinlets, as apical concentrations within the Laramian Bihor pluton;

e) quartz molybdenite impregnations and veinlets within the hydrothermal quartzites related to the hornfelses belonging to the Arieşeni Unit.

Occurrences

The studied material has been collected from the $\text{Mo}+\text{Bi}\pm\text{W}$ (scheelite) mineralizations associated with Ca-skarns from the Blidar Contact, IX level. The Ca-skarn bodies occurring on a recrystallized protolith (hornfelses, marbles) are very well developed within the detrital-carbonate complex belonging to the Codru Nappes system (Liassic Rhetian) that supports a tectonic cover, the Arieşeni Unit (Permian). These thermal and metasomatic products are intimately connected with the Laramian Bihor pluton.

The skarn bodies have a banded texture due to alternating wollastonite and grossularite zones and contain sometimes porphyroblasts of andradite, sillite and idocrase. The $\text{Mo}+\text{Bi}\pm\text{W}$ (scheelite) mineralizations form impregnations, veinlets and nests within hydrothermally altered skarns (Cioflica, Vlad, 1971).

Joseite-A is found as foliaceous aggregates with slightly yellowish lead-grey lustre, occurring as impregnations in the garnet-wollastonite skarns, associated with cisalite, emplectite, tetradymite, bismuthinite and native bismuth. The grain size is variable from a few microns to one centimeter.

Mineralogical features

Joseite-A has been studied by optical, X-ray, electron microprobe and microhardness means.

Optical properties. In the hand specimens and under the microscope, joseite-A appears as platy or long, prismatic crystals, with a low polishing hardness, distinct cleavages parallel to the elongation. The color is white, sometimes with slightly cream tints. The birefractance is too low to be observed. The spectral reflectance is high. The anisotropism is very weak, showing brownish, blue or grey tints. No twins have been observed.

X-ray diffraction. Mineral powder has been analysed using a PW 1840 diffractometer with CoK with 35 Kv and 45mA. The results are presented in Table 1. The diffraction lines are similar to those of joseite-A from "Selected Powder Diffraction Data For Minerals".

Microhardness. Joseite-A has been tested using a LECO M 400 hardness instrument. The microhardness value for 50 g load is 45 kg/mm^2 . The indentation is almost perfect, showing only slightly concavities on one side. Some shells are on the upper half of the indentation.



Table 1
X-rays diffraction pattern for joseite-A
from Băița Bihor Ore Deposit

No.	d (Å)	I/Imax	hkl
1	4.4072	12.57	009
2	3.6140	11.11	012
3	3.3122	17.03	001̄2̄
4	3.0849	100.00	107
5	2.5761	6.18	011̄1̄
6	2.2491	28.56	011̄1̄
7	2.1223	14.51	110
8	2.0593	7.00	101̄6̄
9	1.9740	4.26	011̄7̄
10	1.8924	14.11	002̄1̄
11	1.7861	3.14	111̄5̄
12	1.7515	4.71	027
13	1.6572	7.57	002̄1̄
14	1.5735	4.83	201̄4̄
15	1.4134	4.48	112̄1̄

Chemical composition. The compositional data of joseite-A, by electron microprobe mean (Jeol 733 Suprobe, 15kv and 30.19 nA electronic beam), are given in Table 2. Native metals and galena for the lead and sulphur have been used as standards.

Table 2
Electron microprobe analyses of joseite-A from
Băița Bihor Ore deposit compared with
other analyses from literature

Elements	Băița Bihor (Romania)	Magadan (Russia)	Nagakuki (Japan)
Bi	81.8970	81.2	82.16
Te	11.1006	10.7	10.56
S	6.2120	6.1	6.52
Sb	0.0233	—	—
Pb	0.4953	1.8	0.22
Cu	0.0179	—	—
Se	0.1622	0.5	0.10
As	0.0417	—	—
Total	99.95	100.3	99.56

The chemical composition of joseite-A from Băița Bihor ore deposit compared with available chemical analyses of joseite-A in the literature, as Magadan, Russia (zavyalov, Begigov,

1983) and Nagakuki, Japan (Kato et al., 1994) shows similarities. Joseite-A from Băița Bihor points up slightly higher Pb and Se amounts than joseite-A from Nagakuki and lower Pb and Se contents than joseite-A from Magadan. Only Te is higher than both cited joseite-A.

The formula calculated on the basis of 7 total atoms is $(\text{Bi}_{4.04}\text{Pb}_{0.02})$. The analyses of joseite-A show slightly higher (Bi+Pb) and (S+Se) contents as compared with the ideal Bi_4TeS_2 formula. The substitutions of Pb for Bi and Se for S are minor and Cu, Sb, As are only as traces.

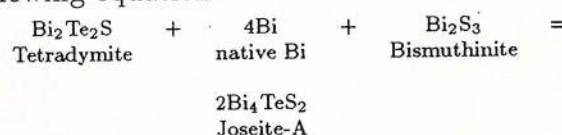
Discussion

Joseite-A appears in the Mo+Bi±W skarn deposits from Băița Bihor in the same association with cosalite, emplectite, tetradymite, bismuthinite and native-bismuth.

The deposition paragenetic sequence is the following: bismuthinite-Pb and Bi sulfides-Bi sulfosalts-Bi sulfotellurides. This deposition sequence points up the change of a_s . The a_s had high values at the beginning of the paragenetic sequence and low values toward the end of the crystallization process, due to the variations of a_s/a_{te} ratio, but no passing into the Bi-telluride stability field.

The increasing a_{Te} has determined the instability of bismuthinite coexisting with native bismuth and tetradymite, which has been experimentally demonstrated by Glatz (1967) in the $\text{Bi}_2\text{S}_3 - \text{Bi}_2\text{Te}_3$ binary system.

According to Kato et al. (1944) the generation of joseite-A could be interpreted as in the following equation:



The equation we presented could be real for Băița Bihor ore deposit, where the association bismuthinite, tetradymite, joseite-A is very common. Although not very well spread,



the association bismuthinite – native bismuth has been described, but in a sulfur-rich environment (with sulfides, especially chalcopyrite). Its stability may relate the absence of tellurium on the occasion of the formation of this association unless temperature is significant to the formation of joseite-A.

The chemical composition Bi_3TeS by Koch (1948) and Grassely (1948) corresponds to the protojoseite according to the Zawylov, Begizov (1983) data, but this is an unapproved mineral. The composition $\text{Bi}_3\text{Te}_{0.8}\text{S}_{1.9}$ according to Cioflica, Vlad (1979) is almost similar to those of joseite-A, but slightly different. These chemical differences in the group of trigonal bismuth chalcogenides could be due to the transitions in the composition of the solid solution of these chalcogenides, but the lack on any experimental data in the Bi-Te-S system makes us unable to the other interpretations.

References

- Cioflica, G., Vlad, Ș., Stoici, S. (1971) Répartition de la minéralisation dans les skarns de Băița Bihorului. *Rev. Roum. Geol., Geophys., Geogr., serie Geologie*, 15, 1, p. 43–58, Bucurest.
- , Vlad, Ș., Volanschi, E., Stoicu, A. (1977) Skarnele magneziene cu mineralizațiile de la Băița Bihorului. *St. Cerc. Geol., Geofiz., Geogr., seria Geologie*, 22, p. 39–57, București.
- , Vlad, Ș. (1979) Bi sulfosalts related to Laramian skarns of the Bihor Mountains (Northern Apuseni, Romania). *Rev. Roum. Geol., Geophys., geogr., Geologir*, 23, 1, p. 15–21, București.
- , Lupulescu, M. (1994) Joseite-A in bismuth mineralization of Bihor Mountains (Romania): its mineralogic characteristics and genetic significance, 16th General Meeting Abs., IMA, Pisa, Italy, p. 77.
- , Lupulescu, M. (1995) New data on Joseite-A from Băița Bihor mine (Bihor Mountains, Romania), 3rd Mineralogical Symposium. *Rom. J. Mineralogy, Suppl.* 1, 77, p. 12, București.
- Glatz, A.C. (1967) The Bi_2Te_3 – Bi_2S_3 system and the synthesis of the mineral tetradymite. *Amer. Miner.*, 52, p. 161–170.
- Grassely, G. (1948) Analyses of some bismuth minerals. *Acta Szeged*, 2, p. 24–30.
- Kato, A., Shimizu, M., Suzuki, Y., Okada, Y., Komuro, Y. (1994) Joseite-A from Nagakuki, Hanawa - cho, Fukushima Prefecture, Japan. *Bull. Natn. Sci. Mus., Tokyo, Ser. C*, 20(4), p. 141–147.
- Koch, S. (1948) Bismuth minerals in the Carpathian Basin. *Acta Szeged*, 2, p. 17–22.
- Kwac, T.A.P. (1987) W-Sn skarn deposits and related metamorphic skarns and granitoids. *Developments in Econ. Geol.*, 24, Amsterdam, Elsevier, p. 439.
- Stoici, D.S. (1974) Studiul geologic și petrografic al bazinului superior al Crișului Negru-Băița Bihor, cu privire specială asupra mineralizațiilor de bor și a skarnelor magneziene. *Stud. Tehn. Econ., Inst. Geol., seria I, Mineralogie-Petrografie*, 7, p. 1–169.
- Zavayalov, E.N., Begizov, V.D. (1983) New data on the constitution and nomenclature of bismuth sulphotellurides of joseite family. *Zapiski Vses. Mineralog. Obshch.*, 112, p. 589–601, (in Russian).



RECENT DISCOVERY OF TELLURIDES IN THE VEZHNALI ORE DEPOSIT, LESSER CAUCASUS

S.F. VELIZADE, A.B. SHIRALIYEV, E.N. EFENDIYEVA, N.F. NAGIYEV, T.G. MUSTAFAYEV

Geological Institute of Azerbaijan

H. Savid Avenue, 29a, 370143 Baku 143, Azerbaijan

Key words: Lesser Caucasus. Hydrothermal ore. Tellurides. Microprobe analyses.

Abstract: Several gold, silver and bismuth tellurides, i.e. petzite, hessite, calaverite, volynskite, tellurobismuthite and tetradymite were recently identified in the ores of the Vejnali hydrothermal deposit. The tellurides have been analysed by a CAMECA electron microprobe and the results computed by using a PUMA software.

Introduction

The area of the Vejnali deposit consists of Middle Devonian metamorphosed carbonate rocks, Tithonian-Valanginian volcanogenic and volcano-sedimentary and Hauterivian-Barremian terrigenous rocks, which were intruded by granitoids of different ages. Large hydrothermally alteration zones host ores forming veins, disseminations as well as combined types of ore bodies. Druses and breccias are locally developed within the ore bodies.

Mineral Content of the Ores

The main minerals are pyrite, chalcopyrite, galena, quartz, calcite, accompanied by various amounts of native gold, sphalerite, magnetite, hematite, pyrrhotite, ankerite, aragonite etc. Subordinately there occur native silver, native tellurium, cubanite, rutile anatase as well as garnet, zircon etc. (Shiraliyev, 1968). The well-developed supergene alteration zones contain goethite, covellite, chalcocite, malachite and more rarely azurite, anglesite, cerussite.

The Tellurides

The presence of tellurides in the Vejnali ores has been only recently reported (Velizade et al., 1995). Electron microprobe analyses enabled the identification of the following tellurides: petzite, hessite, calaverite, volynskite, tellurobismuthite and tetradymite. The analyses were performed by a CAMECA electron microprobe at the IGEM of the Russian Academy of Sciences. The working conditions were: accelerating voltage 20 kv, intensity of the absorbed electrons 10–40 nA, area of measurement 2 μm , measurement time at one point 10 seconds. Several measurements were performed on different points and grains, that were averaged as presented in the Table. The standards used were metallic Au, Ag and Bi (L_{α}) as well as CuFeS_2 and Zn (K_{α}). The measured relative intensities were converted into concentration values by using a CANON-CX computer with a PUMA software (Boronikhin and Tsepin, 1980). The results are given in the Table.



Table
Chemical composition of tellurides (wt %)

Minerals	Bi	Au	Ag	Fe	Cu	Zn	Te	S	Total	Formulae
Petzite	0.06	$\frac{25.37}{25.22}$	$\frac{41.87}{41.62}$	0.49	—	0.01	$\frac{32.92}{32.68}$	$\frac{0.75}{0.48}$	$\frac{101.47}{100.00}$	$Ag_{3.013}Au_{1.000}(Te_{1.883}S_{0.17})_{2.0}$
Petzite	0.15	$\frac{25.10}{24.94}$	$\frac{42.11}{41.84}$	0.26	0.01	0.02	$\frac{33.36}{33.06}$	$\frac{0.43}{0.16}$	$\frac{101.44}{100.00}$	$Ag_{2.994}Au_{0.977}(Te_{1.960}S_{0.040})_{2.000}$
Vollhyskite	$\frac{35.94}{39.26}$	$\frac{0.11}{0.12}$	$\frac{18.37}{18.74}$	0.22	—	0.03	$\frac{44.24}{44.88}$	0.29	$\frac{99.20}{100.00}$	$(Ag_{0.988}Au_{0.003})_{0.991}Bi_{0.987}Te_{2.000}$
Tetradymite	$\frac{54.94}{58.70}$	4.09	1.72	0.28	0.04	0.03	$\frac{35.84}{37.20}$	$\frac{4.16}{4.10}$	$\frac{101.10}{100.00}$	$Bi_{2.197}Te_{2.280}S_{1.000}$
Calaverite	0.07	$\frac{39.19}{39.34}$	$\frac{4.27}{4.29}$	0.34	0.13	0.02	$\frac{55.99}{56.15}$	$\frac{0.63}{0.22}$	$\frac{100.64}{100.00}$	$(Au_{0.908}Ag_{0.181})_{1.089}(Te_{1.969}S_{0.032})_{2.00}$
Hessite	0.37	$\frac{0.23}{0.23}$	$\frac{63.86}{64.14}$	0.42	0.03	0.01	$\frac{35.82}{35.63}$	0.53	$\frac{101.27}{100.00}$	$(Ag_{2.129}Au_{0.004})_{2.133}Te_{1.000}$
Hessite	0.53	$\frac{0.56}{0.57}$	$\frac{62.46}{63.02}$	0.38	0.01	0.02	$\frac{36.53}{36.37}$	$\frac{0.45}{0.04}$	$\frac{100.94}{100.00}$	$(Ag_{2.050}Au_{0.010})_{2.060}(Te_{0.996}S_{0.004})_{1.000}$
Tellurobismuthite	$\frac{50.28}{52.23}$	0.27	0.28	0.20	0.02	0.08	$\frac{46.49}{47.75}$	$\frac{0.29}{0.02}$	$\frac{97.91}{100.00}$	$Bi_{2.004}(Te_{2.995}S_{0.005})_{3.00}$

The figures given as denominator mean theoretical values of the elements

Petzite is the most frequently found telluride, forming fine veinlets in pyrite, that is locally intensively replaced by petzite. As a rule the petzite is intimately intergrown with sphalerite, chalcopyrite, tetradymite, a fact which at least in part may explain the relatively high concentrations of Cu, Fe and Zn in the analyses. The mode of presentation of tellurides is shown in Plate I (Figs. 1,2) and the scanning images are given in Plate II (Figs. 1-8).

Calaverite forms small grains or aggregates, commonly included in petzite or hessite or filling the interstices between them. The calaverite grains are 0.01 mm in size, more rarely reaching 0.1 mm.

Hessite forms small euhedral to anhedral grains and is associated with tellurobismuthite and tetradymite. The analyses gave a Ag:Te ratio very close to the theoretical 2:1 value.

Volynskite grains are always irregular in shape and together with tellurobismuthite form thin rims around the petzite aggregates.

Tellurobismuthite forms small aggregates of tabular grains up to 0.01-0.03 mm in size. It is closely intergrown with volynskite and tetradymite. The composition is near the theoretical formula of Bi_2Te_3 .

Tetradymite occurs as isolated tabular grains, commonly associated with tellurobismuthite. An excess of Bi and Te in the formula obtained by computing the analytical data may be explained by the fine intergrowth with tellurobismuthite.

Conclusions

The tellurides belong to late stages in the evolution of the ore deposits suggesting increasing Te fugacity by decreasing temperature.

Aknowledgements

The authors express their gratitude to A.I. Tsepin, Moscow, who carried out the microprobe analyses and to Dr. G. Udubaş for the assistance in the preparation of the paper publication and improving the English version.

References

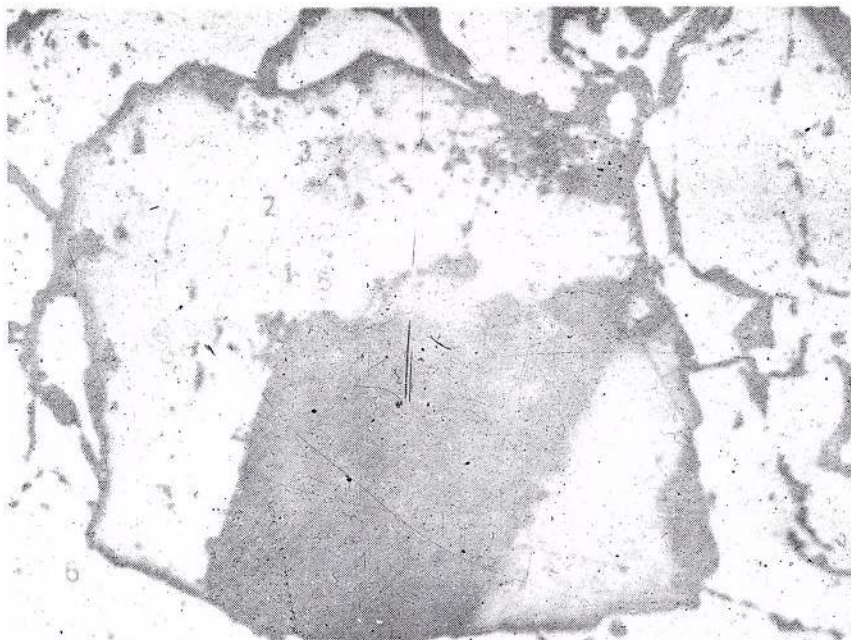
- Boronikhin, V.A., Tsepin, A.I. (1980) Programme for computing the corrections and statistical processing of EPMA measurements (in Russian). In: Equipments and methods in the Röntgen analysis (*Apparatura i metodi röntgenovskovo analize*), 23, Leningrad, Mashinostroenie Publ. House.
- Shyalyev, A.B. (1968) Composition and formation conditions of gold-polymetallic ores of the Vezhnali deposit. Doctoral thesis, Univ. of Baku.
- Velizade, S.F., Shilaliev, A.B., Efendieva, E.N., Nagiyev, N.F. (1995) Tellurium minerals in ore of the Vezhnalinsk deposit (Lesser Caucasus Mountains). *Rom. J. Mineralogy*, 77, Suppl. 1, p. 49-50, Bucureşti.



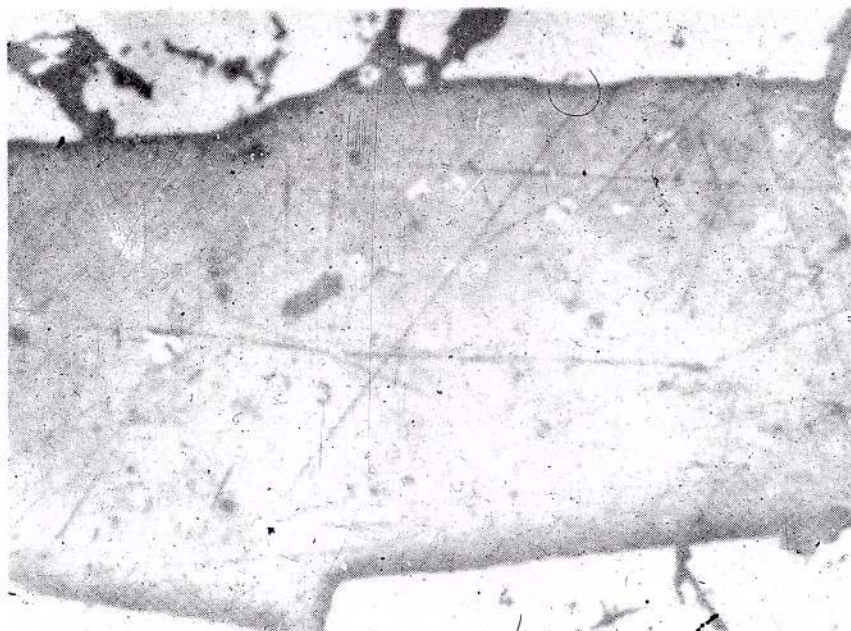
Plate I

Fig. 1 – Mode of presentation of telluride minerals: 1, petzite; 2, volynskite; 3, tellurobismuthite; 4, tetradymite; 5, native gold; 6, pyrite; 7, quartz. Polished section, X80.

Fig. 2 – Calaverite inclusions (1) in an intergrowth of hessite (2) and petzite (3), included in pyrite (4). Polished section, X200.



a



b

Rom. J. Mineralogy, vol. 78, București, 1997



Institutul Geologic al României

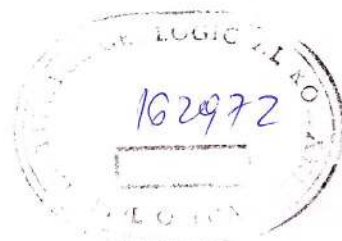
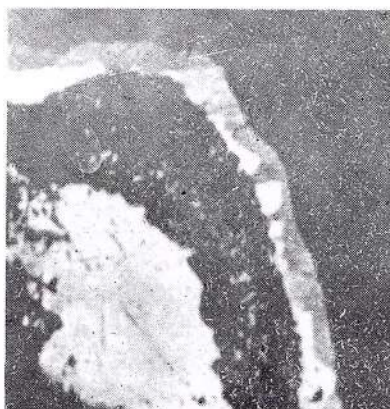


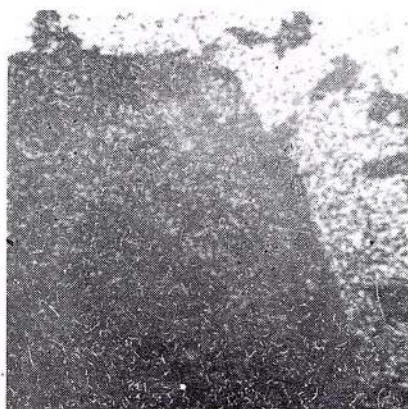
Plate II

Figs. 1–8 SEM images of tellurides in reflected electrons (3) and X-rays: AuL_α (4), AgL_α (5), BiL_α (6), FeK_α (7), CuK_α (8), TeK_α (9), SK_α (10). It can be seen that a tetradymite nucleus is successively enveloped by chalcopyrite+tetradymite, tellurobismuthite+volynskite and petzite.

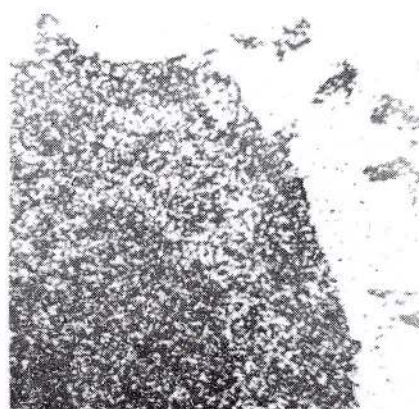




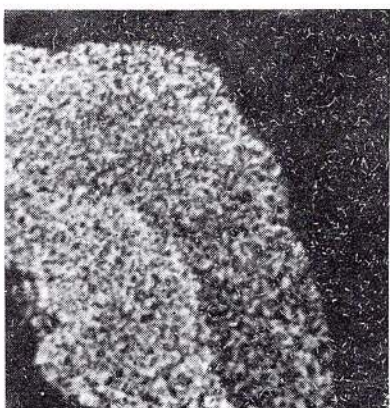
1



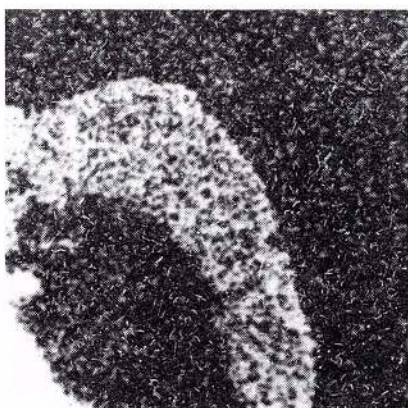
2



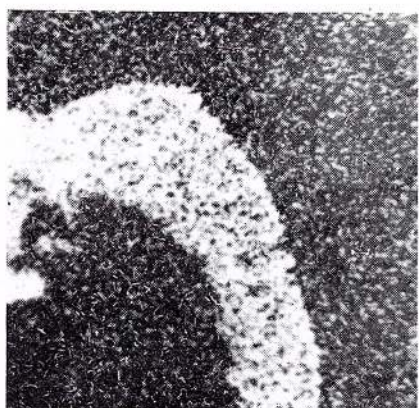
3



4



5



6



7



8

Rom. J. Mineralogy, vol. 78, București, 1997



Institutul Geologic al României





PARAGENETIC MINERAL ASSOCIATIONS OF SULPHIDE ORES, SOUTHERN SLOPE OF THE GREAT CAUCASUS

S.F. VELIZADE, A.B. SHIRALIYEV, E.N. EFENDIYEVA

Geological Institute of Acad. Sci. Azerbaijan

H. Savid Avenue, 29a, 370143 Baku 143, Azerbaijan

Key words: Great Caucasus (southern slope). Black shale. Pyrite ore. Polymetallic ore. Parageneses. Regional zoning.

Abstract: The Jurassic black shale series developed on the southern slope of the Great Caucasus Mts contains several polymetallic ore occurrences and deposits displaying compositional variations and different modes of presentation. The ores are polygenetic in character and their space distribution supports the idea of a quite well-developed regional zoning.

Introduction

On the southern slope of the Great Caucasus the Jurassic black shale series contains a number of ore deposits/districts, such as Filizchai, Katsdag, Katekh, Zhihikh, and ore occurrences (Katsmaly, Cheder, Gumbulchai etc.) with sulphide ores showing a great variety of mineral associations and a well-developed regional distribution of dominant sulphide associations. Pyrite-polymetallic, chalcopyrite-pyrrhotite, "intermediate", polymetallic-quartz and lead-zinc ore types can be found together within the deposit or may dominate in one or another ore deposit or occurrence. In addition, the ore bodies display different modes of presentation, i.e. there are massive ores, bedded, spotted and breccia like ores.

Mineral composition

The ores contain a great number of minerals, but pyrite, pyrrhotite, sphalerite, galena, chalcopyrite, quartz and carbonates are the most widespread and quantitatively the most

important (Velizade, 1982; Zlotnik-Khotkevich, 1970; Yusifov, 1969). Antimony sulphosalts, such as boulangerite, jamesonite, bournonite, meneghinite, etc., as well as tin, bismuth and tellurium bearing minerals are present in some deposits. By combining the fabric analysis with some geochemical criteria the polygenetic character of the ores as a whole could be recognized. The succession in time of the paragenetic mineral association in all the ore deposits or occurrences studied is obvious and largely similar, but their space distribution is different leading to a quite well-developed regional zoning (Fig.).

Mineral association

The complex analysis of the ores resulted in distinguishing several paragenetic mineral associations. According to their age relations they are, as follows:

1. The early pyrite generation contains fine-grained, colloform and globular pyrite grains or aggregates, which can be found in all the



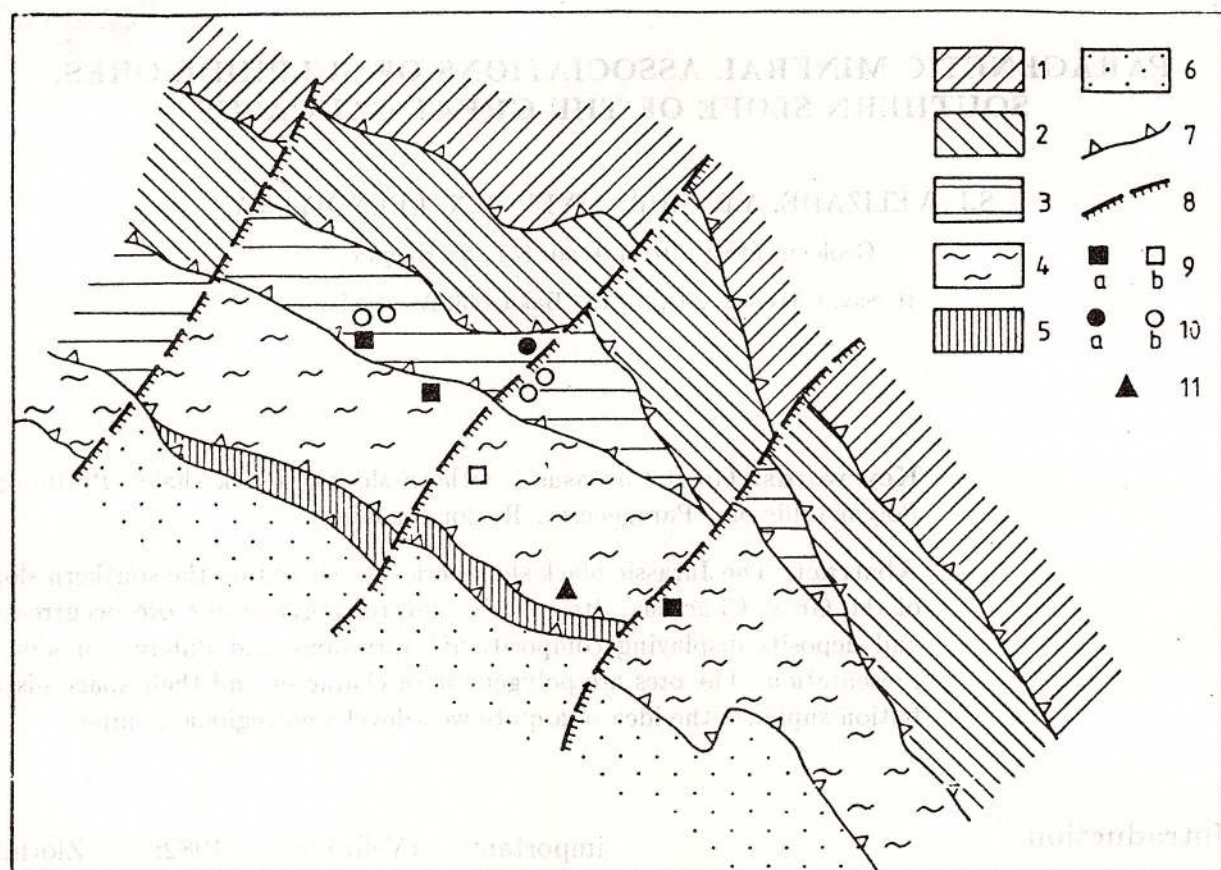


Fig. - Scheme of ores objects distribution on the southern slope of the Great Caucasus on Azerbaijan territory (compiled on N.K. Kurbanov's material, 1982). 1, Alpine foredeep trough; 2-6, Structural-formational zones: 2-Metluta-Akhtychai, 3-Goytkhsko-Tfansk, 3-Goytkhsko-Tfansk, 4-Chkhaltta-Sarybash, 5-Duruginsk, 6-Transcaucasian median mass; 7, Longitudinal upthrust fault; 8, Cross transform faults ore deposits (a) and occurrences (b); 9, Pyrite-polymetallic; 10, Chalcopryite-pyrrhotite; 11, Lead-Zinc ores.

deposits. However, this first stage of mineralization is characteristic of the deposits situated in the southern part of the area, with an obvious decrease towards north, i.e. in the Katsdag deposit and Katsmaly and Kekhnamedan occurrences, where it is less developed and sometimes preserved only as relics.

2. The next association consists of arsenopyrite and pyrite and is widely developed in the massive and bedded ores of the Filizchai and Katsdag deposits. The grains of pyrite are mainly euhedral or show a skeletal development. The arsenopyrite subordinately occurs and sometimes forms some small euhedral grains. Both minerals replace the first generation pyrite and are replaced by the base metal

sulphides of the next association.

3. The association fahlore - chalcopryite - galena - sphalerite is best developed in the polymetallic ores of the Filizchai, Katekh and Katsdag deposits and to some extent in the "intermediate" ores of the Filizchai, Zhikhikh and especially of the Katsdag deposit. The ores of this association are economically the most important and consist of anhedral, fine grains of sulphides, among which the sphalerite predominates, as well as of various amounts of tetrahedrite, tennantite, freibergite. Quantitatively the galena amount considerably increases southwards, being the most important ore mineral of the Katekh, Cheder and Gumbulchai deposits.

4. The association carbonate – chalcopryrite – galena – sphalerite – pyrite is only locally developed, such as in the base metal ores of the Katekh, Filizchai and Katsdag deposits. The sulphides typically form concentric aggregates with a zonal arrangement, sometimes bordering the mineral aggregates of earlier associations.

5. A sulphosalts-rich association is locally developed in the base metal ores of the Filizchai deposit and consists of boulangerite, jamesonite, bournonite, gudmundite, meneghinite, cosalite, famatinite, semseyte, emplectite, etc.

6. The galena – sphalerite – chalcopryrite – pyrrhotite association is the most important one and is widely distributed especially in the ore deposits of the northern part of the studied area. It typically forms the chalcopryrite-pyrrhotite and the "intermediate" ores of the Katsdag and Zhihikh districts and is less developed in the ores of the Filizchai deposit. The main ore mineral is pyrrhotite forming granular aggregates. The association also includes some rarely met minerals, such as cobaltite, stannite, mackinawite, cubanite, epidote.

7. The chalcopryrite – quartz association is composed by various amounts of the above-mentioned minerals and sphalerite, galena, a monoclinic variety of pyrrhotite, native bismuth, tellurobismuthite, hessite, petzite, altaite, hedleyite, nagyagite, volynskite etc. The leading mineral is the quartz, forming veins, nests or pockets which host the ore minerals. The Filizchai, Katsdag and Zhihikh deposits exhibit best such chalcopryrite rich ores.

8. The siderite – pyrite association is closing the multistage mineralizing processes in the area. Although it is only locally developed the final association could be traced in a number of deposits, mainly in the Katsdag and Zhihikh ore districts and to a lesser extent in the ores at Katsmaly, Tenross, Chugak. Besides pyrite there are also marcasite, magnetite, quartz etc. Pyrite is as a rule euhedrally developed, as are also marcasite and quartz. Skeletal crystals as well as bird's eye structures may in places be observed.

Conclusions

The complex analysis of the ores contained by the Jurassic black shale series developed on the southern slope of Great Caucasus led to the separation of several paragenetic mineral associations that occur in most of the ore deposits and occurrences but greatly differ as concerns their quantitative distribution. A regional zoning can be thus traced: a higher temperature ore zone is present in the northern part of the studied area and a lower temperature one in the southern part.

Acknowledgements. The authors gratefully appreciate the assistance of Dr. G. Udubaşu in the preparation of the final version of the paper.

References

- Kurbanov, N.K. (1982)** The main stages of combined copper-polymetallic deposits formation and their correlation with evolution stages of Alpine terrigenous geosynclinal of Great Caucasus. Papers of Scientific-Research Geologic Exploration Institute, 168, (in Russian).



PLANT REMNANTS REPLACED BY COPPER MINERALS, RONGJING COPPER DEPOSIT, SICHUAN, CHINA

Z.M.CAO, X.Q.HU, D.Q.SHUAI

Dept. Mineral. Resources, Chengdu Institute of Technology.

Chengdu 610059, P.R. China.

Key words: Copper minerals. Plant remnants. Bornite. Plant remnants. Replacement. Rongjing Deposit. Sichuan. China.

Abstract: Plant remnants replaced by bornite, chalcopryite and covellite are described from Rongjing deposit, Sichuan Province, where at least three stages have been depicted. Wood cell textures and textures reminiscent of wood leaves have thus been developed. Finally, an attempt was made in order to classify the organic matter related ore textures, in which both sulphides and oxides can equally occur.

Introduction

Ore minerals replacing plant or faunal remnants have been reported in several occurrences in the world, e.g. Ramdohr (1969), Tufar (1968), Udubaşa (1984) etc. In the last time plant remnants replaced by copper minerals were also recognized in some ore deposits in China, such as Lonchi and Naxi in the Sichuan Province and Dayao in the Yunnan Province (Shuai, 1988). At Rongjing wood cell textures inherited by chalcopryite and bornite as well as peculiar textures reminiscent of plant leaves have been observed, too. The present paper deals with a detailed description of such replacement textures.

Geologic Setting of the Copper Deposit

The Rongjing copper deposit is situated in a structural unit consisting of Triassic sandstones rich in carbonaceous matter and asphalt, with which large amounts of copper

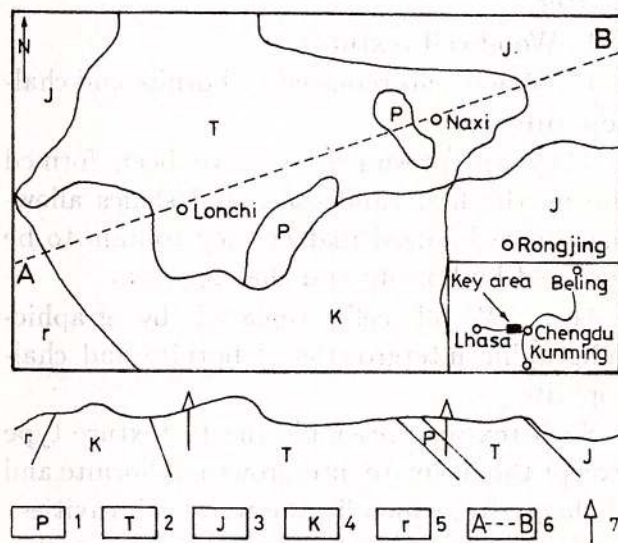


Fig. 1 - Sketch map of the deposits and cross profile. 1, Permian basalt; 2, Triassic sandstone; 3, Jurassic sandy ravel; 4, Cretaceous silt-shale; 5, granite; 6, profile line; 7, ore occurrence.

minerals associate either by adsoption or replacement or both. The ore source seems to be at least in part closely related to magmatic



activity. Three stages of mineralization have been depicted with quite different PT parameters. They are:

Stage I: Early hydrothermal, with a low temperature bornite-chalcocite association;

Stage II: Intermediate supergene, with a partial replacement of bornite by covellite;

Stage III: Late hydrothermal, with a more complex, medium temperature mineral association containing also pyrite, galena and sphalerite, superposed on the early copper-rich assemblages.

Such a succession of mineralizing stages is somewhat unusual and it is responsible for the presence of very different texture types preserved within the deposit.

Texture Types of the Ore Minerals

The textures so far recognized in the Rongjing ores can be classified according to both the dominant ore mineral and the type of replaced plant remnant and/or carbonaceous matter.

1. Wood cell textures.

1a. Wood cells replaced by bornite and chalcopyrite.

They are presumed to have been formed during the first sandstones and shales allowing the carbonized matter they contain to be replaced by bornite and chalcopyrite.

1b. Wood cells replaced by graphic-subgraphic intergrowths of bornite and chalcopyrite.

Such textures resemble the 1a texture type except the intimate intergrowth of bornite and chalcopyrite, which fill the wood cell cavities.

1c. Wood cells replaced by bornite, covellite and chalcopyrite.

Such textures probably appeared as a direct result of superposed mineralizing stages, one of them being related to supergene transformations. Bornite has replaced first the inner parts of the carbonized wood cell texture, then bornite was bordered by covellite during the supergene stage, and finally chalcopyrite of the

stage III further replaced the previous texture by including the bornite – covellite intergrowth in a chalcopyrite matrix (Pl. Fig. 1).

1d. Wood cells replaced by chalcopyrite.

As a dominant mineral of the late hydrothermal stage chalcopyrite shows great varieties of wood cell textures resulting both by direct replacement of the carbonized wood (Pl., Fig. 2) and by replacement of other types of mineralized wood cells. Such chalcopyrite rich textures exhibit also different deformation patterns, i.e. ordered or disordered deformations, either due to compression or extension.

2. Textures reminiscent of replaced wood leaves.

2a. Textures containing bornite and chalcopyrite. Such a texture is shown in Figure 3 of the plate and it appears as if the leaf limb would have been first replaced by bornite and then the leaf nervures or even the leaf stalks by chalcopyrite. A selective replacement could also be invoked but the explanation would be even more difficult.

2b. Distorted leave-like textures.

They are similarly featured but seemingly late remobilization of chalcopyrite resulted in much more complicated aspects (Pl., Fig. 4) that only in part are reminiscent of wood leaves.

Discussion

It is obvious that the organic matter replaced ores and their textures can be divided into two main types According to the timing of processes giving rise to the deposition of the organic matter and that of the ore minerals.

1. Simultaneous deposition of organic matter and ore minerals leading to the occurrence of fine-grained ore minerals as disseminations in black shales or black shale like rocks. This is a feature typical of syngenetic processes and can also called direct biomineralization processes. The Mansfeld-Lubin copper mineralizations carrying also PGE is a typical example. The framboidal pyrite widely found in a

large variety of occurrences can also be added.

2. Later circulation of ore-bearing solutions through rock sequences containing organic remnants can also produce precipitation of ore minerals. It signifies epigenetic type of mineralization or indirect biomineralization. The textures produced may reflect selective replacement of different parts of the fossilized plants or animals or even of other mineral components of the primary rock. Features suggesting late replacement of wood remnants were largely identified in the copper ores at Rongjing as presented above. A more detailed classification of biological fabric types was presented by Shuaj (1988).

Features typical of both main types of organic matter related ore mineralization can be found in the same deposit the textures resulted in such cases may be called composite textures derived both from combination of syngenetic and epigenetic (or direct and indirect biomineralization) processes and from succeeding multistage epigenetic events. The Laerma gold deposit in Gansu Province, China, is such an example, where diagenetic framboidal pyrite is accompanied by late, hydrothermal pyrite overgrowths which result in the development of euhedral pyrite grains growth around pyrite framboids. Such aspects were also described by Udubaşa (1986) in some ores hosted by brecciated black shale in Romania.

The classification of the organic matter related ores and ore textures may therefore be based on the leading ore mineral(s) and on the type of organic matter they associate with. If sulphides predominate the texture may be called S (sulphide) type ore textures; if oxides are the main minerals then the texture may be named O type. By appearing both sulphides and oxides the texture may be called S-O type etc. The classification may further include the type of organic matter or the parts of the replaced plants, e.g. either wood cells (S-1) or wood leaves (S-11) as well as the chief replacing ore mineral, e.g. S-I-1 type for cases when only one ore mineral is presented in the

wood cells or S-11-2 type when leave-like textures consist of two minerals. Such features were thoroughly described from the ores of the Rongjing deposit.

The composite textures are important in deciphering the evolution stages of a deposit or in depicting its polygenetic character. The Rongjing deposit is an example where ore textures helped in the reconstruction of the three stages of the mineralization process, all of them related to late circulation of ore bearing solutions through a rock sequence rich in fossilized plant remnants. A quite different example is the Chengu deposit, Hunan Province, where the ore beds consist of dominant framboidal pyrite without having any apparent effects of epigenetic processes. The deposit belongs to the direct (bio)mineralization type and contains textures typical of syngenetic processes. If the textures are of biological nature or not it is a matter of further debate.

There are some other ore deposits in China showing evidences of both types of processes and textures, e.g. the Ertai gold deposit in the Shannxi Province and the Longtang lead-zinc deposit in the Sichuan Province. Here both syngenetic or diagenetic (or direct) mineral deposition and late, epigenetic or indirect mineralization took place resulting in typical composite textures.

By detailed investigation of the relation between the ore minerals and the organic matter it is thus possible to recognize features typical of genetically different processes. The study of the Rongjing ore deposit enabled us to depict several stages of mineralization, all of them with specific textures relating the copper ore minerals and the fossilized plant remnants.

Aknowledgements. The assistance of Dr. G. Udubaşa is gratefully acknowledged.



References

- Ramdohr, P. (1969)** The ore minerals and their intergrowth. Pergamon Press, Oxford, 1174 p.
- Shuai, D.O. (1988)** Biological fabric of ore minerals. Sichuan University Press, Chengdu, China.
- Tufar, W. (1968)** Pyritisierte Hölzer eozänen Alters aus Ost-Holstein. *Meyniana*, 18, 65–78.
- Udubaşa, G. (1984)** Iron sulfides in sedimentary rocks: some occurrences in Romania. In: A. Wauschkuhn, C. Kluth, R.A. Zimmermann (eds.) *Syngensis and epigenesis in the formation of mineral deposits*. Springer, Berlin, p. 28–35.

Received: October 1995

Revised form: May 1996

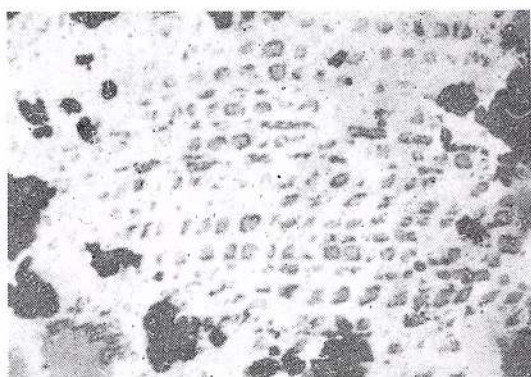
Accepted: September 1996

Plate

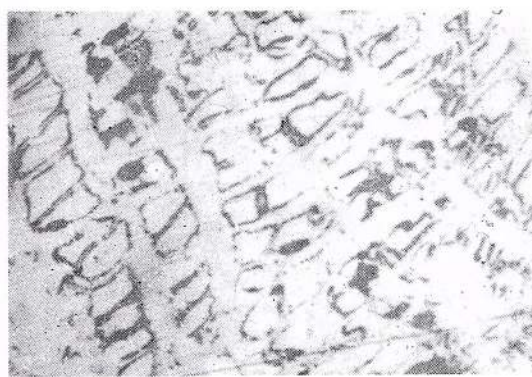
- Fig. 1** – Chalcopyrite (white) contains loose wood-cell texture of bornite (grey) and covellite (deep grey) with ordered arrangement. Quartz takes on black in the photo. Reflection light, 100X.
- Fig. 2** – Residual, loose wood-cell texture comprises chalcopyrite (white) and quartz (black). Reflection light, 100X.
- Fig. 3** – Leave-like texture consisting of bornite (grey) and chalcopyrite (white). Quartz is black in the photo. Reflection light, 100X.
- Fig. 4** – Leave-like texture composed of bornite (grey) and chalcopyrite (white). Quartz is black. Reflection light, 100X.



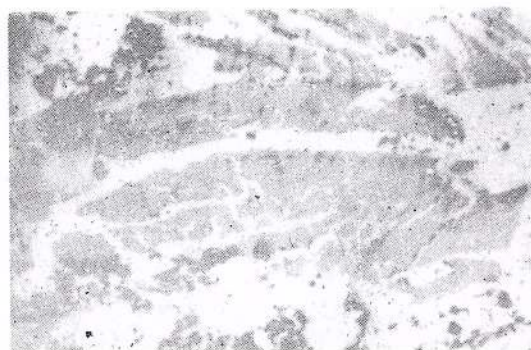
Z.M. CAO et al. PLANT REMNANTS REPLACED BY COPPER MINERALS, RONGJING DEPOSIT



1



2



3



4

Rom. J. Mineralogy, vol. 78, București, 1997



Institutul Geologic al României

THE POSSIBILITIES OF GEOLOGICAL CORRELATION ON THE BASIS OF EXTRATERRESTRIAL SPHERULES OCCURRING IN HUNGARY

Cs. H. DETRE, Gy. DON, L. DOSZTÁLY, E. RÁLISCH-FELGENHAUER, Á. SIEGL-FARKAS

Geological Institute of Hungary. Stefánia út 14, H.-1143, Budapest

Key words: Exaterrestrial spherules. Lithostratigraphic correlation. Hungary.

On the basis of the investigations carried out in Hungary until now we can perform spherule-based geological correlations in the following periods:

PERMIAN

Late Permian "Bellerophon Kalk": Bükk Mts., Nagyvisnyó (NE Hungary): glassy spherules with rich *Bellerophonitidae* and *Nautiloidae* fauna.

Permian – Traissic boundary

Bükk Mts., Gerennavár; Bálvány (NE Hungary): limestones with late Permian *Brachiopods* and early Triassic *Lamellibranchiata*. Rare occurrence of glassy spherules. A probable part of a global belt (see: Miono, 1993 Miono et al., 1995).

TRIASSIC

Middle Triassic, Anisian stage, Pelsonian substage, Balatonites balatonicus zone: Aszófő (Balaton Higland): glassy spherules; Misina, Mecsek Mts (South Hungary): "extremely small spherules".

Ladinian – Carnian stage: Recsk Mts (NE Hungary): glassy spherules. Glassy spherules occurrences of similar age are known from Greece, Italy and Austria (Pötschener Kalk).

Norian – Rhaetian stage: Several occurrences in the Buda Mts with limited possibilities

of correlation (Glassy spherules).

JURASSIC

Hettangian – Sinemurian stage: Mecsek Mts (S Hungary): Rare occurrence of glassy spherules.

Bathonian – Callovian stage: Recsk Mts (Glassy spherules).

Callovian – Oxfordian stage: Gerecse Mts (Kálvária Hill, tata): The oldest known occurrence of magnetic spherules. In the case of both Jurassic occurrences wide-ranging correlation is impossible.

CRETACEOUS

Upper Cretaceous, Upper Santonian – Lower Campanian stage: A wide zone of occurrence of glassy and magnetic spherules extending in Hungary: Magyarpolány 42 borehole (W Hungary) to Nekézseny (NE Hungary) (Glassy and magnetic spherules).

Campanian – Maastrichtian stage: Isolated occurrences in W Hungary.

The Upper Cretaceous occurrences have to be interpreted as belonging to the global Upper Cretaceous belt rich in spherule zones.

EOCENE

Upper Eocene: Csetény borehole 72 (NW Hungary): Glassy spherules. It can be associated with the global occurrence-belt.



OLIGOCENE

Very rich occurrences (mainly magnetic spherules) were found in the Cserhát Mts (N Hungary) without correlation possibilities.

MIOCENE

Badenian stage: Sopron borehole 89 (W Hungary). Several localities were identified in the Börzsöny Mts (N Hungary) and Bükkmogyorósd (Bükk Mts, NE Hungary, see: Dávid, A., Rácz, A., 1995) with glassy and magnetic spherules.

May be these Badenian occurrences are within "actio radius" of the Ries meteorite crater, therefore they probably are impact spherules. However, the distinction of the genetic types of spherules is not sure at the present time (About Ries see: Preuss, E., Schmidt-Kaler, H., 1970).

PLIOCENE

Pannonian stage: Very rich occurrences of glassy spherules were found in the Little Hungarian Plain (NW Hungary, see: Szöör, Gy. et al., 1995).

PLEISTOCENE

A lot of magnetic spherules from various localities.

HOLOCENE

Placer type sediments bearing a large amount of glassy and magnetic spherules make up all investigated areas along Hungarian rivers. More than 80% of the magnetic spherules belong to the "industrial type", with high Cu, Mn, Cr, V, Zn, Li peaks.

Expected occurrences:

First of all new occurrence localities would be expected in the formations of slow sedimentation, e.g. in the various Triassic formations of the Mecsek Mts (S Hungary) and Bükk Mts (NE Hungary), further in the Jurassic limestones of the Bakony Mts (Transdanubia).

The main directions of the further research: Upper Devonian limestone in the Szendrő Mts (NE Hungary). A potential part of the Upper Devonian global occurrence (see: Wang, K., 1992; Claeys, P. et al., 1992; Bouska, V., 1993; Claeys, P., Casier, J.G., 1994).

Eocene – Oligocene boundary:

Vásárosmajor (in Budapest area) 1. borehole: a potential part of the global occurrence belt of this time interval (see: Glass, B.P. et al., 1986; Bohor, B.F., Betterton, W.S., 1991; Pollastro, R.M., Bohor, B.F., 1993; Xiao Zhifeng et al., 1994).

These investigation are supported by the OTKA grant no. T 014958.

References

- Bouška, V. (1993) Sklenene sférule devonského štáti. *Geologický Průzkum*, 11–12/1993, p. 362–363.
- Claeys, P., Casier, J.G., Margolis, S.V. (1992) Microtectites and mass extinctions: Evidences for a Late Devonian asteroid impact. *Science*, 257, p. 1102–1104.
- Claeys, P., Casier, J.G. (1994) Microtectite-like impact glass associated with in Frasnian-Famenian boundary mass extinction. *Earth and Planetary Science Letters*, 122, p. 303–315.
- Dávid, A., Rácz, A. (1995) Contribution to the knowledge of spherulite occurrences of North-Hungary – a preliminary report – In: Detre, Cs. H. and Szöör, Gy. eds. *Proceedings of the International Meeting: Spherulites and (Palaeo) ecology*, p. 121–124, Debrecen.
- Glass, B.P., Hall, C.M., York, D. (1986) $^{40}\text{Ar}/^{39}\text{Ar}$ laser-probe dating of North America tectite fragments Barbados and the age of the Eocene-Oligocene boundary. *Chem. Geol. (Isotope Geoscience Section)*, 59, p. 181–329.
- Gyuricza, Gy. (1995) Iron spherulites in unconsolidated sediments in Hungary. In: Detre, Cs.H. and Szöör, Gy. eds. *Proceedings of the International Meeting: Spherulites and (Paleo) ecology*, p. 125–130, Debrecen.
- Miono, S., Nakayama, Y., Shoji, M., Nakanishi, A. (1993) Origin of microspherules in Palaeozoic – Mesozoic bedded chert Estimated by PIXE analysis. *Nuclear Instruments and Methods in Physics Research*, B 75, p. 435–439, North Holland.
- Miono, S. (1995) Origin of Microspherules in Palaeozoic – Mesozoic Bedded Chert as estimated from its Morphology. *Il Nuovo Cimento*, 18/1, p. 9–13.



- Pollastro, R.M., Bohor, B.F. (1993) Origin and clay-mineral genesis of the Cretaceous/Tertiary Boundary Unit, Western Interior of North America. *Clay and Clay Minerals*, 41, p. 7-25.
- Preuss, E., Schmidt-Kaler, H. (Red.) (1970) Das Ries. Geologie, Geophysik und Genese eines Kraters. *Geol. Bavarica*, 61, p. 478.
- Szöör, Gy., Korpás-Hódi, M., Don, Gy., Beszeda, I. (1995) Microspherules from the sediments of Borehole Nagylózs-1, Hungary. In: Dete, Cs.H. and Szöör, Gy. eds.: *Proceedings of the International Meeting: Spherulites and (Palaeo) ecology*, p. 87-110, Debrecen.
- Rálich-Felgenhauer, E., Beszeda, I., Rózsa, P., Braun, M. (1995) "Extremely small spherules" from Middle Triassic of Mecsek Mts, Hungary. In: Dete, Cs.H. and Szöör, Gy. eds. *Proceedings of the International Meeting: Spherulites and (Palaeo) ecology*, p. 111-120, Debrecen.
- Wang, K. (1992) Glassy microspherules (microtektites) from an Upper Devonian limestone. *Science*, 256, p. 1547-1550.
- Xiao Zhifeng, Ouyang Ziyuan, Lin Wenzhu (1994) Simulation of the climatic effect of giant extraterrestrial body impacts on the earth in Cenozoic. *Abstr. Internat. Meeting Spherulites (Micrometeorites) in the Carpathian Basin*, p. 10, Budapest.

BOOK REVIEW

László Trunkö. Geology of Hungary. Gebrüder Borntraeger, Berlin – Stuttgart, 1996. Hardcover, 464 pp. Price: 15 DM, ISBN 3-443-11023-1

This synthesis on the geology of Hungary represents a concise and complete presentation of the stratigraphy and structure of the main structural units of Hungary. This new edition of a book first published in German in 1969 required an entirely new conception not only for the general ideas, but also for the details, in order to keep up with the tremendous amount of papers published during the last three decades which shed a new light on the tectonics, sedimentological and stratigraphic issues.

The geology of Hungary is treated in thirteen chapters. The book also includes a list of geographical names and one of stratigraphical names and major tectonic units and structures. The book is based on a large volume (47 pages) of references.

The almost generally accepted structural model of Hungary is a puzzle of plates of different origin, whose recent configuration was achieved in the Lower or Middle Miocene, whilst the beginning of the movements, though still debated, has probably started in the Middle or Upper Cretaceous. There are three main units, separated by the Mid-Hungarian Lineament: Transdanubicum and Bkkium (Pelso Unit) to the North and Tisza Unit to the South. A few smaller units are scattered north of Transdanubicum and Bükkium: the Alpine Unit (regarded as part of the Alps, consists of a Penninic window near Koszeg, Lower Austroalpine series near Sopron and Upper Austroalpine - Graz Paleozoic - in the basement of the Little Plain), Vepor Unit, Zemplen Subunit. They are largely covered by Tertiary deposits.

The first eight chapters of the book present the stratigraphy and tectonics of the major structural units of the country: the Transdanubian Mid-Mountains, Igal Unit, Alpine Unit, Vepor Unit, the NE-Hungarian Mountains (Bükk and Rudabnya) and Tisia (Tisza) Unit.

A substantial chapter of the book is dedicated to the Cenozoic in Hungary, including detailed stratigraphy of the Paleogene, Neogene and Quaternary deposits, with their flora and fauna. A special chapter treats the tectonics of the Paleogene and Neogene basins.

Magmatism is grouped in pre-Variscan events, Variscan plutonism and volcanism, Triassic basic-intermediate volcanism, Cretaceous basic-alkaline volcanism in Tisia and Cretaceous subvolcanic rocks, the andesitic volcanism of the Eocene, the acidic-intermediate volcanism of the Miocene and the basaltic volcanism of the Pannonian.

Chapter 12 represents a general outline of the pre-Variscan, Variscan and Alpine tectonic events and of geotectonical conceptions.

A special chapter is dedicated to natural resources: ores (non-ferrous metals, iron-manganese-titanium ores, uranium and bauxite), sources of energy (crude oil and gas, coal, geothermal energy and thermal water) and nonmetallic raw materials.

This volume provides the reader new data and good, up-to-date reviews. It is therefore a good source and will be useful for all people interested in the region, which makes this volume worth having in personal or institutional libraries.

A. Seghedi



ON THE MORPHOLOGICAL DISTINCTION BETWEEN SPHERULES OF EXTRATERRESTRIAL, TERRESTRIAL AND INDUSTRIAL ORIGIN BY MEANS OF SEM AND EDAX EXAMINATION OF SAMPLES TAKEN FROM THE PLACERS OF CRIȘU NEGRU, ROMANIA

Orsolya KÁKAY-SZABÓ

Hungarian Geological Survey, 1143 Budapest Stefánia út 14, Hungary

Árpád HADNAGY

Geological Institute of Romania, str. Caransebeș nr. 1, 78344 București 32, Romania

Key words: Micrometeorites. Extraterrestrial, Terrestrial and Industrial Spherules. Morphogenetic, Glassy Tektite. Silicate-rich Spherules. Iron-rich Spherules.

Abstract: Samples were taken from the placer of Crișu Negru at 24 sites which yielded 52 granules among which 24 pieces were of extraterrestrial, 7 pieces of terrestrial and 18 pieces of industrial origin. The three genetic types are easy to distinguish with SEM and EDAX examinations by their morphological and chemical properties. The sites where the samples were taken yield on map points which show the places from where the material of granules of different genetic types erode. In conclusion it appears possible both to localize the primary sites of extraterrestrial materials and to measure the industrial environmental pollutions and also the spherule field of dispersion. The data are important in view of environment protection.

24 samples were collected from placers in Crișu Negru and examined by the aim of SEM and EDAX. As a result of the examinations three main genetic types can be discerned: extraterrestrial, terrestrial and industrial (Fig. 1).

EXTRATERRESTRIAL TYPE can be divided into two subtypes.

A. Spherules formed in the upper part of the atmosphere.

1. Glassy tektites (Pl. I, Figs. 1, 2)

Size: 100-200 μ m

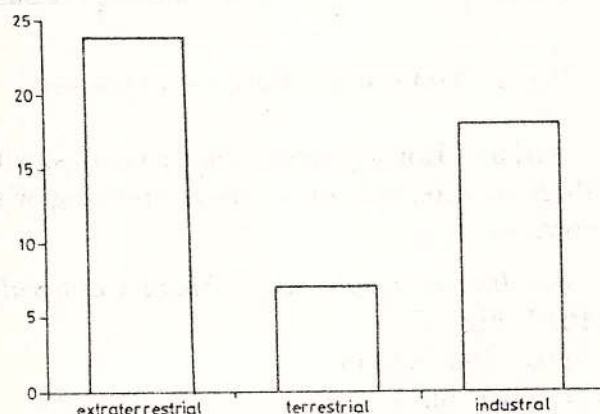


Fig. 1 - Frequency of the three genetic types of spherules.



Colour: honey yellow, brownish yellow

Chemical composition is given in Figure 2

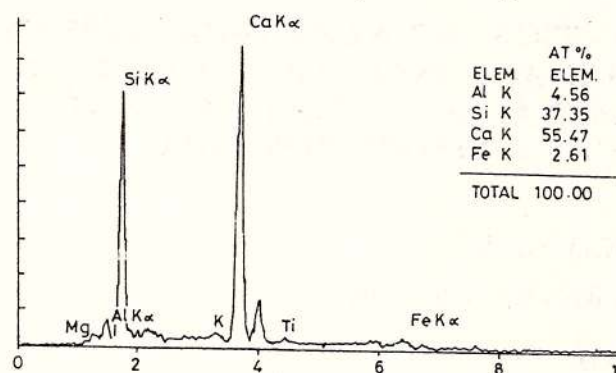


Fig. 2 – EDAX graph of glassy tektites.

Surface: homogeneous, strongly viscous, transparent material, with gaseous bubbles and with crystallites ordered in direction of spinning with craters of bubbles.

2. *Silicate-rich spherules* (Pl. I, Figs. 3, 4)

Size: 150–300 μm

Colour: black

Chemical composition is given in Figure 3

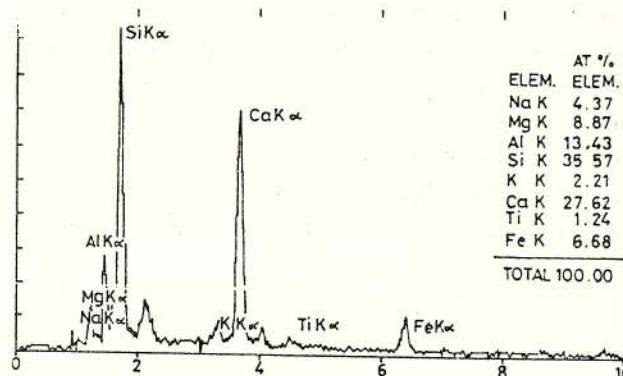


Fig. 3 – EDAX graph of silicate-rich spherulite.

Surface: Homogeneous, highly viscous, with fibers in direction of a strong spinning with carvings.

3. *Iron-rich spherules "Magnetospherules"* (Pl. I, Figs. 5, 6)

Size: 150–200 μm

Colour: black

Chemical composition is shown in Figure 4

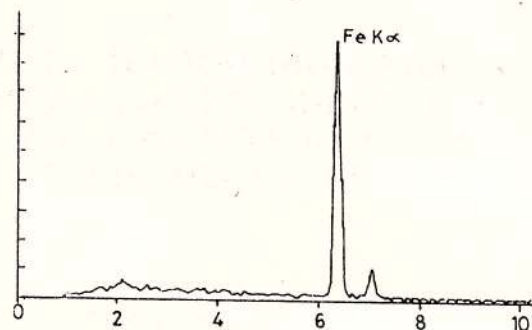


Fig. 4 – EDAX graph of a iron-rich spherule.

Surface: built from octahedral pieces ordered in direction of spinning with joints resulting in a surface carved by parallel lines; the small holes on the surface result from the exits of gaseous content suggesting the original behaviour of its material.

These are micrometeorites resulted from meteorite entering the atmosphere and their dismembering and fast heating, which afterwards slowly float and cool reaching the Earth's surface. The slow cooling enables the primary features to inherit.

B. *Spherules formed in the lower layers of the atmosphere*

4. *Perfectly homogenized Fe- and silicate-rich spherules* (Pl. II, Figs. 1, 2)

Size: 150–300 μm

Colour: black

Chemical composition: on the surface they are Fe-rich (Fig. 5) in the interior Si >> Ca > Al > Mg > Fe > K > Ti

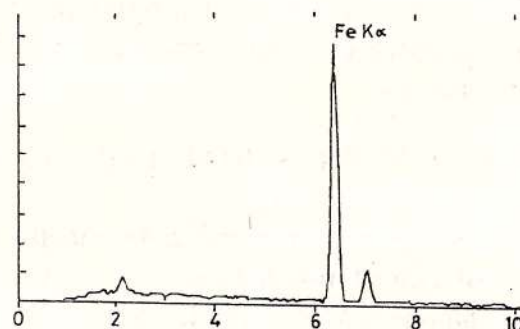


Fig. 5 – EDAX graph of B4 spherule type (rim).

Surface is rough showing small octahedral crystals building up an iron-rich crust on the drop surface. The iron-rich crust has formed by recrystallization of primary Fe-Si drop (Shymanovich et al., 1993) by entering the lower atmosphere.

5. *Partly homogenized silicate-rich spherules "Siderospherules"* (Pl. II, Figs. 3, 4)

Size: 180–300 μm

Colour: black with glassy appearance

Chemical composition: Fe and Si > Ca > Al > Mg > Na > K > Ti (Figs. 6a, 6b).

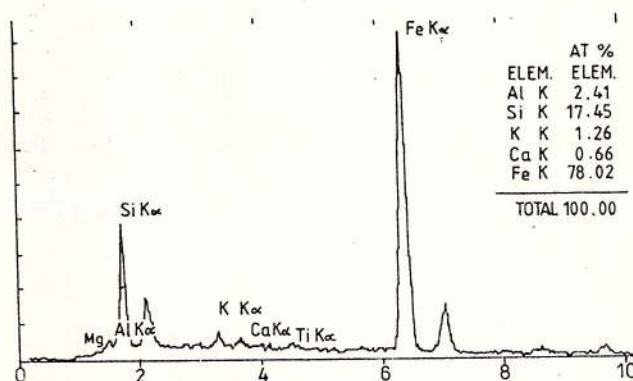


Fig. 7 – EDAX graph of B6 spherule type

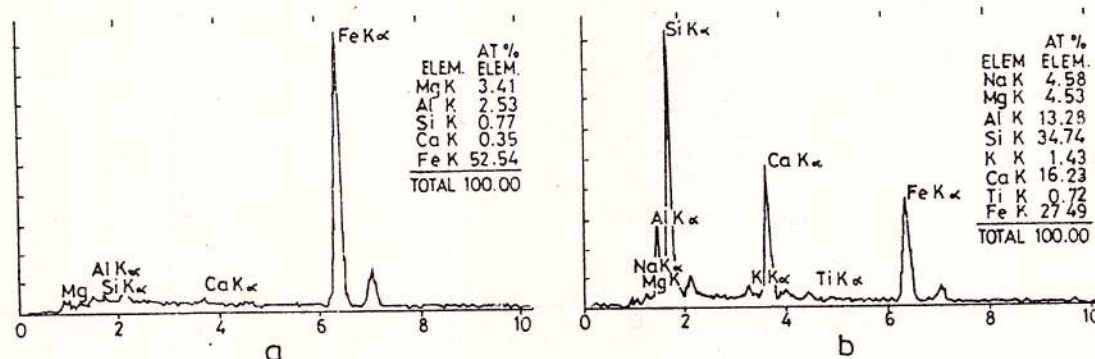


Fig 6 – EDAX graph of B5 spherule type, showing both iron rich parts (a) and silicate-rich parts (b).

Surface is rough formed by iron octahedra floating in the silicate material.

6. *Non-homogenized silicate-rich spherules* (Pl. II, Fig. 5)

Size: 180–350 μm

Colour: black with glassy appearance

Chemical composition: both Fe and Si are present (Fig. 7)

Surface: rough. It is supposed that such spherules have formed by a meteorite dismembering near the earth's surface, as the caloric energy of a drop decreases. The distance from the earth's surface plays thus an important role in the formation of iron-rich or silicate-rich spherules as well as in the phase separation (Pl. III).

TERRESTRIAL SPHERULES

7. *Limonite rounded grains with relict pyrite* (Pl. IV, Figs. 1, 2)

Size: 500–600 μm

Colour: dark brown, metallic yellow green

Chemical composition: iron is dominant (Fig. 8)

Surface: irregular.

INDUSTRIAL TYPE

8. *Titanium-rich grains* (Pl. IV, Figs. 3, 4)

Size: 200–400 μm

Colour: shiny black

Chemical composition:

Ti >> Si > Fe > Mn > Ca > Al > K (Fig. 9)

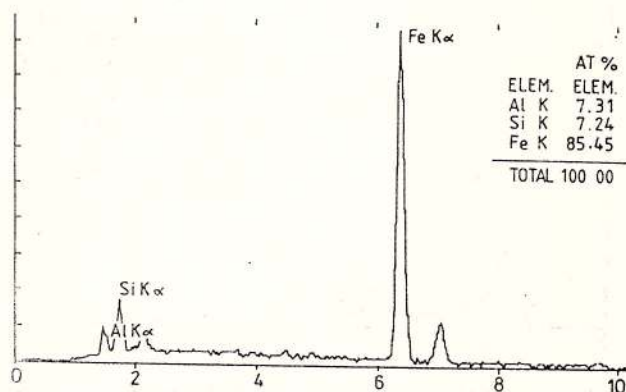


Fig. 8 - EDAX graph of a spherule of type 7.

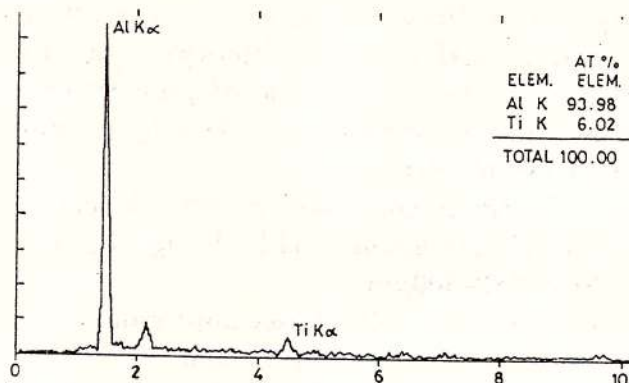


Fig. 10 - EDAX graph of an Al-rich spherule.

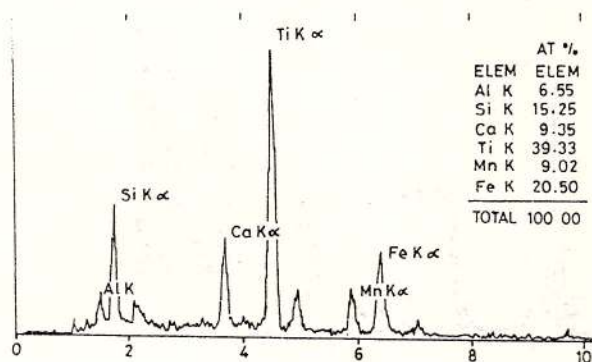


Fig. 9 - EDAX graph of a Ti-rich spherule.

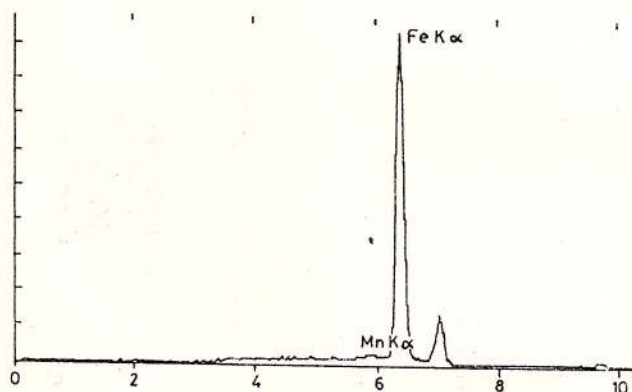


Fig. 11 - EDAX graph of grain of an Fe-rich spherule.

Surface: generally smooth shiny; bubble craters are present.

9. Aluminium-rich spherules (Pl. IV, Figs. 5, 6)

Size: 200–350 μm

Colour: light gray

Chemical composition: Al >> Ti (Fig. 10)

Surface: rough, paste-like

10. Iron-rich grains (Pl. V, Figs. 1, 2)

Size: 300–400 μm

Colour: black

Chemical composition: Fe > Mn (Fig. 11)

Surface: carved with octahedral crystals; the inner parts have gaseous bubbles.

11. Silicate grains (Pl. V, Figs. 3, 4)

Size: 220 μm

Colour: glassy milkwhite

Chemical composition:

Si >> Ca >> Al > Mg > K > Ti (Fig. 12)

Surface: paste-like, inner bubbles.

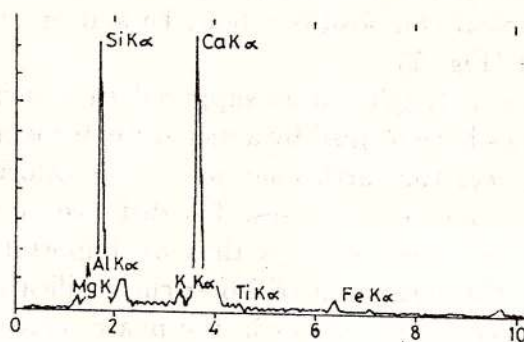


Fig. 12 - EDAX graph of a silicate spherule.

By their properties above, it is possible to distinguish the Extraterrestrial, Terrestrial and Industrial material according to the following characteristics:

meteorites were observed to fall, which all were chondrite meteorites (B. Mauritz et al., 1953; K. Sztrókay, M. Földváry, 1953; K. Sztrókay et al., 1961). By searching and studying the

	Extraterrestrial materials	Industrial materials
Size	100–280 μm	150–350 μm
Shape	drop, sphere	sphere, rarely drop
Figures	Glassy tektites Pl. I, Figs. 1,2; Pl. VI, Figs. 1,3,5	Ti industrial PL. VI, Figs. 2,4,6
Surface	soft material of high viscosity, uniform surface fibers, bubble craters Fig. 3 of soft edges with ordered crystalline in	no fibers, smooth shiny surface, hard crystal parts arranged without order, sharp bubble craters with edges on the boundaries
Colour	honey yellow	shiny black, glassy black
Chemical composition	$\text{Ca} > \text{Si} > \text{Al} > \text{Mg} > \text{K} > \text{Ti}$	there is always a small amount of Mn high Ti content

	"Magnetospherules"	Similarities	Industrial iron
Size	120–200 μm		200–300 μm
Colour		metallic black	
Figures	Pl. I, Figs. 5,6; Pl. III, Fig. 3; PL. VII, Figs. 1,3		Pl. V, Figs. 1,2; PL. VII, Figs. 2,4
Surface	octahedral units of different size, ordered in direction of spinning, carved surface at the edges of octahedral plates Pl. VII, Fig. 1	the octahedra on the surface yield gaps at joints	the octahedral plates build up the surface in an irregular way; the surface of the octahedral crystal Pl. V, Fig. 2; Pl. VII, Fig. 2
Inner structure	cavities produced by the gas content, the disc plates are saw edged, the solid parts show signs of gas bubbles Pl. VII, Fig. 3		structure like that of loose dirt with cavities Pl. VII, Fig. 4

DISTINCTION OF EXTRATERRESTRIAL AND TERRESTRIAL MATERIALS

Their morphologies, size and chemical compounds are completely different. The terrestrial material have a bigger size and their shapes are either formules or with edges not like those of regular spherules. Their chemical composition is easy to distinguish.

DIFFERENCES BETWEEN EXTRATERRES- TRIAL AND INDUSTRIAL MATERIALS

In their distinction the structure of material of spherules has a decisive role especially in case of spherules with pure iron content. The amounts of extraterrestrial material (52%) in the examined material show that in the second half of the last century and at the beginning of this century by every 10-th to 15-th year

micrometeorites there is a possibility to discover meteorite impacts, their periodicity and frequency through the geological ages.

References

- Mauritz, B., Hegedús, M., Szelényi, T. (1953) A Kisvarsányi meteorkö. *Földtani Közlöny*, 83, p. 138–146.
- Shymanovich, S., Kolosova, T., Raukas, A., Tiirmaa, R. (1933) Extraterrestrial spherules in the surroundings of Kaali meteorite craters. *Proc. Estonian Acad. Sci. Geol.*, 42/3, p. 127–133.
- Sztrókay, K., Földváry, M. (1953) A somogygyei Mike községben hullott meteorit vizsgálata. *Földtani Közlöny*, 83, p. 243–256.



Sztrókey, K., Tolnay, V., Földváry-Vogel
(1961) Mineralogical and chemical properties
of the carbonaceous meteorite from Kaba. *Hun-*
gary. Acta Geol., 7, p. 57-103.

Plate I

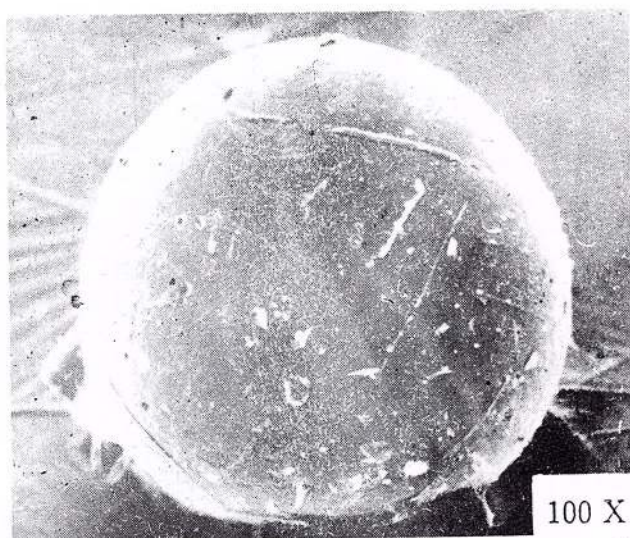
Extraterrestrial spherules. SEM photographs.

Figs. 1, 2 – Glassy tektite.

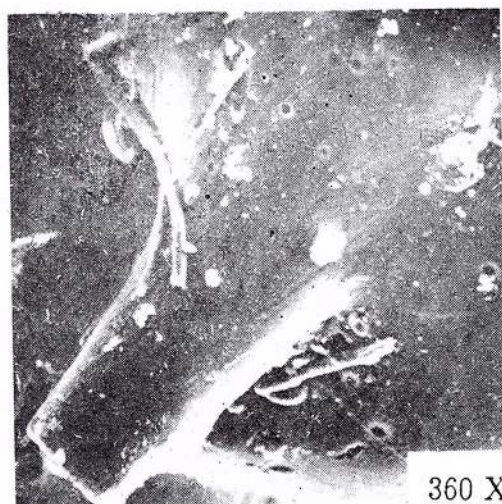
Figs. 3, 4 – "Siderosphrules".

Figs. 5, 6 – Iron-rich spherules.

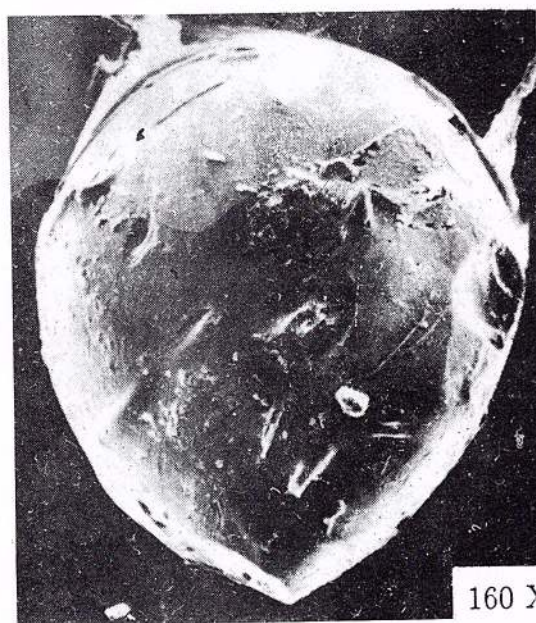




100 X
1

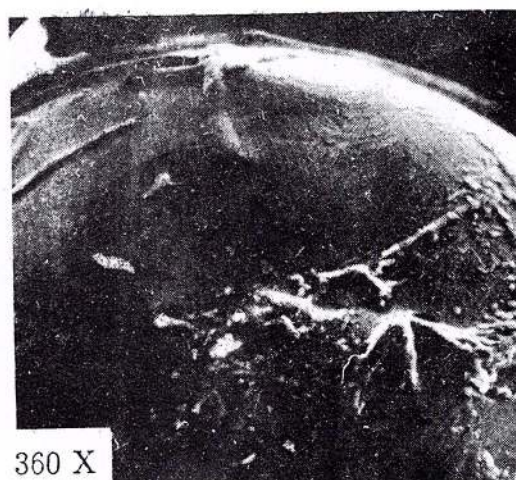


360 X
2



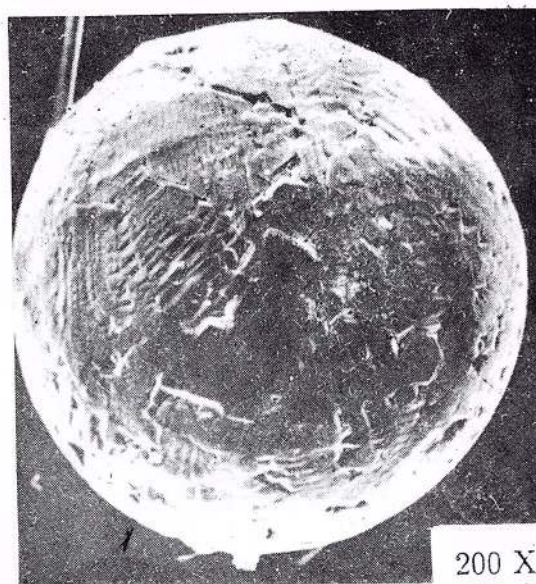
3

160 X



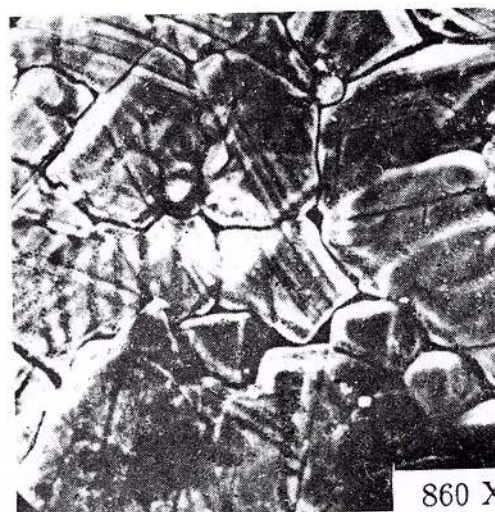
4

360 X



5

200 X



6

860 X

Plate II

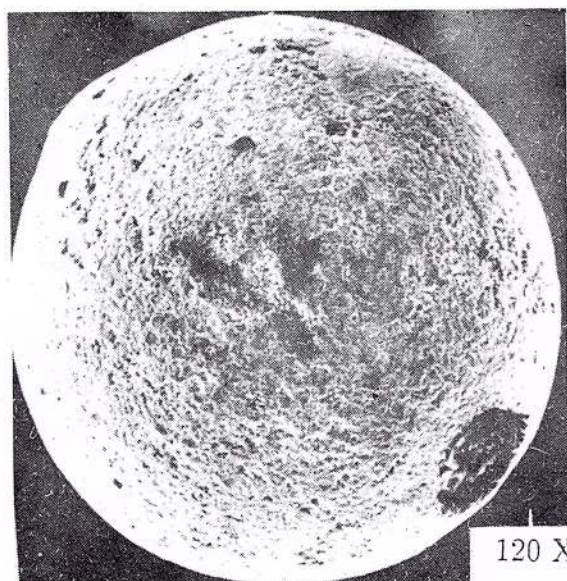
Extraterrestrial spherules. SEM photograph.

Fig. 1, 2 – Homogeneous Si-Fe spherules – type B4.

Fig. 3, 4 – Homogeneous Si-Fe spherules – type B5.

Fig. 5 Non-homogenized Fe-Si spherules.

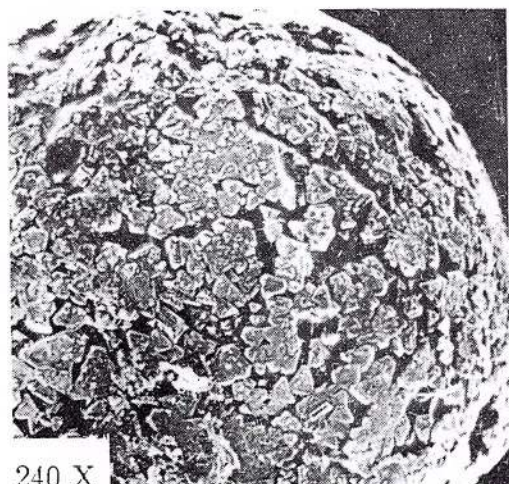




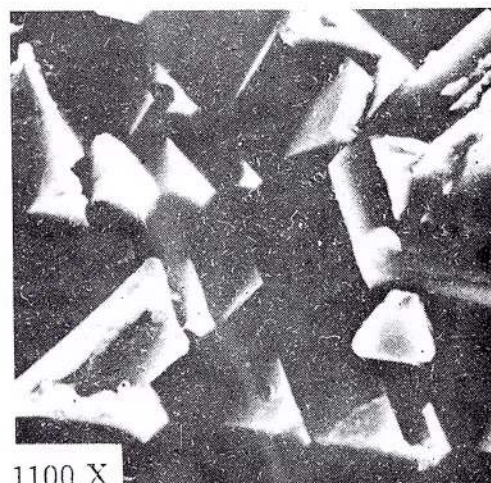
1



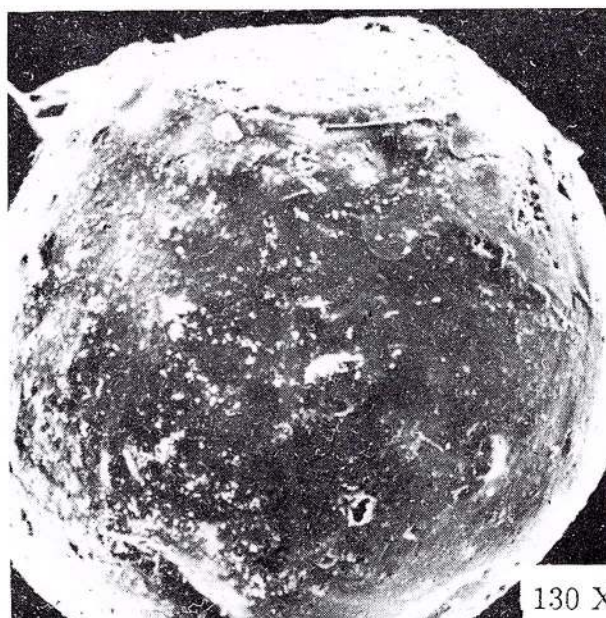
2



3



4



5

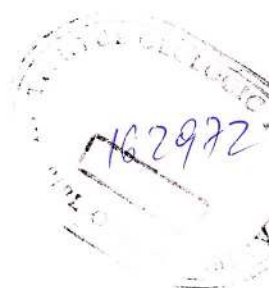


Plate III

Main genetic types

- A.** Spherules formed in the upper part of the atmosphere.
- B.** Spherules formed in the lower layers of the atmosphere.



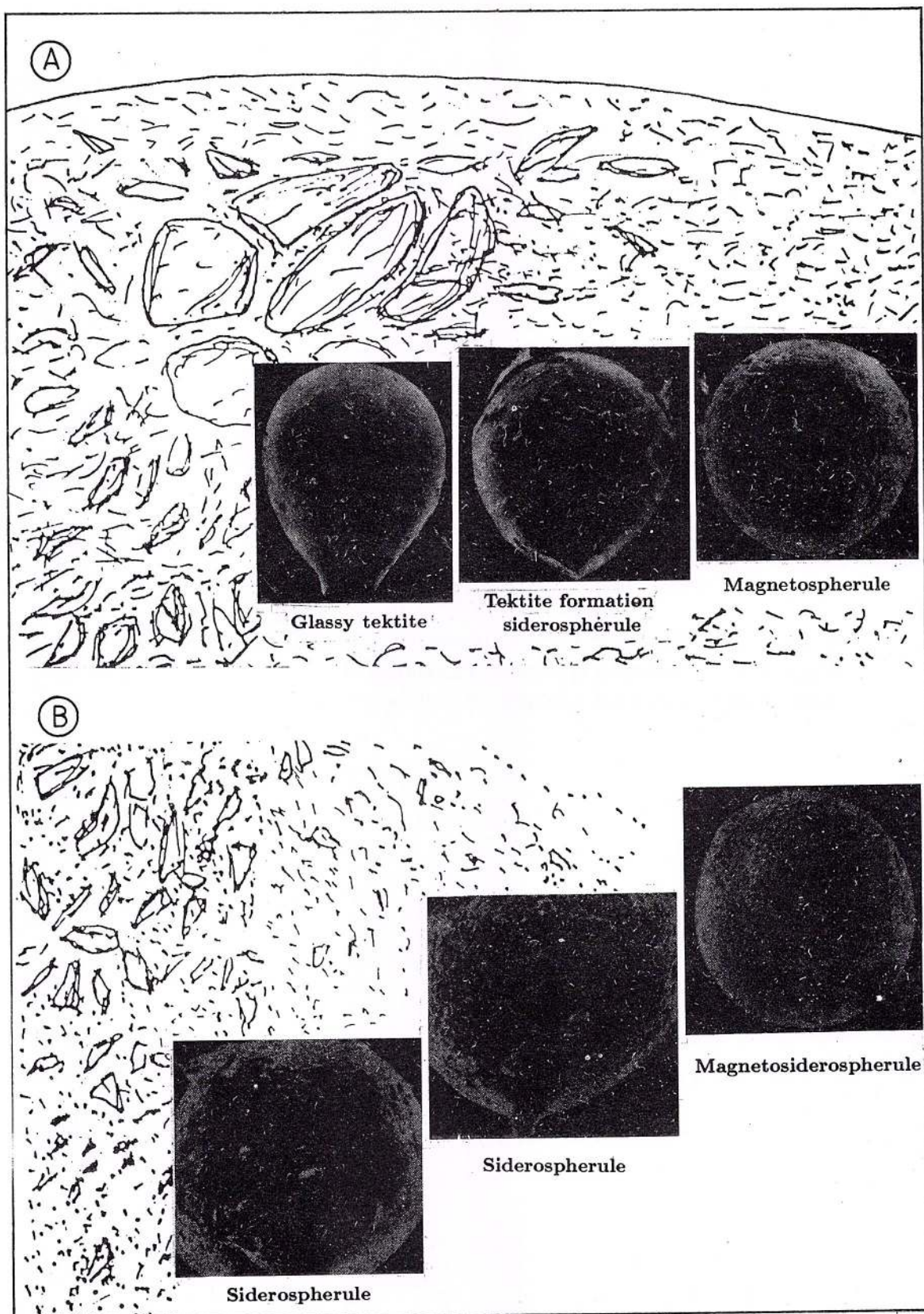
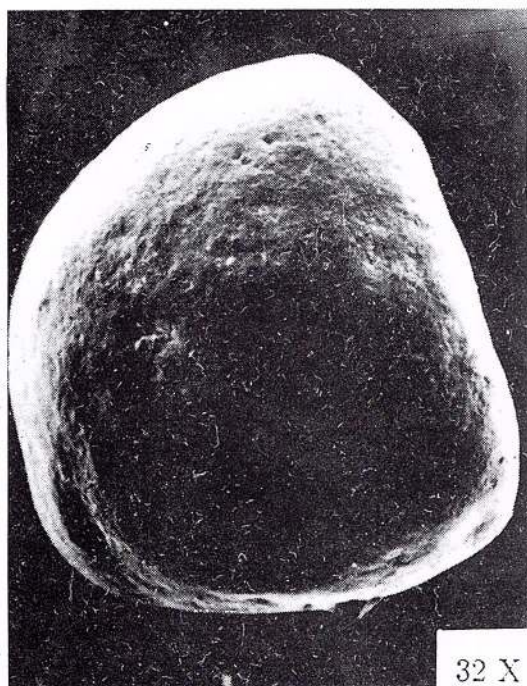


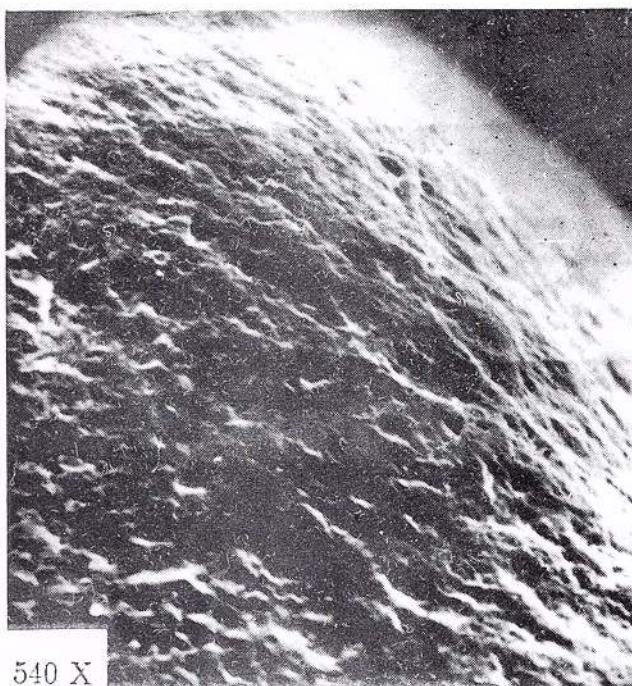
Plate IV

- Figs. 1, 2** – SEM photographs. Terrestrial spherules. Limonite grains.
Figs. 3, 4 – Industrial spherules. Titanium-rich.
Figs. 5, 6 – Industrial spherules. Aluminium-rich.

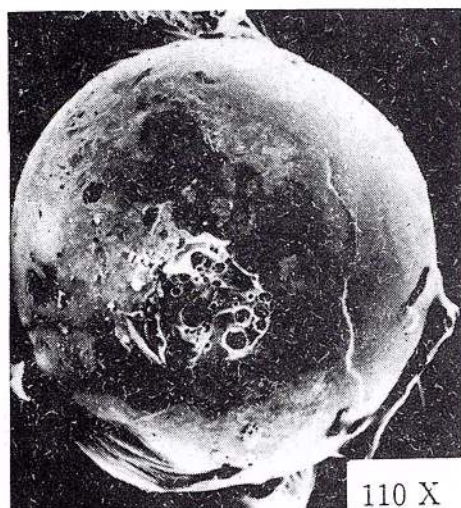




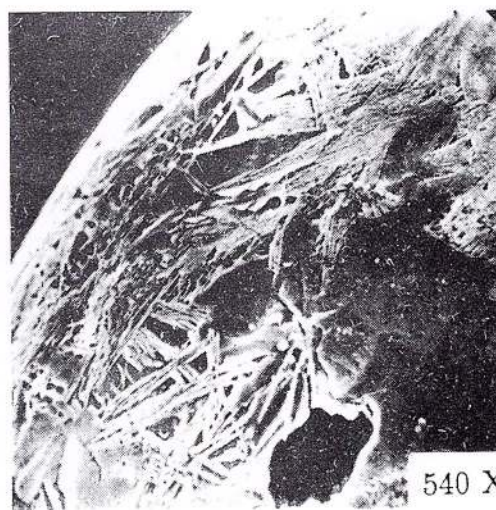
32 X
1



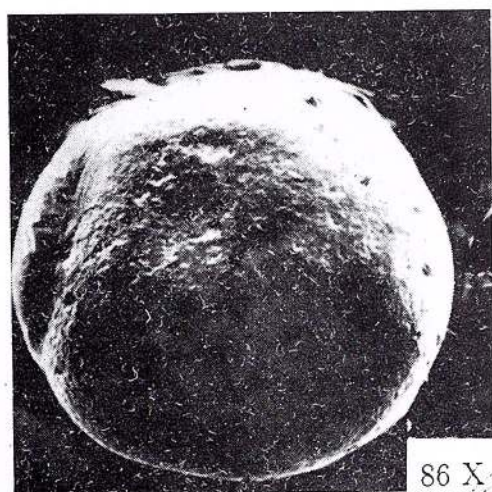
540 X
2



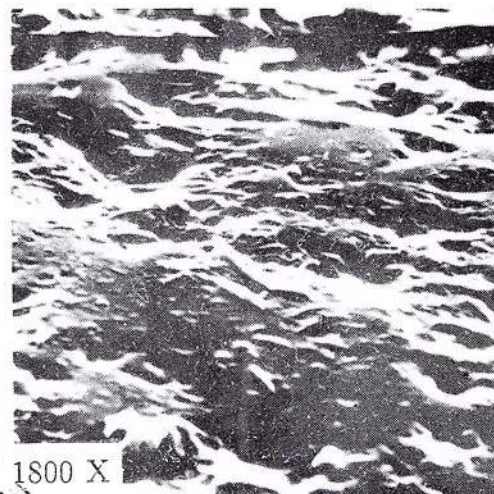
110 X
3



540 X
4



86 X
5



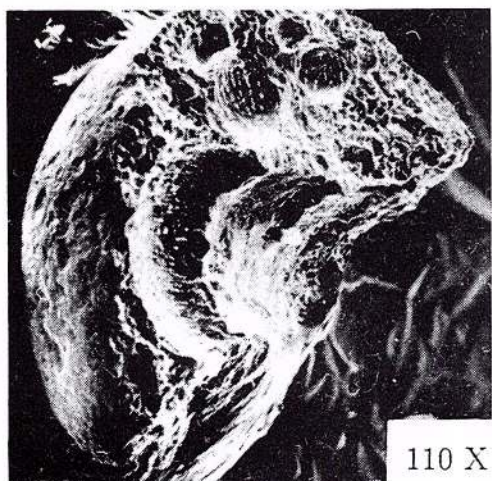
1800 X
6

Plate V

Figs. 1, 2 – Industrial spherules. SEM photographs. Fe-rich grains.

Figs. 3, 4 – Industrial spherules. SEM photographs. Silicate-rich grains.

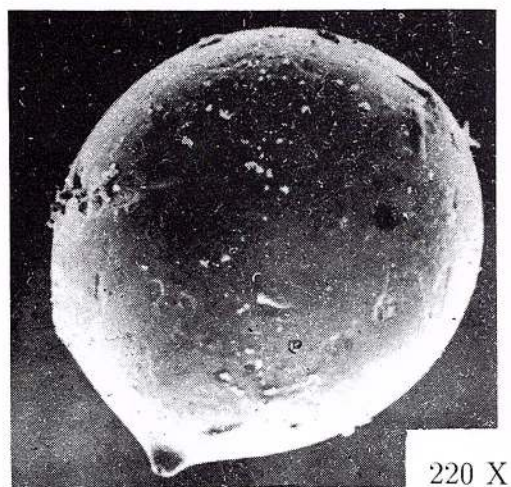




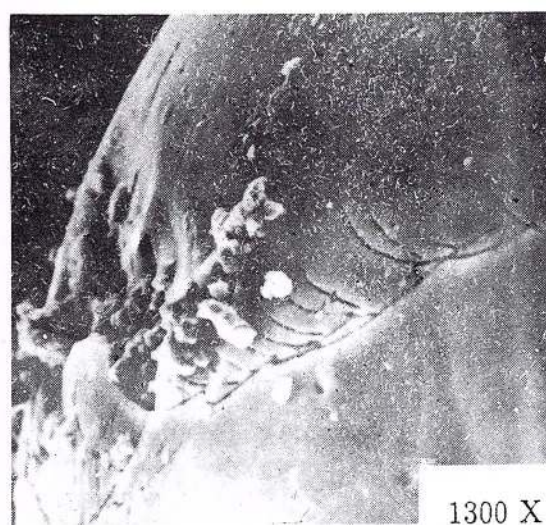
1



2



3



4

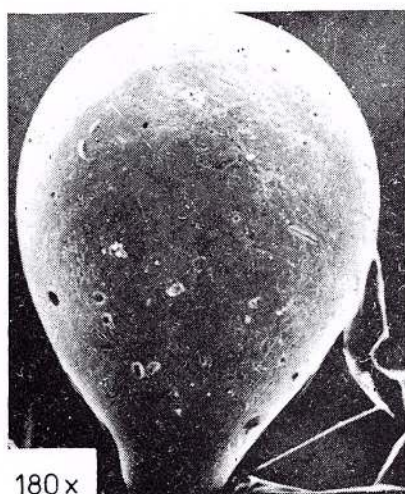
Plate VI

Morphological differences between extraterrestrial and industrial spherules

Figs. 1, 2, 5 – Glassy tektites.

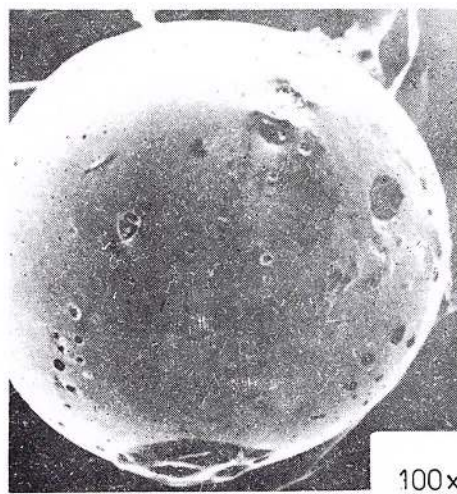
Figs. 2, 4, 6 – SEM photographs. Titanium-rich spherules.





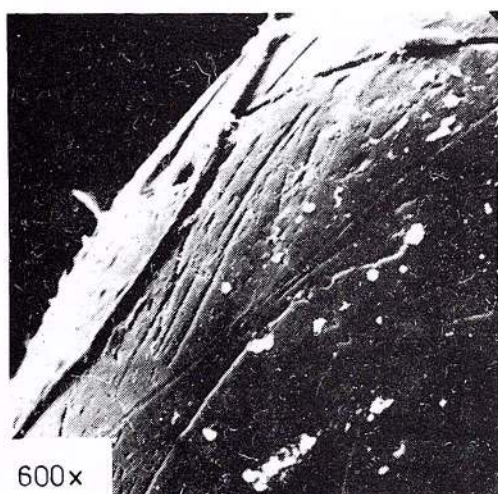
180x

1



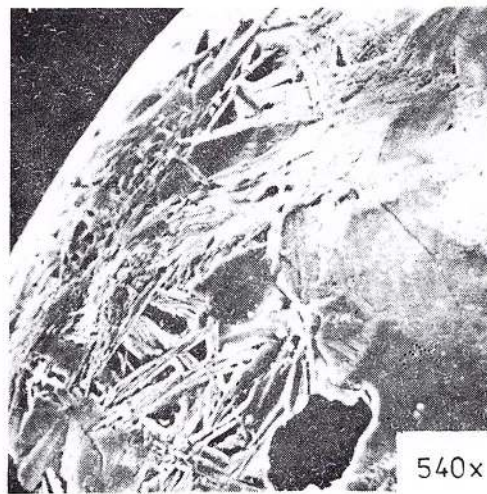
2

100x



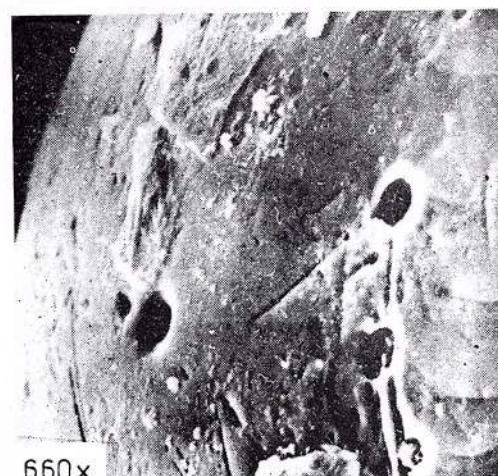
600x

3



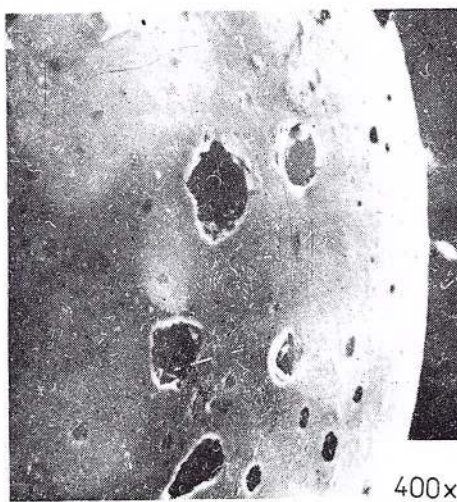
4

540x



660x

5



6

400x

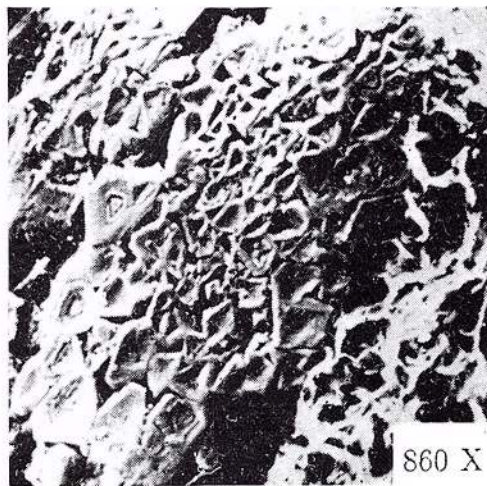
Plate VII

Morphological difference between the extraterrestrial iron-rich spherules
and the industrial iron-rich spherules (SEM photographs)





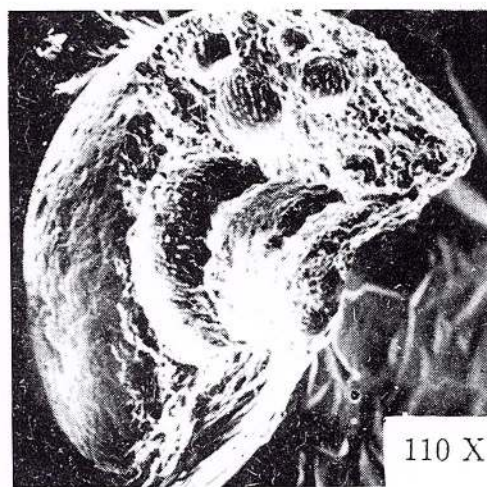
1



2



3



4

Rom. J. Mineralogy, vol. 78, București, 1997



Institutul Geologic al României



THE STRUCTURE OF SYNTHETIC ZIPPEITE

Renaud VOCHTEN, Laurent van HAVERBEKE, Karel van SPRINGEL

Departement Scheikunde – Experimentele Mineralogie, Universiteit Antwerpen (RUCA)

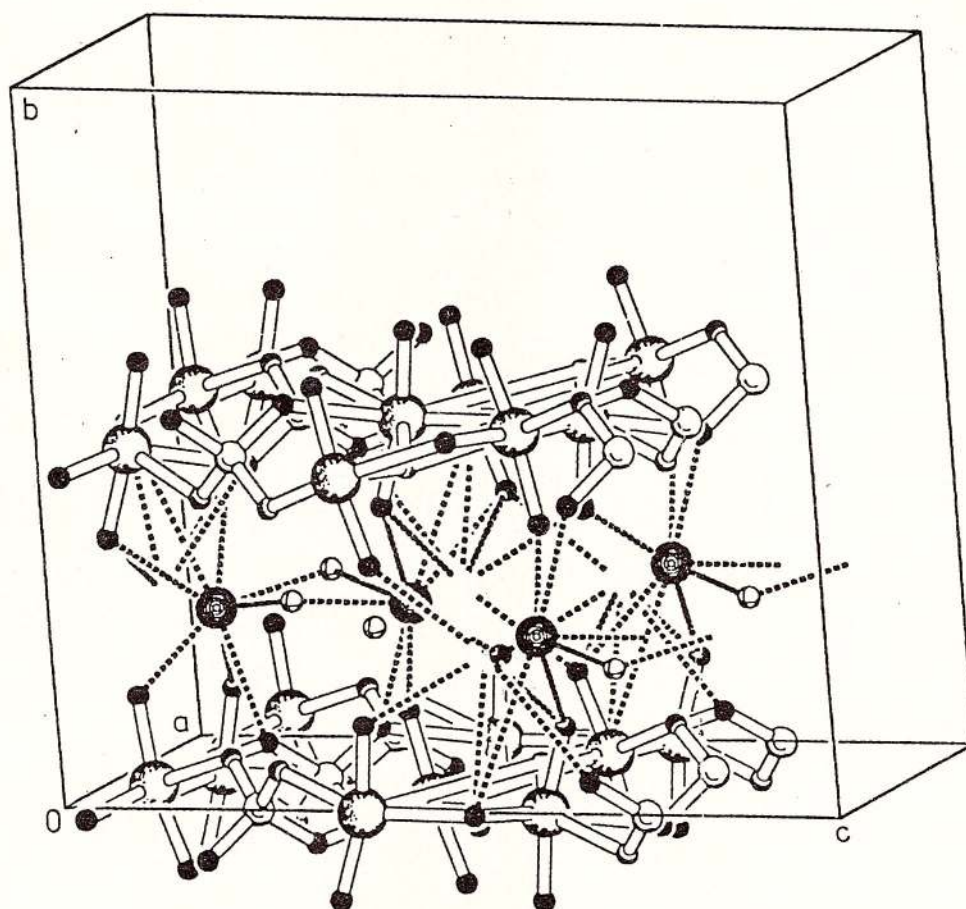
Middelheimlaan 1, B-2020 Antwerpen, Belgium

Norbert BLATON, Oswald M. PEETERS

Laboratorium voor analytische chemie en medicinale fysiochemie, Faculteit Farmaceutische Wetenschappen,

Katholieke Universiteit Leuven, Van Evenstraat 4, B-300 Leuven, Belgium

Zippeite was synthesized by adjusting a UO_2SO_4 solution containing K_2SO_4 to a pH of 3.6 by means of KOH and keeping it for 75 hours at 150°C at an approximate pressure of 3.5 MPa. The crystals are yellow and well-formed. Chemical analysis gives $\text{K}(\text{UO}_2)_2(\text{SO}_4)(\text{OH})_3 \cdot \text{H}_2\text{O}$ as the composition. The strongest lines of the X-ray pattern correspond to d values of 7.06, 3.51, 3.14, 2.86 and 3.65 Å. The pattern is identical to the pattern of natural



zippeite. Single-crystal X-ray studies revealed the composition $\text{K}(\text{OH}_2)_2\text{SO}_4(\text{OH})_3 \cdot \text{H}_2\text{O}$. The crystals are monoclinic, space group C2/c , with a 8.755(3), b 13.987(7), c 17.730(7) Å, β 104.13(3)°, and $Z=8$. The density D_m is 4.8 and D_X is 4.7 g/cm³. The crystal structure was solved by Patterson methods. The structure has been refined to an unweighted residual of 0.053. Zippeite possesses a layer structure parallel to (010). $\text{UO}_4(\text{OH})_3$ pentagonal bipyramids are the building blocks of a unique pattern of double polyhedra linked along the a axis by edge-sharing of OH-groups.

The $\text{UO}_4(\text{OH})_3$ chains are joined by chains of SO_4 polyhedra into infinite $(\text{UO}_2)_2(\text{OH})_2\text{SO}_4$ sheets. Two $(\text{UO}_2)_2(\text{OH})_2\text{SO}_4$ sheets sandwich planar layers of K^+ , OH^- and H_2O at $y \approx 1/4$ and $3/4$. The crystals show a moderate fluorescence between 520 and 620 nm, with unresolved bands at room temperature, but with three distinct bands at 77 K. The infrared spectrum was recorded, and the most important bands were assigned. The optical parameters were determined. The crystals have a moderate solubility, with the solubility product found to be $10^{-42.60}$.



STANDARDISATION OF POLYTYPE SUFFIXES

E.H. NICKEL

(Vice-Chairman, I.M.A. Commission on New Minerals and Mineral Names)

Division of Mineral Products, CSIRO, Wembely, WA 6014 Australia

The Commission on New Minerals and Mineral Names (CNMMN) of the International Mineralogical Association has published guidelines on a number of matters dealing with mineralogical nomenclature, including polytype nomenclature (e.g. Nickel and Mandarino, 1987). In essence, polytypes are distinguished by alphanumeric symbols appended to the name and jointed to it by a hyphen. The numeric part of the symbol represents the layering periodicity, and the alphabetic part, rendered in italic print, represents the crystallographic system. For example, wurtzite *4H* is a hexagonal wurtzite polytype with a periodicity of 4 times the c-dimension of the wurtzite parent.

Prior to the publication of these guidelines, various other polytype symbols had been used in the mineralogical literature and, in an effort

to standardise polytype nomenclature, members of the CNMMN decided that previous usage should be brought into conformity with current practice, which follows recommendations of the International Union of Crystallography (Guinier et al., 1984). Polytype names in the literature that require changing are as follows (Table)

It is quite likely that the mineralogical literature contains additional examples of polytype symbols that do not confirm to the recommended usage. Such names should also be revised to bring them into conformity. The recommended alphabetic symbols are as follows: cubic, *C*; hexagonal, *H*; rhombohedral, *R*; tetragonal, *Q* (for quadratic); orthorhombic, *O*; monoclinic, *M*; and triclinic, *A* (for anorthic).

Original Name	Present Name	Reference
Anandite-2 Or	Anandite-2 O	Filut et al. (1958)
Gageite-1 Tc	Gageite-1 A	Ferraris et al. (1987)
Hilgardite-1 Tc	Hilgardite-1 A,	Ghose (1985)
Hilgardite-3 Tc	Hilgardite-1 A	Ghose (1985)
Pyrophyllite-1 Tc	Pyrophyllite-1 A	Wardle and Brindley (1972)
Sapphirine-1 Tc	Sapphirine-1 A	Merlino (1973)
Tyretskite-1 Tc	Tyretskite-1 A	Ghose (1985)
Wollastonite-1 T	Wollastonite-1 A	Henmi et al. (1978)
Wollastonite-3 T	Wollastonite-3 A	Henmi et al. (1983)
Wollastonite-4 T	Wollastonite-4 A	Henmi et al. (1983)
Wollastonite-5 T	Wollastonite-5 A	Henmi et al. (1983)
Wollastonite-7 T	Wollastonite-7 A	Henmi et al. (1978)



References

- Ferraris, G., Mellini, M., Merlino, S. (1987) Electron-diffraction and electron-microscopy study of balangeroite and gageite: Crystal structures, polytypism, and fibre texture. *American Mineralogist* 72, p. 382-391.
- Filut, M.A., Rule, A.C., Bailey, S.W. (1985) Crystal structure refinement of anandite - 2 Or, a barium- and sulfur-bearing trictahedral mica. *American Mineralogist*, 70, p. 1298-1308.
- Ghose, S. (1985) A new nomenclature for the borate minerals in the hilgardite ($\text{Ca}_2\text{B}_5\text{O}_9\text{Cl}\cdot\text{H}_2\text{O}$)/tyretskite ($\text{Ca}_2\text{B}_5\text{O}_9\text{OH}\cdot\text{H}_2\text{O}$) group. *American Mineralogist*, 70, p. 636-637.
- Guiner, A. et al. (1984) Nomenclature of polytype structures. Report of the International Union of Crystallography Ad-Hoc Committee on the Nomenclature of Disordered, Modulated and Polytype Structures. *Acta Crystallographica*, A40, p. 399-404.
- Henmi, C., Kusachi, I., Kawahara, A., Henmi, K. (1978) 7 T wollastonite from Fuka, Okayama Prefecture. *Mineralogical Journal*, 9, p. 169-181.
- , Kawahara, A., Henmi, K., Kusachi, I., Tekeuchi, Y. (1983) The 3 T, 4 T, 5 T polytypes of wollastonite from Kushiro, Hiroshima Prefecture, Japan. *American Mineralogist*, 68, p. 156-163.
- Merlino, S. (1973) Polymorphism in sapphirine. *Contributions to Mineralogy and Petrology*, 41, p. 23-29.
- Nickel, E.H., mandarino, J.A. (1987) Procedures involving the IMA Commission on New Minerals and Mineral Names, and guidelines on mineral nomenclature. *Schweiz. Mineral. Petrogr. Mitt.*, 67, p. 185-210, (also published in other mineralogical journals).
- Wardle, R., Brindley, G.W. (1972) The crystal structures of pyrophyllite, 1 Tc and of its dehydroxylate. *American Mineralogist*, 57, p. 732-750.



MINERAL NAMES APPLIED TO SYNTHETIC SUBSTANCES*

Ernest H. NICKEL

Division of Exploration and Mining, CSIRO, Wembley, WA 6014, Australia

(Vice-Chairman, I.M.A. Commission on New Minerals and Mineral Names)

Introduction

Guidelines in mineral nomenclature published by the Commission on New Minerals and Mineral Names (CNMMN) of the International Mineralogical Association (Nickel and Mandarino, 1987) include the following statement: "If an artificial substance has given a name, and a mineral corresponding to that substance is subsequently discovered, the name given to the artificial substance does not necessarily have to be applied to the mineral". However, when the artificial substance corresponds to an existing mineral, it is commonly referred to by name of its mineralogical analogue. Ideally, mineral names should be given only to naturally-occurring substances formed by geological processes, yet it is recognized that a mineral name is a convenient short-hand way of referring to a synthetic substance that corresponds to a particular mineral. Following requests from editors of several major mineralogical journals for guidance in the editorial treatment of manuscripts containing such names, members of the CNMMN have discussed this question with a view to making recommendations acceptable to the mineralogical community. The recommendations are as follows:

Recommendations

1. Unmodified mineral names are not to be used for synthetic substances corresponding to existing minerals, chemical analogues of existing minerals, or hypothetical minerals.

2. If the synthetic substance has a simple formula, then preference should be given to the use of a chemical formula instead of a mineral name.

3. Synthetic substances that correspond to existing minerals with long or complex chemical formulae may be given mineral names suitably modified to clearly indicate their synthetic origin. Thus, for example, a synthetic topaz can be referred to as **synthetic topaz**, **synth-topaz** or **topaz (synth)**.

4. Synthetic substances that are chemical analogues of existing minerals with long or complex chemical formulae may also be given mineral names suitably modified to clearly indicate their synthetic origin. Thus, for example, a synthetic hydroxyl analogue of topaz can be referred to as **Synthetic OH-topaz**, **synth-OH-topaz** or **Topaz-(OH)-synth**.

5. If modified mineral names are used as indicated above, then this usage should extend throughout the published paper, including title, text, figure captions, and table captions.

* (Publication of this paper has been authorized by the Commission on New Minerals and Mineral Names of the International Mineralogical Association)



6. In languages other than English, the translated equivalents of "synthetic" and "synth" may be used in modified mineral names.

7. Abstractors and compilers should faithfully copy the modified mineral names in their abstracts and/or compilations, and not refer to synthetic products by unmodified mineral names.

Reference

- Nickel, E.H., Mandarino, J.A. (1987) Procedures involving the IMA Commission on New Minerals and Mineral Names and guidelines on mineral nomenclature. (The journal reference is varied to correspond to the journal to which the manuscript has been submitted).



NEW MINERALS RECENTLY APPROVED BY THE COMMISSION ON NEW MINERALS AND MINERAL NAMES INTERNATIONAL MINERALOGICAL ASSOCIATION

The information given here is provided by the Commission on New Minerals and Mineral Names, I.M.A. for comparative purpose and as a service to mineralogists working on new species.

Each mineral is described in the following format:

IMA No. (any relationship to other minerals)
Chemical Formula
Crystal system, space group
unit cell parameters
Colour; lustre; diaphaneity.
Optical properties.
Strongest lines in the X-ray powder diffraction pattern.

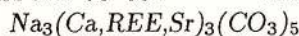
The names of these approved species are considered confidential information until the authors have published their description or released information themselves.

No other information will be released by the commission

J.A. Mandarino,
Commission on New Minerals and Mineral Names
International Mineralogical Association

1993 PROPOSALS

IMA No. 93-001 **The calcium-analogue of burbankite and khanneshite.**



Hexagonal: $P6_3mc$, $P6_2c$ or $P6_3mmc$

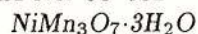
a 10.447 c 6.318 Å

Deep orange; vitreous; translucent.

Uniaxial (-), ω 1.636, ε 1.631.

5.20 (4), 3.68 (3), 3.01 (5), 2.601 (10), 2.130 (60), 1.649 (3).

IMA No. 93-002 **The nickel-analogue of chalcophanite.**



Hexagonal (trigonal): $R\bar{3}$ or $R3$

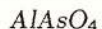
a 7.514 c 20.52 Å

Very dark brown to almost black; submetallic to vitreous; opaque, but translucent in thin plates.

Uniaxial (-), ω > 2.00, ε 1.97.

6.84 (10), 4.01 (2), 2.219 (3), 1.884 (2), 1.575 (2).



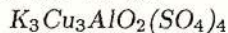
IMA No. 93-003 **The arsenate-analogue of berlinite.**Hexagonal (trigonal): P3_121 or P3_221

a 5.031 c 11.226 Å

Colourless, white, cream; vitreous; transparent.

Uniaxial (+), ω 1.596, ϵ 1.608.

4.36 (20), 4.06 (31), 3.442 (100), 2.359 (15), 1.873 (16), 1.4202 (11).

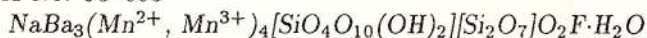
IMA No. 93-004 **The aluminum-analogue of klyuchevskite.**Monoclinic: I2 a 18.423 b 5.139 c 18.690 Å β 101.72°

Dark green; vitreous; transparent.

Biaxial (+), α 1.542, β 1.548, γ 1.641, 2V(meas.) unknown, 2V(calc.) 30°.

9.15 (84), 9.04 (100), 7.20 (52), 3.781 (37), 3.757 (33), 2.786 (21).

IMA No. 93-005

Orthorhombic: Pnma

a 23.42 b 12.266 c 7.181 Å

Black with a green shade; vitreous to greasy; translucent.

Biaxial (+), α 1.767, β 1.793, γ 1.871, 2V(meas.) 60–65°, 2V(calc.) 62°.

4.580 (5), 3.303 (9), 2.999 (10), 2.715 (5), 2.655 (10), 2.156 (4), 1.648 (5).

No. 93-006 **A tetragonal polymorph of rooseveltite.**Tetragonal: $\text{I4}_1/\text{a}$

a 5.085 c 11.69 Å

White to yellowish white; earthy; opaque.

Uniaxial (+), mean $n > 2.0$.

4.660 (11), 3.066 (100), 2.546 (12), 1.797 (11), 1.581 (10), 1.551 (17).

IMA No. 93-008

Orthorhombic: Pnma

a 9.0615 b 5.6727 c 7.2672 Å

Colourless to white and yellowish; vitreous; transparent to translucent.

biaxial, mean n calculated from Gladstone-Dale is 1.308.

4.472 (75), 3.540 (90), 3.183 (100), 2.8982 (80), 2.5362 (65), 2.2822 (65), 2.1631 (70).

IMA No. 93-009 **A tetragonal polymorph of bismite.**Tetragonal: $\text{P4}_2/\text{n}$ or P4_22_12

a 8.08 c 6.46 Å

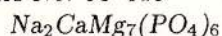
Green, yellowish; adamantine; translucent.

Uniaxial (+), ω 2.13, ϵ 2.18.

5.73 (7), 3.44 (5), 3.16 (10), 3.01 (4), 2.56 (4dif.), 2.02 (5), 1.902 (6).



IMA No. 93-010 The magnesium analogue of fillowite and johnsomervilleite.

Hexagonal (trigonal): $R\bar{3}$

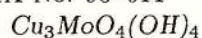
a 14.967 c 42.595 Å

Colourless; vitreous; transparent.

Uniaxial, indices of refraction calculated from reflectance values: n_1 1.60, n_2 1.62.

3.694 (S), 3.558 (M), 2.960 (S), 2.753 (S), 2.500 (M), 2.126 (M), 1.851 (M).

IMA No. 93-011



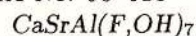
Orthorhombic: Pnnm

a 8.499 b 12.527 c 6.067 Å

Dark green; adamantine; transparent.

Biaxial (+), α slightly < 1.89, β unknown, γ slightly < 1., $2V(\text{meas.})$ 74° . 5.471 (S), 3.754 (S), 3.043 (S), 2.591 (VS), 1.519 (S).

IMA No. 93-013

Monoclinic: $P2_1/c$ a 8.215 b 11.989 c 6.076 Å β 96.22°

Colourless; vitreous; transparent.

Biaxial (+), α 1.4240, β 1.4320, γ 1.4415, $2V(\text{meas.})$ 85.5° , $2V(\text{calc.})$ 85.6° .

6.758 (7), 4.250 (9), 3.643 (8), 3.148 (7), 3.063 (8), 3.030 (7), 2.840 (7), 2.125 (8).

IMA No. 93-016

Cubic: $\text{Pa}\bar{3}$

a 6.502 Å

Steel black; metallic; opaque.

In reflected light: bright white with a yellowish tint, moderate anisotropism, no bireflectance, nonpleochroic. R: (51.0%)470nm, (52.6%)546nm, (52.9%)589nm, (49.2%)650nm.

2.89 (70), 1.955 (100), 1.735 (80), 1.250 (80), 1.207 (70), 1.148 (70), 1.054 (70).

IMA No. 93-017

Cubic: $\text{Pa}\bar{3}$

a 6.413 Å

Steel black; metallic; opaque.

In reflected light: bright white with bluish tint, no anisotropism, no bireflectance, nonpleochroic.

R: (44.3 %)470nm, (46.0%)546nm, (46.9%)589nm, (45.5%)650nm.

2.86 (70), 1.93 (100), 1.235 (80), 1.132 (90), 1.040 (80), 0.9780 (80).

IMA No. 93-018

Hexagonal: $P\bar{3}m1$

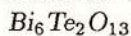
a 3.933 c 5.390 Å

Steel black; metallic; opaque.



In reflected light: bright yellowish white with bluish tint, moderate anisotropism with bluish or yellowish tint, no bireflectance, nonpleochroic. R_o & R_E : (41.4, 49.0%)470nm (40.2, 48.2%)546nm, (41.1, 49.0%)589nm, (45.2, 51.2%)650nm.
2.85 (100), 2.10 (80), 1.95 (60), 1.580 (70), 1.160 (60), 1.110 (70).

IMA No. 93-019



Orthorhombic: space group unknown

a 5.689 b 10.791 c 5.308 Å

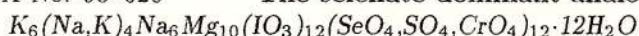
Yellow green to light green; adamantine; transparent.

Biaxial n's > 2. In reflected light, R: (14.8%)470nm, (13.0%)546nm, (13.2%)589nm, (13.6%)650nm.

3.146 (100), 2.841 (80), 2.694 (20), 1.956 (10), 1.695 (20), 1.631 (10).

IMA No. 93-020

The selenate-dominant analogue of 93-021



Hexagonal: $P\bar{3}c1$

a 9.590 c 27.60 Å

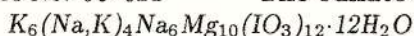
Pale yellow; vitreous; transparent.

Uniaxial (-), ω 1.655, ϵ 1.642.

13.75 (30), 7.10 (20), 3.974 (16), 3.561 (100), 3.082 (32), 3.058 (39), 2.715 (39).

IMA No. 93-021

The sulfate-dominant analogue of 93-020



Hexagonal: $P\bar{3}c1$

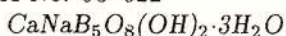
a 9.4643 c 27.336 Å

Pale yellow; vitreous; transparent.

Uniaxial (-), ω 1.622, ϵ 1.615.

13.67 (50), 7.05 (40), 3.927 (100), 3.515 (24), 3.023 (41), 2.681 (33), 2.3273 (12).

IMA No. 93-022



Monoclinic: $P2_1/c$

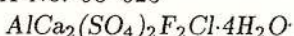
a 6.506 b 13.280 c 11.462 Å β 92.97°

White; silky to pearly; translucent.

Biaxial (-), α 1.540, β 1.554, γ 1.558, 2V(meas.) 60°, 2V(calc.) 56°.

8.64 (100), 6.62 (30), 4.18 (17), 2.868 (26), 2.845 (16), 2.795 (17), 2.587 (15).

IMA No. 93-023



Tetragonal: $I4/m$

a 6.859 c 13.310 Å

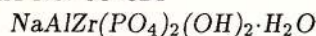
White; vitreous; transparent.

Uniaxial (+), ω 1.509, ϵ 1.526.

6.67 (60), 3.922 (50), 3.729 (40), 3.431 (100), 3.335 (80), 3.052 (40), 2.483 (40).



IMA No. 93-024



Monoclinic: space group unknown

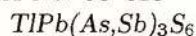
a 20.840 b 9.871 c 11.195 Å β 104.41°

Pale pinkish orange; vitreous; translucent.

Biaxial, n's vary from 1.62 (parallel to fibres) to 1.64 (normal to fibres)

8.865 (40), 4.128 (80), 3.711 (65), 3.465 (60), 3.243 (35), 2.603 (100).

IMA No. 93-025

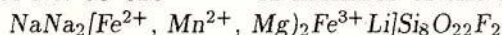
Monoclinic: $\text{P2}_1/\text{a}$ a 8.444 b 23.97 c 5.844 Å β 113.58°

Brilliant black, but dark red in thin fragments; metallic to submetallic; opaque, but translucent in thin fragments.

In reflected light: greyish white, clearly visible anisotropism from bluish to very weak reddish visible bireflectance, nonpleochroic. R_{\min} & R_{\max} : (29.7, 35.4%)470nm, (28.8, 33.1 %)546nm, (26.7, 30.3%)589nm, (26.6, 29.9%)650nm.

5.346 (32), 3.998 (74), 3.816 (54), 3.587 (86), 2.823 (100), 2.778 (84), 2.670 (58).

IMA No. 93-026

A member of the amphibole groupMonoclinic: $\text{C2}/\text{m}$ a 9.792 b 17.938 c 5.3133 Å β 103.87°

Bluish black to black; vitreous; opaque.

Biaxial (+), α 1.675, β 1.683, γ 1.694, $2V(\text{meas.})$ 87°, $2V(\text{calc.})$ 81°.

8.426 (45), 4.481 (54), 3.404 (57), 2.985 (38), 2.710 (100), 2.585 (38), 2.536 (92).

IMA No. 93-028

Hexagonal: $\text{P6}_3/\text{mmc}$

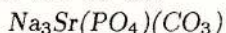
a 4.316 c 5.510 Å

White, greyish-black to black (when oxidized); metallic; opaque.

In reflected light: white with light yellow tint, clear anisotropism light yellow with a brown tint, faint bireflectance, nonpleochroic. R_o & R_E : (65.4, 65.2 %)470nm, (76.7, 74.8 %)546nm, (80.5, 77.9 %)589nm, (82.8, 79.5 %)650nm.

3.726 (34), 3.087 (38), 2.218 (100), 2.159 (57), 1.546 (31), 1.258 (25), 1.256 (26).

IMA No. 93-030

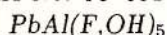
Monoclinic: P2_1 a 9.187 b 6.707 c 5.279 Å β 89.98°

Colourless to white; vitreous; transparent.

Biaxial (-), α 1.520, β 1.564, γ 1.565, $2V(\text{meas.})$ 20°, $2V(\text{calc.})$ 17°.

3.35 (50), 2.708 (100), 2.648 (90), 2.172 (100), 2.080 (50), 1.891 (80), 1.676 (50), 1.415 (70).

IMA No. 93-031

Triclinic; P1 or $\text{P}\bar{1}$ 

a 6.259 b 6.791 c 5.053 Å α 90.92° β 107.45° γ 104.45°

White to colourless; vitreous; transparent.

Biaxial (-), α 1.629, β 1.682, γ 1.691, 2v(meas.) 41°, 2V(calc.) 44°.

4.42 (100), 4.05 (35), 3.221 (40), 2.595 (70), 2.190 (65), 2.030 (50), 2.015 (40).

IMA No. 93-032

CaVOSiO_4

Monoclinic: C2/c

a 6.526 b 8.691 c 7.032 Å β 113.88°

Deep red; adamantine; transparent.

Biaxial (sign unknown), $\alpha \sim 1.95$, β unknown, γ 2.105, 2V(meas.) unknown.

4.90 (W), 3.22 (VS), 2.97 (M), 2.59 (S), 2.271 (W), 1.641 (W).

IMA No. 93-034

$(\text{Y,Ca,Na,REE})_4\text{Si}_5\text{O}_{15} \cdot n\text{H}_2\text{O}$ 4 ~ 4

Triclinic: P1 or P1̄

a 9.245 b 9.689 c 5.510 Å α 97.44° β 100.40° γ 116.70°

White; vitreous; translucent.

Biaxial (-), α 1.602, β 1.607, γ 1.611, 2V(meas.) 73°, 2V(calc.) 83°.

8.44 (80), 8.01 (50), 4.51 (50), 3.76 (70), 2.973 (100), 2.930 (60).

IMA No. 93-035

The chromium-dominant analogue of schreyerite

$(\text{Cr,V})_2\text{Ti}_3\text{O}_9$

Monoclinic: C2/c, Cc, P2₁/c, P2/c or Pc

a 7.03 b 5.02 c 18.83 Å β 119.60°

Black; metallic; opaque.

In reflected light: white, faint anisotropism, faint bireflectance, faint pleochroism pale brown.

R_{\min} & R_{\max} : (18.1, 20.1 %)470nm, (18.5, 19.9 %)546nm, (18.4, 19.8 %)589nm, (18.6, 20.9 %)650nm.

2.88 (2), 2.75 (3), 2.43 (2), 1.635 (3), 1.386 (2).

IMA No. 93-036

$\text{BaCuSi}_4\text{O}_{10}$

Tetragonal: P4/ncc

a 7.441 c 16.133 Å

Blue; vitreous; transparent.

Uniaxial (-), ω 1.633, ε 1.593.

8.055 (100), 4.031 (35), 3.544 (15), 3.200 (21), 2.688 (18), 2.395 (19), 2.016 (26).

IMA No. 93-037

The K-dominant analogue of gainesite.

$\text{NaKZr}_2(\text{Be,Al,Ca,Mn})(\text{PO}_4)_4 \cdot 2\text{H}_2\text{O}$

Tetragonal: I4₁/amd

a 6.570 c 17.142 Å

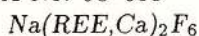
Intense bluish purple or pale lilac; vitreous; transparent.

Uniaxial (+), ω 1.624, ε 1.636.

6.161 (100), 4.291 (25), 3.286 (50), 3.039 (30), 2.895 (20).



IMA No. 93-038

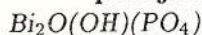
Hexagonal: $\text{P}\bar{3}$

a 6.099 c 11.066 Å

Pale pink to colourless; vitreous; transparent.

Uniaxial (+), ω 1.483, ϵ 1.503.

5.29 (70), 3.036 (100), 2.146 (70), 1.757 (80), 1.152 (40), 0.9189 (40).

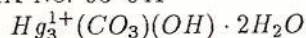
IMA No. 93-040 The PO_4 -analogue of atelesite and a monoclinic polymorph of
petitjeaniteMonoclinic: $\text{P}2_1/\text{c}$ a 6.954 b 7.494 c 10.869 Å β 107.00°

White to yellow; adamantine; translucent.

Biaxial (+), α 2.05, β 2.06, γ 2.09, 2V(meas.) 45°, 2V(calc.) 61°.

4.268 (17), 3.271 (51), 3.254 (100), 3.145 (34), 2.727 (29), 1.885 (16).

IMA No. 93-041

Orthorhombic: Pcab

a 11.130 b 11.139 c 10.725 Å

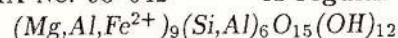
Black to very dark red-brown; sub-metallic to adamantine; opaque.

In reflected light: grey with slight bluish tinge, weak anisotropism (dull and dark greys and browns), weak to moderate bireflectance, nonpleochroic. R_{\min} & R_{\max} :

(11.4, 12.15 %)470nm, (10.95, 11.6 %)546nm, (10.85, 11.5 %)589nm, (10.7, 11.2 %)650nm.

4.84 (50), 2.969 (70), 2.786 (70), 2.648 (100), 2.419 (60), 1.580 (50).

IMA No. 93-042 A regular interstratification of amesite and clinochlore

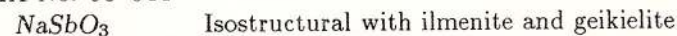
Monoclinic: Cm a 5.323 b 9.214 c 21.45 Å β 94.43°

Colourless to very pale green; nacreous; translucent.

Biaxial (+), α 1.575, β 1.575, γ 1.581, 2V(meas.) 0°, 2V(calc.) 0°.

7.1 (100), 4.61 (60), 3.560 (80), 2.557 (400), 2.427 (60), 1.536 (70).

IMA No. 93-044

Hexagonal: $\text{R}\bar{3}$

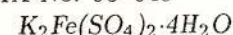
a 5.302 c 15.932 Å

Colourless; pearly; transparent.

Uniaxial (-), ω 1.184, ϵ 1.631.

5.30 (53), 3.00 (55), 2.650 (67), 2.365 (69), 1.874 (100), 1.471 (69).

IMA No. 93-045 The Fe-analogue of leonite

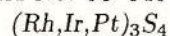
Monoclinic: $\text{C}2/\text{m}$ 11.843 b 9.552 c 9.945 Å β 94.89°

Colourless to light yellow; vitreous; transparent.



Biaxial (+), α 1.497, β 1.501, γ 1.509, 2V(meas.) 73° , 2V(calc.) 71° .
4.776 (30), 3.504 (52), 3.439 (100), 3.330 (48), 3.051 (29), 2.405 (30), 2.389 (49).

IMA No. 93-046



Monoclinic: F2/m

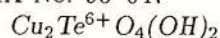
a 13.44 b 10.749 c 10.448 Å β 118.32 $^\circ$

Megascopic colour not observed; metallic; opaque.

In reflected light: pale slightly brownish grey, weak anisotropism in greys and browns, weak bireflectance, pleochroism weak. R_1 & R_2 : (47.2, 48.9 %)470nm, (48.4, 50.3 %)546nm, (49.1, 50.7 %)589nm, (49.8, 51.0%)650nm.

3.156 (100), 3.081 (100), 2.957 (90), 2.234 (60), 1.871 (80), 1.791 (90), 1.532 (70).

IMA No. 93-047



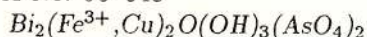
a 0.905 b 5.206 c 4.604 Å β 98.69 $^\circ$

Medium leaf green; adamantine; transparent.

In reflected light: pale grey, weak anisotropism with brown rotation tints, weak bireflectance, nonpleochroic. The mean index of refraction calculated from the reflectances at 589nm is 2.00.

4.506 (40), 4.337 (60), 3.838 (50), 2.891 (70), 2.598 (100), 1.834 (40), 1.713 (40), 1.500 (40).

IMA No. 93-048



Triclinic: P1 or P1

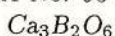
a 4.569 b 6.162 c 8.993 Å α 94.56 $^\circ$ β 99.68 $^\circ$ γ 94.31 $^\circ$

Brown-yellow; adamantine; transparent to translucent.

Biaxial (-), α 2.04, β 2.10 (calc.), γ 2.11, 2V(meas.) 45° .

8.822 (62), 3.749 (100), 3.596 (77), 3.468 (58), 2.903 (69), 2.810 (51), 2.685 (48).

IMA No. 93-049



Hexagonal: R3c or R3c

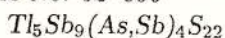
a 8.638 c 11.850 Å

Greyish white; vitreous; transparent.

Uniaxial (-), ω 1.726, ϵ 1.630.

2.915 (100), 2.756 (61), 2.493 (44), 2.160 (19), 2.044 (21), 1.976 (18), 1.895 (75).

IMA No. 93-050



Triclinic: P1

a 7.393 b 8.707 c 17.58 Å α 103.81 $^\circ$ β 91.79 $^\circ$ γ 109.50 $^\circ$

Black; metallic; opaque.

In reflected light: white, distinct to strong anisotropism with blue or blue-green colours, weak to medium bireflectance, pleochroism white to white with grey-blue tints.

R_{min} & R_{max} : (34.0, 36.7 %)470nm, (32.0, 34.9 %)546nm, (30.5, 33.0 %)589nm, (28.1, 29.7 %)650nm.



3.459 (100), 3.388 (64), 3.177 (54), 3.076 (65), 2.802 (44), 2.287 (57), 1.736 (38).

IMA No. 93-051



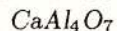
monoclinic: space group unknown

a 9.717 b 7.280 c 6.559 Å β 95.00°

Yellow; metallic; opaque.

In reflected light: yellow, strong anisotropism with orange, yellow-orange and greenish grey colours, distinct bireflectance, pleochroism greyish brown, orange, yellow orange. R_{\min} & R_{\max} : (19.5, 32.1 %)470nm, (23.8, 36.8 %)546nm, (24.6, 37.4 %)589 nm, (25.1, 37.3 %)650nm. 2.709 (10), 2.419 (8), 2.323 (7), 1.92 (6), 1.758 (8), 0.9605 (6), 0.9576 (7).

IMA No. 93-052



Monoclinic: C2/c

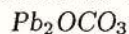
a 12.94 b 8.910 c 5.446 Å β 107.0°

Colourless to white; vitreous; transparent.

Biaxial (+), α 1.6178, β 1.6184, γ 1.6516, 2V(meas.) 12°, 2V(calc.) 15.5°(synthetic material).

4.460 (43), 3.609 (13), 3.515 (100), 2.882 (13), 2.605 (36), 2.440 (21), 1.764 (20).

IMA No. 93-053



Orthorhombic: P2₁22₁ or P2₁2₁2₁

a 9.294 b 9.000 c 5.133 Å

White; waxy; transparent to opaque.

The mean index of refraction calculated from the reflectance value at 589nm is 2.09.

6.49 (30), 4.02 (40), 3.215 (100), 3.181 (90), 2.858 (40), 2.564 (35).

IMA No. 93-054

The Se-analogue of pyrite



Cubic: Pa3

a 5.783 Å

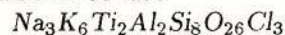
Black; metallic; opaque.

In reflected light: pink-yellow, no anisotropism, no bireflectance, nonpleochroic.

R: (42.4 %)470nm, (42.7 %)546nm, (45.7 %)589nm, (49.8 %)nm.

2.888 (50), 2.588 (100), 2.364 (80), 2.045 (40), 1.743 (50), 1.546 (60), 1.1131 (40).

IMA No. 93-055



Monoclinic: C2/m

a 10.37 b 16.32 c 9.16 Å β 105.6°

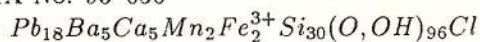
Colourless; vitreous; transparent.

Biaxial (+), α 1.601, β 1.625, γ 1.654, 2V(meas.) 85°, 2V(calc.) 86°.

8.22 (71), 3.50 (42), 3.157 (35), 3.049 (100), 2.900 (71), 2.835 (84).



IMA No. 93-056

Hexagonal: $R\bar{3}$

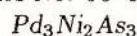
a 9.863 c 79.45 Å

Colourless; adamantine; transparent.

Uniaxial (-), ω 1.845, ε 1.815.

13.4 (50), 4.43 (30), 3.98 (30), 3.32 (100), 3.11 (40), 2.969 (40), 2.671 (80).

IMA No. 93-057

Hexagonal: $P6_3/m$, $P6_3$ or $P6_322$

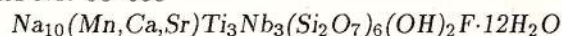
a 8.406 c 6.740 Å

Megascopic colour not observed; metallic; opaque.

In reflected light: rose, distinct anisotropism from light grey to greyish-brown, no birefractance, nonpleochroic. R_{min} & R_{max} : (48.4, 50.2 %)470nm, (51.2, 53.2 %)546nm, (53.2, 55.3 %)589nm, (56.6, 58.7 %)650nm.

2.626 (10), 2.477 (10), 2.429 (8), 2.283 (7), 1.978 (7), 1.818 (7), 1.781 (7).

IMA No. 93-058

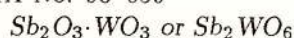
Monoclinic: Pm , $P2$ or $P2/m$ a 5.468 b 7.18 c 31.1 Å β 94.0°

Colourless, white, silvery, pale pink or cream; greasy to pearly; transparent to translucent.

Biaxial (+), α 1.608, β 1.630, γ 1.660, 2V(meas.) 82°, 2V(calc.) 83°.

15.56 (9), 5.16 (6), 3.11 (10), 2.850 (7), 2.665 (7), 2.627 (7), 2.217 (6), 1.795 (6).

IMA No. 93-059

Orthorhombic: probably $P22_12_1$

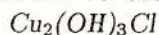
a 8.59 b 9.58 c 6.12 Å

Green to dark green; pearly to dull; translucent to opaque.

Biaxial (+), α 2.285, β 2.40, γ 2.58, 2V(meas.) large, 2V(calc.) 82°.

3.32 (10), 3.06 (10), 2.98 (4), 2.73 (6), 2.46 (5), 1.919 (4).

IMA No. 93-060 A monoclinic polymorph of atacamite, botallackite and paratacamite

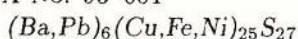
Monoclinic: $P2_1/n$ a 6.157 b 6.814 c 9.104 Å β 99.65°

Green to dark greenish black; adamantine; translucent to transparent.

Biaxial (-), indices of refraction could not be measured because mineral reacts with immersion liquids, 2V(meas.) 75°.

5.44 (100), 2.887 (40), 2.767 (60), 2.742 (70), 2.266 (60), 2.243 (50), 1.704 (50).

IMA No. 93-061

Cubic: $Pm\bar{3}m$

a 10.373 Å

Megascopic colour unknown; metallic; opaque.



In reflected light: pale brownish grey, no anisotropism, no bireflectance, nonpleochroic.

R: (22.0 %)470nm, (24.85 %)546nm, (26.2 %)589nm, (27.55 %)650nm.

3.460 (40), 3.281 (40), 2.996 (90), 2.378 (90), 1.835 (100), 1.779 (40).

IMA no. 93-062

$(Pd,Ag)_2Te$

Tetragonal: $P4_222$, $P4_2/m$ or $P4_2$

a 8.913 c 6.098 Å

Megascopic colour unknown; metallic; opaque.

In reflected light: brownish-rose, distinct to strong anisotropism from white to rose-brown,

distinct bireflectance, pleochroic from brownish-grey, to violet-rose. R_{min} & R_{max} :

(38.7, 48.7 %)470nm, (44.0, 55.5 %)546nm, (47.3, 58.2 %)589nm, (50.7, 60.7 %)650nm.

3.051 (96), 2.825 (10), 2.553 (4), 2.231 (6), 2.042 (5), 1.326 (3).



Erratum

Romanian Journal of Mineralogy, 76/2, p. 95–100.

MICROCHEMICAL DATA ON ANDRADITE GARNETS WITH IRISATIONS FROM OCNA DE FIER, BANAT, ROMANIA

Lucreția GHERGARI¹, Ștefan NICOLESCU², Ioan MĂRZA¹, Constantin GRUESCU³

¹ Universitatea "Babeș-Bolyai", Catedra de Mineralogie, Str. Kogălniceanu nr. 1, RO-3400 Cluj-Napoca

² Department of Geology, Earth Sciences Centre, University of Gothenburg, S - 413 81 Gothenburg, Sweden; e-mail: nicolec@gvc.gu.se

³ Str. Vale, nr. 113, RO-1736 Ocna de Fier

Due to an unfortunate error, REE data were inaccurately given in the original paper (Ghergari *et al.*, 1995). The section on REE elements should have read:

Rare earth element (REE) analyses were performed by solution ICP-MS. REE abundances are low (Σ REE = 31 ppm, Tab. 3), much lower than in associated felsic igneous rocks, but in good agreement with REE data on non-iridescent garnets from the deposit. As other investigated grandite samples, the light rare earth element (LREE) enrichment and negative Ce anomaly are diagnostic for Ocna de Fier garnets (Fig.). The full genetic significance of this behaviour will be discussed elsewhere (Nicolescu, Corneli, *in prep.*).

References

- Evensen, N.M., Hamilton, P.J., O'Nions, R.K. (1978) Rare-earth abundances in chondritic meteorites. *Geochim. Cosmochim. Acta*, 42, p. 1199–1212.
- Ghergari, L., Nicolescu, Șt., Mărza, I., Gruescu, C. (1995) Microchemical data on andradite garnets with irisations from Ocna de Fier, Banat, Romania. *Rom. J. Mineral.*, 76/2, p. 95–100.
- Nicolescu, Șt., Cornell, D.H. (in prep.) Genetic significance of major and rare earth elements geochemistry of primary and secondary skarn minerals in the Ocna de Fier-Dognecea deposit (Banat, SW Romania).

Table

REEs	ppm
La	5.23
Ce	11.89
Pr	1.98
Nd	9.52
Sm	1.24
Eu	0.23
Gd	0.49
Tb	0.05
Dy	0.25
Ho	0.05
Er	0.14
Tm	0.02
Yb	0.10
Lu	0.02
Σ REEs	31.20

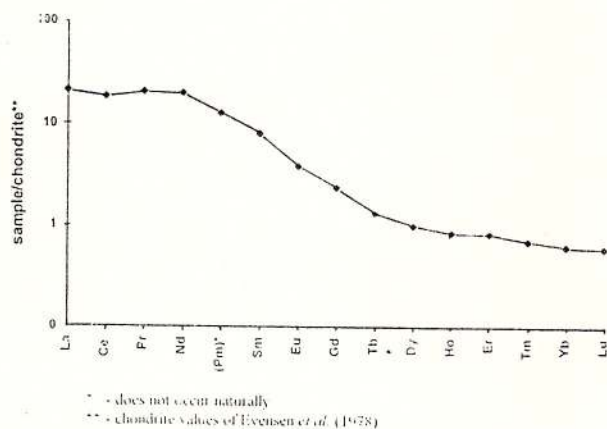


Fig. – REE Abundances in Ocna de Fier Iridescent Andradite



INSTRUCȚIUNI PENTRU AUTORI

ROMANIAN JOURNAL OF MINERAL DEPOSITS publică contribuții științifice originale referitoare la acest domeniu.

Vor fi acceptate numai lucrările care prezintă concis și clar informații noi. Manuscrisul va fi supus lecturii critice a unuia sau mai multor specialiști; după a doua revizie nesatisfăcătoare din partea autorilor va fi respins definitiv și nu va fi înapoiat.

Manuscrisele trebuie prezentate, de regulă, în engleză sau franceză; cele prezentate în limba română trebuie să fie însoțite de un rezumat, în engleză sau franceză, de maximum 10 % din volumul manuscrisului.

Lucrările trebuie depuse, în două exemplare, la secretariatul Comitetului de redacție, inclusiv ilustrațiile în original. Manuscrisul trebuie să cuprindă: textul (cu o pagină de titlu, care este și prima pagină a lucrării), bibliografie, cuvinte cheie, abstract, ilustrații, explicații ale figurilor și planșelor, și un sumar cu scop tehnic.

Se va adăuga o filă separată cu un colontitlu de maximum 60 semne și un sumar, în care se va indica ierarhia titlurilor din text în clasificarea zecimală (1; 1.1; 1.1.1), care nu trebuie să depășească patru categorii.

Textul va fi dactilografiat la două rânduri (31 rânduri/pagină și 64 semne/rând), pe o singură parte a colii, cu un spațiu liber de 3-4 cm în partea stângă a paginii și nu trebuie să depășească 20 pagini dactilografiate (inclusiv bibliografia și figurile).

Prima pagină a textului va cuprinde: a) titlul lucrării (concis, dar informativ), cu un spațiu de 8 cm deasupra; b) numele întreg al autorului (autorilor); c) instituția (instituțiile) și adresa (adresele) pentru fiecare autor sau grup de autori; d) text.

Notele de subsol se vor numerota consecutiv.

Citările din text trebuie să includă numele autorului și anul publicării. Exemplu: Ionescu (1970) sau (Ionescu, 1970). Pentru doi autori: Ionescu, Popescu (1969) sau (Ionescu, Popescu, 1969). Pentru mai mult de doi autori: Ionescu et al. (1980) sau (Ionescu et al., 1980). Pentru lucrările care se află sub tipar, anul publicării va fi înlocuit cu "in press". Lucrările nepublicate și rapoartele vor fi citate în text ca și cele publicate.

Abstractul, maximum 20 rânduri (pe filă separată), trebuie să fie în limba engleză și să prezinte pe scurt principalele rezultate și concluzii (nu o simplă listă cu subiecte abordate).

Cuvintele cheie (maximum 10) trebuie să fie în limba engleză sau franceză, corespunzător limbii în care este lucrarea (sau abstractul, dacă textul este în română), prezentate în succesiune de la general la specific și dactilografiate pe pagina cu abstractul.

Bibliografia se va dactilografia la două rânduri, în ordine alfabetică și cronologică pentru autorii cu mai mult de o lucrare. Abrevierile titlului jurnalului sau ale editurii trebuie să fie conforme cu recomandările respectivelor publicații sau cu standardele internaționale.

Exemple:

a) jurnale:

Giuşcă, D. (1952) Contributions à l'étude cristallographique des niobates. *An. Com. Geol.*, XXIII, p. 259-268, București.

– , Pavelescu, L. (1954) Contribuții la studiul mineralogic al zăcămintului de la Mușca. *Comm. Acad. Rom.*, IV, 11-12, p. 658-991, București.

b) publicații speciale:

Strand, T. (1972) The Norwegian Caledonides. p. 1-20. In: Kulling, O., Strand, T. (eds.) *Scandinavian Caledonides*, 560 p., Interscience Publishers.

c) cărți:

Bălan, M. (1976) Zăcămintele manganifere de la Iacoveni. *Ed. Acad. Rom.*, 132 p., București.

d) hărți:

Ionescu, I., Popescu, P., Georgescu, G. (1990) Geological Map of Romania, scale 1:50,000, sheet Câmpulung. *Inst. Geol. Geofiz.*, București.

e) lucrări nepublicate sau rapoarte:

Dumitrescu, D., Ionescu, I., Moldoveanu, M. (1987) *Report. Arch. Inst. Geol. Geofiz.*, București.

Lucrările sau cărțile publicate în rusă, bulgară, sârbă etc. trebuie menționate în bibliografie transliterând numele și titlurile. Exemplu:

Krashenninnikov, V. A., Basov, I. A. (1968) *Stratigrafiya kainozoa*. Trudy GIN, 410, 208 p., Nauka, Moscow.

Ilustrațiile (figuri și planșe) trebuie numerotate și prezentate în original, pe coli separate (hârtie de calc), bune pentru reprodus. Dimensiunea liniilor, a literelor și a simbolurilor pe figuri trebuie să fie suficient de mare pentru a putea fi citite cu ușurință după ce au fost reduse. Dimensiunea originalului nu trebuie să depășească suprafața tipografică a paginii: lățimea coloanei 8 cm, lățimea paginii 16,5 cm, lungimea paginii 23 cm, pentru figuri, iar pentru planșele liniare nu trebuie să depășească dimensiunile unei pagini simple (16,5/23 cm) sau duble (23/33 cm) și trebuie să fie autoexplicativă (să includă titlul, autori, explicație etc.). Scară grafică obligatorie.

Ilustrațiile fotografice (numai alb-negru) trebuie să fie clare, cu contrast bun și grupate pe planșe de 16/23 cm. În cadrul fiecărei planșe număratoarea fotografiilor se repetă (de. ex. Pl. I, fig. 1, Pl. II, fig. 1).

Tabelele vor fi numerotate și vor avea un titlu. Dimensiunea originală a tabelor trebuie să corespundă dimensiunilor tipografice menționate mai sus (8/16,5 sau 16,5/23).

Autorii vor primi un singur set de corectură, pe care trebuie să-l înapoieze, cu corecturile corespunzătoare, după 10 zile de la primire. Numai greșelile de tipar trebuie corectate; nu sunt acceptate modificări.

Autorii vor primi gratuit 30 de extrase pentru fiecare lucrare.

Comitetul de redacție



INSTRUCTIONS TO AUTHORS

ROMANIAN JOURNAL OF MINERAL DEPOSITS publishes original scientific contributions dealing with any subject of this field.

Only papers presenting concisely and clearly new information will be accepted. The manuscript will be submitted for critical lecture to one or several advisers. Papers will be definitely rejected after a second unsatisfactory revision by the authors. The manuscripts will not be returned to the authors even if rejected.

Manuscripts are preferred in English or French. Manuscripts submitted in Romanian will be accompanied by an abstract in English or French (maximum 10 per cent of the manuscript volume).

Papers should be submitted in duplicate to the secretary of the Editorial Board, including the reproduction ready original figures. The manuscript should comprise: text (with a title page which is the first page of it), references, key words, abstract, illustrations, captions and a summary for technical purposes.

Author(s) should add a separate sheet with a short title (colontitle) of maximum 60 strokes and a summary indicating the hierarchy of headings from the text listed in decimal classification (1; 1.1; 1.1.1) but not exceeding four categories.

Text should be double-spaced typed (31 lines/page with 64 strokes each line) on one side of the paper only, holding an empty place of 3–4 cm on the left side of the page. The text cannot exceed 20 typewritten pages (including references and figures).

Front page (first page of the text) should comprise: a) title of the paper (concise but informative) with an empty space of 8 cm above it; b) full name(s) of the author(s); c) institution(s) and address(es) for each author or group of authors; d) text.

Footnotes should be numbered consecutively.

Citations in the text should include the name of the author and the publication year. Example: Ionescu (1970) or (Ionescu, 1970). For two authors: Ionescu, Popescu (1969) or (Ionescu, Popescu, 1969). For more than two authors: Ionescu et al. (1980) or (Ionescu et al., 1980). For papers which are in course of print the publication year will be replaced by "in press". Unpublished papers or reports will be cited in the text like the published ones.

Abstract, of maximum 20 lines (on separate sheet), must be in English, summarizing the main results and conclusions (not a simple listing of topics).

Key words (max. 10 items), in English or French, following the language used in the text (or the *Resumé* if the text is in Romanian), given in succession from general to specific, should be typed on the abstract page.

References should be typed in double-line spacing, listed in alphabetical order and chronological order for authors with more than one reference. Abbreviations

of journals or publishing houses should be in accordance with the recommendations of the respective publications or with the international practice.

Examples:

a) journals:

Giușcă, D. (1952) Contributions à l'étude cristallographique des niobates. *An. Com. Geol.*, XXIII, p. 259–268, București.

– , Pavelescu, L. (1954) Contribuții la studiul mineralogic al zăcămintului de la Mușca. *Comm. Acad. Rom.*, IV, 11–12, p. 658–691, București.

b) special issues:

Strand, T. (1972) The Norwegian Caledonides. p. 1–20. In: Kulling, O., Strand, T. (eds.) *Scandinavian Caledonides*, 560 p., Interscience Publishers.

c) books:

Bălan, M. (1976) Zăcămintele manganifere de la Iacobeni. *Ed. Acad. Rom.*, 132 p., București.

d) maps:

Ionescu, I., Popescu, P., Georgescu, G. (1990) Geological Map of Romania, scale 1:50,000, sheet Cîmpulung. *Inst. Geol. Geofiz.*, București.

e) unpublished papers or reports:

Dumitrescu, D., Ionescu, I., Moldoveanu, M. (1987) Report. *Arch. Inst. Geol. Geofiz.*, București.

Papers or books published in Russian, Bulgarian or Serbian etc. should be mentioned in the references transliterating the name and titles. Example:

Krashennnikov, V. A., Basov, I. A. (1968) *Stratigrafiya kainozoiă*. Trudy GIN, 410, 208 p., Nauka, Moscow.

Illustrations (figures and plates) must be numbered and submitted as originals on separate sheets (tracing papers), ready for reproduction. The thickness of the lines, lettering and symbols on figures should be large enough to be easily read after size-reduction. The original size should not extend beyond the print area of the page: column width 8 cm, page width 16.5 cm, page length 23 cm for figures; the width of line drawings should not extend over a single (16.5/23) or double (23/33 cm) page area and must be selfexplanatory (including title, authors, legend etc.). The graphic scale is obligatory.

Photographic illustrations (black-and-white only) must be of high quality and should be grouped into plates 16/23 cm in size. Each plate should have the photos numbered, i.e. Pl. I, Fig. 1; Pl. II, Fig. 1.

Tables should be numbered and entitled. Original size of the tables should correspond to the above mentioned (8/16.5 or 16.5/23) dimensions of the printing area.

Author(s) will receive only one set of preprint proofs which must be returned, with corrections, 10 days after receiving them. Only printing errors should be corrected, no changes in the text can be accepted.

Thirty offprints of each paper are supplied to the author(s) free of charge.

Editorial Board



Institutul Geologic al României





Toate drepturile rezervate editurii Institutului Geologic al României
All rights reserved to the Geological Institute of Romania

*Editat cu sprijinul Ministerului Cercetării și Tehnologiei –
Colegiul Consultativ pentru Cercetare Științifică și Dezvoltare Tehnologică*

*Edited with the support of the Ministry of Research and Technology –
Advisory Board for Scientific Research and Technologic Development*

Translation and language review by:
Adriana Năstase, Mariana Borcoș

Editorial Staff:
Anca Andăr

Illustration:
Paraschiv Toader

Printing: Valerian Vlad



(Contents continued from front cover)

Glauconitic minerals from the Transylvanian Basin. New mineralogical data. D. POP, I. BEDELEAN.....	71
Palygorskite in magnesian skarns from Băița Bihor (Rézbanya): A second romanian occurrence and a review. ȘT. MARINCEA, M. CIULAVU, I. VANGHELIE.....	87
Sepiolite from Dealul Măgurenilor-Preluca Veche, Maramureș District, Romania. I. KALMÁR, P. KOVÁCS-PALFFY, M. FÖLDVARI.....	97
Mineral composition and bloating effect of clayshale from Mežica Pb-Zn ore deposit (Slovenia). P. TOMŠE, B. MITRIČ.....	107
Once again on the joseite-A from the skarns deposits from Băița Bihor mine (Apuseni Mts, Romania). G. CIOFLICA, M. LUPULESCU.....	113
Recent discovery of telurides in the Vezhnali ore deposit, Lesser Caucasus. S.F. VELIZADE, A.B. SHIRALIYEV, E.N. EFENDIYEVA, N.F. NAGIYEV, T.G. MUSTAFAYEV.....	117
Paragenetic mineral associations of sulphides ores, southern slope of the Great Caucasus. S.F. VELIZADE, A.B. SHIRALIYEV, E.N. EFENDIYEVA.....	121
Plant remnants replaced by copper minerals, Rongjing copper deposit, Sichuan, China. Z.M. CAO, X.Q. HU, D.Q. SHUAI.....	125
The possibilities of geological correlation on the basis of extraterrestrial spherules occurring in Hungary. Cs. H. DETRE, Gy. DON, L. DOSZTÁLY, E. RÁLISCH-FELGENHAUER, A. SIEGL-FARKAS.....	129
On the morphological distinction between spherules of extraterrestrial, terrestrial and industrial origin by means of SEM and EDAX examination of samples taken from the placers of Crișu Negru, Romania. O. KÁKAY-SZABÓ, Á. HADNAGY.....	133
The structure of synthetic Zippeite. R. VOCHTEN, L. VAN HAVERBEKE, K. VAN SPRINGEL, N. BLATON, O.M. PEETERS.....	139
Standardisation of polytype suffixes. E.H. NICKEL.....	141
Mineral names applied to synthetic substances. E.H. NICKEL.....	143
New minerals recently approved by the Commission on New Minerals and Mineral Names International Mineralogical Association.....	145

